Population balance modeling and passivity-based control of particulate processes, applied to the *Silgrain*® process

Marta Dueñas Díez
Telemark University College
Faculty of Technology
Porsgrunn, Norway

Thesis submitted to the
Norwegian University of Science and Technology
for the degree of
philosophiae doctor (PhD)

In memory of my beloved father
and
to my mother

Preface

This thesis is submitted in partial fulfillment of the requirements for the degree of *philosophiae doctor* (PhD) at the Norwegian University of Science and Technology (NTNU) and Telemark University College (HiT). The research has been carried out with financial support from the Research Council of Norway through the project 142994/432, and with some additional financial support from Elkem ASA and from ISA (the Instrumentation, Systems, and Automation society) through the Norman E. Huston scholarship. The financial support from these sources is gratefully acknowledged.

When I started in the summer of 2000, the intention of this work was to investigate the "Integration of process control based on mechanistic models with statistical process monitoring", i.e. the work would cover three fields: mechanistic modeling, process control, and statistical process monitoring, and the obtained results would be tested with an industrial process. The selected case study turned out to belong to a class of systems that has attracted and is still attracting much attention from the research community, i.e. particulate processes. Modeling and process control of particulate processes are active areas of research, with certain challenges that remain unresolved. This made us place more focus on the modeling and control tasks than originally planned. The title of the thesis has thus been changed to "Population balance modeling and inventory passivity-based control of particulate processes" to better reflect the contents of this work.

Although there is one single name on the cover of this thesis, this work would have not been possible without the guidance, help and support of many people. Working towards this degree has been challenging, interesting, enjoyable, hard sometimes, and definitely worthy. I have had the opportunity to meet and collaborate with a number of brilliant people that deserve recognition.

First of all, I am indebted to my main supervisor associate professor dr.ing. Bernt Lie for a good number of reasons: for encouraging me to study for a PhD degree, for the skilful scientific guidance, for the non-scientific help in many occasions (like when my car broke down), for an amazing patience (to handle my mediterranean character), for reading and correcting diverse reports, articles, and the drafts of this thesis, and for the optimistic encouragement I got from you when

I needed it. Your broad overview of engineering topics (and non-engineering topics) impresses me. I really hope that we can continue collaboration in the future.

My sincere gratitude also goes to my co-supervisor dr.tech. Magne Fjeld, whose broad expertise both at the academic level and the industrial level has had a clear contribution to the fruitful collaboration with the industrial partner. I am thankful for the way you directed the meetings with Elkem ASA, for the supervision, for your contribution to direct the focus of the thesis towards key areas, and for reading and correcting reports, articles and the drafts of the thesis. I also want to thank Sissel and you for the inspiring *hyttetur* (cottage trip), which gave me the energy I needed to finalize the writing of the thesis.

I want to thank my other co-supervisor dr.ing. Rolf Ergon, for his participation and guidance in this project. Although less focus was placed in this thesis to the area you work most with, I really appreciate that you took the time to participate in the meetings, to read diverse written material, to give useful comments and suggestions, and to participate in our graduate student lunch breaks. I am also thankful to Målfrid and you for the boat trip last summer to *Jomfruland*.

I have much to thank Elkem ASA for besides the financial support. Thank you for providing me with a challenging process to model, for allowing me to carry out experiments at the laboratory and plant scale, for sharing process knowledge with me, and for the enthusiasm that the project members have shown. The following employees at Elkem Research Centre and Elkem Bremanger deserve to be mentioned: Geir Ausland, Einar Andersen, Håvard Sørheim, Birte Skofteland, Thomas Realfsen, Vegard Olsø, and Marit G. Dolmen. In particular, I am sincerely grateful to Geir Ausland and Einar Andersen for being so enthusiastic and involved. Geir, although I might once have suggested you were demanding, I really appreciate that you pushed me to rethink my arguments and to improve the model. I am also very grateful to Einar Andersen for an active participation in the establishment of the model foundations, and for your tremendous help in the measurement campaign carried out at the Bremanger plant. It will be difficult to forget the day you jumped on to a transport track and below the transport belt trying to catch a large *representative* sample of the feedstock.

From January to June 2001 I visited Prof. B. Erik Ydstie at Carnegie Mellon University in Pittsburgh (USA) for the first time. This visit was very inspiring, and had an important impact on the part of this thesis on control. Erik, I am thankful to you for introducing me to the fascinating field of nonlinear control. Thank you to you and your students (Vianey, Edgar, Duncan, Dimitrios, Jennifer, Martin, Ashish, and Christy) for making me feel as any other member of your group of graduate students. I am also grateful to Prof. Larry Biegler, from whom I learnt a lot about numerical methods.

And now my colleagues, with whom I have shared many moments these years.

Thanks to dr.ing. Tor Anders Hauge for the scientific help, the help with administrative and bureaucracy issues, and for your patience. In addition to your good work, your ability to keep your desk always neat really amazed me. Thank you very much to (very soon PhD) Glenn-Ole Kaasa for the interesting discussions on nonlinear control, for teaching me mindmapping (which I use ever since to organize my ideas), and thanks to Linn and you for giving me my first pair of skis. Thanks to Beathe Furenes, with whom it has been a pleasure to share office for over a year now. It was great to have somebody to talk to in the good and the hard times, and I really appreciate the help I got from you in so many aspects: encouragement, skiing techniques, house search, etc. Thanks also to Urmila Datta for so many enjoyable conversations and advice, and for the times you have invited me to delicious Indian food. Thanks to Inger Hedvik Matveyev for contributing to have such a positive working environment, and so enjoyable lunch breaks, and thank you for the delicious Chinese food. Thanks to all the other regular members of the lunch breaks: Nils-Olav, Anette, Gerhard, Dawn, and Thomas.

And now it comes the people who did not contribute scientifically to my work but that were crucial for my well-being. My friends: Paul Arild, Jesús María, Nobuaki, Ann Eli, Marte, Ine, Dagmara, Xiao Li, Serena, Amalia, and others, that have done their best to drag me out of the office from time to time. Very special warm thanks to my boyfriend Ingo Brigandt who has certainly managed to get my mind away from engineering for a little while every day since we met. Although we are physically separated by some thousands of km most of the year, I feel you have been close to me all along. Those minutes talking on the phone every day are a highlight.

Finally, the people to whom I really owe everything: my family. My family has been the most important emotional support of my life. My three brothers José, Aurelio, and Agustín, and my sister Ana have been an example to follow to me. My eldest brother José has a brilliant career as gynecologist. My brothers Aurelio and Agustín had a very good ability to combine the university duties with social life while they studied Medicine and Economics, respectively. My sister Ana is the most intelligent and hard-working person I have ever known, being a brilliant microbiologist. I am thankful for the close relationship we have always had. Indeed, I am in Norway thanks to her — she took me to Norway for holiday back in 1996. Finally, my parents, to whom I dedicate this thesis. My mother, Aurora Díez, who is a very intelligent brave woman that has an impressive strength to handle the difficulties that life gives us, and who has always been devoted to the well-being of her husband and children. And my father, José Dueñas, who was a great man, a loving father and who had so many precious qualities: generosity, honesty, tenacity, intelligence,... The memory of his unconditional support and encouragement is always with me.

Summary

This thesis deals with the systematic development of mechanistic models of particulate processes for the purposes of nonlinear controller design and implementation. The methods investigated in this thesis were illustrated with an industrial hydrometallurgical process called the *Silgrain*® process (Elkem ASA), for which a model and a controller strategy have been developed from scratch.

The class of processes studied in this thesis, particulate processes, has attracted and still attracts a great deal of interest from the international research community. Particulate processes are characterized by the presence of a continuous phase and a dispersed phase comprised of entities that have a distribution of properties. Such a distribution of properties has an important impact on the process operation and quality of the final products. Moreover, most of process industries contain one or more stages that involve particulate processes, among them the major Norwegian companies: Elkem, Hydro, Borealis, Statoil, etc.

A systematic method to PBE modeling was suggested, consisting of the following stages: establishment of model purpose and model foundations, building of the model structure, determination of the constitutive relations, selection of a solution method, parameter estimation and model validation. Such an approach is general to any type of process, but when dealing with particulate processes special care should be placed on some of these stages. The method was thoroughly illustrated with the development of the model of the two reactors of the *Silgrain*® process. The model was based on the traditional balance equations of mass, energy, and momentum, and on a balance of the distribution of properties, called the population balance equation (PBE). This is the first time PBE is used to model a hydrometallurgical leaching reactor where disintegration takes place. An experimental laboratory campaign had to be carried out in order to determine the constitutive equations of the disintegration event. Another experimental campaign at the plant level was carried out to gather data for parameter estimation and model validation. The results of the fitting were satisfactory. Besides the particular contribution of developing a detailed model for the case study, some general contributions of this research were:

- it was shown how dividing the model into compartments according to the

regions that are observed in practice in the reactors is key to obtaining realistic models;

- it was discussed how the widely used assumption of complete mixing provides unrealistic models. Instead, the compartmentalization approach combined with a balance of forces on the entities to define the interflows among compartments improves the realism of PBE models to a great extent;

- it was shown that the use of a systematic parameter identifiability analysis prior to parameter estimation can be very useful, and even essential. PBE models are large in size, typically nonlinear in the parameters, and many parameters may not be identifiable from the available measurements. Hence, if no parameter identifiability analysis is carried out, the parameter estimation algorithm may break down, or give very poor parameter estimates.

An approach to process control called inventory passivity-based control was selected in this thesis, since this method handles nonlinear processes, is based on dynamic models, and it has suitable stability properties. In order to apply this method to particulate processes, the theory was extended in this thesis to handle rectangular systems, i.e. systems where the number of available manipulated variables is less than the number of inventories. Both chemical reaction networks and particulate processes fall under such a class of systems. An stability proof has been developed, by linking inventory passivity-based control to a relevant theory of nonlinear chemical dynamics, called the Feinberg Deficiency Theorems. In addition to stability, some other implementation issues were discussed in the thesis, such as the handling of constraints on the manipulated variables, the robustness of the controller against disturbances and model errors, the importance of observers, and the adaptation of the approach to semibatch control. Finally, the thesis also discussed the role of inventory passivity-based control within the framework of plantwide control, and the integration of inventory passivity-based control with a statistical process monitoring approach.

Contents

Nomenclature

It is useful to provide a list of symbols and notation used in this thesis. A few symbols of temporary nature that are used only in specific contexts are omitted to restrict the length of the list.

Latin letters

a	Particle *breakage frequency* function
b	Birth probability distribution function
$\bar{b}$	Discrete birth probability distribution function
B	Birth rate
C	Molar concentration
clip	Strictly increasing sigmoid function
D	Death rate
D	Reactor Diameter
D_{cut}	Cut size
D_p	Particle diameter
E	Activation energy (kinetic rate)
e	Output error
f	Mass probability distribution function
f	State function of a dynamic model
g	Acceleration of gravity
g	Time-varying coefficient (method of weighted residuals)
g	Output function of a dynamic model
h	Specific enthalpy
h	Heat transfer coefficient
h	Input function of a dynamic model
J	Cost function (optimization)
K	Proportional constant of a controller
k	Preexponential factor (kinetic rate)
k	Heat conductivity
L	Observer gain
l	Linkage classes

N	Mole number
N	Number of intervals (discretization method)
$\dot{N}$	Molar flow rate
n_c	Number of complexes in a reaction network
n_s	Number of species in a reaction network
M	Mass
$\dot{M}$	Mass flow rate
M_w	Molecular weight
m	Moment of a distribution
P	Pressure
P	Partition matrix
p	Generation or disappearance term in the inventory balance
$\dot{Q}$	Heat loss
q	Volumetric flow rate
r	Reaction rate
r	Radius
S	Sensitivity matrix (identifiability analysis)
S	Sliding function
s	Rank of a reaction network
s_{ij}	Sensitivity of i-th output to j-th parameter
Sc	Scaling matrix (nonlinear least squares)
sc_{ij}	Scale required to calculate s_{ij}
T	Temperature
t	Time
U	Internal energy
u_{sup}	Superficial velocity
u_o	Actual fluid velocity
V	Volume
V	Storage function (passivity theory)
v	Inventory or extensive variable
$\mathbf{v}$	Velocity vector
v_i	Time derivative of internal coordinate ($\frac{d\zeta_i}{dt}$)
W	Component mass
$\dot{W}$	Component mass flow rate
w	Component weight fraction
w	Supply function (passivity theory)
x	Representative size
x	Internal state of a dynamic system
x	Intensive variable
y	Model output
y	Controlled inventories

$\bar{y}$	Deviation of controlled inventory from the desired setpoint
y_m	Measured variable
z	Axial direction
z	Uncontrolled inventories
$\bar{z}$	Deviation of uncontrolled inventory from the steady-state value

Greek Symbols

α	Measure of conversion
β	Fraction of reaction via HCl
γ	Reaction order (kinetic rate)
γ	Collinearity index (parameter identifiability)
Δ	Uncertainty
ΔH_r	Reaction enthalpy
δ	Importance ranking parameter (parameter identifiability)
δ	Deficiency of a chemical reaction network
ϵ	Daughter particle size
ε	Void fraction
ζ	*Internal* coordinate
θ	Model parameter
λ	Eigenvalue
π	Momentum
$\dot{\pi}$	Momentum flow rate
ρ	Density
Σ	Surface to volume ratio
Φ	Discrete population density distribution
ϕ	Basis function (method of weighted residuals)
ϕ	Transport term in the inventory balance
φ	Weighting function (method of weighted residuals)
ψ	*intensive* population density distribution
Ψ	*extensive* population density distribution
$\dot{\Psi}$	population density distribution *flow*

Abbreviations

ARMAX	AutoRegressive Moving Average with eXternal Input
ARX	AutoRegressive with eXternal Input
BDF	Backward Differentiation Formulas
CSTR	Continuous Stirred Tank Reactor
CV	Controlled Variable
DAE	Differential and Algebraic Equations

GUI	Graphical User Interface
HR	First Leaching Reactor (from *hovedreaktor* = main reactor)
MV	Manipulated Variable
NDF	Numerical Differentiation Formulas
ODE	Ordinary Differential Equations
PBE	Population Balance Equation
PDAE	Partial Differential and Algebraic Equations
PDE	Partial Differential Equation
PID	Proportional, Integral, and Derivative
PSD	Particle Size Distribution
SNA	Stoichiometric Network Analysis
SPM	Statistical Process Monitoring
UR	Second Leaching Reactor (from *utlutningsreaktor* = leaching reactor)

Subscripts

acid	relative to the acid and/or acid compound
feed	relative to the inlet to the HR
in	relative to the inlet flow to a compartment
max	maximum
min	minimum
Me	metallic component, i.e. Fe, Al and Ca
RI	relative to the disintegration region of the HR
RII	relative to the storage region of the HR
RIII	relative to the sedimentation region of the UR
RIV	relative to the dissolution region of the UR
out	relative to the outflow from the reactor
overflow	relative to the overflow of the UR
sediment	relative to the sedimentation flow in the UR
solid	relative to the particulate phase
surroundings	relative to the surroundings
tapping	relative to a tapping flow

Chapter 1

Introduction

1.1 Background

The goal of this thesis is to establish a systematic strategy for the development of PBE models of particulate processes to be used for the purposes of design and implementation of automatic control, and to illustrate the suggested modeling and control strategies with a real industrial particulate process, the *Silgrain*® process.

Particulate processes are characterized by a presence of a continuous phase and a disperse phase made up of entities with a distribution of properties, and where the distribution of properties strongly affects the operation of the process and the product quality. Particulate processes are encountered in a considerable number of applications: crystallization, agglomeration, grinding, dissolution, leaching, etc. Many valuable products are obtained in these processes. Therefore, it is of great interest to focus attention on particulate processes, and how to improve their performance. Automatic control is known to improve process operation, and to reduce process and product variability.

The modeling of particulate processes has been studied for several decades now, and a tool named Population Balance Equation (PBE) has become the most widely-used modeling approach for such processes. Despite the active research on this topic, the PBE remains being a tool for the academic community, and not for the industrial community. A reason may be that the simplest way to use the PBE, i.e. assuming complete mixing, may not provide realistic models. Accounting for the spatial distribution of the properties increases realism, but the resulting models become mathematically challenging, and impractical for industrial application. Establishing a systematic strategy for the development of PBE models that both represent realistically the operation of industrial units and that are mathematically simple enough to be used in online applications, is thus a first step towards a more widely use of PBE models in industry.

The second objective is that of developing a control strategy for particulate processes, a strategy that exploits the process information contained in the PBE model. There are several control theories that are based on mechanistic nonlinear models, and that could be studied. One theory that has not been studied in the framework of particulate processes before, is inventory passivity-based control. Such an approach is chosen in this thesis because it has some advantageous features related to stability and robustness, and the controller design is relatively straightforward. Extending inventory passivity-based control to reactive systems and particulate systems is thus believed to be an interesting area of research.

1.2 Outline of the thesis

The thesis is composed of three parts. Part I presents the suggested PBE modeling methodology, and its application to the case study. Part II describes inventory passivity-based control, the extension of the theory to reactive systems and particulate systems, the application to the case study, and the analysis of certain practical issues. Part III summarizes the conclusions of the thesis. Finally, some complementary chapters are included as appendices at the end of the thesis.

In more detail: Chapter 2 gives an introduction to mathematical modeling, particulate processes, and modeling of particulate processes. A systematic PBE modeling strategy is described in Chapter 3, where emphasis is put on the most challenging stages. Such a methodology is illustrated in a thorough way with the development of the the *Silgrain*® model in Chapter 4. A general introduction to process control, and a review of the control methodologies that have been applied to particulate processes, are given in Chapter 5. Chapter 6 introduces inventory passivity-based control, shows the suggested methodology for rectangular systems, discusses in detail the requirements that have to be met to ensure stability, compares the approach with other approaches of nonlinear control, discusses the link of the methodology to thermodynamics, and illustrates the use of the methodology with a benchmark chemical reactor and with the *Silgrain*® model. Some issues related to the practical implementation of inventory passivity-based control are analyzed in Chapter 7, namely: the presence of input constraints, the robustness of the approach, the need for an observer, the possibility of semibatch control, the role of the approach within plantwide control, and the combination of the control strategy with statistical monitoring. The main body of the thesis concludes with Chapter 8, which presents the concluding remarks and gives some ideas for future research.

1.3 Main Contributions

The contributions of this thesis regarding PBE modeling are:

- A systematic approach to PBE modeling is suggested. The approach itself is not original, and is based on standard modeling techniques. The contribution consists in how attention is drawn to the stages that require special care when dealing with particulate processes, due to the special features of such processes. The application of compartmentalization as a way to achieve more realistic models is original, although the idea of compartmentalization itself has been used in reaction engineering for a long time. This thesis stresses the importance of compartmentalization and description of connections based on distinguishable physical phenomena in the process. The work on PBE modeling and compartmentalization has been presented in (Dueñas Díez, Ausland, Fjeld & Lie 2001) (later published in (Dueñas Díez, Ausland, Fjeld & Lie 2002)), (Dueñas Díez & Lie 2003*c*), (Dueñas Díez, Ausland & Lie 2003*a*), and (Dueñas Díez, Ausland & Lie 2003*b*) (submitted to *Powder Technology*).

- The systematic approach to parameter identifiability prior to parameter estimation is not original, but it is the first time that such an approach is applied to particulate processes. This part of the work will be presented in (Dueñas Díez, Andersen, Fjeld & Lie 2004), and is submitted to *Chemical Engineering Science*.

- The model of the *Silgrain*® process is entirely original, including the determination of the constitutive equations describing particle disintegration. Two experimental campaigns have been necessary for model development: one at laboratory scale for the determination of constitutive equations, reported in (Dueñas Díez 2001) (confidential), and one at the plant scale for gathering data for model validation, reported in (Dueñas Díez 2003) (confidential). Diverse versions of the model have been presented in (Dueñas Díez & Lie 2000), (Dueñas Díez, Ausland, Fjeld & Lie 2002) and (Dueñas Díez et al. 2003*b*).

The contributions of this thesis regarding inventory passivity-based control are:

- The application of inventory passivity-based control to particulate processes is new. This work has been reported in (Dueñas Díez, Lie & Ydstie 2001), (Dueñas Díez, Ydstie & Lie 2002*a*), (Dueñas Díez, Ydstie & Lie 2002*b*), (Dueñas Díez & Lie 2003*a*) and (Dueñas Díez & Lie 2003*b*).

- The stability proof reported in (Farschman, Viswanath & Ydstie 1998) has been extended in this thesis to account for systems with chemical reaction

and particulate systems. Such systems are typically rectangular, i.e. systems with less manipulated variables than inventories. A detectability requirement is introduced in this thesis, and a way to check detectability, based on a published technique of nonlinear chemical dynamics, is suggested. It is the intention to submit such new theoretical results for publication in an international journal in the field of process control.

- Some issues that are important for the practical implementation of inventory passivity-based control, such as the presence of input constraints and robustness, are discussed, and some methods taken from literature are tested in simulation with the *Silgrain*® process, being thus tested for the first time on a particulate process.

Part I

Modeling of Particulate Processes

Chapter 2

Introduction

2.1 Modeling

A model is a representation of a certain real system or event of interest. This is quite a general definition. Hence, a toy, a drawing, a picture, a computer programme or a set of equations fall under such a definition. Here, the interest is focused on mathematical modeling. A simple but proper definition of a mathematical model is the following:

> A mathematical model is a representation, in mathematical terms, of certain aspects of a nonmathematical system. The arts and crafts of mathematical modeling are exhibited in the construction of models that not only are consistent with themselves and mirror the behavior of their prototype, but also serve some exterior purpose. (Aris 1999*b*)

The type of model to be used is thus determined to a large extent by the final purpose of the model. For example, in process engineering a dynamic model describing the time evolution of the system is needed for process control, whereas a static (or steady-state) model might be suitable for process optimization.

There are two main types of mathematical models: *mechanistic* models and *empirical or data-oriented* models. Mechanistic models try to describe the mechanisms that lie behind, and drive the evolution of a system. In process engineering, mechanistic models are based on the application of well-established balance laws of mass, energy and momentum to the system under study. In such applications, mechanistic models are also referred to as first-principle models. In contrast, entirely empirical models are just based on experience. Available data from the system are used to find a mathematical function that conveniently reproduces these data. Empirical models are also referred to as black-box models or identification

models. Some authors may argue that mechanistic models are also empirical because the mechanisms are derived from experience. However, such a classification of models into mechanistic and empirical is widely accepted.

Some other differences between mechanistic and empirical models are summarized below:

- Empirical models may often require more exhaustive experimentation on the real system than mechanistic models.
- Empirical models are valid for the range of conditions at which experimental data were obtained, whereas mechanistic models typically have a broader range of validity.
- The set of candidate models that are commonly used for empirical dynamic modeling are simple: linear on the states and time-invariant. In contrast, mechanistic models are typically nonlinear.
- For complex systems, building up mechanistic models may be very time-consuming.

Note that purely mechanistic models are rare. Experimental data are typically required to find expressions for certain terms of the balance laws or for the values of certain parameters in the model. For this reason, this type of models combining well-established balance laws with experimentally-obtained constitutive relations are sometimes called *gray-box* models.

There is a vast literature both on building of mechanistic and empirical models. Some basic references on building of mechanistic models are (Bird, Stewart & Lightfoot 2002) and (Aris 1999*b*), and on empirical models are (Ljung 1999) and (Nelles 2001).

2.2 Particulate processes

Particulate processes are present in a very wide range of industrial applications, such as crystallization, precipitation, leaching, grinding, biotechnology, and many others. The presence of particulate products in our daily life is also notable: pharmaceutical products, food (coffee, cocoa powder...), and detergents are a few examples. Even natural events such as the formation of rain drops or the predator-pray dynamics may be considered particulate processes. Particulate processes may thus seem very different from one another, and there is a large amount of research dedicated to each and one of these processes. However, there exists a number of characteristics common to all particulate processes that makes it possible to

study particulate processes within the same framework. Such characteristics are the following:

- The presence of a continuous phase (liquid, gaseous, or solid) and a dispersed phase made of individual entities. The dispersed phase is thus a population of entities of some kind. For example, we may have a crystallizer with a population of crystals immersed in a liquid phase, or we may have a bioreactor with a population of cells immersed in a liquid phase.

- The population of entities shows a distribution of one or more properties of interest, which affects the operation of the process and the quality of the product. In a crystallizer, the crystals are distributed in shape and size. In a bioreactor, the cells have a distribution of age.

- The presence of complex phenomena that causes dynamic changes in the property distribution. Examples of such complex phenomena:

  - Nucleation, i.e. birth of new entities;
  - Disintegration or breakage, i.e. disappearance of entities;
  - Growth;
  - Agglomeration;

The field of particulate processes is multidisciplinary not only because of the wide range of applications and products, but also because of the existence of three scale levels of interest:

- Microscale, i.e. considering one entity.

- Mesoscale, i.e. considering the interaction among some entities and the complex phenomena affecting them.

- Macroscale, i.e. considering the whole population and the integration of the particulate process within the entire production process.

Such a multiscale interest is also encountered in more traditional process industry, where microscale would refer to the molecular level, mesoscale would refer to the operation unit level and macroscale to the plantwide level.

2.3 Mechanistic models of particulate processes

Extensive research in the last five decades has been dedicated to the modeling of particulate processes. Increasing demands on product quality, and the need for operation optimization have enhanced this effort. Mechanistic models are widely used since the development of the Population Balance Equation (PBE) in 1964, by two groups of researchers studying crystal nucleation and growth, (Hulburt & Katz 1964) and (Randolph 1964). A good review on the use of the PBE is given in (Ramkrishna 1985) and (Ramkrishna 2000). Some of the reasons that explain the success of mechanistic modeling in the field of particulate processes are:

- the ability of the PBE approach to account for the complex phenomena taking place in the process,
- the lack of instrumentation to measure distributed properties, and in turn, the difficulty of obtaining extensive and complete experimental data that are required to identify an empirical model,
- the type of operation. A great deal of particulate processes operate in semi-batch or batch modes. Hence, a dynamic model is needed.

The next chapter describes a systematic modeling methodology for particulate processes. Such a methodology is subsequently illustrated in chapter 4 with the modeling of an industrial hydrometallurgical leaching process.

Chapter 3

Modeling of particulate processes

3.1 Modeling methodology

The development of mechanistic models of process systems, including particulate systems, can be carried out quite systematically. Figure 3.1 summarizes such a systematic approach to modeling.

Naturally, the first stage in the development of a model is to define the purpose of the model. The model complexity, the validity region of the model, and the required time to develop the model depend to a great extent on the final purpose of the model. Then, as much information about the system as possible should be gathered, not only regarding the physical, chemical, and/or biological mechanisms taking place in the system, but also about the equipment design and mode of operation. Based on such a knowledge about the system and on the purpose of the model, the next stage is to choose the model type and to establish the main principles and assumptions for the model. In most cases, this is the most important stage in model-building. Once the basis for the model and the main assumptions are established, the next stage is to build up the structure of the model by application of the balance laws and/or the PBE. Once this is done, modeling continues by determining the constitutive relations that define the transport flows, the reaction rates, and any other complex phenomena taking place in the system. The next stage is to find a solution method for the resulting mathematical model. The final stage is to validate the model using real data. This is a key stage, particularly if the model is to be used for prediction purposes.

Note that mathematical modeling is often a dynamic and iterative process. New knowledge about some aspects of the system may force the modeler to change or extend the existing model. Modeling of particulate processes is challenging and time-consuming. Changing the structure of such a model may be costly. The three first stages mentioned in figure 3.1 are thus even more crucial when dealing with

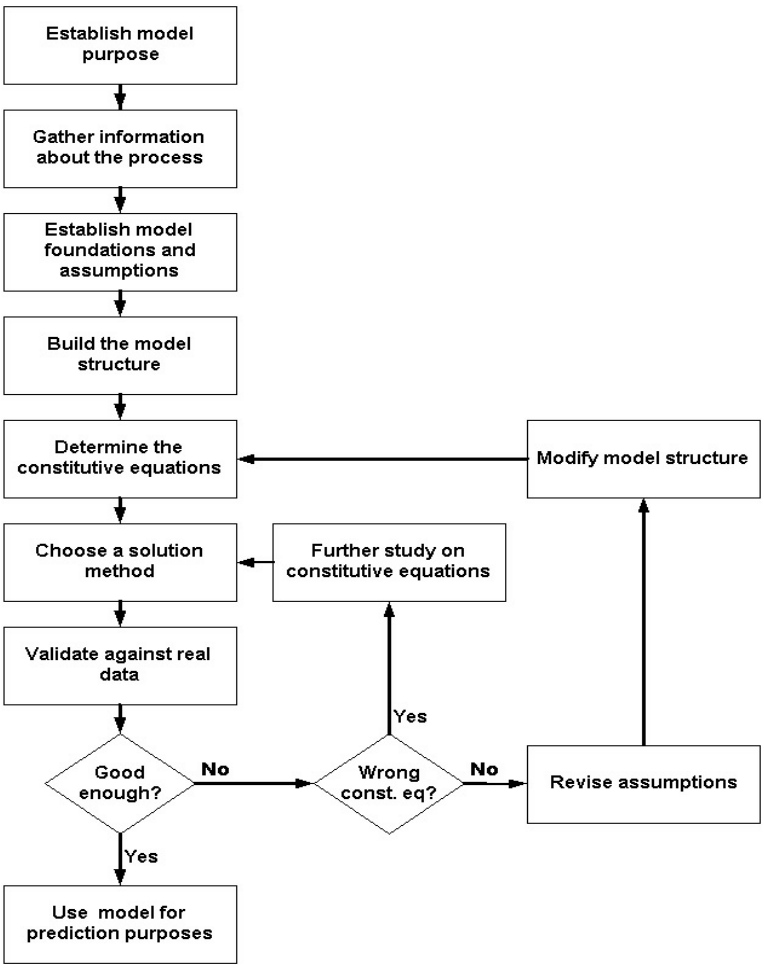

Figure 3.1: A systematic way to develop mechanistic models of process systems.

particulate processes than with other types of unit operations. If the validation using real data turns out to give unsatisfactory results, it is worth to check first whether a change in the constitutive relations may correct the problem. If this is not the case, then the assumptions need to be revised and changes in the structure of the model may be needed.

3.2 Establishing the model foundations and assumptions

As stressed in the previous section, the crucial stages in model building are: gathering of information, and establishment of model foundations and assumptions. As much information as possible should be gathered on:

- the phenomena affecting the continuous phase and the disperse phase, such as chemical reaction, nucleation, agglomeration, breakage, etc., as well as the factors affecting these phenomena,
- the flow regimes in the system, and the interaction between the continuous and disperse phases,
- the equipment design and operation, if an existing unit is to be modelled.

As regards model foundations and assumptions, some guidelines are given in the subsections below.

3.2.1 Define the coordinates and variables of interest

The coordinate system should be defined first. In the particulate processing field it is typical to distinguish between *external* and *internal* coordinates.

External coordinates are used to denote position (x, y, z) and time (t). The external coordinates are thus defined for both the continuous phase and the dispersed phase. If the properties of the system experience dynamic changes with time, then a dynamic model accounting for the time coordinate t may be used. In contrast, if the properties of the system remains constant with time, a steady-state model may be used. If the properties of interest of the continuous phase and/or the dispersed phase vary according to the position in the system, then a model distributed in the external coordinates should be used. Such models are called *microscopic or distributed*. In contrast, when space distribution can be neglected, *macroscopic* models can be used.

Internal coordinates (ζ) are defined for the dispersed phase only. They refer to the properties of the entities in the population that can be given values for each

individual entity, thus characterizing the entities. For example, when referring to a population of crystals, some possible internal coordinates would be: crystal size, crystal shape, and crystal composition. Or when referring to a population of cells, some possible internal coordinates would be: cell age, cell size. Note that the more internal coordinates we use, the more complex the model would be. Moreover, the internal coordinates to be used involve additional simplifications. If entity size is to be defined with a unique coordinate, a regular spherical shape may be assumed.

As regards the variables of interest, it is convenient to distinguish between *extensive* and *intensive* variables. *Extensive* variables are proportional to the size of the system. Some examples are: mass, component mass, energy and momentum. In contrast, *intensive* variables are those whose value is independent of the size of the system. Some examples are: concentration, temperature and pressure.

For the dispersed phase, a density distribution function $f(\zeta)$ in terms of the internal coordinates ζ should be defined. Physically,

$$\int_{\zeta_{\text{low}}}^{\zeta_{\text{up}}} f(\zeta) d\zeta \tag{3.1}$$

is the fraction of entities in the population that lie in the property interval $\left[\zeta_{\text{low}}, \zeta_{\text{up}}\right]$. Hence, depending on how the fraction of entities is defined, different density distribution functions may be defined for the same population of entities. The *fraction of entities* can be defined in terms of the number of entities, the length of entities, the area of entities or the volume of entities. The PBE was originally defined in terms of the number of entities (Hulburt & Katz 1964) and (Randolph 1964), and it remains the most used definition in literature. However, note that in many applications other definitions may be more suitable.

3.2.2 Define the number of compartments

In many industrial particulate systems it is possible to identify regions where there is a marked change in properties from one region to the next. Such changes typically arise due to the interaction between the continuous and dispersed phase, and due to hydrodynamic considerations. In particular, when the entities in the population show a wide range of sizes, and the difference in densities between the continuous and dispersed phase is relatively large, segregation is likely to occur. Hence, the fine entities may be concentrated in one region of the reactor, while the coarser entities may be concentrated in another region. More importantly, very different physical events may also be localized in different regions. For example, breakage may only happen in the region where coarse entities are encountered, or agglomeration and growth may be predominant in the region with the fine entities.

It is important to account for these physically differentiated regions. The number of compartments to be used in the model is thus defined by the number of regions that are physically identifiable in the system. Note that for establishing the number of compartments, information about the unit design and operation is required. Note also that in the literature some references to compartmental modeling are found (Ma, Braatz & Taffi 2002), but with a different meaning. There, the unit is divided into a finite but large number of compartments without much physical significance. The division in compartments is done in order to solve a spatially distributed model, i.e. is just an approximate way to solve the equations. The approach used in literature assumes, in most cases, fixed volume of the compartments, whereas in the approach suggested here the volume of compartments is allowed to vary.

3.3 Building the model structure

Once the model foundations and assumptions are established, the model structure may be built by applying the corresponding balance laws and PBE to each compartment. Now, depending on whether spatial distribution is ignored or considered, the model to be constructed will be *macroscopic* or *microscopic*, respectively. These two types of models are discussed separately.

3.3.1 Macroscopic balance laws and macroscopic PBE

A *macroscopic* model is used when the spatial distribution of the properties of interest may be ignored. Macroscopic models may be obtained by two different ways: by integrating the microscopic balances over the entire volume of the system, or by writing the balance laws directly for the macroscopic region of interest[1] (Bird et al. 2002). The latter approach is typically the easiest. A balance law is given by the following equality:

$$\text{Accumulation} = \text{Inflow} - \text{Outflow} + \text{Generation} - \text{Disappearance}, \tag{3.2}$$

i.e. the rate of accumulation of a certain extensive property of the system is equal to the rate of property added to the system by convective flow, minus the rate of the property extracted from the system by convective flow, plus the rate of generation of the property within the system, minus the rate of disappearance of the property within the system. A pictorial representation of the balance is given in Figure 3.2. For example, the total mass balance would be given by

[1] the whole system of interest or each of the compartments if the system has been divided in several compartments.

Figure 3.2: Application of a balance law.

Table 3.1: Balance laws of mass, energy and momentum

Total mass balance	$\frac{dM}{dt} = \dot{M}_{\text{in}} - \dot{M}_{\text{out}}$
Component mass balance	$\frac{dW_i}{dt} = \dot{W}_{i,\text{in}} - \dot{W}_{i,\text{out}} + r_i V$
Energy	$\frac{dE}{dt} = \dot{E}_{\text{in}} - \dot{E}_{\text{out}} + \dot{W} + \dot{Q}$
Momentum	$\frac{d\pi}{dt} = \dot{\pi}_{i,\text{in}} - \dot{\pi}_{i,\text{out}} + \sum F_j$

$$\frac{dM}{dt} = \dot{M}_{\text{in}} - \dot{M}_{\text{out}}, \tag{3.3}$$

where M is the total mass within the system/compartment, $\dot{M}_{\text{in}}$ is the mass flowrate entering the system by the inflow, and $\dot{M}_{\text{out}}$ is the mass flowrate leaving the system with the outflow.

Table 3.1 summarizes the traditional balance laws of mass, energy and momentum, whose derivation can be found in excellent references such as (Bird et al. 2002).

Note that the balance laws are formulated in terms of extensive variables. These models may be reformulated in terms of intensive variables, but this requires simplifications such as for example constant volume.

In the original work by (Hulburt & Katz 1964) and (Randolph 1964), the macroscopic PBE was derived by integration of the microscopic PBE over the entire volume of the system, yielding the following balance

$$\underbrace{\frac{1}{V}\frac{\partial\left(V\psi\right)}{\partial t}}_{\text{Accumulation}} = \underbrace{\sum_j \frac{q_j\psi_j}{V}}_{\text{Inflow}-\text{Outflow}} + \underbrace{B - D - \sum_{i=1}^{m}\frac{\partial\left(v_i\psi\right)}{\partial\zeta_i}}_{\text{Generation}-\text{Disappearance}}, \tag{3.4}$$

where

$\psi\left(t,\zeta_1,\zeta_2,\ldots,\zeta_m\right)$ is the multidimensional population density distribution with internal coordinates $\zeta_1,\zeta_2,\ldots,\zeta_m$. Note that this density distribution is defined in terms of an intensive variable: the number of entities *per unit*

volume, i.e. a number concentration. Hence,

$$\int_{\zeta_{i,\text{low}}}^{\zeta_{i,\text{up}}} \cdots \int \psi d\zeta_1 d\zeta_2 \ldots d\zeta_m \tag{3.5}$$

represents the number of entities *per unit volume* with property values in the ranges $\left[\zeta_{i,\text{low}}, \zeta_{i,\text{up}}\right]$ for $i = 1, ..., m$.

$\psi_j\left(t, \zeta_1, \zeta_2, \ldots, \zeta_m\right)$ is the multidimensional population density distribution, given in number of entities per unit volume, corresponding to the jth influent/effluent.

V is the volume of the macroscopic region of interest, that contains the continuous and the dispersed phase.

B and D are the *birth* and *death* functions, respectively, and were defined as follows

$$B = \frac{\text{(birth of entities)}}{\left(\begin{array}{c}\text{unit}\\ \text{time}\end{array}\right)\left(\begin{array}{c}\text{unit}\\ \text{volume}\end{array}\right)\left(\begin{array}{c}\text{unit}\\ \text{property}\end{array}\right)} \tag{3.6}$$

$$D = \frac{\text{(death of entities)}}{\left(\begin{array}{c}\text{unit}\\ \text{time}\end{array}\right)\left(\begin{array}{c}\text{unit}\\ \text{volume}\end{array}\right)\left(\begin{array}{c}\text{unit}\\ \text{property}\end{array}\right)}. \tag{3.7}$$

The *birth* and *death* functions are very general and can thus be used to model a broad class of phenomena affecting particulate processes. In particular, these terms are useful to model discrete phenomena such as nucleation or breakage.

$\sum_{i=1}^{m} \frac{\partial(v_i \psi)}{\partial \zeta_i}$ represents a continuous generation or disappearance of entities, where $v_i = d\zeta_i/dt$ is the time rate or change of property ζ_j. This term may be used to model growth or dissolution phenomena.

The macroscopic PBE is mostly used as defined by (Hulburt & Katz 1964) and (Randolph 1964), as shown in equation 3.4. However, using the number of entities as the way to express fractions of the population is not always the best choice. A mass-based distribution of the particle volume seems to be a better choice for comminution, sintering and granulation applications, as discussed in (Verkoeijen, Pouw, Meesters & Scarlett 2002). A mass-based distribution is also the best choice for the case investigated in the present work, as will be discussed in Chapter 4.

It has already been noted that macroscopic models may be formulated by integrating microscopic balances — this is the approach used in equation 3.4 — but

that is often simpler to work directly with macroscopic quantities. This means that it may be advantageous to work directly with a extensive population distribution function Ψ rather than the intensive population distribution function ψ in equation 3.4. Hence,

$$\int_{\zeta_{i,\text{low}}}^{\zeta_{i,\text{up}}} \cdots \int \Psi d\zeta_1 d\zeta_2 \ldots d\zeta_m \tag{3.8}$$

represents the fraction (number, mass, volume...) of entities in the macroscopic region of interest with property values in the ranges $\left[\zeta_{i,\text{low}}, \zeta_{i,\text{up}}\right]$. The macroscopic PBE can thus be rewritten as follows:

$$\frac{\partial \Psi}{\partial t} = \sum_j \dot{\Psi}_j + (B - D) V - \sum_{i=1}^{m} \frac{\partial (v_i \Psi)}{\partial \zeta_i}, \tag{3.9}$$

where

$$\int_{\zeta_{i,\text{low}}}^{\zeta_{i,\text{up}}} \cdots \int \dot{\Psi}_j d\zeta_1 d\zeta_2 \ldots d\zeta_m, \tag{3.10}$$

represents the fraction of entities per unit time with property values in the ranges $\left[\zeta_{i,\text{low}}, \zeta_{i,\text{up}}\right]$ entering or leaving the macroscopic region with the stream j.

3.3.2 Microscopic balance laws and microscopic PBE

A *microscopic* model is used when there exists a spatial distribution of the properties of interest, and when such a spatial distribution has important consequences for the operation of the process and/or the quality of the product. Microscopic models are generally more difficult to solve than macroscopic models.

A microscopic model can be obtained by writing the corresponding balance law over a volume element $\Delta x \Delta y \Delta z$, fixed in space, through which a continuous phase and the dispersed phase are flowing. Then, both sizes of the equation are divided by the volume element. Then, by taking the limit as Δx, Δy and Δz approach zero, a partial differential equation is obtained.

For example, if the mass balance law is applied to the volume element in Figure 3.3, the following balance is obtained

$$\begin{aligned} \Delta x \Delta y \Delta z \frac{\partial (\rho)}{\partial t} &= \Delta y \Delta z \left[(\rho v_x)|_x - (\rho v_x)|_{x+\Delta x} \right] \\ &\quad + \Delta x \Delta z \left[(\rho v_y)|_y - (\rho v_y)|_{y+\Delta y} \right] \\ &\quad + \Delta x \Delta y \left[(\rho v_z)|_z - (\rho v_z)|_{z+\Delta z} \right], \end{aligned} \tag{3.11}$$

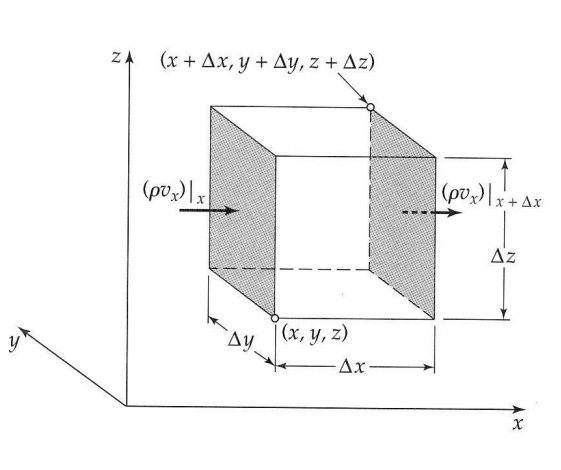

Figure 3.3: Volume element for the application of a microscopic conservation law. Taken from (Bird et al. 2002)

Table 3.2: Microscopic balance laws of mass, energy and momentum

Continuity Equation (total mass)	$\frac{\partial \rho}{\partial t} = -\left(\nabla \cdot \rho \mathbf{v}\right)$
Component mass balance	$\rho \frac{D\boldsymbol{\omega}_\alpha}{Dt} = -\nabla \cdot \mathbf{j}_\alpha + r_\alpha$
Energy	$\rho C_p \frac{D\boldsymbol{T}}{Dt} = -\left(\nabla \cdot \mathbf{q}\right) - \left(\boldsymbol{\tau} : \nabla \mathbf{v}\right)$
Momentum	$\rho \frac{D\mathbf{v}}{Dt} = -\nabla p - \left(\nabla \cdot \boldsymbol{\tau}\right)$

where ρ is the density of the volume element, v_x, v_y and v_z are the fluid velocities in the x, y and z directions, respectively. By dividing equation 3.11 by $\Delta x \Delta y \Delta z$ and taking the limit as Δx, Δy and Δz approach zero, and using the definitions of the partial derivatives, we get

$$\frac{\partial \rho}{\partial t} = -\left(\frac{\partial}{\partial x}\rho v_x + \frac{\partial}{\partial x}\rho v_y + \frac{\partial}{\partial x}\rho v_z\right), \tag{3.12}$$

that can be written in a more concise way by using vector notation:

$$\frac{\partial \rho}{\partial t} = -\left(\nabla \cdot \rho \mathbf{v}\right). \tag{3.13}$$

Table 3.1 summarizes the traditional microscopic balance laws of mass, energy and momentum, whose derivation can be found in excellent references such as (Bird et al. 2002).

The microscopic PBE was derived in an analogous way, yielding the following balance

$$\frac{\partial \psi}{\partial t} = -\left(\nabla \cdot \mathbf{v}\psi\right) - \sum_{i=1}^{m} \frac{\partial \left(v_i \psi\right)}{\partial \zeta_i} + B - D. \tag{3.14}$$

Note that the microscopic PBE is written in terms of ψ (*intensive* density distribution function) and not in terms of Ψ (*extensive* density distribution function). But this is in accordance with the microscopic balances of mass, energy and momentum, which are also written in terms of intensive variables (density, component mass concentration, temperature and velocity).

3.4 Defining the constitutive relations

Once the structure of the model is defined, the next step is to find mathematical expressions for the *constitutive relations*. The constitutive relations provide the specific information on the phenomena taking place within the system.

> When we make a balance to obtain a differential equation, we are invoking a *natural law.* [...] In expressing the elements of the balance in terms of dependent variables, we use certain properties of the materials involved. These are sometimes called *constitutive relations* because they invoke the constitutions of the various components. They are not principles applying to everything, as are natural laws, but apply only to the materials in question. (Aris 1999*b*)

Hence, the constitutive relations "particularize" the model, i.e. the model is transformed from a general model that may represent a variety of systems to a model that is specific for the system under study. The internal coupling between the balances is typically provided by the constitutive relations. Moreover, the nonlinear behavior of particulate processes is typically related to the constitutive relations.

For the continuous phase, the constitutive relations describe:

- the transport flows, e.g. flow by gravity, pumped flow, etc.
- the chemical reaction terms, e.g. reaction rates, reaction enthalpy, etc.
- the dissipative terms, e.g. friction terms, heat loss, etc.

For the dispersed phase, the constitutive relations describe:

- the transport flows.
- the birth and death terms, e.g. nucleation rates, breakage rates, agglomeration rates, etc.
- multiple phase interactions, e.g. bed packing, critical sizes, etc.

Table 3.3: Some references on phenomenological research of particulate processes.

Application	**Phenomena**	**References**
Crystallization	Birth { Primary Nucleation, Secondary Nucleation } Growth { Surface Integration }	Randolph et al.(1988) Tavare (1995) Mersmann et al.(2002) Mohan et al.(2002)
Granulation	Birth { Drop controlled nuclea., Mechanical dispersion, Intermediate regime } Growth { Induction Growth, Steady Growth, Rapid Growth }	Pietsch (2001) Wauters (2001) Litster (2003)
Bioreactors	Birth { Cell birth } Growth { Cell Growth } Death { Budding }	Ramkrishna (2000)

For the determination of constitutive relations corresponding to the continuous phase, advantage can be taken of the extensive research available on the phenomenological laws of transport phenomena (Bird et al. 2002), and on reaction engineering (Aris 1999*a*), (Levenspiel 1972), (Fogler 1992), (Froment & Bischoff 1990).

As regards the dispersed phase the emphasis is placed on establishing the mechanisms and phenomenological laws for the events affecting the entities of the population. However, the development of such theories has not yet come as far as in the case of continuous media. The great variety and diversity of particulate processes makes the establishment of such general phenomenological laws difficult. However, the modeler may take advantage of the existing results within each subfield of particulate processes. Table 3.3 gives some references on such phenomenological research. In many cases, tailor-made experimental studies may be necessary to find expressions for the constitutive relations. A possible approach is the following:

1. Isolate each of the phenomena affecting the particulate process. For example, in a crystallization problem, it would be necessary to study nucleation and growth separately.

2. Design a series of batch experiments to identify the factors that influence the phenomena under study.

3. Based on the factors that have the strongest influence, design a new series of batch experiments in order to find the desired rates.

4. Fit the results from batch experiments to appropriate mathematical expressions.

Such an approach is similar to the kinetic studies that are carried out in reaction engineering to determine reaction rates (Aris 1999*a*) (Levenspiel 1999).

Another approach that is being used in particulate processing is the so-called *inverse problem* approach (Ramkrishna 2000). It consists in extracting the behavior of single particles from measurements made on the population. The approach relies on the exploitation of self-similar behavior. For further details, see (Ramkrishna 2000) and (Mahoney, Doyle III & Ramkrishna 2002).

3.5 Solution methods

Once the model is built, the next stage is to find a solution method for the model. The application of the macroscopic PBE together with the balance laws of mass, energy and momentum results in a system of *integrodifferential* equations, whereas the application of the microscopic PBE leads to a system of *partial integrodifferential* equations. The integrodifferential term, i.e. an integral function of the density distribution function, usually appears in the birth term. Such systems are difficult to solve mathematically.

Extensive research has been focused on developing methods to solve PBE models. For a quite complete review of solution methods, see (Ramkrishna 2000).

The main idea behind a good deal of the analytical and numerical methods that are available to solve PBE models, is to transform the *integrodifferential equations* into a system of ordinary equations (ODE) or into a system of differential and algebraic equations (DAE), that may, in turn, be solved by well-known standard algorithms. As for a system of *partial integrodifferential* equations, the system may be transformed into a system of partial differential equations (PDE) or into a system of partial differential and algebraic equations (PDAE).

A method that has been extensively used in the past is the *method of moments*, which was already suggested in (Hulburt & Katz 1964). Note that this method is widely used in statistics. The jth moment of a given density distribution $\Psi(t, \zeta)$ with internal coordinate ζ is defined as:

$$m_j = \int \zeta^j \, \Psi(t, \zeta) \, d\zeta, \tag{3.15}$$

where integration extends for all possible values of ζ. In certain cases, if the moment definition in equation 3.15 is applied to the PBE model for a certain number of indexes $j = 0, 1, 2, \ldots, n$, a closed and finite set of ODE is obtained. However, in other cases where the constitutive relations are relatively complex,

the moment transformation would lead to a set of ODE that is not closed. Some applications of the method of moments are discussed in e.g. (Randolph 1964), (Randolph & Larson 1988), and (Diemer & Olson 2002).

A more general method is the method of *weighted residuals*, which consists in expanding the population density distribution $\Psi(t,\zeta)$ in terms of a finite number of basis functions $\phi_k(\zeta)$:

$$\hat{\Psi}(t,\zeta) = \sum_{k=1}^{N} g(t)\,\phi_k(\zeta), \tag{3.16}$$

where $g(t)$ are time-varying coefficients. Since equation 3.16 is an approximation of $\Psi(t,\zeta)$, the right hand side and the left hand side of the PBE in equation 3.9 do not match, and a residual function can be calculated as follows

$$R(t,\zeta) = \left.\frac{\partial \Psi}{\partial t}\right|_{\Psi=\hat{\Psi}} - \left|\sum_{j}\dot{\Psi}_j + (B-D)V - \sum_{i=1}^{m}\frac{\partial(v_i\Psi)}{\partial\zeta_i}\right|_{\Psi=\hat{\Psi}}. \tag{3.17}$$

Finally, the residual is forced to be orthogonal to a complete set of weighting functions $\varphi(t)$, i.e. the inner product of the residual with the set of weighting functions is set equal to zero

$$\int R(t,\zeta)^T\,\varphi(t)\,dt = 0. \tag{3.18}$$

The selection of basis functions and weighting functions determines the type of method of weighted residuals. Hence, the method of moments is obtained when Laguerre polynomials are chosen as basis functions and $\varphi_j = \zeta^j$ as the weighting functions. Some examples about the use of the method of weighted residuals in particulate processes can be found in (Ramkrishna 1971), (Ramkrishna 1973), (Bathia & Chakraborty 1992), (Christofides 2002).

As regards numerical methods, those based on coordinate discretization of the continuous PBE are reported to be the most attractive from the computational point of view (Kumar & Ramkrishna 1996*a*). Discretization techniques aim at the formulation of PBE in discrete internal coordinate space. This is done by integrating the continuous PBE over a discrete size interval, say ζ_i to ζ_{i+1}

$$\int_{\zeta_i}^{\zeta_{i+1}}\frac{\partial\Psi(t,y)}{\partial t}dy = \int_{\zeta_i}^{\zeta_{i+1}}\left|\sum_{j}\dot{\Psi}_j + (B-D)V - \sum_{i=1}^{m}\frac{\partial(v_i\Psi)}{\partial\zeta_i}\right|dy, \tag{3.19}$$

where the discrete population density distribution $\phi_i(t)$ is given by

$$\phi_i(t) = \int_{\zeta_i}^{\zeta_{i+1}}\Psi(t,y)\,dy, \tag{3.20}$$

and the number of intervals used to represent the total population of particles is N, i.e. $i = 1, 2, ...N$. The main disadvantage of coordinate discretization methods is that the discretized model may in some cases not be consistent with the number and mass balance laws, or any other integral property of interest associated to the entire population. Often, the accuracy of the solutions is improved by using finer discretization grids, but this is incurring very high computational costs. Some references on discretization methods are (Gelbardt & Seinfeld 1978), (Litster, Smit & Hounslow 1995), (Kumar & Ramkrishna 1996a), (Kumar & Ramkrishna 1996b), (Ramkrishna 2000).

Monte Carlo methods, which are based on artificial realization of the system behavior by simulation and by averaging all of the sample paths, have also been used (Ramkrishna 2000).

3.6 Model validation

Once a solution model is chosen for the PBE model, and the model is implemented in a programming environment, everything is ready for the model to be used for simulation purposes. However, the results given by the model should not be trusted until the model is validated, not only in a qualitative but also in a quantitative way by comparing it with data measured on the real system.

Mechanistic models are never perfect since they are based on idealizations and simplifications of the real system. There may be phenomena or interactions that are not accounted for in the model. Often some of the parameters of the model are taken from the literature and/or estimated from qualitative information. Therefore, a quantitative comparison of the simulation results with real data is important, and may indicate whether further parameter estimation is needed or not, or whether some of the assumptions in the model should be reconsidered or not. Moreover, validation of models should be carried out at two levels:

- the dynamic level, i.e. check that the model is able to properly predict the transient behavior of the system.
- the static level, i.e. check that the model correctly predicts the steady-state conditions.

There are thousands of references on PBE modeling. In a recent forum on particle technology[2], 80% of the attendants claimed to have used or be using population balances in their research. Surprisingly, there is still little material published on validation of PBE models. Moreover, of the published papers on this

[2]The 5th UK Particle Technology Forum (Sheffield, UK, July 2003)

issue, the vast majority validate models using experimental data from laboratory scale units (Matthews, Miller & Rawlings 1996), (Alopaeus, Koskinen, Keskinen & Majander 2002), (Immanuel, Cordeiro, Sundaram, Meadows, Crowley & Doyle III 2002), (Gerstlauer, Motz, Mitrovic & Gilles 2002) and (Zeaiter, Romagnoli, Barton, Gomes, Hawkett & Gilbert 2002), but not experimental data from industrial units. Very often the validation is limited to graphical comparison of the simulation results with the experimental data, and the results are just used to qualitatively judge whether the assumptions in the constitutive relations seem correct or not. In some cases, parametric sensitivity of the model is studied. Therefore, validation and parameter estimation of PBE models is an area that should (and probably will) be paid more attention in the future research. The challenges are not trivial:

- Gathering good experimental data is still difficult, particularly as regards the population density distributions. Even measuring the initial state of the system may be problematic.
- Computational issues are important. PBE models are large and nonlinear. Therefore, if nonlinear optimization is used for parameter fitting, the problem may be computationally demanding. In addition, global optimality is difficult, if not impossible, to prove for these types of nonlinear optimization problems.
- The models may have a large number of parameters, as compared to the number of available measurements, which makes the parameters non-identifiable or poorly-identifiable.

Fortunately, parameter identifiability and parameter estimation in mechanistic models has been widely studied in other areas of engineering (Walter & Pronzato 1997). The systematic approach described in (Brun, Reichert & Künsch 2001) seems well suited to particulate processes. This method is suited for large simulation models, and provides identifiability diagnosis for parameter subsets. Figure 3.4 summarizes the main stages of the approach. As indicated in the Figure 3.4, the stages are grouped into three categories: stages related to the experimental campaign, stages related to identifiability analysis, and stages related to estimation. Note also that some stages have been highlighted by a grey background in the boxes. These stages are not automatized, they require direct analysis from the modeler. The remaining stages may be implemented such that they are carried out in the computer. Let us take a closer look at each of the stages:

1. Experiment design. It consists in establishing the experiments that should be carried out to obtain data for parameter estimation and model validation.

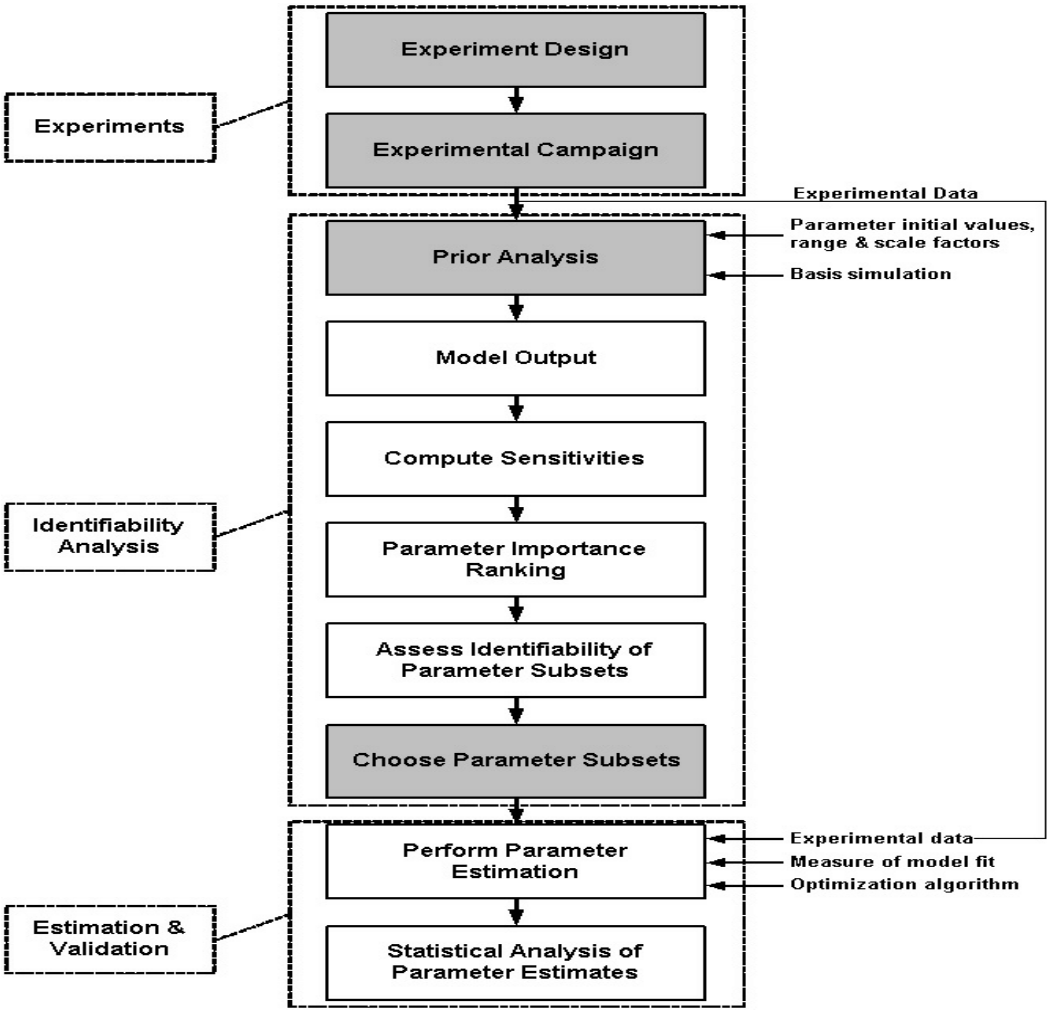

Figure 3.4: Systematic approach to parameter identifiability and estimation.

The feasible measurements, the region of operating conditions to be considered, the measurement location, and the sampling interval, among other factors, should be decided. Moreover, the experiment designer should make sure that the excitation carried out to the process allows to validate both the steady-state behavior and the dynamic behavior of the model.

2. Experimental campaign.

3. Prior analysis. Once the data are obtained, they should be analyzed to check their quality. If poor quality data are used in the parameter estimation, the resulting parameter estimates will be even poorer. The experimental data have to be treated to adapt them to the parameter estimation, and outliers should be detected and eliminated. In addition, the basis simulation to compare the model results with the real data should be established. The inputs and the initial values for the simulation have to be specified. Then, the parameters θ of the model should be listed, as well as their initial values θ_0 and range of values $\Delta\theta$. Since the parameters and/or outputs of the model may have different orders of magnitude, proper scaling factors should be found.

4. Model output. This stage involves the generation of simulated data by using the model. Such a simulation should resemble the operation of the system during the data gathering campaign.

5. Compute sensitivities. The sensitivity s_{ij} is a measure of the change in the ith model output y_i caused by a change in the jth parameter value θ_j. Again, for the sake of comparison, scaled sensitivities should be used. For large complex models that are solved numerically, the easiest way to calculate sensitivities is by a finite difference approximation:

$$s_{ij} = \mathrm{sc}_{ij} \frac{y_i(\theta_j) - y_i(\theta_{j,0})}{\theta_j - \theta_{j,0}}. \tag{3.21}$$

where sc_{ij} are proper scaling factors. The sensitivity matrix S can be then constructed from the s_{ij} values.

6. Parameter importance ranking. The norm of each column of the sensitivity matrix is a quantitative measure of the importance of each individual parameter. A large norm $\|s_j\|$ means that a change in the jth parameter θ_j has an important effect on the model outputs, making it identifiable from the measured data. Now, there are different types of norm, so that the parameter importance ranking can be done in different ways. (Brun et al. 2001)

recommend the use of the following measure:

$$\delta_j^{\text{msqr}} = \sqrt{\frac{1}{n}\sum_{i=1}^{n} s_{ij}^2} \tag{3.22}$$

as ranking criterion.

7. Identifiability of parameter subsets. The parameter importance ranking gives an idea of the effect of each *individual* parameter on the outputs. However, the *joint* influence of the parameters needs to be studied too. Collinearity among parameters arise when the changes caused in an output by a change in one parameter, can be cancelled by a change in another parameter. Parameter collinearity thus results in ill-conditioning and poor identifiability. According to (Brun et al. 2001), such compensation effects can be looked for by checking the degree of near linear dependence among the columns subsets s_j of the scaled sensitivity matrix. The columns s_j of a matrix S are said to be linearly dependent if there exists a vector $\boldsymbol{\beta}$ such that $S\beta = 0$. Then, a measure of near collinearity is to look for the linear combination $S\beta$ that has minimal norm under the constraint $\|\beta\| = 1$. In (Brun et al. 2001) the collinearity index γ_K was defined as follows:

$$\gamma_K = \frac{1}{\min_{\|\beta\|=1} \left\| \tilde{S}_K \beta \right\| = 1} = \frac{1}{\sqrt{\lambda_K}}, \tag{3.23}$$

where $\tilde{S}_K$ is a $n \times k$ submatrix of $\tilde{S}$ containing those columns that correspond to the parameters of the subset K, $\tilde{S}$ is the re-scaled sensitivity matrix with columns

$$\tilde{s}_j = \frac{s_j}{\|s_j\|}, \tag{3.24}$$

and where λ_K is the smallest eigenvalue of $\tilde{S}_K^T \tilde{S}_K$. A high value of the collinearity index indicates that the parameter subset K is poorly identifiable even if the individual parameters that composes it are among the top parameters of the parameter importance ranking.

8. Based on the results of the parameter importance ranking and identifiability analysis, the most suitable subset(s) are chosen.

9. Parameter estimation. This is the first stage at which the measured data are directly used. A measure of model fit and an optimization algorithm should be selected. Table 3.4 summarizes some of the most common criteria used as measure of model fit. There are also many optimization algorithms

Table 3.4: Measures of model fit.

Least Squares	$\min \ J = \frac{1}{n} \sum_{i=1}^{n} \left(y\left(\hat{\theta}\right) - y_{\text{data}} \right)^T \left(y\left(\hat{\theta}\right) - y_{\text{data}} \right)$
Least Modulus	$\min \ J = \frac{1}{n} \sum_{i=1}^{n} \left\lvert \left(y\left(\hat{\theta}\right) - y_{\text{data}} \right) \right\rvert$
Maximum likelihood	$\max \ J = f_{\text{joint}}\left(y_{\text{data}}, \hat{\theta}\right)$

that may be used. Hence, if the least squares criterion is chosen as measure of model fit, several algorithms are available: the Gauss-Newton method, the Levenberg-Marquadt method, Quasi-Newton methods, etc. For details about algorithms, see (Nocedal & Wright 1999) or (Walter & Pronzato 1997).

10. Statistical analysis of parameter estimates. It is advisable to analyze the certainty of the estimates, and to evaluate whether the fitting is appropriate or not. There is a number of measures of statistical accuracy for parameters: standard errors, biases and confidence intervals. There are also different methods to estimate these measures of statistical accuracy: large-sample theory methods (Lehmann 1998), bootstrap methods (Efron & Tibshirani 1993), jackknifing, etc. It is also important to measure how well the model with the estimated parameters predicts the response values of future observations. Again, several methods are available: cross-validation, Cp statistics, Scwartz's criterion, etc.

Once the parameter estimates are obtained and their certainties are analyzed, a decision is made on whether the model is sufficiently realistic or if, on the contrary, the model needs to be revised.

3.7 Model uses

Once a PBE model is built and validated, it can be used for many different purposes. Some of the most common uses are:

- Simulation. The model is used to resemble the operation of the system, and to analyze how the system would response to changes in the inputs and/or operation of the system.

- Nonlinear analysis. Complex dynamic behavior, such as self-sustained oscillations, has been reported for industrial particulate process units, see for example (Randolph & Larson 1988). Bifurcation and stability analysis can

thus be carried out to map operation and/or parameter regions where different patterns of behavior may be encountered. Since PBE models are complex and nonlinear, such studies will typically require numerical analysis. (Pathath & Kienle 2002) gives an example of a crystallization application.

- Process control. There is extensive research on use of PBE models to design a control system. A review of different PBE model-based methods that have been suggested in the literature is given in section 5.2.

- Process optimization. The simulation results can be used to establish changes in the inputs and/or operation of the system that improves the process yield (Lestage, Pomerleau & Hodouin 2002) and (Zeaiter, Romagnoli, Barton & Gomes 2002).

- Operator training. PBE models can be used, combined with a proper graphical user interface, to train operators.

- Roll-out. A model corresponding to a given system can be easily changed to model another system for which the main foundations remain the same. The constitutive relations or the parameter values are the elements that have to be modified or identified for the new model. This is particularly attractive for companies having many similar processes, since the subsequent models are comparatively easy to develop once the first one is developed, see (Glemmestad, Ertler & Hillestad 2002) and (Hauge 2003).

3.8 Conclusions

This chapter discusses a systematic approach to mechanistic modeling of particulate processes. The approach consists of the following stages: establishment of model foundations, building of the model structure, determination of the constitutive relations, selection of a solution method and model validation. Such an approach is general to any type of process, but when dealing with particulate processes special care should be placed on some of these stages. Special emphasis was put on the establishment of model foundations. The widely-used assumption of complete-mixing turns out to be unrealistic in many instances, and should thus be avoided. A compartmentalization of the unit based on distinguishable regions in the unit is suggested. A macroscopic balance is used for each compartment, and the connections among compartments should be defined based on the physics and hydrodynamics of the process.

Once the model is built, the model has to be "particularized" by defining the constitutive relations. The determination of constitutive relations corresponding

to the continuous phase is fairly straightforward, since extensive research results are available on the phenomenological laws of transport phenomena and on reaction engineering. As regards the dispersed phase, general phenomenological laws for the events affecting the entities of the population have not yet been established. However, the modeler may take advantage of the existing results within each subfield of particulate processes, or tailor-made studies can be carried out.

The mathematical solution of PBE models is typically more challenging than the solution of other types of process models, mainly due to the fact that the PBE is a balance on a property distribution function. Hence, a macroscopic PBE typically results in a system of integrodifferential equations, whereas a microscopic PBE model typically results in a system of functional partial integrodifferential equations. Fortunately, extensive research results are available on this topic. In contrast, the area of parameter estimation and model validation of PBE models has not been studied to such a large extent yet. The main challenges encountered are:

- Gathering good experimental data is still difficult, particularly as regards the population density distributions.
- Computational issues are important. PBE models are large and nonlinear. Of particular importance is the fact that some parameters may be collinear for the given measurements, which results in ill-conditioning of the optimization problem, and poor parameter identifiability.

The use of a systematic parameter identifiability analysis prior to parameter estimation was discussed in this chapter. Such an analysis provides a subset of parameters with two important properties: the measurements are highly sensitive to the selected parameters, and the selected parameters are not collinear with each other. In other words, the analysis provides the selection of parameters that can be identified from the available data. Parameter estimation and validation of PBE models will probably attract the attention of the research community in the coming years.

Chapter 4

Modeling of the *Silgrain*® Process

4.1 Introduction

The systematic approach to modeling of particulate processes that was presented in chapter 3 is applied in this chapter to an industrial leaching process for production of Silicon (Si) from Ferrosilicon (FeSi) . The process, called the *Silgrain*® process, is patented and is owned by the Norwegian company Elkem ASA.

Si is an important industrial material. Si is widely used in metallurgical applications, both as a constituent of various alloys and as an oxidizer in steelmaking . It is also a basic material for the chemical industry:

> Silicon shows a rich variety of chemical properties and it lies at the heart of much modern technology. Indeed, it ranges from such bulk commodities as concrete, clays, and ceramics, through more chemically modified systems such as soluble silicates, glasses, and glazes, to the recent industries based on silicone polymers and solid state electronics devices. (Greenwood & Earnshaw 1997)

Si is the basis of modern electronics, due to its properties as a semiconductor. More than 90% of all electronic components are based on Si. One of the most recent applications of Si is as a feedstock for the multi-crystalline photovoltaic industry, i.e. for solar cell production. Indeed, the use of Si in the solar industry has rocketed in the last decade, and is expected to continue growing (Sarti & Einhaus 2002). Elkem ASA supplies *Silgrain*® Si metal products to companies that produce polysilicones (polycrystalline silicone), which are used in the manufacture of semi-conductors such a microchips for computers, plates for solar panels, and so-called optoelectronic components for communication systems. Nearly 80% of the silicon metal used by the Japanese IT industry is delivered by Elkem ASA,

and it is estimated that half of all the PC's in the world contain Si metal from Elkem ASA[1].

The *Silgrain®* process is based on hydrometallurgical leaching. Leaching is the extraction of a soluble constituent from a solid by means of a solvent (Richardson & Harker 2002). Leaching processes thus belong to the field of particulate processes; leaching is encountered in a wide range of applications such as metal extraction, wastewater treatment and food industry. In some applications it is the liquid phase with the extracted compounds that constitute the product of interest, whereas in other applications it is the purified solid phase that constitutes the product. In general, some of the factors influencing the rate of extraction in a leaching process are: the particle size, the solvent composition, the temperature, and the agitation of the solid phase (Richardson & Harker 2002). In the *Silgrain®* process, the metallic impurities present in the FeSi solid phase, mainly iron Fe, aluminum Al, and calcium Ca, are dissolved in a hot acidic solution. A feature that distinguishes the *Silgrain®* process from other leaching processes is the rapid disintegration of FeSi into small grains during the reaction. The product thus consists of highgrade Si metal grains, and this is why the product was trademarked *Silgrain®* .

Several references on mechanistic modeling of leaching reactors can be found in the literature. These mathematical models can be divided into two categories:

1. General heterogeneous models, such as *fixed-bed reactor models* or *fluidized-bed reactor models*. They are developed for catalytic heterogeneous reactions, but have also been applied to non-catalytic heterogeneous reactors (Froment & Bischoff 1990), (Kunii & Levenspiel 1991), (Levenspiel 1972). The general heterogeneous models do not account directly for the changes occurring in the solid phase, but they focus mainly on the changes occurring in the fluid phase.

2. Models accounting for the special nature of particulate material, the most-used approaches being: the *segregated flow model*, the *multiple convolution integral* and the *PBE approach*. The *segregated flow model* (Dixon 1995), (Dixon 1996) assumes that each particle in a steady-state flow leaching reactor behaves as a tiny batch reactor. Hence, a probability integral is solved for the expected value of the fraction of solids unreacted with respect to mass-weighted distributions of residence time and particle size. The main drawback of this model is the assumption that the system operates at steady-state. The *multiple convolution integral* model, developed by Dixon (Dixon 1995), (Dixon 1996), is an extension of the segregated model to multistage leaching reactors, but it has also the drawback that it can only be applied to

[1] as reported in http://www.elkem.no/

steady-state reactors. The first references on the application of the *PBE approach* to hydrometallurgical leaching assumed steady-state conditions are (Herbst 1979), (Crundwell & Bryson 1992) and (Herbst & Asihene 1993). The transient behavior of hydrometallurgical leaching reactors was first reported in (Rubisov & Papangelakis 1995), (Rubisov & Papangelakis 1996*a*) (Rubisov & Papangelakis 1996*b*). No references[2] to PBE modeling of leaching processes where particle disintegration takes place are reported in the literature.

Some incentives for developing a dynamic model of the *Silgrain*® process are:

- Customer requirements become tighter with time, making it necessary to achieve better control over the system. A mechanistic model could be used as basis for process control and quality control.
- Increased productivity of the process is desired, and the main way to achieve this is by enhancing the disintegration of particles. A model that captures the essence of the disintegration mechanism can be used for the purpose of process optimization.
- Experimentation on the physical process is difficult and expensive. It would be much easier and cheaper to do a simulation analyses of the model.

From the academic point of view modeling the *Silgrain*® process presents interesting challenges. Firstly, phenomenological modeling of the disintegration process is challenging. Subsequently, testing whether compartmental PBE modeling provides a realistic model of the industrial plant or not is of great interest.

Before this project was initiated, mechanistic dynamic modeling of the *Silgrain*® process had not been attempted. Empirical modeling had previously been tested, but the results were not very satisfactory for the leaching part of the process. On the other hand, information was available on process design (Aas 1971), process operation[3], and phenomenological research of the process (Kolflaath 1960), (Andreassen 1995).

The present chapter describes the development of a mechanistic model of the *Silgrain*® process, following the systematic approach that was presented in chapter 3. Section 4.2 describes the process operation. The model foundations and assumptions are discussed in section 4.3. Subsequently, the model structure is established in section 4.4. The establishment of constitutive relations is then discussed in section 4.5. The numerical solution of the model is studied in section 4.6. Parameter estimation and model validation is presented in section 4.7. Finally, some possible uses of the model are listed in section 4.8.

[2]other than published work related to this PhD thesis.

[3]Elkem ASA has been running the process since the 1970*s*.

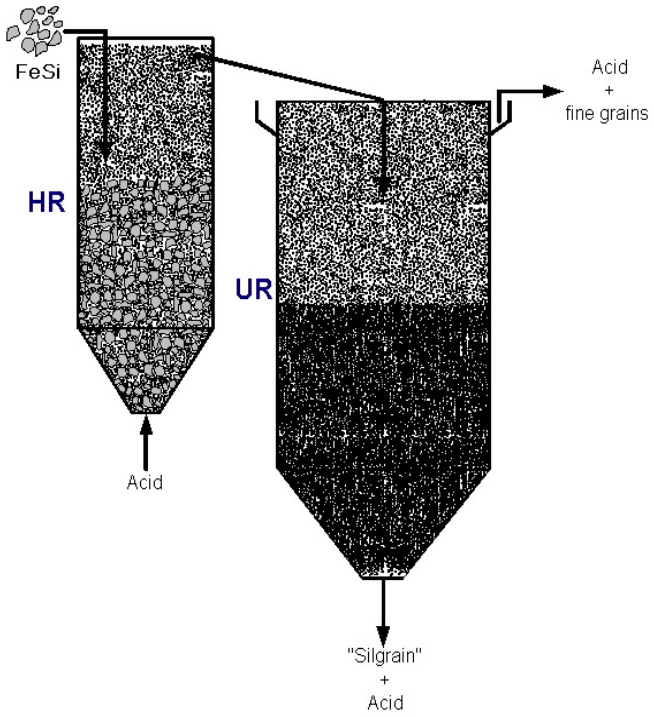

Figure 4.1: Simplified sketch of the two reactors in the *Silgrain*® process.

4.2 Description of the *Silgrain*® process

As mentioned in the previous section, the *Silgrain*® process is a hydrometallurgical leaching process where high-purity Si metal is produced by leaching lumps of $90-94\%$ FeSi in a hot acidic solution of ferric chloride ($FeCl_3$) and hydrochloric acid (HCl). The acid attacks the crystalline structure of the FeSi, selectively dissolving the intermetallic phases containing the impurities of Fe, Al and Ca, while leaving the Si unattacked. Leaching is assumed to proceed according to the following reduction-oxidation reactions (Aas 1971):

$$\mathrm{Me} + 2\,\mathrm{FeCl_3} \longrightarrow \mathrm{MeCl_2} + 2\,\mathrm{FeCl_2} \tag{4.1}$$

$$\mathrm{Me} + 2\,\mathrm{HCl} \longrightarrow \mathrm{MeCl_2} + \mathrm{H_2} \tag{4.2}$$

where Me represents a metallic impurity in the intermetallic phases, i.e. any of the species Fe, Al, and Ca .

A simplified sketch of the two reactors in the process is shown in Figure 4.1. FeSi lumps of relatively large size are fed in a semibatch mode at the top of the

main reactor (HR) and sink towards the bottom. A relatively large flow of hot acidic solution is fed in a continuous mode at the bottom of the HR . Contact between the FeSi lumps and the hot acidic solution results in the leaching of the metallic impurities and the subsequent disintegration of the lumps. The fine grains generated in the disintegration process are displaced upwards through particle buoyancy and hydrodynamic thrust from the acid flow. The lumps that are only partially disintegrated, are still large in size, and remain in the bottom of the HR until they are further disintegrated. The stream flowing from the HR to the second reactor (UR) consists of acid and the fine disintegrated material. The top of the UR is designed as a sedimentation chamber, where most of the Si grains sediment while most of the acid leaves the reactor by the overflow on the top. Only very fine grains are entrained in the overflow stream. The sedimented grains in the UR react with the remaining acid in the packed bed. This is believed to proceed through pure chemical dissolution, and not through further disintegration. Tapping of the *Silgrain®* product at the bottom of the UR is carried out in a semibatch mode. After tapping, the product is subjected to diverse operations such as: filtering, drying, weighting and packing. The overflow from UR is first circulated through a heating tank, and later on the composition of the acid is adjusted to the desired operational values before the acid is recirculated to the HR.

According to (Aas 1971), a successful production of *Silgrain®* depends on the following factors: chemical composition and intermetallic phase composition of FeSi, chemical composition of the leaching acid, leaching time, and temperature.

Further details about the *Silgrain®* process can be found in (Aas 1971) and (Andreassen 1995).

4.3 Model foundations and assumptions

A mechanistic model of the *Silgrain®* process should be dynamic and should be able to reproduce the main phenomena taking place in the process, as well as the responses of the system due to changes in the inputs or in the operation of the process.

4.3.1 Choice of coordinates and variables of interest

As described in section 4.2, the dispersed phase experiences important changes in the particle size due to particle disintegration. In turn, the particle size affects the rate at which disintegration takes place. It is thus natural to consider the particle size as the internal coordinate of interest to be used in the PBE approach. There are many ways to define particle size: volume diameter, surface diameter, drag diameter, sieve diameter, sauter diameter, ..., but here the most simple def-

inition of particle size is used: the particles are assumed to be spherical and the diameter of the sphere is used as particle size. Particles have a random distribution of shapes that it would be very difficult to measure in practice, and shape affects disintegration to a considerably lesser extent than particle size. Therefore the assumption of spherical particles is reasonable. Another factor affecting disintegration is the phase composition of the particles, i.e. the type and amount of intermetallic phases that are present in the material. The phase composition is then a distributed property of the particles. However, the quality of raw material FeSi is controlled, varying within a tight component region. This means that the variation of intermetallic phase composition may also vary within a restricted region. Hence, it is reasonable to neglect the distribution of phase composition and use average values instead, such that the model predicts how these average values evolve with time. The feedstock has a certain amount of inert material, called slug. The slug is not dissolved by the leaching acid and accumulates in the bottom of the HR. For simplicity, the inert content is assumed to be homogeneously distributed among the feedstock. The variables whose transient behavior is intended to be modeled are thus: the particle size distribution (PSD) of active FeSi and slug, the acid composition, the dispersed phase composition (Si, Fe, Al, Ca) and the energy of the system.

Finally, mass is chosen as basis for the PSD function since in the *Silgrain®* process PSD functions are typically measured by sieving and weighting. A number-based PSD function was initially used in the work, see references (Dueñas Díez & Lie 2000) and (Dueñas Díez, Ausland, Fjeld & Lie 2002), but this involved increased computation to adapt the input and output PSD functions to the correct basis. The choice of mass is convenient also from a numerical point of view: Note that there is a relatively small number of large particles and a huge number of small particles. This means that the ratio:

$$\frac{\max\left(\Psi_{\text{number}-\text{based}}\right)}{\min\left(\Psi_{\text{number}-\text{based}}\right)}$$

is a very large number, giving ill-conditioned problems. However, if mass fraction is used, the ratio

$$\frac{\max\left(\Psi_{\text{mass}-\text{based}}\right)}{\min\left(\Psi_{\text{mass}-\text{based}}\right)}$$

is several orders of magnitude smaller.

4.3.2 Choice of compartments

In order to choose the number of compartments, attention is paid to the design and operation of the *Silgrain®* process. Only the fine disintegrated particles can be

entrained with the upward fluid, and flow out from the HR . This means that if the HR was modelled as one unique compartment and it was assumed that the PSD flowing out from the HR equals the PSD within the reactor, then the model would clearly be providing wrong results. The model would indicate that all particles can appear in the effluent from the HR, no matter their size.

Two regions are clearly identifiable in the HR:

- *Disintegration* region (compartment I): the bottom part of the HR, where the feedstock is interacting with the leaching acid, resulting in disintegration. The disintegrated material that is fine enough to be entrained by the countercurrent acid flows out from this region, whereas the coarse material remains in this region until it is further disintegrated.

- *Storage* region (compartment II): the top part of the HR, where the fine material transported by the fluid remains for a short time before being further transported to the UR. Since the residence time is short, it can be assumed that no reaction is taking place.

As regards the UR, two clearly differentiated regions are also identified:

- *Sedimentation* region (compartment III): the top of the UR, where most of the acid is separated from the particles. The acid leaves the UR by the overflow on the top, whereas the particles sediment.

- *Dissolution* region (compartment IV): the bottom of the UR, where the particles have sedimented and formed a packed bed. The particles interact with the acid in the bed causing a further dissolution of the impurities. The product material is intermittently pumped out at the bottom of the UR, in a semibatch mode. Due to this type of operation, spatial gradients in the properties, such as composition and temperature, are expected within this region. Time-variant behavior of the profiles is also expected, due to the semibatch tapping. Hence, a microscopic model accounting for spatial variations is chosen for this region.

Figure 4.2 sketches the division in compartments for the *Silgrain*® process.Let us analyze now the flow among compartments, and some other assumptions related to each compartment.

- Compartment I (HR):

  - Hydrodynamic considerations can be used to relate the PSD of the dispersed phase leaving the reactor with that of the dispersed phase

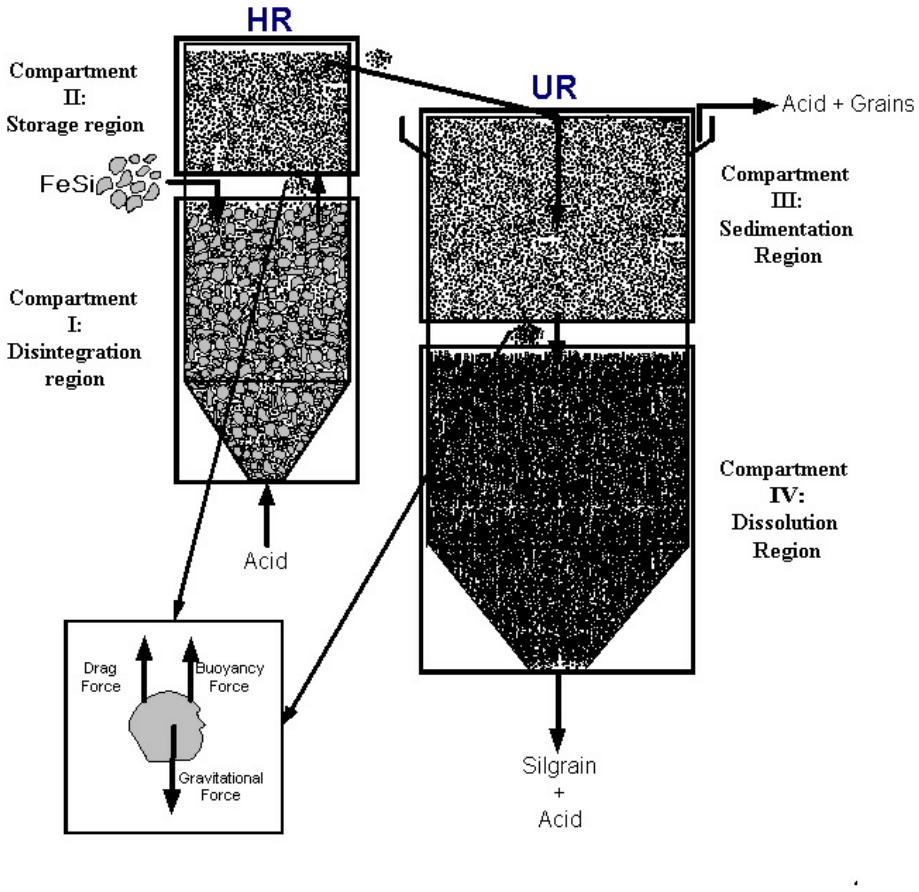

Figure 4.2: Compartmental modeling of the *Silgrain*® process.

within the reactor. Hence, a particle in compartment I is subjected to three forces: the gravitational force, the drag force, and the thrust force exerted by the upward flow. For a certain particle size, to which we will refer as *cut-size*, the free-falling velocity of the particle equals the velocity of the upward acid. Particles smaller than the *cut-size* are displaced by the upflow to the *storage* region, whereas particles larger than the *cut-size* remain in the *disintegration* region.

- The volume of the region is not constant, it may vary with time. This region contains a random packing of a population of particles with distributed sizes and shapes. Such a packing is impossible to predict, and impossible to measure in the current industrial implementation. However, it is not unreasonable to assume that the packing occurs in a pattern that is more or less constant. Therefore, a constant packed bed void fraction is assumed and used in the model.
- The FeSi feedstock contains a certain amount of inert material, which is assumed to be evenly distributed among the feedstock. This inert material does not disintegrate, hence it accumulates in compartment I. Once too much inert is accumulated in the reactor, tapping of inerts is carried out at the bottom of the reactor.
- A very high flowrate of acid is used, as compared to the amount of FeSi fed to the system. The high flowrate generates a great deal of turbulence within the reactor. Therefore, assuming homogeneous temperature within the HR (compartments I and II) is a good approximation. In other words, the completely mixed conditions can be assumed for the energy balance. Further assumptions with respect to the energy balance are the following:
  - The kinetic energy and the potential energy are negligible as compared to the internal energy.
  - The liquid and the solid phases are assumed to be incompressible.
  - Specific enthalpies are a function of temperature and composition (i.e. reaction enthalpies are accounted for).
  - The heat capacities of the liquid and solid phases are assumed to be constant. However, the bulk heat capacity is allowed to vary depending on the ratio of solid phase/liquid phase, as follows:

$$c_p = c_{p,\text{liquid}}\ \varepsilon + c_{p,\text{solid}}\,(1-\varepsilon) \tag{4.3}$$

    where ε is the void fraction of the packed bed.
  - The densities of the liquid phase and the solid phase are assumed to be constant. However, the bulk density is allowed to vary depending

on the ratio of solid phase/liquid phase, as follows:

$$\rho = \rho_{\text{liquid}}\varepsilon + \rho_{\text{solid}}\left(1-\varepsilon\right). \tag{4.4}$$

  - Disintegration is the main event taking place in this compartment, and has an important effect on the PSD .
  - Chemical composition changes occur both to the acid phase and to the solid phase.

- Compartment II (HR):
  - It is reasonable to assume completely mixed conditions in compartment II, so that the slurry flowing from this compartment to compartment III have the same properties (PSD, solid composition, acid composition) as the slurry within the region.
  - The slurry leaves compartment II by gravity flow. The corresponding flowrate can thus be calculated by applying Bernoulli's law between the slurry level and the outlet through which the slurry flows from compartment II to the UR .
  - The volume of this region varies with time.
  - The residence time of the slurry in this compartment is relatively short as compared to the residence time in compartment I. Hence, dissolution or reaction can be neglected.

- Compartment III (UR):
  - The total volume of the UR (V_{UR}) is constant, but the volumes of compartment III (V_{RIII}) and IV (V_{RIV}) are variable and are related as follows:
$$V_{\text{UR}} = V_{\text{RIII}} + V_{\text{RIV}}. \tag{4.5}$$
  - The top part of the UR is designed so that most of the acid is separated from the dispersed phase. The exact flow conditions within this region are unknown, but it is believed that the grains sediment in an approximately constant pattern, such that constant bed void fraction can be assumed for the sedimented slurry.
  - The residence time within compartment III is much smaller than the residence time in compartment IV. For this reason, the separation of particles from the acid phase is assumed to occur instantaneously. The particles are split among the two flows leaving compartment III: the overflow and the sedimentation flow (i.e. flow to compartment IV). The splitting function depends on size, and has a sigmoid shape.

  - The assumption of instantaneous separation implies the following:
    * since particles do not accumulate in the region, any volume change in this compartment can only be caused by the liquid phase.
    * changes in the solid composition in the flow coming from compartment III cause instantaneous changes in the solid composition of the overflow and sedimentation flow.
  - Reaction, dissolution, and heat exchange effects in compartment III are neglected.

- Compartment IV (UR):
  - The stream leaving this compartment is a controlled flow. Moreover, tapping is not carried out continuously, but in a cyclic way.
  - Dissolution is the main phenomenon taking place in this compartment. Disintegration is not considered since the remains of intermetallic phases are now located on the external surface of the Si grains as opposed to the feedstock, where the intermetallic phases were encountered within the particles.
  - Property profiles are believed to exist in this compartment, and should not be neglected. Therefore, a microscopic model accounting for spatial distribution should be used. However, only distribution in the axial direction is considered. In other words, plug-flow with radial perfect mixing is assumed.

4.4 Model structure

Based on the model foundations and model assumptions that were established in section 4.3, the structure of the model can now be built. Tables 4.1, 4.2, 4.3, and 4.4 summarize the structure of the *Silgrain*® model. The initial conditions and boundary conditions that are necessary to solve the model are also indicated. Tables 4.1 and 4.2 show the PBE, the total mass balances, the component balances of the acid phase and the solid phase for the HR, whereas table 4.3 shows the energy balance for the whole HR. Table 4.4 shows the model of the UR .

Some words about notation are necessary. References to compartment I, II, III or IV are indicated with subscripts RI, RII, RIII and RIV, respectively. Subscript in refers to a influent into the compartment, whereas subscript out refers to an effluent of the compartment. Superscript Me indicates a balance for each of the metallic impurities, i.e. Fe, Al, and Ca. Superscript acid indicates a balance for

Table 4.1: Structure of HR-model (Compartment I): PBE, mass, and component balances. I.C. = Initial Condition

Compartment I:	
PBE I.C. $\Psi_{\mathrm{RI}}^{\mathrm{active}}(0, D_p)$	$\frac{d\Psi_{\mathrm{RI}}^{\mathrm{active}}}{dt} = \dot{\Psi}_{\mathrm{RI,in}}^{\mathrm{active}} - \dot{\Psi}_{\mathrm{RI,out}}^{\mathrm{active}} + B - D$ $\dot{\Psi}_{\mathrm{RI,in}}^{\mathrm{active}} = \dot{M}_{\mathrm{feed}} \Psi_{\mathrm{feed}} \left(1 - w_{\mathrm{feed}}^{\mathrm{inert}}\right)$ $\dot{\Psi}_{\mathrm{RI,out}}^{\mathrm{active}}(D_p, t) = \begin{cases} B - D & \text{for } D_p \leq D_{\mathrm{cut}} \\ 0 & \text{for } D_p > D_{\mathrm{cut}} \end{cases}$
PBE I.C. $\Psi_{\mathrm{RI}}^{\mathrm{inert}}(0, D_p)$	$\frac{d\Psi_{\mathrm{RI}}^{\mathrm{inert}}}{dt} = \dot{\Psi}_{\mathrm{RI,in}}^{\mathrm{inert}} - \dot{\Psi}_{\mathrm{RI,out}}^{\mathrm{inert}}$ $\dot{\Psi}_{\mathrm{RI,in}}^{\mathrm{inert}} = \dot{M}_{\mathrm{feed}} \Psi_{\mathrm{feed}} w_{\mathrm{feed}}^{\mathrm{inert}}$ $\dot{\Psi}_{\mathrm{RI,out}}^{\mathrm{inert}} = q_{\mathrm{RI,tapping}}^{\mathrm{inert}} \Psi_{\mathrm{RI}}^{\mathrm{inert}}$
Comp. mass bal. (solid) I.C. $W_{\mathrm{RI}}^{\mathrm{Me}}(0)$	$\frac{dW_{\mathrm{RI}}^{\mathrm{Me}}}{dt} = \dot{W}_{\mathrm{RI,in}}^{\mathrm{Me}} - \dot{W}_{\mathrm{RI,out}}^{\mathrm{Me}} - r_{\mathrm{RI}}^{\mathrm{Me}} M_w^{\mathrm{Me}} V_{\mathrm{RI}}$ $\dot{W}_{\mathrm{RI,in}}^{\mathrm{Me}} = \dot{M}_{\mathrm{feed}} w_{\mathrm{RI,in}}^{\mathrm{Me}}$ $\dot{W}_{\mathrm{RI,out}}^{\mathrm{Me}} = \left(\int_{Dp,\mathrm{min}}^{Dp,\mathrm{max}} \dot{\Psi}_{\mathrm{RI,out}}^{\mathrm{active}} d\zeta\right) w_{\mathrm{RI,out}}^{\mathrm{Me}}$ $W_{\mathrm{RI}}^{\mathrm{Me}} = \left(\int_{Dp,\mathrm{min}}^{Dp,\mathrm{max}} \Psi_{\mathrm{RI}}^{\mathrm{active}} d\zeta\right) w_{\mathrm{RI}}^{\mathrm{Me}}$ $V_{\mathrm{RI}} = \frac{\left(\int_{Dp,\mathrm{min}}^{Dp,\mathrm{max}} \Psi_{\mathrm{RI}}^{\mathrm{active}} d\zeta + \int_{Dp,\mathrm{min}}^{Dp,\mathrm{max}} \Psi_{\mathrm{RI}}^{\mathrm{inert}} d\zeta\right)}{\rho_{\mathrm{solid}} (1 - \varepsilon_{\mathrm{RI}})}$
Comp. mole bal. (acid) I.C. $N_{\mathrm{RI}}^{\mathrm{acid}}(0)$	$\frac{dN_{\mathrm{RI}}^{\mathrm{acid}}}{dt} = \dot{N}_{\mathrm{RI,in}}^{\mathrm{acid}} - \dot{N}_{\mathrm{RI,out}}^{\mathrm{acid}} + r_{\mathrm{RI}}^{\mathrm{acid}} V_{\mathrm{RI}}$ $\dot{N}_{\mathrm{RI,in}}^{\mathrm{acid}} = q_{\mathrm{feed}}^{\mathrm{acid}} C_{\mathrm{RI,in}}^{\mathrm{acid}}$ $\dot{N}_{\mathrm{RI,out}}^{\mathrm{acid}} = q_{\mathrm{RI,out}}^{\mathrm{acid}} C_{\mathrm{RI,out}}^{\mathrm{acid}}$ $N_{\mathrm{RI}}^{\mathrm{acid}} = V_{\mathrm{RI}} \varepsilon_{\mathrm{RI}} C_{\mathrm{RI}}^{\mathrm{acid}}$ $q_{\mathrm{RI,out}}^{\mathrm{acid}} = q_{\mathrm{feed}}^{\mathrm{acid}} - \varepsilon_{\mathrm{RI}} \frac{dV_{\mathrm{RI}}}{dt}$

Table 4.2: Structure of HR-model (Compartment II): PBE, mass, and component balances. I.C. = Initial Condition

Compartment II:	
PBE I.C. $\Psi_{\mathrm{RII}}(0, D_p)$	$\frac{d\Psi_{\mathrm{RII}}}{dt} = \dot{\Psi}_{\mathrm{RII,in}} - \dot{\Psi}_{\mathrm{RII,out}}$ $\dot{\Psi}_{\mathrm{RII,in}} = \dot{\Psi}^{\mathrm{active}}_{\mathrm{RI,out}}$ $\dot{\Psi}_{\mathrm{RII,out}} = \frac{q_{\mathrm{RII,out}}}{V_{\mathrm{RII}}}\Psi_{\mathrm{RII}}$
Total mass bal. I.C. $M_{\mathrm{RII}}(0)$	$\frac{dM_{\mathrm{RII}}}{dt} = \dot{M}_{\mathrm{RII,in}} - \dot{M}_{\mathrm{RII,out}}$ $\dot{M}_{\mathrm{RII,in}} = \int_{Dp,\min}^{Dp,\max} \dot{\Psi}_{\mathrm{RI,out}} d\zeta + q^{\mathrm{acid}}_{\mathrm{RI,out}}\rho_{\mathrm{acid}}$ $\dot{M}_{\mathrm{RII,out}} = q_{\mathrm{RII,out}}\left(\rho_{\mathrm{acid}}\varepsilon_{\mathrm{RII}} + \rho_{\mathrm{solid}}\left(1-\varepsilon_{\mathrm{RII}}\right)\right)$ $M_{\mathrm{RII}} = \int_{Dp,\min}^{Dp,\max} \Psi_{\mathrm{RII}} d\zeta + \varepsilon_{\mathrm{RII}} V_{\mathrm{RII}}\rho_{\mathrm{acid}}$
Comp. mass bal. (solid) I.C. $W^{\mathrm{Me}}_{\mathrm{RII}}(0)$	$\frac{dW^{\mathrm{Me}}_{\mathrm{RII}}}{dt} = \dot{W}^{\mathrm{Me}}_{\mathrm{RII,in}} - \dot{W}^{\mathrm{Me}}_{\mathrm{RII,out}}$ $\dot{W}^{\mathrm{Me}}_{\mathrm{RII,in}} = \dot{W}^{\mathrm{Me}}_{\mathrm{RI,out}}$ $\dot{W}^{\mathrm{Me}}_{\mathrm{RII,out}} = q_{\mathrm{RII,out}}\left(1-\varepsilon_{\mathrm{RII}}\right)\rho_{\mathrm{solid}} w^{\mathrm{Me}}_{\mathrm{RII}}$ $W^{\mathrm{Me}}_{\mathrm{RII}} = \left(\int_{Dp,\min}^{Dp,\max} \Psi_{\mathrm{RII}} d\zeta\right) w^{\mathrm{Me}}_{\mathrm{RII}}$
Comp. mole bal. (acid) I.C. $N^{\mathrm{acid}}_{\mathrm{RII}}(0)$	$\frac{dN^{\mathrm{acid}}_{\mathrm{RII}}}{dt} = \dot{N}^{\mathrm{acid}}_{\mathrm{RII,in}} - \dot{N}^{\mathrm{acid}}_{\mathrm{RII,out}}$ $\dot{N}^{\mathrm{acid}}_{\mathrm{RII,in}} = \dot{N}^{\mathrm{acid}}_{\mathrm{RI,out}}$ $\dot{N}^{\mathrm{acid}}_{\mathrm{RI,out}} = q_{\mathrm{RII,out}}\varepsilon_{\mathrm{RII}} C^{\mathrm{acid}}_{\mathrm{RII}}$ $N^{\mathrm{acid}}_{\mathrm{RII}} = V_{\mathrm{RII}}\varepsilon_{\mathrm{RII}} C^{\mathrm{acid}}_{\mathrm{RII}}$

Table 4.3: Structure of HR-model: energy balance.

$$\left(V_{\mathrm{RI}}\,\rho c_{p\,\mathrm{RI}} + V_{\mathrm{RII}}\,\rho c_{p\,\mathrm{RII}}\right)\frac{dT_{\mathrm{HR}}}{dt} = \dot{H}_{\mathrm{in}} - \dot{H}_{\mathrm{out}} + \sum_{\mathrm{Me}}\left(-\Delta H_{\mathrm{Me}}\right) r^{\mathrm{Me}}_{\mathrm{RI}} V_{\mathrm{RI}} - \dot{Q}_{\mathrm{surroundings}}$$

$$\dot{H}_{\mathrm{in}} = \dot{M}_{\mathrm{feed}} c_{p\mathrm{solid}}\left(T^{\mathrm{solid}}_{\mathrm{feed}} - T_{\mathrm{ref}}\right) + q^{\mathrm{acid}}_{\mathrm{feed}}\rho_{\mathrm{acid}} c_{p\mathrm{acid}}\left(T^{\mathrm{acid}}_{\mathrm{feed}} - T_{\mathrm{ref}}\right)$$

$$\dot{H}_{\mathrm{out}} = q_{\mathrm{RII,out}}\left|\rho c_p\right|_{\mathrm{RII}}\left(T_{\mathrm{HR}} - T_{\mathrm{ref}}\right)$$

$$\rho c_{p\,i} = \rho_{\mathrm{acid}} c_{p\mathrm{acid}}\varepsilon_i + \rho_{\mathrm{solid}} c_{p\mathrm{solid}}\left(1-\varepsilon_i\right) \quad i = \mathrm{RI}, \mathrm{RII}$$

Table 4.4: Structure of UR model. Initial conditions and boundary conditions are indicated in the first column.

UR vol. bal.	$q_{\mathrm{RIII,in}} = q_{\mathrm{RIII,overflow}} + q_{\mathrm{RIV,tapping}}$
Compartment III:	
PBE	$\frac{d\Psi_{\mathrm{RIII}}}{dt} = 0 = \dot{\Psi}_{\mathrm{RIII,in}} - \dot{\Psi}_{\mathrm{RIII,out}} - \dot{\Psi}_{\mathrm{RIII,overflow}}$ $\dot{\Psi}_{\mathrm{RIII,overflow}} = \mathrm{split}\,(Dp)\,\dot{\Psi}_{\mathrm{RIII,in}}$ $\dot{\Psi}_{\mathrm{RIII,out}} = (1 - \mathrm{split}\,(Dp))\,\dot{\Psi}_{\mathrm{RIII,in}}$ $q_{\mathrm{RIII,out}} = \frac{\int_{Dp,\min}^{Dp,\max} \dot{\Psi}_{\mathrm{RIII,out}} d\zeta}{\rho_{\mathrm{solid}}\,(1 - \varepsilon_{\mathrm{design}})}$
Solid comp.mass b.	$w^{\mathrm{Me}}_{\mathrm{RIII,out}} = w^{\mathrm{Me}}_{\mathrm{RIII,overflow}} = w^{\mathrm{Me}}_{\mathrm{RII,out}}$
Acid comp.mole b.	$\frac{dN^{\mathrm{acid}}_{\mathrm{RIII}}}{dt} = \dot{N}^{\mathrm{acid}}_{\mathrm{RIII,in}} - \dot{N}^{\mathrm{acid}}_{\mathrm{RIII,out}} - \dot{N}^{\mathrm{acid}}_{\mathrm{RIII,overflow}}$ $\dot{N}^{\mathrm{acid}}_{\mathrm{RIII,in}} = \dot{N}^{\mathrm{acid}}_{\mathrm{RI,out}}$ $\dot{N}^{\mathrm{acid}}_{\mathrm{RIII,out}} = q_{\mathrm{RIII,out}}\,\rho_{\mathrm{solid}}\,(1 - \varepsilon_{\mathrm{design}})\,C^{\mathrm{acid}}_{\mathrm{RIII}}$ $\dot{N}^{\mathrm{acid}}_{\mathrm{RIII,overflow}} = q_{\mathrm{RIII,overflow}}\,\rho_{\mathrm{solid}}\,(1 - \varepsilon_{\mathrm{overflow}})\,C^{\mathrm{acid}}_{\mathrm{RIII}}$ $N^{\mathrm{acid}}_{\mathrm{RIII}} = V_{\mathrm{RIII}} C^{\mathrm{acid}}_{\mathrm{RII}}$
Energy bal.	$T^{\mathrm{Me}}_{\mathrm{RIII,out}} = T^{\mathrm{Me}}_{\mathrm{RIII,overflow}} = T^{\mathrm{Me}}_{\mathrm{RII,out}}$
Compartment IV:	
PBE $\psi_{\mathrm{RIV}}\,(0, z, D_p)$ $\psi_{\mathrm{RIV}}\,(t, z_{\mathrm{boundary}}, D_p)$	$\frac{\partial \psi_{\mathrm{RIV}}}{\partial t} = -\frac{\partial\,(v_z \psi_{\mathrm{RIV}})}{\partial z} - \frac{\partial\,(v_{D_p} \psi_{\mathrm{RIV}})}{\partial D_p}$ $v_z = \frac{q_{\mathrm{RIII,out}} - q_{\mathrm{RIV,tapping}}}{\pi D^2_{\mathrm{UR}}}$
Total mass bal. $M_{\mathrm{RIV}}\,(0)$	$\frac{dM_{\mathrm{RIV}}}{dt} = \dot{M}_{\mathrm{RIV,in}} - \dot{M}_{\mathrm{RIV,out}}$ $\dot{M}_{\mathrm{RIV,in}} = q_{\mathrm{RIII,out}}\,(\rho_{\mathrm{acid}} \varepsilon_{\mathrm{design}} + \rho_{\mathrm{solid}}\,(1 - \varepsilon_{\mathrm{design}}))$ $\dot{M}_{\mathrm{RIV,out}} = q_{\mathrm{RIV,tapping}}\,(\rho_{\mathrm{acid}} \varepsilon_{\mathrm{tapping}} + \rho_{\mathrm{solid}}\,(1 - \varepsilon_{\mathrm{tapping}}))$ $\varepsilon_{\mathrm{tapping}} = \frac{\int_{Dp,\min}^{Dp,\max} \psi_{\mathrm{RIV}}\,(z_{\mathrm{tapping}}, \zeta)\,d\zeta}{\rho_{\mathrm{solid}} q_{\mathrm{RIV,tapping}}}$
Solid comp.mass b. $w^{\mathrm{Me}}_{\mathrm{RIV}}\,(0, z)$ $w^{\mathrm{Me}}_{\mathrm{RIV}}\,(t, z_{\mathrm{boundary}})$	$\frac{\partial w^{\mathrm{Me}}_{\mathrm{RIV}}}{\partial t} = -\frac{\partial\,(v_z w^{\mathrm{Me}}_{\mathrm{RIV}})}{\partial z} + \frac{r^{\mathrm{Me}}_{\mathrm{RIV}} M^{\mathrm{Me}}_{w}}{\rho_{\mathrm{solid}}}$ $\varepsilon_{\mathrm{RIV}} = \frac{\int_{Dp,\min}^{Dp,\max} \psi_{\mathrm{RIV}} d\zeta}{\rho_{\mathrm{solid}}}$
Acid comp.mole b. $C^{\mathrm{acid}}_{\mathrm{RIV}}\,(0, z)$ $C^{\mathrm{acid}}_{\mathrm{RIV}}\,(t, z_{\mathrm{boundary}})$	$\frac{\partial C^{\mathrm{acid}}_{\mathrm{RIV}}}{\partial t} = -\frac{\partial\,(v_z C^{\mathrm{acid}}_{\mathrm{RIV}})}{\partial z} + \frac{r^{\mathrm{acid}}_{\mathrm{RIV}}\,(1 - \varepsilon_{\mathrm{RIV}})}{\varepsilon_{\mathrm{RIV}}}$
Energy bal. $T_{\mathrm{RIV}}\,(0, z)$ $T_{\mathrm{RIV}}\,(t, z_{\mathrm{boundary}})$	$\frac{\partial T_{\mathrm{RIV}}}{\partial t} = -\frac{\partial\,(v_z T_{\mathrm{RIV}})}{\partial z} - \frac{\dot{Q}_{\mathrm{surroundings}}}{\rho C_p} + \frac{r_j \Delta H_j \varepsilon_{\mathrm{RIV}}}{\rho C_p}$

each of the reactants and products components in the acid phase, i.e. $FeCl_3$, HCl, $FeCl_2$, $AlCl_3$, and $CaCl_2$.

The model, as presented in this section, is not complete. The disintegration, chemical reaction, and some of the flow terms need to be specified, and values for the parameters and the initial conditions (I.C.) and boundary conditions (B.C.) have to be selected. The structure of the model or some of its parts would be valid for any other particulate processes as long as the corresponding assumptions are still reasonable.

4.5 Constitutive relations

The model must now be "particularized" by defining the constitutive relations, and finding values for the parameters. The constitutive relations that have to be specified in the *Silgrain®* model are the following:

- the disintegration terms.
- the reaction rates.
- the heat exchange terms and reaction enthalpies.
- the hydrodynamic relations, critical sizes, and bed packing parameters.

4.5.1 Particle disintegration

Although the *Silgrain®* process had not been mathematically modeled prior to this work, some phenomenological work had already been carried out by the process designers and by Elkem ASA. Hence, the patent of the process (Kolflaath 1960) describes the refining of Si with solutions containing chloride ions and metal cations. The leaching solution is compared to another reactive solution that had been used in the past, the hydrochloric acid leaching process. The patent describes some factors affecting reaction, such as composition or temperature, but does not discuss the disintegration mechanism. A tentative theory about the disintegration phenomena was given in (Aas 1971). The theory states that the corrosive attack opens up narrow cracks along the grain boundaries of the Si . H_2 gas is generated during reaction (see equation 4.2). Salt precipitates of the chloride compounds may be formed in the cracks since the pH conditions within the crack differ much from the acidity conditions in the bulk phase due to mass transfer resistance. The combined effect of gas and precipitate formation may be the reason for particle disintegration. This theory was further studied in (Andreassen 1995). Moreover, this work studied some factors affecting disintegration such as acid composition and intermetallic phase composition.

Some references to phenomenological research of the refining of FeSi alloys by acid leaching are found in the literature. Hence, the effect of structural composition, acid composition, and stirring was investigated in (Margarido, Martins, Figueiredo & Bastos 1993*b*) and (Margarido, Figueiredo, Queiróz & Martins 1997). The crackling core model, developed by Park and Levenspiel (1975), was used in (Margarido, Martins, Figueiredo & Bastos 1993*a*) and (Martins & Margarido 1996) to model the FeSi leaching. The crackling core model assumes that the particles are initially nonporous; then, under the action of the reactant the pellet transforms progressively from the outside in, by crackling and fissuring, to form a grainy material, which then continuous reacting according to the shrinking core model (Park & Levenspiel 1975). Conceptually, this model agrees well with the tentative theory suggested in (Aas 1971). However, the crackling core model is not suited for use in the PBE, since the model assumes that all the grains have the same size, thus ignoring the distribution of particle sizes.

No reference has been reported in the literature on PBE modeling of leaching processes where particles disintegrate. However, there are other types of particulate processes where disintegration or breakup phenomena are important, either as the primary event (comminution, emulsion dispersion) or as a secondary event (agglomeration, crystallization). Examples of mathematical descriptions of the birth (B) and death (D) rate functions can thus be found in the granulation (Kapur 1995), comminution (Herbst & Asihene 1993), (Ramkrishna 2000), and emulsion dispersion (Chen, Prüss & Warbecke 1998) literature. Although these particulate processes differ considerably from each other, they model the birth and death rate terms in a similar way, as follows:

$$B - D = \int_{D_p}^{D_{p,\max}} b(D_p, \zeta)\, a(\zeta, \theta)\ \Psi(\zeta, t)\, d\zeta - a(D_p, \theta)\Psi(D_p, t) \tag{4.6}$$

where $a(D_p, \theta)$ is the rate at which a particle of size D_p breaks per unit time, and is thus commonly called the *breakage frequency* function. It is a function of particle size and some other application-dependent parameters θ. In turn, $b(D_p, \zeta)$ is a probability density distribution function that defines the distribution of sizes of *daughter* particles when a *mother* particle of size ζ breaks apart. Some other additional conditions must be fulfilled:

- a mother particle can not generate larger *daughter* particles than itself. This is the reason why the integral limits are selected as indicated in equation 4.6.
- the mass of *daughter* particles originated from breakage of a *mother* particle of size ζ must be less than or equal to the mass of the mother particle:

$$\int_{D_{p,\min}}^{D_p} b(\epsilon, D_p)\, a(D_p)\ \Psi(D_p, t)\, d\epsilon \leq a(D_p)\Psi(D_p, t). \tag{4.7}$$

The birth and death terms of the *Silgrain®* process have been modeled according to equation 4.6. Some experimental work was necessary to find mathematical expressions for $a(D_p, \theta)$ and $b(D_p, \zeta)$. The available phenomenological information was used to design the laboratory experimental campaign. The experiments were carried out in the laboratories at Elkem Research Centre (Kristiansand, Norway). A brief description of the experiments is given below, but the operational parameters have been omitted to protect confidential information. The experimental campaign is described in more detail in a confidential report (Dueñas Díez 2001).

Batch leaching tests (performed at Elkem Research Centre)

Batch leaching tests were carried out, and special care was paid so that the operating conditions resembled the conditions encountered in compartment I of the HR. The influence of the following variables was studied:

- Temperature.
- Leaching acid composition.
- Leaching time.
- Particle size.

The chemical composition and intermetallic phase composition of the FeSi material used for the experiments was characterized and representative of the regular feedstock to the *Silgrain®* process. The disintegration and impurity removal rates were followed by measuring the change of composition in the solid phase.

Each leaching test involved the following stages:

1. Preparation of the feed and the acid.
   (a) The material was grinded to the chosen particle size. Batches of FeSi with the same weight, the same number of particles, and a homogeneous distribution of shapes were used.
   (b) The acid composition was manipulated to the chosen set of values.
2. The acid was heated up to the chosen temperature.
3. Once the chosen temperature was reached, the FeSi was added. A constant and representative acid/solid ratio was used.
4. The temperature was kept constant during the duration of the test.

Figure 4.3: Experimental setup for batch leaching experiments. Picture taken by the author at Elkem Research Centre, Kristiansand, Norway.

5. Once the final time was reached, the vessel was quenched to stop the reaction. The solid phase was then separated from the liquid phase by vacuum filtering.

6. The solid phase was dried, and then sieved.

7. The sieved fractions were weighted, and subjected to chemical analysis to determine the impurity content.

Some of the leaching equipment is shown in Figures 4.3 and 4.4. In view of the results, it was concluded that the disintegration rate is mainly influenced by temperature and by the initial particle size, in such a way that the smaller the initial particle size and/or the higher the temperature, the faster the disintegration is. The leaching acid composition does not have an important effect on the final PSD, as long as the composition lies within the operation range of the *Silgrain®* process. Therefore, this factor can be neglected in the birth and death rates. A disintegration pattern was observed: the PSD of daughter particles was bimodal with a mode located around a *fixed* particle size in the fine range and with a *mobile* mode whose location is dependent on the *mother* particle size. This led to the following theory: when the acid attacks FeSi, the intermetallic phases are dissolved, causing a particle to break up into a small number of still relatively large particles and a large number of Si grains, which are quite fine. The large daughter particles are subject to acid attack and breakup, giving rise again to grains and

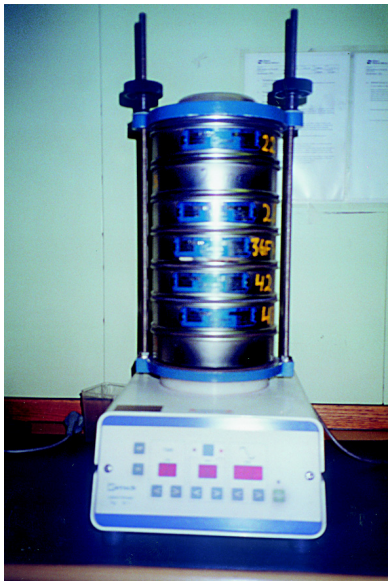

Figure 4.4: Sieve equipment. Picture taken by the author at Elkem Research Centre, Kristiansand, Norway.

intermediate sizes. This process repeats until all the material is disintegrated into grains. Figure 4.5 sketches the suggested model of disintegration, and indicates qualitatively how the PSD of daughter particles varies with disintegration.

Based on the results of this experimental campaign, the following mathematical expression was suggested to describe the *breakage frequency*:

$$a(D_p, T) = \begin{cases} \dfrac{k_a \exp\left(k_T T\right)}{D_p^n} & \text{for } D_p \leq D_{\text{grain}} \\ 0 & \text{for } D_p > D_{\text{grain}} \end{cases}, \tag{4.8}$$

where k_a, k_T, n and D_{grain} are the fitting parameters and where particles smaller than the average size of Si grains D_{grain} do not experience further disintegration. As regards the density distribution function of *daughter* particles, the *static* mode around a fixed point D^* was modeled with an exponential distribution function whereas the mobile mode was modeled with a log-normal distribution function, as follows:

$$b(\epsilon, \zeta) = \underbrace{A_1 \exp\left(-\beta_1 \left(1 - \frac{\epsilon}{D^*}\right)^2\right)}_{\text{static mode}} + \underbrace{\frac{A_2}{\epsilon} \exp\left(-\beta_2 \log^2\left(1 - \frac{\epsilon\,\zeta}{(\zeta - \epsilon)\,(0.6\,\epsilon^3)^{1/3}}\right)\right)}_{\text{mobile mode}}, \tag{4.9}$$

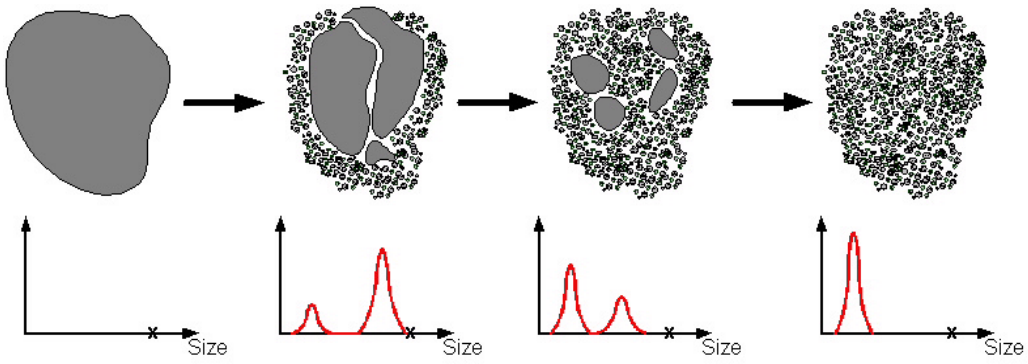

Figure 4.5: Disintegration model.

where ζ represents the size of the *mother* particle, ϵ represents the size of the *daughter* particles, and where A_1, A_2, β_1, β_2, D^* are the fitting parameters. Note that mass fraction is used as basis for $b(\epsilon, \zeta)$. The Generalized Reduced Gradient (GRG) nonlinear optimization algorithm (Edgar, Himmelblau & Ladson 2001), available in Excel , was used to fit experimental data to equations 4.9 and 4.8, with satisfactory results. Figure 4.6 shows good agreement between the fitted curve $b(\epsilon, \zeta)$ and experimental results. The parameter estimates and the axis in Figure 4.6 have been omitted to protect confidential information.

4.5.2 Reaction rates

The experimental campaign carried out to determine the birth and death terms also provided information about the chemical reactions. In view of the results, it can be concluded that when particle disintegration takes place, a part of the metallic impurities in the FeSi feedstock have been removed. The grains show a considerable lower content of impurities, whereas the disintegrated material that is still large in size contains approximately the same proportion of metallic impurities as the feedstock. Moreover, the conversion observed in the grains was nearly independent of temperature and acid composition. However, the conversion is still lower than that of the product material tapped in the UR. Therefore, a part of the chemical work takes place in the HR, and the remaining in the UR. The kinetic rates in the two reactors are different, mainly due to unalike flow and solid/liquid ratio conditions. The solid/liquid ratio is considerably lower in compartment I than in compartment IV. Moreover, there exists more turbulence in compartment I than in compartment IV. This means that both the rate limiting stage and the magnitude of the reaction rate are different for the two reactors. The chemical reaction is closely linked to disintegration in compartment I, whereas a considerably slower

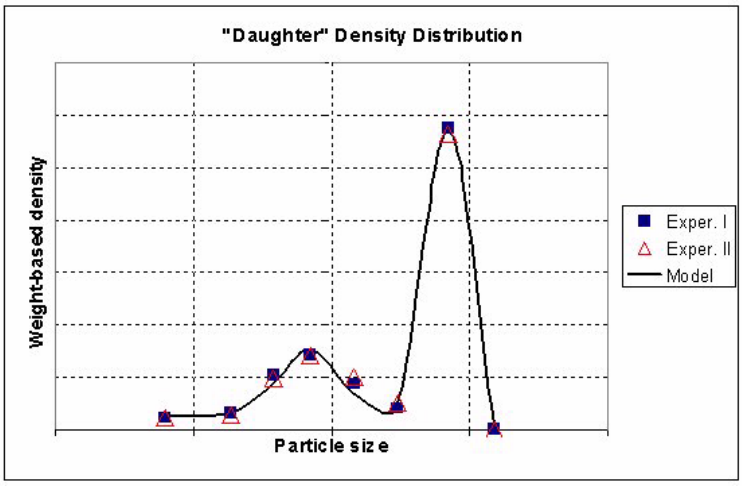

Figure 4.6: Fitted $b(\epsilon, \zeta)$ vs. experimental data.

reaction is observed in compartment IV. Figure 4.7 depicts how reaction evolves with time in compartments I and IV.

A fairly simple kinetic model can be used for compartment I:

$$w_{\mathrm{RI,out}}^{\mathrm{Me}} = \alpha^{\mathrm{Me}} w_{\mathrm{RI}}^{\mathrm{Me}} \tag{4.10}$$

$$r_{\mathrm{RI}}^{\mathrm{Me}} = -\frac{\int_{Dp,\min}^{D\,\mathrm{cut}} (B - D)\, d\zeta}{M_w^{\mathrm{Me}} V_{\mathrm{RI}}} \alpha^{\mathrm{Me}} w_{\mathrm{RI}}^{\mathrm{Me}}, \tag{4.11}$$

where α^{Me} is a measure of conversion. It must be in the range:

$$0 \leq \alpha^{\mathrm{Me}} \leq 1, \tag{4.12}$$

and is assumed to be constant[4]. Note that the integral term in equation 4.11 represents the mass of grains generated during disintegration in compartment I. Now, taking into account the stoichiometry of the chemical reactions (see equations 4.1 and 4.2) the reaction rates of the acid components can be formulated in terms

[4] α^{Me} varies with the phase composition of the feedstock, but since it is assumed that such a composition does not vary considerably, then it is reasonable to assume a constant value for α^{Me}.

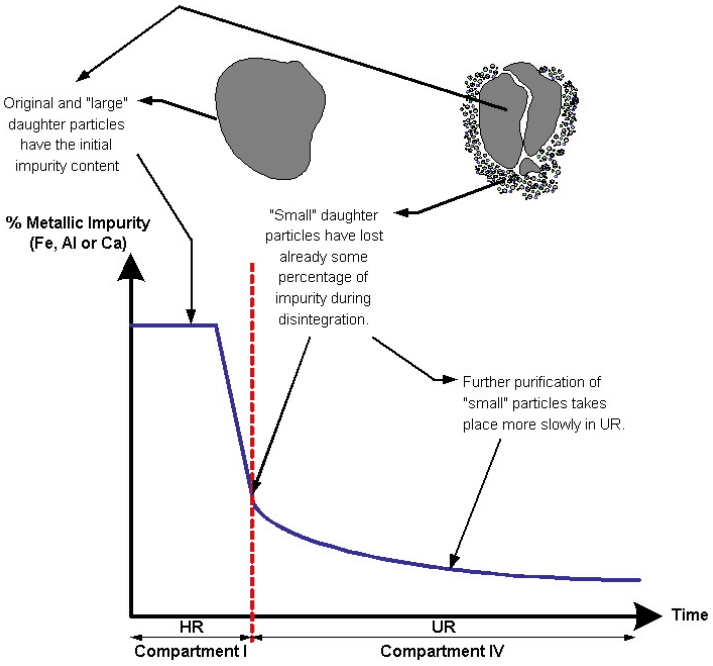

Figure 4.7: Evolution of chemical reaction in compartments I and IV.

of the reaction rates of the metallic impurities as follows:

$$\begin{pmatrix} r_{\mathrm{RI}}^{\mathrm{FeCl_3}} \\ r_{\mathrm{RI}}^{\mathrm{HCl}} \\ r_{\mathrm{RI}}^{\mathrm{FeCl_2}} \\ r_{\mathrm{RI}}^{\mathrm{AlCl_3}} \\ r_{\mathrm{RI}}^{\mathrm{CaCl_2}} \end{pmatrix} = \begin{pmatrix} 2\beta_{\mathrm{RI}}^{\mathrm{Fe}} & 3\beta_{\mathrm{RI}}^{\mathrm{Al}} & 2\beta_{\mathrm{RI}}^{\mathrm{Ca}} \\ 2\left(1-\beta_{\mathrm{RI}}^{\mathrm{Fe}}\right) & 3\left(1-\beta_{\mathrm{RI}}^{\mathrm{Al}}\right) & 2\left(1-\beta_{\mathrm{RI}}^{\mathrm{Ca}}\right) \\ -3\beta_{\mathrm{RI}}^{\mathrm{Fe}}-\left(1-\beta_{\mathrm{RI}}^{\mathrm{Fe}}\right) & -3\beta_{\mathrm{RI}}^{\mathrm{Al}} & -2\beta_{\mathrm{RI}}^{\mathrm{Ca}} \\ 0 & -3 & 0 \\ 0 & 0 & -2 \end{pmatrix} \begin{pmatrix} r_{\mathrm{RI}}^{\mathrm{Fe}} \\ r_{\mathrm{RI}}^{\mathrm{Al}} \\ r_{\mathrm{RI}}^{\mathrm{Ca}} \end{pmatrix}, \tag{4.13}$$

where β^{Me} is the fraction of reacted metallic impurity Me that was dissolved by reaction with iron chloride $\mathrm{FeCl_3}$, whereas $1-\beta^{\mathrm{Me}}$ is the fraction that was dissolved by reaction with HCl. The values for the parameters α^{Me} and β^{Me} were obtained from the laboratory experimental data.

In turn, the following kinetic model is assumed for compartment IV:

$$r_{\mathrm{RIV}}^{\mathrm{Me}} = -\underbrace{k_{\mathrm{RIV}}^{\mathrm{Me}} \exp\left(-\frac{E^{\mathrm{Me}}}{RT}\right)}_{\text{kinetic constant}} \left(C_{\mathrm{RIV}}^{\mathrm{FeCl_3}}\right)^{\gamma_1^{\mathrm{Me}}} \left(C_{\mathrm{RIV}}^{\mathrm{HCl}}\right)^{\gamma_2^{\mathrm{Me}}} \left(w_{\mathrm{RIV}}^{\mathrm{Me}}\right)^{\gamma_3^{\mathrm{Me}}}, \tag{4.14}$$

where $k_{\mathrm{RIV}}^{\mathrm{Me}}$ is the preexponential factor and E^{Me} is the activation energy of the reaction. Hence, it is assumed that the kinetic constant follows Arrhenius' law for

temperature dependence. Note also that if any of the reactants (Me, HCl or $FeCl_3$) gets depleted, then the reaction rate goes to zero. Again, the reaction rates of the acid compounds can be calculated according to stoichiometry as indicated by equation 4.13, but where $\beta_{\mathrm{RI}}^{\mathrm{Me}}$ is substituted by the corresponding values of compartment IV $\beta_{\mathrm{RIV}}^{\mathrm{Me}}$. Laboratory tests resembling the operation of the UR were attempted in order to obtain data for parameter estimation ($k_{\mathrm{RIV}}^{\mathrm{Me}}, E^{\mathrm{Me}}, \gamma_1^{\mathrm{Me}}, \gamma_2^{\mathrm{Me}}, \gamma_3^{\mathrm{Me}}, \beta_{\mathrm{RIV}}^{\mathrm{Me}}$), but unfortunately the data were not representative. Therefore, the parameters ($k_{\mathrm{RIV}}^{\mathrm{Me}}$) were tuned based on a trial-and-error approach using computer simulations.

4.5.3 Dissolution rate

The chemical reactions in compartment IV not only cause changes in the composition of the solid phase and acid phase, but also cause changes in the particle size. Since the impurities are now concentrated on the external surface of the Si grains, the particle shrinks when the impurities are dissolved. Note, however, that the changes in particle size are thus not as dramatic as in compartment I, where disintegration was taking place.

The continuous shrinking of particles is modeled in the PBE through the following term:

$$\frac{\partial \left(v_{D_p}\psi_{\mathrm{RIV}}\right)}{\partial D_p} = \frac{\partial}{\partial D_p}\left(\frac{dD_p}{dt}\psi_{\mathrm{RIV}}\right), \tag{4.15}$$

where v_{D_p} is the rate of change of particle diameter by chemical reaction. Now, if we define the total metallic dissolution rate r as follows

$$r_w = \sum_{\mathrm{Me}} M_w^{\mathrm{Me}} r_{\mathrm{RIV}}^{\mathrm{Me}} = M_w^{\mathrm{Fe}} r_{\mathrm{RIV}}^{\mathrm{Fe}} + M_w^{\mathrm{Al}} r_{\mathrm{RIV}}^{\mathrm{Al}} + M_w^{\mathrm{Ca}} r_{\mathrm{RIV}}^{\mathrm{Ca}}, \tag{4.16}$$

where r_w is given in dissolved mass per unit time and unit particle volume, whereas $r_{\mathrm{RIV}}^{\mathrm{Me}}$ is given in dissolved mol per unit time and unit particle volume. Moreover, r_w can also be defined as:

$$r_w = -\frac{1}{\frac{\pi}{6}D_p^2}\frac{d\left(\frac{\pi}{6}D_p^3\rho_{\mathrm{solid}}\right)}{dt} = -\frac{3\rho_{\mathrm{solid}}}{D_p}v_{D_p}. \tag{4.17}$$

Hence, if equations 4.16 and 4.17 are combined, it is obtained that

$$v_{D_p} = -\frac{D_p}{3\rho_{\mathrm{solid}}}r_w = -\frac{D_p}{3\rho_{\mathrm{solid}}}\sum_{\mathrm{Me}} M_w^{\mathrm{Me}} r_{\mathrm{RIV}}^{\mathrm{Me}}. \tag{4.18}$$

4.5.4 Heat of reaction and overall heat transfer coefficients

The reactions shown in equations 4.1 and 4.2 are exothermic. The heat of reaction can be estimated from thermodynamics. The *standard* heat of reaction

$\Delta H^\circ{}_{r,298.15\,\mathrm{K}}$, i.e. the enthalpy change when the reactants are in their standard states at 298.15 K and 1 bar and react to produce products in their standard states at 25 °C and 1 bar. $\Delta H^\circ{}_{r,i}$ can be estimated from the standard heat of formation $\Delta H^\circ{}_f$ of reactants and products as follows

$$\Delta H^\circ{}_{r,298.15\,\mathrm{K}} = \sum \nu_{\text{product } i}\, \Delta H^\circ{}_{f,i} - \sum \nu_{\text{reactant } i}\, \Delta H^\circ{}_{f,i}, \tag{4.19}$$

where $\nu_{\text{product } i}$ is the stoichiometric coefficients corresponding to product i and $\nu_{\text{reactant } i}$ is the stoichiometric coefficient corresponding to reactant i in the reaction under consideration.

However, the heat of reaction does not take place at the standard reference temperature (298.15 K). Hence, the temperature dependence of the heat of reaction has to be considered. The standard heat of temperature at any temperature T can be calculated as follows

$$\Delta H^\circ{}_{r,T} = \Delta H^\circ{}_{r,298.15\,\mathrm{K}} + \int_{298.15\,\mathrm{K}}^{T} \left(\nu_{\text{product } i} C_{p,i}\left(T\right) - \nu_{\text{reactant } i} C_{p,i}\left(T\right)\right) dT, \tag{4.20}$$

where $C_{p,i}$ is the standard heat capacity and subscript i identifies a particular reactant or product. Standard heat capacities are typically a function of temperature.

Data for the standard heat of formations and heat capacities were obtained from the literature (Perry & Green 1984) and from the National Institute of Standards and Technology (NIST) database[5]. The resulting heat of reactions were linear functions of the temperature.

The heat loss to the surroundings can be estimated as follows

$$Q = u_{\text{overall}}\, S \Delta T = u_{\text{overall}}\ S\ \left(T_{\text{HR}} - T_{\text{surroundings}}\right), \tag{4.21}$$

where u_{overall} is the overall heat transfer coefficient, S is the heat transmission surface and ΔT is the overall temperature difference. The limiting stage in the heat transfer is the heat convection from the external surface of the reactor to the air. The value of the overall heat transfer coefficient was taken from the literature (Coulson & Richardson 1978).

4.5.5 Particle and slurry motion

As mentioned in sections 4.2 and 4.3, particle motion has an important effect on the structure of the model. Indeed, particle motion was essential in establishing the number of compartments and the coupling among compartments. Hence, in compartment I a *cut* size was defined in order to differentiate particles that can not leave the compartment from those that can leave the compartment. However,

[5] http://webbook.nist.gov

the factors determining this *cut* size have not been established. It is widely known that some factors that may affect the *cut* size are:

- the larger the fluid velocity, the larger the *cut* size;
- the larger the turbulence, the larger the *cut* size;
- the smaller the difference between acid density and solid density, the larger the *cut* size;

The best way to establish the *cut* size is by making a force balance over the particle:

$$\text{Drag Force} = \text{Gravity Force} - \text{Buoyancy Force}$$

and since we assume the particles are spherical (Coulson & Richardson 1978)

$$R_o \frac{\pi}{4} D_{\text{cut}}^2 = \frac{\pi}{6} D_{\text{cut}}^3 \rho_{\text{solid}} g - \frac{\pi}{6} D_{\text{cut}}^3 \rho_{\text{acid}} g, \tag{4.22}$$

where R_o is the dimensionless drag force, ρ_{solid} and ρ_{acid} are the solid density and the fluid density, respectively, and g is the gravity constant. The drag force is generally a complicated function of the Reynolds number Re, but for turbulent flow ($500 < \text{Re} < 2 \cdot 10^5$), as in the reactor under study, the drag force is approximately independent of the Reynolds number (Coulson & Richardson 1978). For turbulent flow, the dimensionless drag force R_o is given by

$$\frac{R_o}{\rho_{\text{acid}}\, u_0^2} = 0.22, \tag{4.23}$$

where u_0 is the fluid velocity. Substituting 4.23 into equation 4.22 gives

$$\begin{aligned} D_{\text{cut}} &= 0.33 \frac{\rho_{\text{acid}}}{g\,(\rho_{\text{solid}} - \rho_{\text{acid}})} u_0^2 \\ &= 0.33 \frac{\rho_{\text{acid}}}{g\,(\rho_{\text{solid}} - \rho_{\text{acid}})} \left(\frac{u_{\text{sup}}}{\varepsilon_{\text{RII}}^n} \right)^2, \end{aligned} \tag{4.24}$$

where the fluid velocity has been expressed as a function of the the superficial fluid velocity u_{sup} and the void fraction ε_{RII}. The unknown exponent n was tuned by fitting to experimental data.

The other term that has to be defined is the flowrate of the effluent leaving compartment II. This flow is enhanced by gravity. If Bernoulli's equation is applied between the surface of the slurry in the HR (point 1) and the outlet (point 2), then

$$\frac{P_1}{\rho g} + h_1 + \frac{v_1^2}{2g} = \frac{P_2}{\rho g} + h_{\text{out}} + \frac{v_2^2}{2g}, \tag{4.25}$$

where P indicates pressure, v indicates slurry velocity and h indicates height from the reactor bottom. Taking into consideration that both the HR and the UR operate at atmospheric pressure ($P_1 = P_2$) and that the section of the reactor is much larger than the section of the orifice, or what is the same, $v_1 \ll v_2$, then equation 4.25 reduces to

$$v_2 = \sqrt{2g(h_1 - h_{\text{out}})}. \tag{4.26}$$

The flow rate can thus be calculated by multiplying equation 4.26 by the outlet cross-section and, to account for the effect of friction in the outlet, a coefficient of discharge C_D is used, resulting in the following equation

$$q_{\text{RII,out}} = C_D \frac{\pi}{4} D_{\text{outlet}}^2 \sqrt{2g(h_1 - h_{\text{outlet}})}. \tag{4.27}$$

Now, considering that the bottom part of the reactor is semiconical with volume $V_{\text{semiconical}}$ and height $h_{\text{semiconical}}$ and the remaining part of the reactor is cylindrical with reactor diameter D_{HR}, then equation 4.27 can be rewritten in terms of the volumes

$$q_{\text{RII,out}} = C_D \frac{\pi}{4} D_{\text{outlet}}^2 \sqrt{2g\left(\frac{4}{\pi\left(D_{\text{HR}}\right)^2}(V_{\text{HR}} - V_{\text{semiconical}}) + h_{\text{semiconical}} - h_{\text{outlet}}\right)}. \tag{4.28}$$

where

$$V_{\text{HR}} = V_{\text{RI}} + V_{\text{RII}}. \tag{4.29}$$

The dimension-related parameters ($D_{\text{outlet}}, h_{\text{outlet}}, V_{\text{semiconical}}, h_{\text{semiconical}}$ and D_{HR}) are known exactly, whereas a typical value of 0.64 (Coulson & Richardson 1978) is used for C_D.

Finally, in compartment III the particle motion was not modeled by using a unique cut size, but rather by a split function and a constant value for the void fraction of the sedimented material $\varepsilon_{\text{design}}$. The split function that is used here is a function of the type shown in Figure 4.8. The parameters of the split function and the value of $\varepsilon_{\text{design}}$ were selected according to information about the operation of the industrial reactor. The exact values are not known, but approximate values can estimated from other operational data available from the process.

4.6 Model solution

The model, including the constitutive relations, is summarized in tables 4.5, 4.6, 4.7 and 4.8. Once the constitutive relations were defined and values for the parameters are chosen, the model represents only the system under study. The model is no longer valid for diverse similar systems.

The type of mathematical systems encountered are:

Table 4.5: Model of compartment I.

$$\frac{d\Psi_{\mathrm{RI}}^{\mathrm{active}}}{dt} = \dot{\Psi}_{\mathrm{RI,in}}^{\mathrm{active}} - \dot{\Psi}_{\mathrm{RI,out}}^{\mathrm{active}} + B - D$$

$$\dot{\Psi}_{\mathrm{RI,in}}^{\mathrm{active}} = \left(1 - w_{\mathrm{feed}}^{\mathrm{inert}}\right) \dot{M}_{\mathrm{feed}} \Psi_{\mathrm{feed}}$$

$$B - D = \int_{D_p}^{D_{p,\max}} b(D_p, \zeta)\, a(\zeta, T)\ \Psi(\zeta, t)\, d\zeta - a(D_p, \theta)\Psi(D_p, t)$$

$$b = A_1 \exp\left(-\beta_1 \left(1 - \frac{\epsilon}{D^*}\right)^2\right) + \frac{A_2}{\epsilon} \exp\left(-\beta_2 \log^2\left(1 - \frac{\epsilon\,\zeta}{(\zeta - \epsilon)\,(0.6\,\epsilon^3)^{1/3}}\right)\right)$$

$$a(D_p, T) = \begin{cases} \dfrac{k_a \exp\left(k_T T\right)}{D_p^n} & \text{for } D_p \le D_{\mathrm{grain}} \\ 0 & \text{for } D_p > D_{\mathrm{grain}} \end{cases}$$

$$\dot{\Psi}_{\mathrm{RI,out}}^{\mathrm{active}}(D_p, t) = \begin{cases} \dot{\Psi}_{\mathrm{RI,in}}^{\mathrm{active}} + B - D & \text{for } D_p \le D_{\mathrm{cut}} \\ 0 & \text{for } D_p > D_{\mathrm{cut}} \end{cases}$$

$$D_{\mathrm{cut}} = 0.33 \frac{\rho_{\mathrm{acid}}}{g\left(\rho_{\mathrm{solid}} - \rho_{\mathrm{acid}}\right)} \left(\frac{u_{\mathrm{sup}}}{\varepsilon_{\mathrm{RII}}^n}\right)^2$$

$$\frac{d\Psi_{\mathrm{RI}}^{\mathrm{inert}}}{dt} = \dot{\Psi}_{\mathrm{RI,in}}^{\mathrm{inert}} - \dot{\Psi}_{\mathrm{RI,out}}^{\mathrm{inert}}$$

$$\dot{\Psi}_{\mathrm{RI,in}}^{\mathrm{inert}} = \dot{M}_{\mathrm{feed}} \Psi_{\mathrm{feed}} w_{\mathrm{feed}}^{\mathrm{inert}}$$

$$\dot{\Psi}_{\mathrm{RI,out}}^{\mathrm{inert}} = q_{\mathrm{RI,tapping}}^{\mathrm{inert}} \Psi_{\mathrm{RI}}^{\mathrm{inert}}$$

$$\frac{dW_{\mathrm{RI}}^{\mathrm{Me}}}{dt} = \dot{W}_{\mathrm{RI,in}}^{\mathrm{Me}} - \dot{W}_{\mathrm{RI,out}}^{\mathrm{Me}} - r_{\mathrm{RI}}^{\mathrm{Me}} M_w^{\mathrm{Me}} V_{\mathrm{RI}}$$

$$\dot{W}_{\mathrm{RI,in}}^{\mathrm{Me}} = \dot{M}_{\mathrm{feed}} w_{\mathrm{RI,in}}^{\mathrm{Me}}$$

$$\dot{W}_{\mathrm{RI,out}}^{\mathrm{Me}} = \left(\int_{Dp,\min}^{Dp,\max} \dot{\Psi}_{\mathrm{RI,out}}^{\mathrm{active}} d\zeta\right) w_{\mathrm{RI,out}}^{\mathrm{Me}} = \left(\int_{Dp,\min}^{Dp,\max} \dot{\Psi}_{\mathrm{RI,out}}^{\mathrm{active}} d\zeta\right) \alpha^{\mathrm{Me}} w_{\mathrm{RI}}^{\mathrm{Me}}$$

$$W_{\mathrm{RI}}^{\mathrm{Me}} = \left(\int_{Dp,\min}^{Dp,\max} \Psi_{\mathrm{RI}}^{\mathrm{active}} d\zeta\right) w_{\mathrm{RI}}^{\mathrm{Me}}$$

$$V_{\mathrm{RI}} = \frac{\left(\int_{Dp,\min}^{Dp,\max} \Psi_{\mathrm{RI}}^{\mathrm{active}} d\zeta + \int_{Dp,\min}^{Dp,\max} \Psi_{\mathrm{RI}}^{\mathrm{inert}} d\zeta\right)}{\rho_{\mathrm{solid}}\left(1 - \varepsilon_{\mathrm{RI}}\right)}$$

$$r_{\mathrm{RI}}^{\mathrm{Me}} = -\frac{\int_{Dp,\min}^{D\,\mathrm{cut}} (B - D) d\zeta}{M_w^{\mathrm{Me}} V_{\mathrm{RI}}} \alpha^{\mathrm{Me}} w_{\mathrm{RI}}^{\mathrm{Me}}$$

$$\frac{dN_{\mathrm{RI}}^{\mathrm{acid}}}{dt} = \dot{N}_{\mathrm{RI,in}}^{\mathrm{acid}} - \dot{N}_{\mathrm{RI,out}}^{\mathrm{acid}} + r_{\mathrm{RI}}^{\mathrm{acid}} V_{\mathrm{RI}}$$

$$\dot{N}_{\mathrm{RI,in}}^{\mathrm{acid}} = q_{\mathrm{feed}}^{\mathrm{acid}} C_{\mathrm{RI,in}}^{\mathrm{acid}}$$

$$\dot{N}_{\mathrm{RI,out}}^{\mathrm{acid}} = q_{\mathrm{RI,out}}^{\mathrm{acid}} C_{\mathrm{RI,out}}^{\mathrm{acid}}$$

$$N_{\mathrm{RI}}^{\mathrm{acid}} = V_{\mathrm{RI}} \varepsilon_{\mathrm{RI}} C_{\mathrm{RI}}^{\mathrm{acid}}$$

$$q_{\mathrm{RI,out}}^{\mathrm{acid}} = q_{\mathrm{feed}}^{\mathrm{acid}} - \varepsilon_{\mathrm{RI}} \frac{dV_{\mathrm{RI}}}{dt}$$

$$\begin{pmatrix} r_{\mathrm{RI}}^{\mathrm{FeCl_3}} \\ r_{\mathrm{RI}}^{\mathrm{HCl}} \\ r_{\mathrm{RI}}^{\mathrm{FeCl_2}} \\ r_{\mathrm{RI}}^{\mathrm{AlCl_3}} \\ r_{\mathrm{RI}}^{\mathrm{CaCl_2}} \end{pmatrix} = \begin{pmatrix} 2\beta_{\mathrm{RI}}^{\mathrm{Fe}} & 3\beta_{\mathrm{RI}}^{\mathrm{Al}} & 2\beta_{\mathrm{RI}}^{\mathrm{Ca}} \\ 2\left(1 - \beta_{\mathrm{RI}}^{\mathrm{Fe}}\right) & 3\left(1 - \beta_{\mathrm{RI}}^{\mathrm{Al}}\right) & 2\left(1 - \beta_{\mathrm{RI}}^{\mathrm{Ca}}\right) \\ -3\beta_{\mathrm{RI}}^{\mathrm{Fe}} - \left(1 - \beta_{\mathrm{RI}}^{\mathrm{Fe}}\right) & -3\beta_{\mathrm{RI}}^{\mathrm{Al}} & -2\beta_{\mathrm{RI}}^{\mathrm{Ca}} \\ 0 & -3 & 0 \\ 0 & 0 & -2 \end{pmatrix} \begin{pmatrix} r_{\mathrm{RI}}^{\mathrm{Fe}} \\ r_{\mathrm{RI}}^{\mathrm{Al}} \\ r_{\mathrm{RI}}^{\mathrm{Ca}} \end{pmatrix}$$

Table 4.6: Model of compartment II.

$$\frac{d\Psi_{\mathrm{RII}}}{dt} = \dot{\Psi}_{\mathrm{RII,in}} - \dot{\Psi}_{\mathrm{RII,out}}$$
$$\dot{\Psi}_{\mathrm{RII,in}} = \dot{\Psi}^{\mathrm{active}}_{\mathrm{RI,out}}$$
$$\dot{\Psi}_{\mathrm{RII,out}} = \frac{q_{\mathrm{RII,out}}}{V_{\mathrm{RII}}}\Psi_{\mathrm{RII}}$$
$$V_{\mathrm{over}} = V_{\mathrm{RI}} + V_{\mathrm{RII}} - V_{\mathrm{semiconical}}$$
$$q_{\mathrm{RII,out}} = C_D\frac{\pi}{4}D^2_{\mathrm{outlet}}\sqrt{2g\left(\frac{4V_{\mathrm{over}}}{\pi(D_{\mathrm{HR}})^2} + h_{\mathrm{semiconical}} - h_{\mathrm{outlet}}\right)}$$

$$\frac{dM_{\mathrm{RII}}}{dt} = \dot{M}_{\mathrm{RII,in}} - \dot{M}_{\mathrm{RII,out}}$$
$$\dot{M}_{\mathrm{RII,in}} = \int_{Dp,\mathrm{min}}^{Dp,\mathrm{max}}\dot{\Psi}_{\mathrm{RI,out}}d\zeta + q^{\mathrm{acid}}_{\mathrm{RI,out}}\rho_{\mathrm{acid}}$$
$$\dot{M}_{\mathrm{RII,out}} = q_{\mathrm{RII,out}}\left(\rho_{\mathrm{acid}}\varepsilon_{\mathrm{RII}} + \rho_{\mathrm{solid}}\left(1-\varepsilon_{\mathrm{RII}}\right)\right)$$
$$M_{\mathrm{RII}} = \int_{Dp,\mathrm{min}}^{Dp,\mathrm{max}}\Psi_{\mathrm{RII}}d\zeta + \varepsilon_{\mathrm{RII}}V_{\mathrm{RII}}\rho_{\mathrm{acid}}$$

$$\frac{dW^{\mathrm{Me}}_{\mathrm{RII}}}{dt} = \dot{W}^{\mathrm{Me}}_{\mathrm{RII,in}} - \dot{W}^{\mathrm{Me}}_{\mathrm{RII,out}}$$
$$\dot{W}^{\mathrm{Me}}_{\mathrm{RII,in}} = \dot{W}^{\mathrm{Me}}_{\mathrm{RI,out}}$$
$$\dot{W}^{\mathrm{Me}}_{\mathrm{RII,out}} = q_{\mathrm{RII,out}}\left(1-\varepsilon_{\mathrm{RII}}\right)\rho_{\mathrm{solid}}w^{\mathrm{Me}}_{\mathrm{RII}}$$
$$W^{\mathrm{Me}}_{\mathrm{RII}} = \left(\int_{Dp,\mathrm{min}}^{Dp,\mathrm{max}}\Psi_{\mathrm{RII}}d\zeta\right)w^{\mathrm{Me}}_{\mathrm{RII}}$$

$$\frac{dN^{\mathrm{acid}}_{\mathrm{RII}}}{dt} = \dot{N}^{\mathrm{acid}}_{\mathrm{RII,in}} - \dot{N}^{\mathrm{acid}}_{\mathrm{RII,out}}$$
$$\dot{N}^{\mathrm{acid}}_{\mathrm{RII,in}} = \dot{N}^{\mathrm{acid}}_{\mathrm{RI,out}}$$
$$\dot{N}^{\mathrm{acid}}_{\mathrm{RI,out}} = q_{\mathrm{RII,out}}\varepsilon_{\mathrm{RII}}\,C^{\mathrm{acid}}_{\mathrm{RII}}$$
$$N^{\mathrm{acid}}_{\mathrm{RII}} = V_{\mathrm{RII}}\varepsilon_{\mathrm{RII}}C^{\mathrm{acid}}_{\mathrm{RII}}$$

Table 4.7: Energy balance for the HR.

$$\left(V_{\mathrm{RI}}\,\rho c_{p\,\mathrm{RI}} + V_{\mathrm{RII}}\,\rho c_{p\,\mathrm{RII}}\right)\frac{dT_{\mathrm{HR}}}{dt} = \dot{H}_{\mathrm{in}} - \dot{H}_{\mathrm{out}} + \sum_{\mathrm{Me}}\left(-\Delta H_{\mathrm{Me}}\right)r^{\mathrm{Me}}_{\mathrm{RI}}V_{\mathrm{RI}} - \dot{Q}_{\mathrm{surroundings}}$$
$$\dot{H}_{\mathrm{in}} = \dot{M}_{\mathrm{feed}}c_{p\mathrm{solid}}\left(T^{\mathrm{solid}}_{\mathrm{feed}} - T_{\mathrm{ref}}\right) + q^{\mathrm{acid}}_{\mathrm{feed}}\rho_{\mathrm{acid}}c_{p\mathrm{acid}}\left(T^{\mathrm{acid}}_{\mathrm{feed}} - T_{\mathrm{ref}}\right)$$
$$\dot{H}_{\mathrm{out}} = q_{\mathrm{RII,out}}\left|\rho c_p\right|_{\mathrm{RII}}\left(T_{\mathrm{HR}} - T_{\mathrm{ref}}\right)$$
$$\rho c_{p\,i} = \rho_{\mathrm{acid}}c_{p\mathrm{acid}}\varepsilon_i + \rho_{\mathrm{solid}}c_{p\mathrm{solid}}\left(1-\varepsilon_i\right) \quad i = \mathrm{RI}, \mathrm{RII}$$
$$\dot{Q}_{\mathrm{surroundings}} = u_{\mathrm{overall}}\,S\,\left(T_{\mathrm{HR}} - T_{\mathrm{surroundings}}\right)$$
$$\Delta H_{\mathrm{Me}} = \Delta H^0_{\mathrm{Me}} + \Delta H^T_{\mathrm{Me}}T_{\mathrm{HR}}$$

Table 4.8: Model of compartments III and IV.

$$q_{\mathrm{RIII,in}} = q_{\mathrm{RIII,overflow}} + q_{\mathrm{RIV,tapping}}$$

$$\frac{d\Psi_{\mathrm{RIII}}}{dt} = 0 = \dot{\Psi}_{\mathrm{RIII,in}} - \dot{\Psi}_{\mathrm{RIII,out}} - \dot{\Psi}_{\mathrm{RIII,overflow}}$$
$$\dot{\Psi}_{\mathrm{RIII,overflow}} = \mathrm{split}\left(Dp\right)\dot{\Psi}_{\mathrm{RIII,in}}$$
$$\dot{\Psi}_{\mathrm{RIII,out}} = \left(1 - \mathrm{split}\left(Dp\right)\right)\dot{\Psi}_{\mathrm{RIII,in}}$$
$$q_{\mathrm{RIII,out}} = \frac{\int_{Dp,\min}^{Dp,\max} \dot{\Psi}_{\mathrm{RIII,out}} d\zeta}{\rho_{\mathrm{solid}}\left(1 - \varepsilon_{\mathrm{design}}\right)}$$

$$w_{\mathrm{RIII,out}}^{\mathrm{Me}} = w_{\mathrm{RIII,overflow}}^{\mathrm{Me}} = w_{\mathrm{RII,out}}^{\mathrm{Me}}$$

$$\frac{dN_{\mathrm{RIII}}^{\mathrm{acid}}}{dt} = \dot{N}_{\mathrm{RIII,in}}^{\mathrm{acid}} - \dot{N}_{\mathrm{RIII,out}}^{\mathrm{acid}} - \dot{N}_{\mathrm{RIII,overflow}}^{\mathrm{acid}}$$
$$\dot{N}_{\mathrm{RIII,in}}^{\mathrm{acid}} = \dot{N}_{\mathrm{RI,out}}^{\mathrm{acid}}$$
$$\dot{N}_{\mathrm{RIII,out}}^{\mathrm{acid}} = q_{\mathrm{RIII,out}}\,\rho_{\mathrm{solid}}\left(1 - \varepsilon_{\mathrm{design}}\right)\,C_{\mathrm{RIII}}^{\mathrm{acid}}$$
$$\dot{N}_{\mathrm{RIII,overflow}}^{\mathrm{acid}} = q_{\mathrm{RIII,overflow}}\,\rho_{\mathrm{solid}}\left(1 - \varepsilon_{\mathrm{overflow}}\right)C_{\mathrm{RIII}}^{\mathrm{acid}}$$
$$N_{\mathrm{RIII}}^{\mathrm{acid}} = V_{\mathrm{RIII}} C_{\mathrm{RII}}^{\mathrm{acid}}$$

$$T_{\mathrm{RIII,out}}^{\mathrm{Me}} = T_{\mathrm{RIII,overflow}}^{\mathrm{Me}} = T_{\mathrm{RII,out}}^{\mathrm{Me}}$$

$$\frac{\partial \psi_{\mathrm{RIV}}}{\partial t} = -\frac{\partial\left(v_z \psi_{\mathrm{RIV}}\right)}{\partial z} - \frac{\partial\left(v_{D_p}\psi_{\mathrm{RIV}}\right)}{\partial D_p}$$
$$v_{D_p} = -\frac{2}{\rho_{\mathrm{solid}}}\sum_{\mathrm{Me}} M_w^{\mathrm{Me}} r_{\mathrm{RIV}}^{\mathrm{Me}}$$

$$\frac{dM_{\mathrm{RIV}}}{dt} = \dot{M}_{\mathrm{RIV,in}} - \dot{M}_{\mathrm{RIV,out}}$$
$$\dot{M}_{\mathrm{RIV,in}} = q_{\mathrm{RIII,out}}\left(\rho_{\mathrm{acid}}\varepsilon_{\mathrm{design}} + \rho_{\mathrm{solid}}\left(1 - \varepsilon_{\mathrm{design}}\right)\right)$$
$$\dot{M}_{\mathrm{RIV,out}} = q_{\mathrm{RIV,tapping}}\left(\rho_{\mathrm{acid}}\varepsilon_{\mathrm{tapping}} + \rho_{\mathrm{solid}}\left(1 - \varepsilon_{\mathrm{tapping}}\right)\right)$$
$$\varepsilon_{\mathrm{tapping}} = \frac{\int_{Dp,\min}^{Dp,\max} \psi_{\mathrm{RIV}}\left(z_{\mathrm{tapping}}, \zeta\right) d\zeta}{\rho_{\mathrm{solid}} q_{\mathrm{RIV,tapping}}}$$

$$\frac{\partial w_{\mathrm{RIV}}^{\mathrm{Me}}}{\partial t} = -\frac{\partial\left(v_z w_{\mathrm{RIV}}^{\mathrm{Me}}\right)}{\partial z} + \frac{r_{\mathrm{RIV}}^{\mathrm{Me}} M_w^{\mathrm{Me}}}{\rho_{\mathrm{solid}}}$$
$$\varepsilon_{\mathrm{RIV}} = \frac{\int_{Dp,\min}^{Dp,\max} \psi_{\mathrm{RIV}} d\zeta}{\rho_{\mathrm{solid}}}$$
$$r_{\mathrm{RIV}}^{\mathrm{Me}} = -k_{\mathrm{RIV}}^{\mathrm{Me}} \exp\left(-\frac{E^{\mathrm{Me}}}{RT}\right)\left(w_{\mathrm{RIV}}^{\mathrm{Me}}\right)^{\gamma_1^{\mathrm{Me}}}\left(C_{\mathrm{RIV}}^{\mathrm{FeCl_3}}\right)^{\gamma_2^{\mathrm{Me}}}\left(C_{\mathrm{RIV}}^{\mathrm{HCl}}\right)^{\gamma_3^{\mathrm{Me}}}$$

$$\frac{\partial C_{\mathrm{RIV}}^{\mathrm{acid}}}{\partial t} = -\frac{\partial\left(v_z C_{\mathrm{RIV}}^{\mathrm{acid}}\right)}{\partial z} + \frac{r_{\mathrm{RIV}}^{\mathrm{acid}}\left(1 - \varepsilon_{\mathrm{RIV}}\right)}{\varepsilon_{\mathrm{RIV}}}$$
$$\begin{pmatrix} r_{\mathrm{RIV}}^{\mathrm{FeCl_3}} \\ r_{\mathrm{RIV}}^{\mathrm{HCl}} \\ r_{\mathrm{RIV}}^{\mathrm{FeCl_2}} \\ r_{\mathrm{RIV}}^{\mathrm{AlCl_3}} \\ r_{\mathrm{RIV}}^{\mathrm{CaCl_2}} \end{pmatrix} = \begin{pmatrix} 2\beta_{\mathrm{RIV}}^{\mathrm{Fe}} & 3\beta_{\mathrm{RIV}}^{\mathrm{Al}} & 2\beta_{\mathrm{RIV}}^{\mathrm{Ca}} \\ 2\left(1 - \beta_{\mathrm{RIV}}^{\mathrm{Fe}}\right) & 3\left(1 - \beta_{\mathrm{RIV}}^{\mathrm{Al}}\right) & 2\left(1 - \beta_{\mathrm{RIV}}^{\mathrm{Ca}}\right) \\ -3\beta_{\mathrm{RI}}^{\mathrm{Fe}} - \left(1 - \beta_{\mathrm{RIV}}^{\mathrm{Fe}}\right) & -3\beta_{\mathrm{RIV}}^{\mathrm{Al}} & -2\beta_{\mathrm{RIV}}^{\mathrm{Ca}} \\ 0 & -3 & 0 \\ 0 & 0 & -2 \end{pmatrix} \begin{pmatrix} r_{\mathrm{RIV}}^{\mathrm{Fe}} \\ r_{\mathrm{RIV}}^{\mathrm{Al}} \\ r_{\mathrm{RIV}}^{\mathrm{Ca}} \end{pmatrix}$$

$$\frac{\partial T_{\mathrm{RIV}}}{\partial t} = -\frac{\partial\left(v_z T_{\mathrm{RIV}}\right)}{\partial z} - \frac{\dot{Q}_{\mathrm{surroundings}}}{\rho C_p} + \frac{r_j \Delta H_j \Sigma_{\mathrm{RIV}}}{\rho C_p}$$

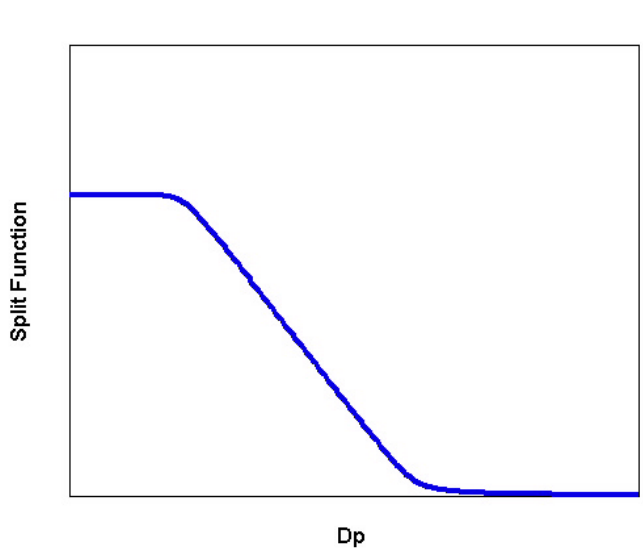

Figure 4.8: Split function.

- compartment I: a system of integrodifferential and algebraic equations.
- compartment II: a system of differential and algebraic equations.
- compartment III: a system of algebraic equations.
- compartment IV: a system of partial differential equations.

Note that compartments I, II and III can be considered a unique system of equations: Integro-DAE. In contrast, compartment IV is of another mathematical nature: Partial-DAE, and must be solved by a different algorithm. The solution of both systems is discussed below.

4.6.1 Solution of compartments I, II and III: Integro-DAE

The system of equations corresponding to compartment I, II and III can be solved by transforming the equations into a DAE system. Since the expressions for birth and death are quite complicated, the differential equations are coupled to each other, and the model is large in size, then the most convenient way to reduce the equations to a DAE is by discretization.

The main idea behind discretization methods is to divide the continuous internal coordinate ζ into a finite number of sections and assign a discrete value for the distribution function in each interval. This is done by integrating the continuous

PBE over a discrete size interval, say $\left[\zeta_i, \zeta_{i+1}\right]$ for $i = 1, \ldots, N$ where N is the number of intervals:

$$\Phi_i = \int_{\zeta_i}^{\zeta_{i+1}} \Psi(\zeta, t)\, d\zeta \tag{4.30}$$

$$\frac{d\Phi_i}{dt} = \int_{\zeta_i}^{\zeta_{i+1}} \left(\sum_j \dot{\Psi}_j^{\text{active}} + B - D \right) d\zeta. \tag{4.31}$$

Note that the terms on the right hand side of equation 4.31 depend on the density distribution function. The problem with discretization is that the new set of equations may not be closed in the set of unknowns, leading to a loss of autonomy (Ramkrishna 2000). Autonomy is restored by expressing the right hand side of equation 4.31 in terms of the discrete density distribution function variables Φ_i. The available discretization methods differ in how the integration is carried out and how autonomy is restored. Here, Φ_i is assumed to be represented by a grid point x_i, such that:

$$\zeta_i \leq x_i \leq \zeta_{i+1} \tag{4.32}$$

$$\Psi(\zeta, t) = \sum_i \Phi_i \delta(\zeta - x_i), \tag{4.33}$$

where $\delta(\zeta - x_i)$ is the Delta Dirac function, i.e.

$$\delta(\zeta - x_i) = \begin{cases} 1 & \text{if } \zeta = x_i \\ 0 & \text{if } \zeta = x_i \end{cases}.$$

Figure 4.9 illustrates how discretization is carried out.The problem with this type of discretization is that since the population of particles is assumed to exist only at representative grid points x_i, the birth and death of particles of these sizes may result in the formation of new particles whose sizes do not match with any other of the representative grid points. Such particles need to be represented through the chosen representative sizes. This difficulty was discussed in detail in (Kumar & Ramkrishna 1997). The strategy suggested in (Kumar & Ramkrishna 1997) is to assign the particles to the adjoining representative sizes such that two preserving properties of interest are preserved, for example number and mass. The technique as shown in (Kumar & Ramkrishna 1997) is not followed here, but the main idea of ensuring that some property of interest is preserved is used in this work. As it was pointed out with inequality 4.7, the mass of *daughter* particles originated from breakage of a *mother* particle of a certain size ζ must be less or equal to the mass of the mother particle. Such a preservation of mass must also

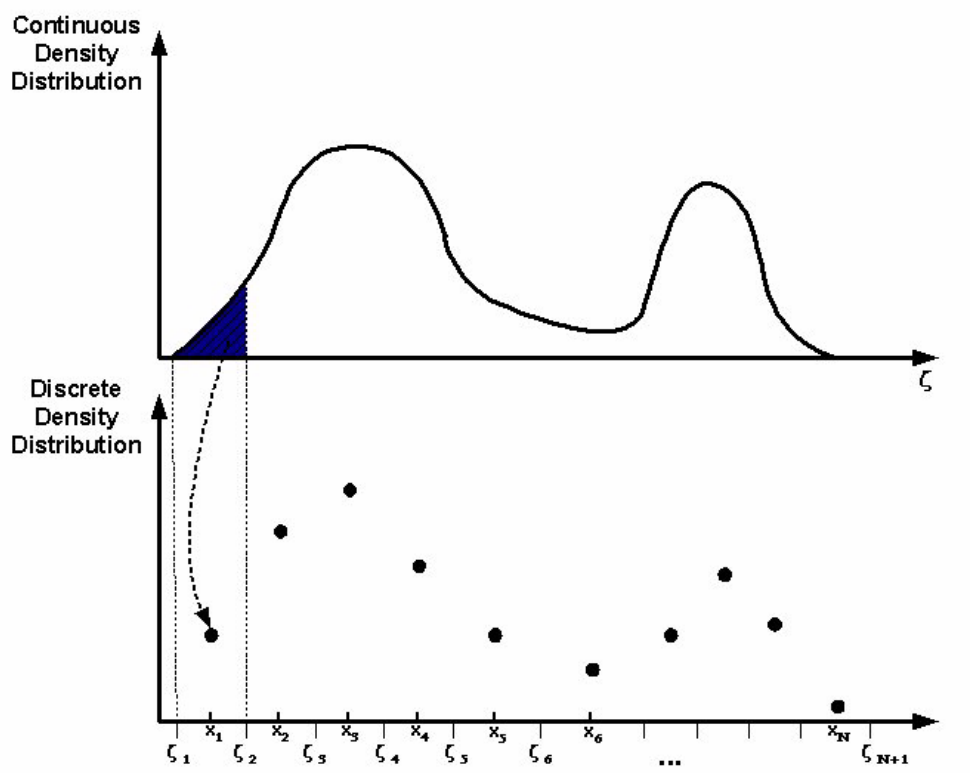

Figure 4.9: Discretization of a continuous density distribution function.

be conserved in the discretized system. To achieve this, the birth and death terms in equation 4.6 are approximated as follows:

$$\int_{\zeta_i}^{\zeta_{i+1}} (B - D)\, d\zeta \approx \sum_{k>i}^{N} \bar{b}(x_i, x_k)\, a(x_k, \theta)\ \Phi_k - a(x_i, \theta)\ \Phi_i, \tag{4.34}$$

where $\bar{b}(x_i, x_k)$ represents the weight fraction of *daughter* particles of representative size x_i that are generated during breakage a *mother* particle of size x_k. $\bar{B}$ thus represents the discretized PSD of daughter particles and is an $N \times N$ matrix

$$\bar{B} = \begin{array}{c} \xrightarrow{\text{Increase in size } x} \\ \begin{pmatrix} \bar{b}(x_1, x_1) & \bar{b}(x_1, x_2) & \dots & \bar{b}(x_1, x_{N-1}) & \bar{b}(x_1, x_N) \\ 0 & \bar{b}(x_2, x_2) & \dots & \bar{b}(x_2, x_{N-1}) & \bar{b}(x_2, x_N) \\ \vdots & \vdots & \ddots & \vdots & \vdots \\ 0 & 0 & \dots & \bar{b}(x_{N-1}, x_{N-1}) & \bar{b}(x_{N-1}, x_N) \\ 0 & 0 & \dots & 0 & \bar{b}(x_N, x_N) \end{pmatrix} \end{array}. \tag{4.35}$$

Since a *mother* particle can not generate *daughter* particles that are larger than itself, $\bar{B}$ is an upper diagonal matrix. And in order to ensure fulfillment of inequality 4.7, the following equivalent discrete inequality is established

$$\sum_{i=1}^{N} \bar{b}_{ik} = 1 \quad \forall k \in [1, \dots, N]\,, \tag{4.36}$$

stating that the sum of all elements in each column must be equal to 1. This implies that the sum of masses of daughter particles is exactly the mass of mother particles, i.e. no material is lost or dissolved during breakage. If material is lost, then a scale $\varkappa < 1$ has to be used in equation 4.36. Therefore, the elements of the matrix shown in equation 4.35 are calculated as follows:

$$\bar{b}(x_i, x_k) = \frac{\int_{\zeta i}^{\zeta_{i+1}} b(\zeta, x_k) d\zeta}{\sum_{k=1}^{N} \left(\int_{\zeta_i}^{\zeta_{i+1}} b(\zeta, x_k) d\zeta \right)}, \tag{4.37}$$

where $b(\zeta, x_k)$ is the continuous density distribution of *daughter* particles shown in equation 4.9.

The selection of the grid is an important stage. The larger the number of intervals, the better the approximation is, but at a larger computational cost. A compromise between precision and computation time has to be found. Moreover, the grid may have equidistant interval sizes or variable interval size, and the representative sizes may be fixed or moving. Here, a nonequidistant fixed grid is

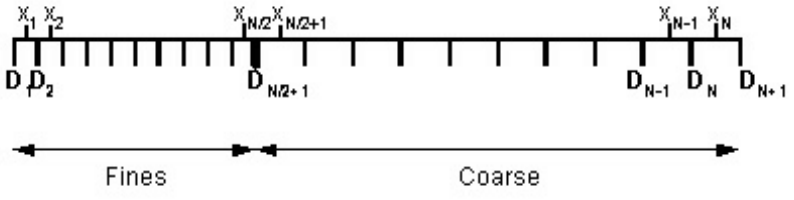

Figure 4.10: Grid used in the *Silgrain®* model.

chosen. The particle size distribution in compartment I is clearly bimodal, with a mode in the range of sizes of Si grains and another mode in the range of sizes of the FeSi feedstock. For this reason, the total number of intervals in the grid was divided into two, half of the intervals corresponding to the *fine* range and the other half to the *coarse* range. In each of the two divisions, equidistant intervals were used. Figure 4.10 sketches such a discretization grid. The total number of intervals was determined by trial-and-error, running simulations with different number of intervals until a further increase in the number of intervals does not provide a significant improvement in precision.

The discrete PBE corresponding to compartment I is the following set of differential equations

$$\frac{d\,\Phi_{i\,\mathrm{RI}}^{\mathrm{active}}}{dt} = \dot{\Phi}_{i\,\mathrm{RI,in}}^{\mathrm{active}} - \dot{\Phi}_{i\,\mathrm{RI,out}}^{\mathrm{active}} + \sum_{k>i}^{N} \bar{b}(x_i, x_k)\, a(x_k, T)\; \Phi_k - a(x_i, \theta)\; \Phi_i, \qquad (4.38)$$

for $i = 1, \ldots, N$. Similarly, the discrete PBE of the inert material is

$$\frac{d\,\Phi_{i\,\mathrm{RI}}^{\mathrm{inert}}}{dt} = \dot{\Phi}_{i\,\mathrm{RI,in}}^{\mathrm{inert}} - \dot{\Phi}_{i\,\mathrm{RI,out}}^{\mathrm{inert}}\,, \qquad (4.39)$$

and the discrete PBE corresponding to compartment II is

$$\frac{d\,\Phi_{i\,\mathrm{RII}}}{dt} = \dot{\Phi}_{i\,\mathrm{RII}} - \dot{\Phi}_{i\,\mathrm{RII}}\,. \qquad (4.40)$$

The moment functions of the PBE appearing in some other parts of the model are thus substituted by summations in the discretized model, for example, as follows:

$$\left(\int_{Dp,\min}^{Dp,\max} \Psi_{\mathrm{RI}}^{\mathrm{active}} d\zeta \right) \rightarrow \sum_{i=1}^{N} \Phi_{i\,\mathrm{RI}}^{\mathrm{active}}\,.$$

Therefore, a large DAE system is obtained when the model of compartments I, II and III is discretized. The model is large in size since each PBE is substituted by N ODEs, but the model can now be solved with well-known standard numerical algorithms.

Remark 1 *The resulting discretised system is an index-*0 *DAE, which is equivalent to an ODE. Originally the PBE was formulated in terms of an intensive density distribution* ψ*, and the resulting discretised system was an index-*1 *DAE (Dueñas Díez, Ausland, Fjeld & Lie 2002). DAE systems are not ODEs (Petzold 1985). The advantages of the formulation as an index-*0 *DAE vs. the formulation as an index-*1 *DAE are: easier initialization of the system of equations and faster calculation. For a brief discussion about the differences between ODE and DAE, please see appendix A.*

Remark 2 *The choice of mass to define the fraction of entities with a certain value of the particle size has implications for the numerical solution of the system. Hence, the resulting system has a several orders of magnitude smaller condition number than a formulation using number to define the fraction of entities with a certain value of the particle size. Hence, scaling is not necessary when mass-fraction is used, whereas scaling was essential when number-fractions were used (Dueñas Díez, Ausland, Fjeld & Lie 2002). Moreover, since the discretised density distribution is related to sieve analysis, there is no longer a need to manipulate or change the basis of the input PSDs and output PSDs. In the case of number-based distribution, several changes of basis were required. The calculation time has thus been further reduced.*

4.6.2 Solution of compartment IV: Functional PDAE

The system of equations corresponding to compartment IV can be solved by transforming the equations into a DAE system. The challenges that are present are:

- *microscopic* balance laws are used, implying that variables depend on time and position.
- a *microscopic* PBE is used, implying that we have a *functional* PDAE, i.e. the partial differential equations are applied to a distribution function, not to a scalar variable.
- a moving boundary between compartments III and IV is encountered. This limits the range of methods to solve PDAEs that can be used here.

The first stage in the solution process is to transform the functional PDAE into a scalar PDAE, i.e. to reduce the dimensionality of the problem with respect to the internal coordinate D_p. Since v_{D_p} is independent of the particle size D_p, a transformation applying a finite number of moments can be used to approximate the

model description, thus eliminating the infinite dimensionality of the continuous distribution. Let us recall that the jth moment is defined as

$$m_j = \int_0^{\infty} D_p^j \psi dD_p = \int_{D_{p,\min}}^{D_{p,\max}} D_p^j \psi dD_p. \tag{4.41}$$

The population balance can now be averaged in the D_p dimension by multiplying by $D_p^j dD_p$ and integrating the resulting equation from zero to the maximum particle size $D_{p,\max}$. Thus,

$$\int_{D_{p,\min}}^{D_{p,\max}} D_p^j \left[\frac{\partial \psi_{\mathrm{RIV}}}{\partial t} + \frac{\partial \left(v_z \psi_{\mathrm{RIV}} \right)}{\partial z} + \frac{\partial \left(v_{D_p} \psi_{\mathrm{RIV}} \right)}{\partial D_p} \right] dD_p = 0. \tag{4.42}$$

Reversing the order of integration and differentiation gives the first two terms as

$$\int_{D_{p,\min}}^{D_{p,\max}} D_p^j \left[\frac{\partial \psi_{\mathrm{RIV}}}{\partial t} + \frac{\partial \left(v_z \psi_{\mathrm{RIV}} \right)}{\partial z} \right] dD_p = \frac{\partial m_j}{\partial t} + \frac{\partial \left(v_z m_j \right)}{\partial z}, \tag{4.43}$$

which assumes that v_z is not a function of D_p. The third term of equation 4.42 needs some manipulation

$$\int_{D_{p,\min}}^{D_{p,\max}} D_p^j \frac{\partial \left(v_{D_p} \psi_{\mathrm{RIV}} \right)}{\partial D_p} dD_p = \int_{D_{p,\min}}^{D_{p,\max}} D_p^j \left[v_{D_p} \frac{\partial \left(\psi_{\mathrm{RIV}} \right)}{\partial D_p} + \psi_{\mathrm{RIV}} \frac{\partial \left(v_{D_p} \right)}{\partial D_p} \right] dD_p, \tag{4.44}$$

where the first integral term on the rhs can be integrated by parts after substituting v_{D_p} by equation 4.18

$$\begin{aligned}
\int_{D_{p,\min}}^{D_{p,\max}} D_p^j v_{D_p} \frac{\partial \left(\psi_{\mathrm{RIV}} \right)}{\partial D_p} dD_p &= \int_{D_{p,\min}}^{D_{p,\max}} D_p^j \left(-\frac{D_p}{3\rho_{\mathrm{solid}}} r_w \right) \frac{\partial \psi_{\mathrm{RIV}}}{\partial D_p} dD_p \\
&= -\frac{r_w}{3\rho_{\mathrm{solid}}} \left[D_p^{j+1} \psi_{\mathrm{RIV}} \right]_{D_{p,\min}}^{D_{p,\max}} \\
&\quad + \frac{r_w}{3\rho_{\mathrm{solid}}} (j+1) \int_{D_{p,\min}}^{D_{p,\max}} D_p^j \psi_{\mathrm{RIV}} dD_p \\
&= \frac{r_w}{3\rho_{\mathrm{solid}}} (j+1) \int_{D_{p,\min}}^{D_{p,\max}} D_p^j \psi_{\mathrm{RIV}} dD_p \\
&= \frac{r_w}{3\rho_{\mathrm{solid}}} (j+1) m_j,
\end{aligned} \tag{4.45}$$

where $D_{p,\min}$ and $D_{p,\max}$ can be chosen such that $\psi_{\mathrm{RIV}}(t, z, D_{p,\min}) = 0$ and $\psi_{\mathrm{RIV}}(t, z, D_{p,\max}) = 0$. The second term of equation 4.42 can be directly writ-

ten in terms of moments as follows

$$\begin{aligned}\int_{D_{p,\min}}^{D_{p,\max}} D_p^j \psi_{\mathrm{RIV}} \frac{\partial\left(v_{D_p}\right)}{\partial D_p} dD_p &= \int_{D_{p,\min}}^{D_{p,\max}} D_p^j \psi_{\mathrm{RIV}} \left(-\frac{r_w}{3\rho_{\mathrm{solid}}}\right) dD_p \\ &= -\frac{r_w}{3\rho_{\mathrm{solid}}} m_j, \end{aligned} \tag{4.46}$$

such that

$$\int_{D_{p,\min}}^{D_{p,\max}} D_p^j \frac{\partial\left(v_{D_p}\psi_{\mathrm{RIV}}\right)}{\partial D_p} dD_p = \frac{r_w}{3\rho_{\mathrm{solid}}} j m_j.$$

The *microscopic* PBE is thus reduced to

$$\frac{\partial m_j}{\partial t} = -\frac{\partial\left(v_z m_j\right)}{\partial z} - \frac{r_w}{3\rho_{\mathrm{solid}}} j m_j, \tag{4.47}$$

which not only gives a set of scalar PBEs, but indeed a set of uncoupled PBEs w.r.t. other moments[6]. The next question to be answered is how many moments are needed, i.e. how large j should be. This question is answered by the coupling with the remaining balance laws. Note that the void fraction in compartment IV is given by

$$\varepsilon_{\mathrm{RIV}} = 1 - \frac{\int_0^{Dp,\max} \psi_{\mathrm{RIV}} dD_p}{\rho_{\mathrm{solid}}} = 1 - \frac{m_0}{\rho_{\mathrm{solid}}}. \tag{4.48}$$

We therefore need at least the 0th moment of the distribution m_0, i.e. the total mass of particles. It is also interesting to follow the first and second moments of the density distribution, i.e. m_1 and m_2, which are related to the average mass of particles, and the standard deviation with respect to the average mass of particles, respectively.

After the moment transformation, the system has been reduced from a functional PDAE to a scalar PDAE. The PDAE should now be further simplified into a DAE, in order to be solved with standard available numerical routines. Compartment IV has variable volume, implying that there exists a moving boundary. This, in turn, limits the appliability of certain solution methods of PDAEs, such as the method of lines. The selected method here is the method of *weighted residuals*, which was already introduced in section 3.5. Such a method shows high-order accuracy and can handle cases with moving boundary. Note that we are mainly interested in the values of the variables at the outlet of the reactor more than in the exact profiles. One particular method of weighted residuals called *collocation* is suitable in such a case, since it is simple and can handle a moving boundary

[6]The moment PBEs are coupled to the other transport laws through r_w.

(Lie 2002). Consider the following general formulation of a PDE

$$\frac{\partial x}{\partial t} + \frac{\partial (v_z x)}{\partial z} = B(x) \tag{4.49}$$

$$s.t. \qquad x(0,z) = x_0(z) \qquad x(t,0) = x_F(t). \tag{4.50}$$

where $x(t,z)$ represents each of the variables of interest, i.e. m_j, $C_{\mathrm{RIV}}^{\mathrm{acid}}, w_{\mathrm{RIV}}^{\mathrm{Me}}$ and T_{RIV}.

A quadratic function is used as trial function:

$$x^*(t,z) = f_{x,0}(t) + f_{x,1}(t)\frac{z}{L} + f_{x,2}(t)\left(\frac{z}{L}\right)^2. \tag{4.51}$$

where L is the distance in the axial direction from the moving boundary to the bottom of the UR. Note that $f_{x,0}$, $f_{x,1}$, $f_{x,2}$ and L depend on time. A Dirac's δ-function is used as weighting function:

$$w(z) = \delta(z - z_i), \tag{4.52}$$

where the z_i's are known as collocation points. The residual function has exactly a zero value for the chosen collocation points:

$$R(t,z_i) = \left|\frac{\partial x^*}{\partial t} + \frac{\partial (v_z x^*)}{\partial z} - B(x^*)\right|_{z=z_i} = 0. \tag{4.53}$$

In this study, two collocation points are used: $z = \frac{L}{2}$ and $z = L$, whereas $z = 0$ represents the moving boundary. The following nomenclature is introduced

$$x^*(t,0) = x_F \tag{4.54}$$

$$x^*\left(t, \frac{L}{2}\right) = x_M \tag{4.55}$$

$$x^*(t,L) = x_L, \tag{4.56}$$

where x_L is the value at the bottom of the UR $(z = L)$, x_M is the value at the intermediate point $z = \frac{L}{2}$, and x_F is the value at the boundary between the separation and reaction regions $z = 0$. Figure 4.11 shows the selection of collocation points. Equation 4.51 can be rewritten in terms of the new nomenclature as follows

$$x^*(t,z) = x_F + (-3x_F + 4x_M - x_L)\frac{z}{L} + (2x_F - 4x_M + 2x_L)\left(\frac{z}{L}\right)^2. \tag{4.57}$$

Now by using the residual condition in equation 4.53, and after some formulae manipulation the PDE in equation 4.49 is transformed into the following set of

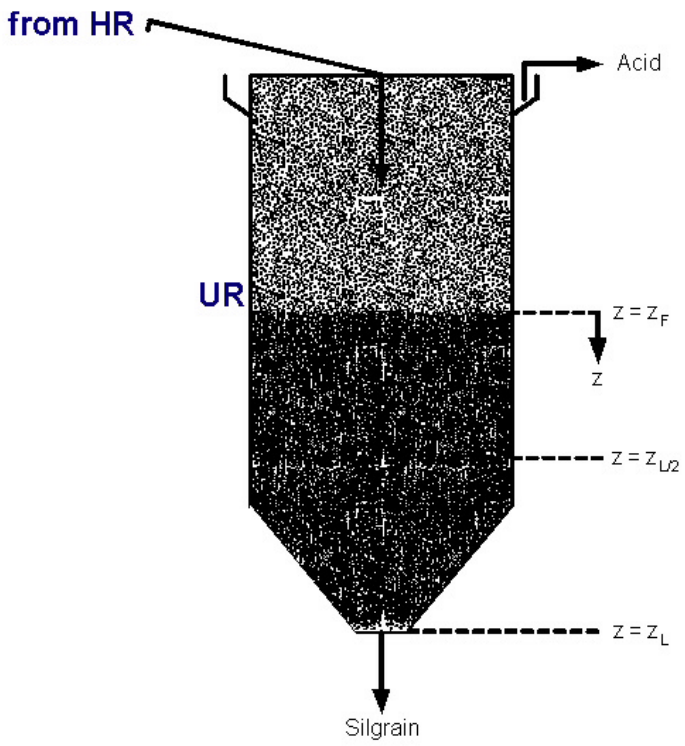

Figure 4.11: Selected collocation points and boundary point for the solution of the model of compartment IV.

ODEs

$$\frac{dx_L}{dt} = \left(\frac{dL}{dt} - v_z\right)\frac{x_F - 4x_M + 3x_L}{L} + B|_{z=L} - x\frac{\partial v_z}{\partial z}\bigg|_{z=L} \tag{4.58}$$

$$\frac{dx_M}{dt} = \left(\frac{1}{2}\frac{dL}{dt} - v_z\right)\frac{x_L - x_F}{L} + B|_{z=\frac{L}{2}} - x\frac{\partial v_z}{\partial z}\bigg|_{z=\frac{L}{2}}, \tag{4.59}$$

where dL/dt is given by the total mass balance for compartment IV. The set of ODEs together with the trial function and other algebraic equations again constitutes an 0-index DAE that can be solved with standard numerical algorithms.

Remark 3 *The main reason why the moment transformation gave a set of closed and uncoupled ODEs is that the birth and death terms are zero, and the dissolution rate v_{D_p} depends only linearly on D_p. Another choice of such a term may have given rise to a more complex set of ODEs.*

Remark 4 *The collocation method gives a zero residual only at the collocation points, but not at any other value of z. In addition, it has been assumed that the profiles fit well to a quadratic function, and only two collocation points are used, which is a fairly small number. No information about the exact profiles within the* UR *was available beforehand nor could be measured in the current industrial setup. This justifies the simple choice of trial function and collocation points. If additional information of the exact profiles was obtained, such a knowledge could be exploited in the selection of basis functions and collocation points.*

Remark 5 *The model of the* HR *and* UR *has been implemented in the widely used problem-solving environment* MATLAB® *and the set of DAEs are solved with the* `ode15s` *routine. The* `ode15s` *code is based on a variant of the Backward Differentiation Formulas (BDFs) called Numerical Differentiation Formulas (NDFs). For further information about* `ode15s`*, see (Shampine, Reichelt & Kierzenka 1999).*

4.7 Parameter estimation and model validation

The last stage in the modeling methodology is to validate the model using experimental data. One of the main reasons why models are built is to applied them for prediction purposes. Modeling results should not be trusted, though, before the model has been compared to experimental data.

As mentioned in section 3.6, validation of PBE models may become a challenging task. PBE models are large-scale and nonlinear in the parameters. In addition, models may be overparametrized, or have poorly identifiable parameters given the available data. Not only do such models have many and different types of

Table 4.9: Parameters of the Silgrain model categorized by type (number of parameters indicated in brackets).

HR	Dimensions	(7)
	Birth Rate	(6)
	Death Rate	(4)
	Kinetic Rate	(4)
	Hydrodynamics	(3)
	Heat Transfer	(1)
UR	Dimensions	(3)
	Kinetic Rate	(16)
	Hydrodynamics Top UR	(3)
	Heat Transfer	(1)
Physical & Thermodynamical Properties	Densities	(2)
	Heat Capacities	(2)
	Constants (gravity,R)	(2)
	Molecular Weights	(8)
	Enthalpies	(8)
Numerical Solution	Population Balance Equation	(4)
	Collocation Method	(2)

parameters (physical constants, birth and death rate parameters, dimensional parameters, etc.) but also the parameter accuracy varies considerably. Hence, some parameters are determined experimentally and are thus quite precise, while for some others only the order of magnitude could be guessed. Table 4.9 summarizes the parameters of the *Silgrain®* model.

Some additional challenges that are particular to PBE model validation are:

- Lack of appropriate measurement techniques. This has been a problem since the origin of PBE modelling. Although progress has been made in developing new measurement techniques for distributed properties, there are still very few sensors that are suitable for industrial and/or online use. In model validation, parameter identifiability is very dependent on how various parameters are projected into model states and subsequently how states are projected onto the measurements.

- The presence of several physically-observable compartments may hinder the accessibility of some measurements that are important in the model, such as measurements related to flows connecting the compartments.

- Coexistence of different scales in the dynamics, i.e. there may be variables with very fast dynamics and others with very slow dynamics. Therefore, care

Table 4.10: Summary of measurement campaign.

Inputs	FeSi *feed* rate
	FeSi *feed* solid phase composition
	FeSi *feed* PSD
	FeSi *feed* inert content
	Ambient temperature
	Silgrain Acid feed rate
	Silgrain Acid temperature
	Silgrain Acid composition
	UR tapping rate
Outputs	HR level of coarse solids
	HR *outflow* temperature
	HR *outflow* solid volumetric fraction
	HR *outflow* PSD
	HR *outflow* acid composition
	UR level of sedimented solids
	UR temperature profile
	Tapping UR solid volumetric fraction
	Tapping UR PSD
	Tapping UR solid phase composition
	Tapping UR solid phase composition

must be paid to sampling rates. Very fast dynamics may be impossible to capture in practice.

The limited measurement availability together with the large number of parameters justify the use of the systematic identifiability analysis and parameter estimation approach presented in section 3.6. The results of the application of such an approach to the *Silgrain*® model are summarized below.

First of all, the regular online measurements that are taken in the *Silgrain*® process are insufficient to estimate parameters or validate the model. Therefore, a special measurement campaign was planned (Dueñas Díez 2003) and carried out at Elkem Bremanger plant at Svelgen (Norway) in May 2003. Table 4.10 summarizes the necessary measurements for the validation. Sampling rates were specified in (Dueñas Díez 2003), but they are omitted here to protect confidential information. Let us just note that there is a large variation in the time constants among variables. Certain variables show very fast dynamics while others evolve slowly with time. Among the special measurements that had to be carried out, let us note two of them: the PSD of the FeSi feedstock and the temperature at certain fixed points of the outer surface of the UR. Figure 4.12 shows a picture taken after

sieving the feedstock. Figure 4.13 shows the location of two of the temperature sensors at the outer surface of the UR. The measurements at the outer surface are used as an indirect way to measure the temperature within the reactor.

Some unexpected difficulties arose during the experimental campaign. Hence, it was impossible to obtain representative samples of the slurry flowing from the HR to the UR. Regarding other variables, less amount of data were obtained than expected, which means that the available data could not divided into an data set for estimation and a test data set, as was desired. Hence, the prediction abilities of the model could not be analyzed. The data were just enough to carry out the parameter identifiability and estimation analysis.

4.7.1 Parameter identifiability and estimation of HR parameters

The methodology presented in section 3.6 and summarized in Figure 3.4 was applied to the HR. The measurements used for studying the parameter identifiability and estimating the HR parameters were the following:

- The time evolution of the boundary between compartment I and compartment II. The operation of the HR was altered to obtain data that are suitable to check how well the model predicts disintegration. Hence, feeding was stopped for a certain period of time so that it could be observed how the volume of compartment I decreases with time. In contrast, the acid flow at the bottom of the HR was kept in the normal operational value. After that, normal semibatch feeding of FeSi was used.

- The time evolution of the temperature at the top of the HR (compartment II) during one normal operational HR-cycle.

Let us comment on each of the stages of the identifiability and estimation analysis.

1. As shown in Figure 3.4, the first stage is a prior analysis. Those parameters that are known exactly, such as reactor dimensions, are omitted from the parameter identifiability analysis. Default values for the parameters $\boldsymbol{\theta}_{\text{default}}$ were already defined in section 4.5, and the outputs to be considered were mentioned above. The most difficult step in this prior analysis is thus to set up the basis simulation that resemble the experimental conditions and the initial values for the simulation. If some initial values are unmeasurable or can not be guessed, then they can be included as parameters in the parameter identifiability analysis. For the HR it was relatively straightforward to set up the basis simulation and the initial values could be measured or guessed.

Figure 4.12: Sieve results of the FeSi feedstock.

Figure 4.13: Location of two temperature sensors at the outer surface of the UR.

2. Once the basis simulation conditions are established, then the model outputs for the default parameter values can be obtained $y_{\text{default}}(t)$. Note that a time series is obtained, since it is desired to validate both the dynamic and static prediction abilities of the model.

3. Local sensitivities are numerically calculated as follows. Each parameter is perturbed at a time to the value $\theta_j = e_j \cdot \theta_{j,\text{default}}$ where e_j is typically in the range $[0.9, 1.1]$. Hence, a simulation is run for this perturbed value of the jth parameter. Then sensitivity of the ith output with respect of the jth parameter is calculated as:

$$s_{ij} \approx \frac{\theta_{j,\text{default}}}{\text{mean}\,(y_{i,\text{default}})} \frac{y_{i,\text{ perturbed}}(t, \theta_j) - y_{i,\text{ default}}(t)}{(e_j - 1) \cdot \theta_{j,\text{default}}}. \tag{4.60}$$

   Note that the mean value of the ith output and the default value of the parameter are used as scaling factors, and that sensitivities are functions of time. Figures 4.14 and 4.15 show the scaled sensitivities versus time. Note that the available outputs are most sensitive to the disintegration parameters $\theta_{10}(k_T)$ and $\theta_{11}(n)$. Note also that the sensitivity functions corresponding to such parameters show a very similar trend, indicating a possible collinearity between these two parameters.

4. In order to determine a quantitative measure of the importance of the individual parameters, the following ranking measure was used:

$$\delta_{i,j}^{\text{msqr}} = \sqrt{\sum_{k=1}^{N} s_{ij}^2(k)}, \tag{4.61}$$

   where k indicates the time instant. In the original work by (Brun et al. 2001), a unique ranking parameter that gives an overall idea of the effect of one parameter on all outputs was calculated. Here the ranking gives an overall idea of the overall effect of one parameter on one output. It is the time evolution that is integrated, not the effect on all outputs simultaneously. Table 4.11 shows the obtained ranking. Observe that the parameter with most effect on both outputs is θ_{10}, i.e. k_a in the *breakage frequency* function, see equation 4.8. The second parameter in the ranking is θ_{11} that is also one of the parameters of the *breakage frequency* function, i.e. the exponent n. Note that the third parameter in the ranking is different for the two outputs, and that the value of the ranking measure has decreased considerably already.

5. Only subsets containing the 3 parameters that ranked best in the parameter importance ranking, i.e. θ_{10}, θ_{11} and θ_7, are used in the identifiability

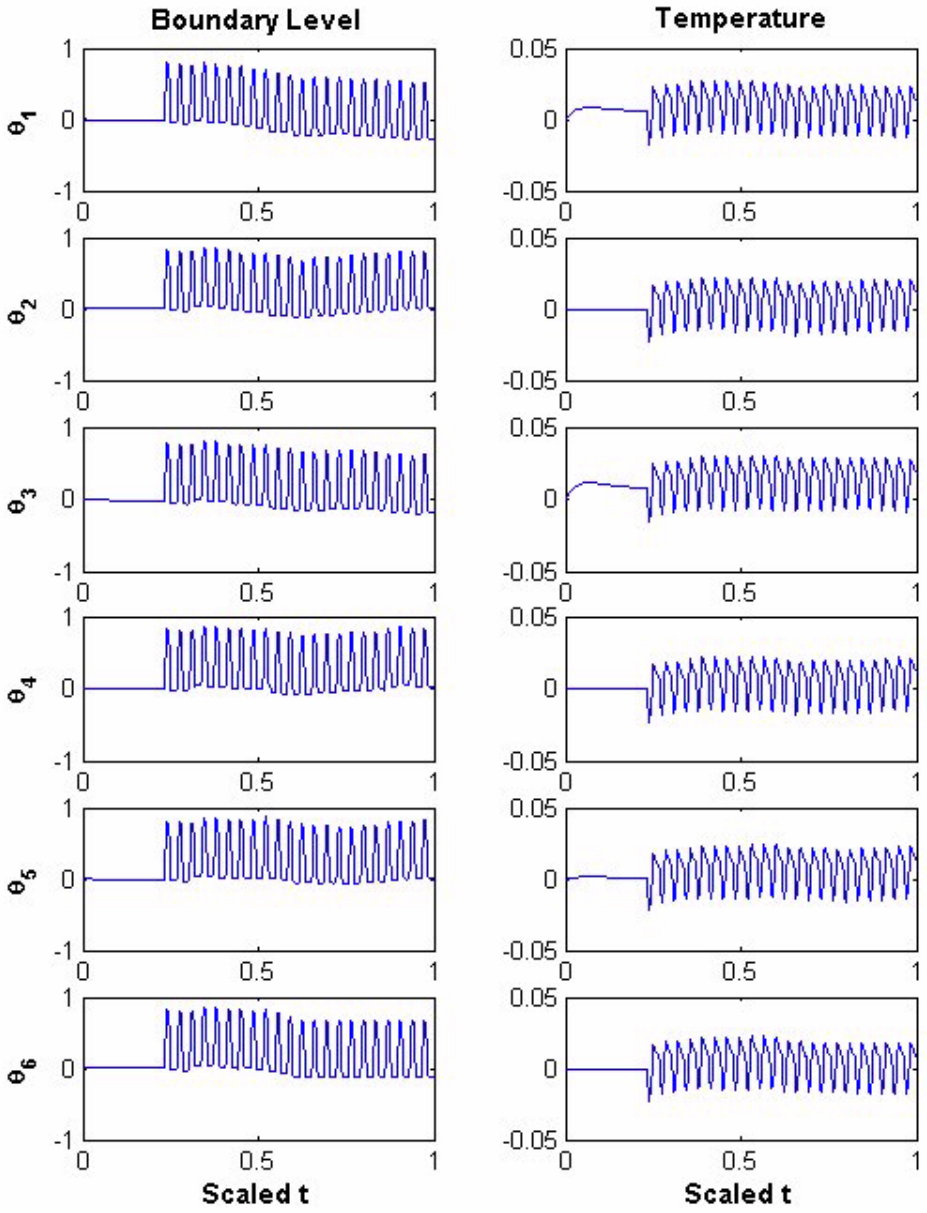

Figure 4.14: Sensitivity of the two HR outputs w.r.t changes in the HR parameters: θ_1 to θ_6 represent the reaction enthalpy parameters ΔH_{Me}.

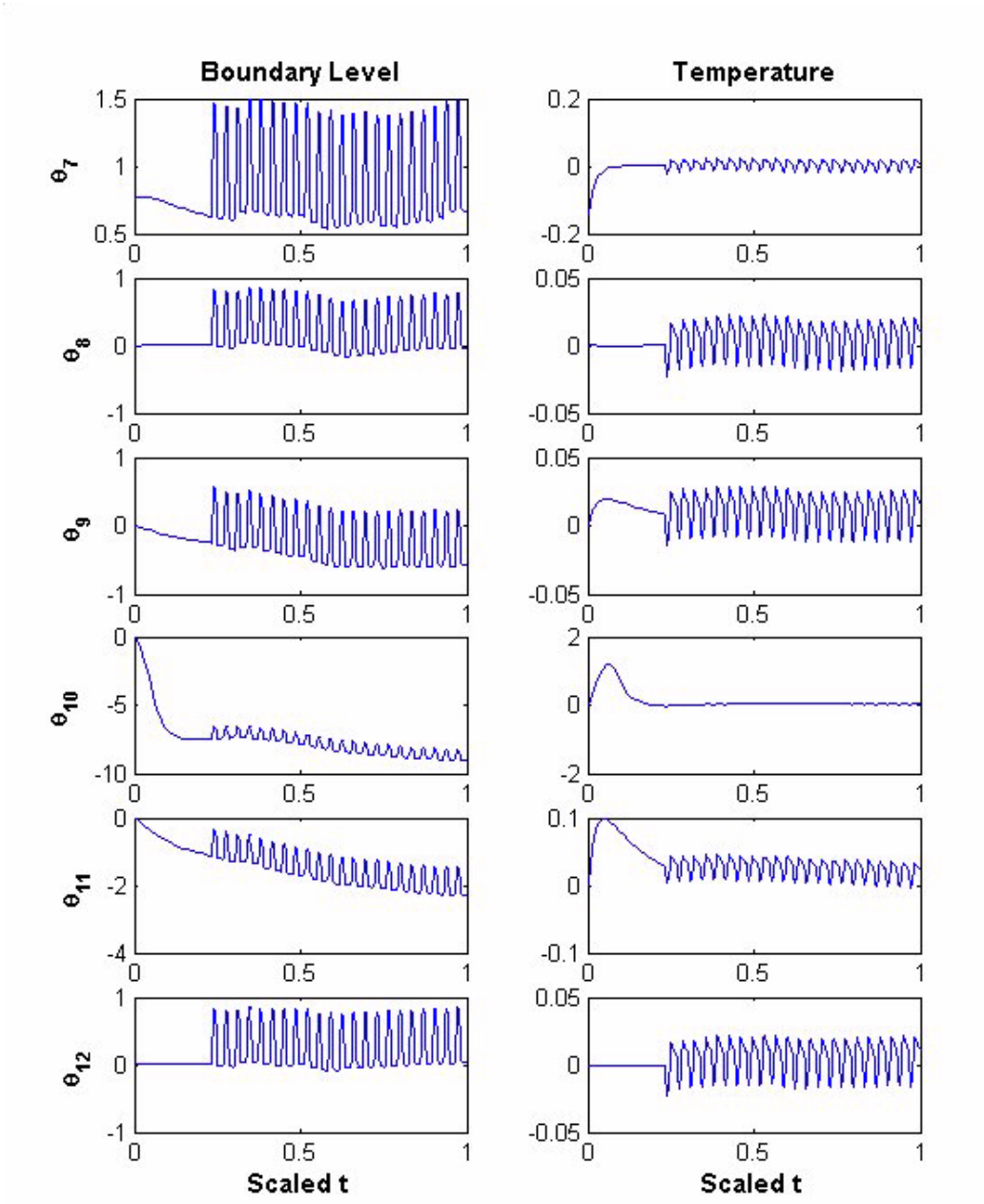

Figure 4.15: Sensitivity of the two HR outputs w.r.t changes in the HR parameters: θ_7 = void fraction; $\theta_8 = \beta$; θ_9, θ_{10} and θ_{11} are the disintegration parameters, and θ_{12} is the overall heat transfer coefficient.

Table 4.11: Ranked parameters according to the importance parameter ranking.

Boundary Level		**Temperature**	
$\delta_{1,j}^{\text{msqr}}$	*Parameter*	$\delta_{2,j}^{\text{msqr}}$	*Parameter*
207.6067	θ_{10}	2.8643	θ_{10}
41.7221	θ_{11}	0.8123	θ_{11}
25.0863	θ_7	0.4798	θ_3
11.2030	θ_{12}	0.4434	θ_9
11.1563	θ_4	0.4131	θ_1
11.1333	θ_5	0.4018	θ_7
10.8031	θ_2	0.3695	θ_5
10.7674	θ_9	0.3481	θ_4
10.6680	θ_8	0.3470	θ_{12}
10.5488	θ_6	0.3447	θ_8
9.9085	θ_3	0.3446	θ_2
9.6036	θ_1	0.3411	θ_6

Table 4.12: Identifiability of parameter subsets.

Parameter Subsets	γ_K
θ_7, θ_{10}, θ_{11}	360.97
θ_{10}, θ_{11}	151.32
θ_7, θ_{10}	56.80
θ_7, θ_{11}	86.72
θ_7	26.35
θ_{10}	25.33

analysis. Table 4.12 shows the results of the identifiability analysis. Remember that the larger the value of the collinearity index γ_K, the poorer the identifiability. Hence, it is clear that the subset containing the three parameters is very poorly identifiable. Subsets $S_{7,10}$ and $S_{7,11}$ show a better identifiability than subset $S_{10,11}$. This indicates a possible strong collinearity between parameters 10 and 11. Figure 4.16 plots the sensitivities corresponding to one parameter vs. the sensitivities to another parameter, which confirms again a strong collinearity between parameters 10 and 11.

6. According to the results in Table 4.12, the most identifiable subset is to choose θ_{10}. Alternatively, only θ_7 or the subset comprised of θ_7 and θ_{10} could also be identified.

7. First, θ_{10} is chosen and parameter estimation is carried out. The nonlinear

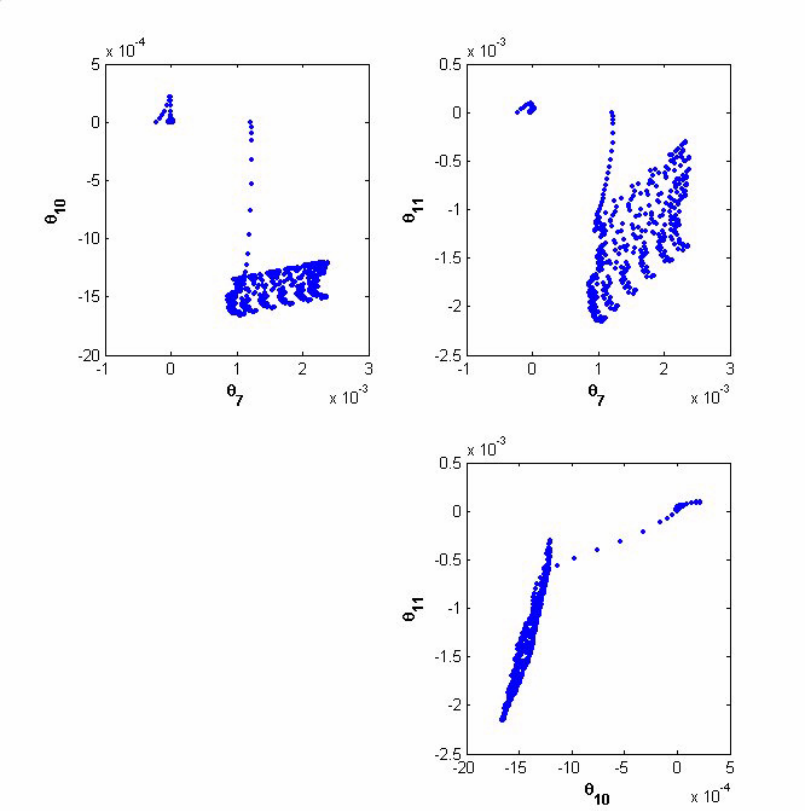

Figure 4.16: Collinearity among parameters.

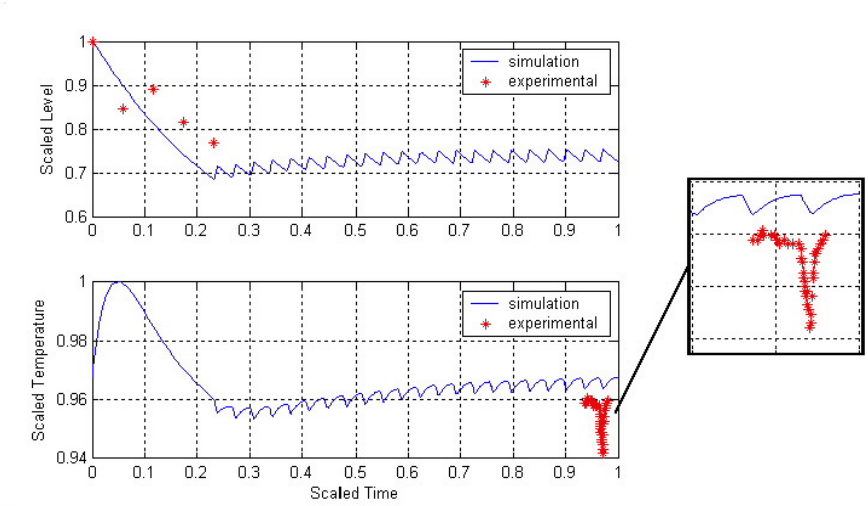

Figure 4.17: Experimental vs. simulation results for HR before parameter estimation, i.e. based on default values for the parameters.

least squares method is used, with the following optimization criteria:

$$\min_{\Delta\theta_{10}} J\left(\Delta\theta_{10}\right) = \sum_{k} \frac{1}{2} \left\{e\left(t_k, \Delta\theta_{10}\right)\right\}^T \mathrm{Sc} \left\{e\left(t_k, \Delta\theta_{10}\right)\right\}, \tag{4.62}$$

where e represents the difference between the experimental output and the simulated output, and Sc is a matrix with the appropriate scaling factors. The estimated parameter is thus

$$\hat{\theta}_{10} = \theta_{10,\text{default}} + \Delta\hat{\theta}_{10}, \tag{4.63}$$

where $\Delta\hat{\theta}_{10}$ is the optimal value provided by the optimization code `lsqnonlin` in MATLAB®. For details about the nonlinear least squares method, see (Walter & Pronzato 1997) and (Nocedal & Wright 1999). Figures 4.17 and 4.18 compare the experimental measurements with the simulation results before and after parameter estimation. From these figures we can conclude that the model fits better to the data after parameter estimation than before. The obtained value for $\Delta\theta_{10}$ was

$$\Delta\theta_{10} = \frac{-0.00065696}{0.047} = -1.3978 \times 10^{-2}\theta_{10,\text{default}} \tag{4.64}$$

corresponding to a value of the cost function of 27.308. Hence, the default value obtained in section 4.5 was quite close to the value obtained after

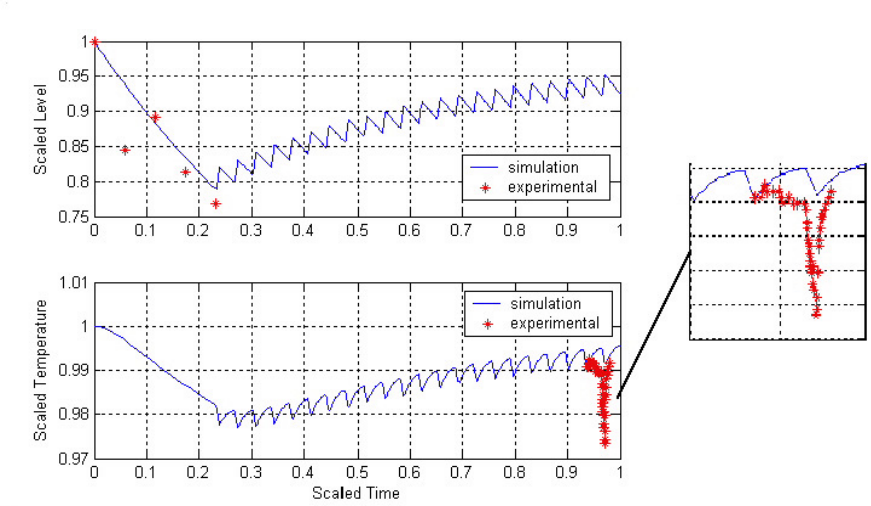

Figure 4.18: Experimental vs. simulation results for HR after parameter estimation.

parameter simulation. Notice, however, how such a small change in the parameter has a noticeable influence on the model response. The subset comprised of parameters θ_7 and θ_{10} is also studied. In this case the cost function is

$$\min_{\Delta\theta_7\ \Delta\theta_{11}} J\begin{pmatrix}\Delta\theta_7\\ \Delta\theta_{10}\end{pmatrix} = \sum_k \frac{1}{2}\left\{e\left(t_k,\ \begin{matrix}\Delta\theta_7\\ \Delta\theta_{10}\end{matrix}\right)\right\}^T \mathrm{Sc}\left\{e\left(t_k,\ \begin{matrix}\Delta\theta_7\\ \Delta\theta_{10}\end{matrix}\right)\right\}. \tag{4.65}$$

Figure 4.19 compares the experimental results with the simulation results after the parameter estimation. The obtained values for $\Delta\theta_7$ and $\Delta\theta_{10}$ are:

$$\Delta\theta_7 = 3.266\,7 \times 10^{-3}\theta_{7,\text{default}} \tag{4.66}$$
$$\Delta\theta_{10} = -1.456\,6 \times 10^{-2}\theta_{10,\text{default}} \tag{4.67}$$

corresponding to a value of the cost function of 27.303. Note that the value of the cost function is very similar to the value obtained when only one parameter was used for parameter estimation.

8. Finally, an analysis of the accuracy of the estimated parameters should be carried out. The model with the estimated parameters should be preferably tested on a new set of experimental data. However, all the available experimental data had to be used for the parameter estimation here. Hence, the estimates of the certainty of the parameter are more optimistic than

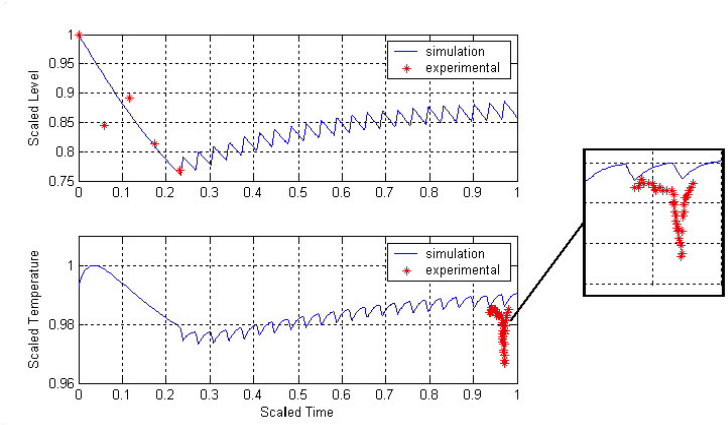

Figure 4.19: Experimental vs. simulation results for HR before parameter estimation (2 parameters).

those that would be obtained with an independent set of data. An order-of-magnitude confidence interval can be obtained by using the following relation (Rawlings & Ekerdt 2002)

$$\left(\theta-\hat{\theta}\right)^{T} H|_{\theta=\hat{\theta}} \left(\theta-\hat{\theta}\right) \leq 2s^{2} n_{p} F\left(n_{p}, n_{d}-n_{p}, \alpha\right), \tag{4.68}$$

where θ is the real value of the parameter, $\hat{\theta}=\theta_{\text{default}}+\Delta\theta$ is the estimated value of the parameter, n_p is the number of estimated parameters, n_d is the number of data points, a is the desired confidence level, F represents the F distribution which is tabulated in statistics handbooks such as (Rice 1995), H is the Gauss-Newton approximation of the Hessian, and s is the sample variance

$$s^{2}=\frac{1}{n_{d}-n_{p}} \sum \left\{e\left(t_{k}, \hat{\theta}\right)\right\}^{T} \mathrm{Sc}\left\{e\left(t_{k}, \hat{\theta}\right)\right\}=\frac{2J\left(\hat{\theta}\right)}{n_{d}-n_{p}}. \tag{4.69}$$

For the parameter estimation with one estimated parameter, $\theta_{10,\text{default}}$, the 95% confidence interval was:

$$\theta_{10,\text{default}}-0.0145\theta_{10,\text{default}} \leq \hat{\theta}_{10} \leq \theta_{10,\text{default}}+0.0145\theta_{10,\text{default}}, \tag{4.70}$$

while for the parameter estimation with two estimated parameters, the 95% confidence interval was:

$$\begin{pmatrix} \theta_7-\hat{\theta}_7 & \theta_{10}-\hat{\theta}_{10} \end{pmatrix} \begin{pmatrix} 1.1778 & 1.1097 \\ 1.1097 & 1.0679 \end{pmatrix} \begin{pmatrix} \theta_7-\hat{\theta}_7 \\ \theta_{10}-\hat{\theta}_{10} \end{pmatrix} \leq 1.71 \cdot 10^{-9}, \tag{4.71}$$

The resulting confidence intervals are relatively narrow, indicating a good approximation of the simulation results to the experimental results.

Therefore, we can conclude that the fitting of the HR model to the available data is satisfactory. As regards the prediction ability of the model, no strong statement should be made yet, since the prediction abilities of the model have not been tested. There was not enough experimental data to split into a data set for estimation and a test data set. But the fact that the model fits well to the experimental data is a positive result.

4.7.2 Parameter identifiability and estimation of UR parameters

The measurements used for studying the parameter identifiability and estimating the UR parameters were the following:

- The time evolution of the interphase level between compartments III and IV.
- The time evolution of the temperature at the top of the UR and of the outer reactor surface temperature at three fixed locations. Such measurements of temperatures are used as an indirect measurement of the temperature profile inside the reactor.
- The time evolution of the average metal impurity composition during one tapping cycle.

The parameters that are studied in the parameter identifiability analysis are: the reaction enthalpies (6 parameters: θ_1 to θ_6), the overall heat transfer coefficient used in the energy balance (1 parameter: θ_7), the initial conditions for the metallic impurity fractions at the outlet ($w^{\mathrm{Me}}_{\mathrm{RIV},E}(0,L)$) and the middle point ($w^{\mathrm{Me}}_{\mathrm{RIV},M}(0,z_M)$) (6 parameters: θ_8 to θ_{13}), the kinetic parameters corresponding to equation 4.14, i.e. $k^{\mathrm{Me}}_{\mathrm{RIV}}$, E^{Me}, γ^{Me}_1, γ^{Me}_2 and γ^{Me}_3 (15 parameters: θ_{14} to θ_{28}), the initial conditions of the temperature profile, i.e. $T_{\mathrm{RIV},E}(0,L)$ and $T_{\mathrm{RIV},E}(0,z_M)$ (parameters θ_{29}, θ_{30}), and a parameter related to the collocation method, θ_{31}.

Let us comment on each of the stages of the identifiability and estimation analysis.

1. The prior analysis of the measurement data is an important stage. Figure 4.20 shows the following UR experimental data: tapping rate, interphase level, temperature at the top of the reactor, and wall temperature at 4 locations on the outer reactor surface. These data reveal systematic trends, which in turn confirm that the evolution of the temperature profile inside

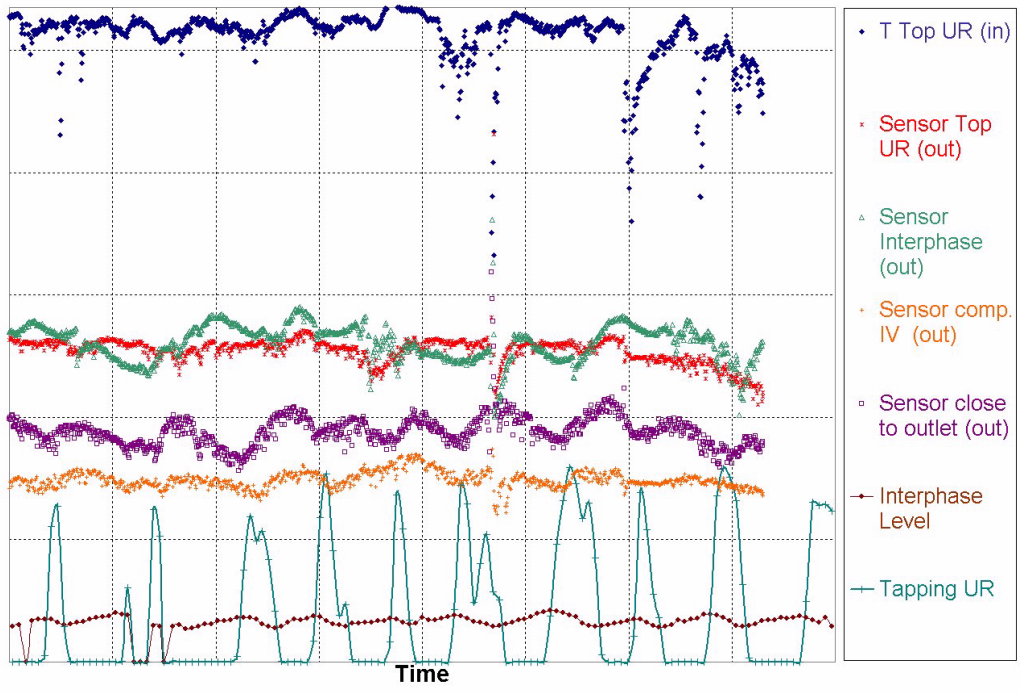

Figure 4.20: UR experimental data: tapping rate, interphase level, temperature at the top, and wall temperature at 4 locations on the outer reactor surface.

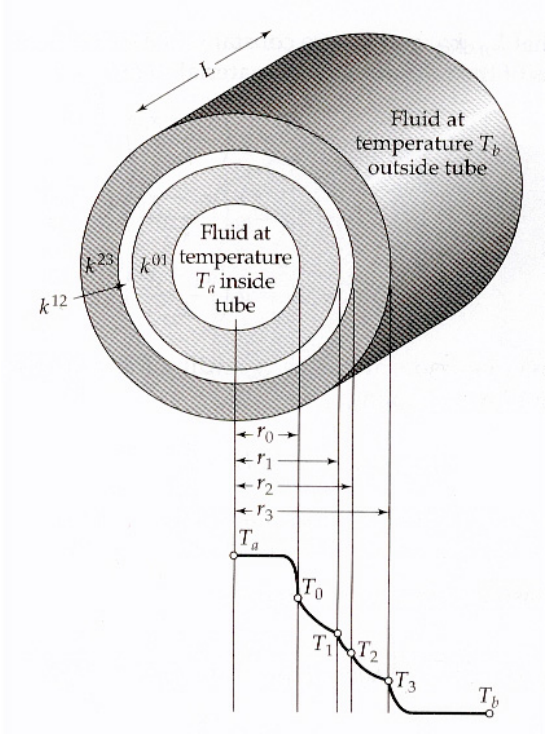

Figure 4.21: Thermal resistances of a composite cylindrical wall. Taken from (Bird et al. 2002)

the reactor can be indirectly followed by measuring wall temperatures at the outer surface. Note that outliers are observed; these must be removed somehow. The outliers are related to problems with the sensors. Hence, the first stage is to make a selection of data. Once this is done, the temperature profile inside the reactor has to be calculated from the measurements on the outside. According to heat transfer theory, we can consider the UR reactor wall as a series of thermal resistances. Figure 4.21 shows the series of thermal resistances corresponding to a composite cylindrical wall. The materials and thicknesses of the different layers in the wall are known. Assuming heat transfer through the wall, the following relation is fulfilled (Bird et al. 2002):

$$q_0 = \frac{T_{\text{in}}(z) - T_3(z)}{\left(\frac{1}{r_0 h_{\text{in}}} + \sum_{j=1}^{3} \frac{\ln(r_j/r_{j-1})}{k_j} \right)}, \tag{4.72}$$

where r_0 is the internal radius of the UR, r_j is the radius of the j-th layer, r_3 is the external radius of the UR, k_j is the heat conductivity of the wall

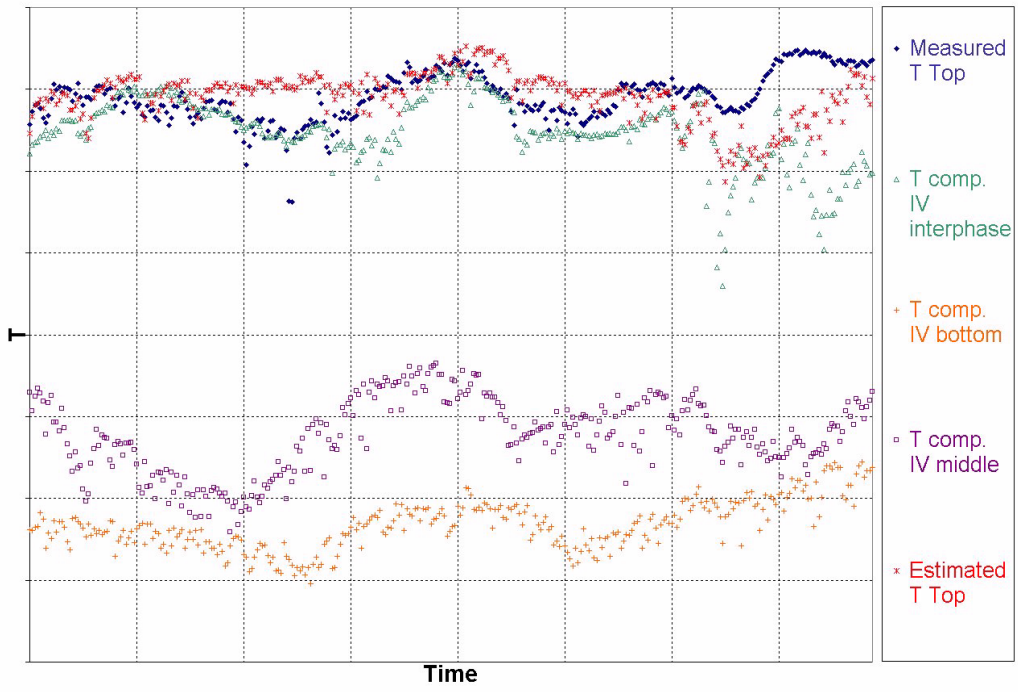

Figure 4.22: Comparison of measured and estimated temperature at the top of the UR, and selected experimental data for model validation: estimated internal temperature at 3 locations in the axial direction of the reactor.

layer, T_3 is the measured T on the outer surface, h_{in} is the heat transfer coefficient from the internal surface to the bulk slurry within the reactor, and q_0 is the heat flux through the wall. Note that $T_{\text{in}}(z)$ is not the only unknown in equation 4.72. The heat flux q_0 and h_{in} are also unknown. In order to solve this difficulty, we can use the measurement data at the top of the reactor, i.e. in compartment III, where both $T_{\text{in}}(z_{\text{top}})$ and $T_3(z_{\text{top}})$ were measured. The data are thus used to estimate the values of q_0 and h_{in} that minimize the error between the calculated $T_{\text{in}}(z_{\text{top}})$ through equation 4.72 and the measured $T_{\text{in}}(z_{\text{top}})$. Then, it is assumed that the obtained values for q_0 and h_{in} can be used for the other sensor locations. This is equivalent to the assumption that the heat transfer conditions do not change much along the reactor. Figure 4.22 shows the estimated values for the temperature inside the reactor for the selected data. As it can be observed, the estimated value of the temperature at the top of the UR does not match completely with the measured values, but it is in the same order of magnitude. The estimated temperature shows more or less the same dynamic trend as the

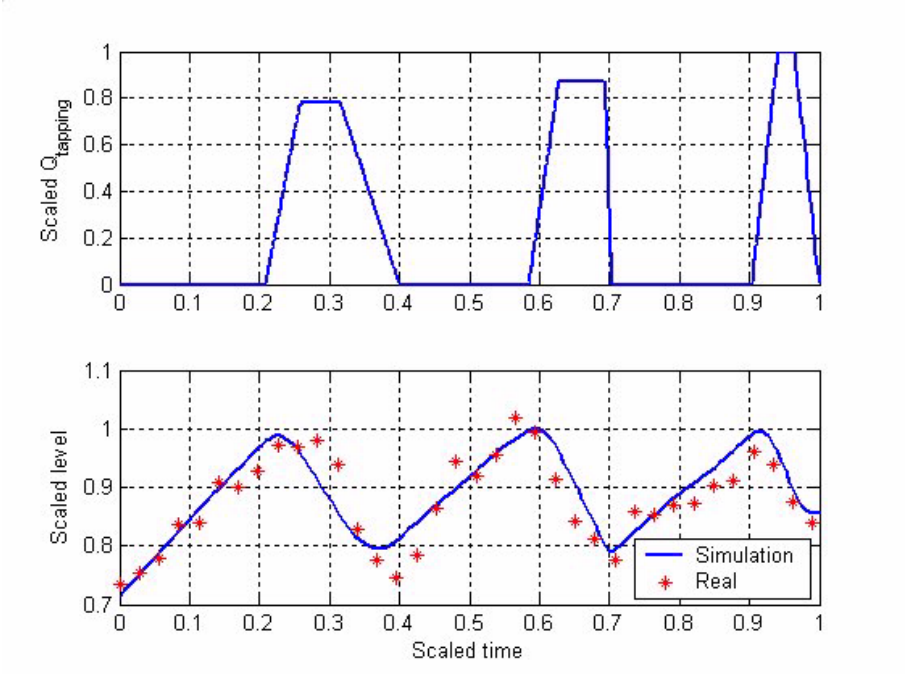

Figure 4.23: Basis simulation vs. real evolution of the interphase level between compartments III and IV.

measured data, although there seems to exist a delay.
Another aspect of the prior analysis is to decide the default values for the parameters. In the case of the HR, many of these parameters were known with a relatively good precision since they had been obtained experimentally or from reliable references in the literature. In contrast, for the UR the parameters were tuned by trial-and-error in a simulation study, so that these default values are not as good as in the case of the HR. Having good default values is important for the parameter estimation. The better the default values, the easier and the faster the parameter estimation is.

2. The basis simulation was then established to resemble the conditions used in the experimental campaign. In order to test the quality of the basis simulation, the interphase level measurements are compared to the values obtained in the simulation. As Figure 4.23 shows, the basis simulation is quite close to the real operation.

3. Then, sensitivities were calculated numerically according to equation 4.60. Due to the large number of parameters (31), graphical analysis of sensitivities is not recommended. The best thing to do is to use the parameter

ranking measure in equation 4.61 to study which parameters are the ones that influence the outputs to the largest extent.

4. The results of the parameter ranking $\delta_{i,j}^{\text{msqr}}$ are summarized in table 4.13. The parameters that affect the outputs most are the initial conditions for the equations describing the axial profiles within compartment IV. Hence, the calculated temperatures are mostly affected by the initial conditions of the temperature profile, i.e. $T_{\text{RIV},E}(0,L)$ and $T_{\text{RIV},M}(0,z_M)$ (parameters θ_{29}, θ_{30}). A parameter related to the collocation method, θ_{31}, has also a notable effect on the calculated temperatures. As regards the metallic impurity weight fractions at the bottom of the UR, the parameters that have the most influence are the respective initial conditions at the outlet (parameters θ_8, θ_9, and θ_{10}), i.e. $w_{\text{RIV},E}^{\text{Fe}}(0,L)$ affects $w_{\text{RIV},E}^{\text{Fe}}(t,L)$ the most, $w_{\text{RIV},E}^{\text{Al}}(0,L)$ affects $w_{\text{RIV},E}^{\text{Al}}(t,L)$ the most, and so on. Other parameters having noticeable influence on the metallic impurity weight fractions are the corresponding activation energies (θ_{15} to $w_{\text{RIV},E}^{\text{Fe}}(t,L)$, θ_{20} to $w_{\text{RIV},E}^{\text{Al}}(t,L)$, and θ_{23} to $w_{\text{RIV},E}^{\text{Ca}}(t,L)$) and the corresponding reaction orders γ_3^{Me} (parameters θ_{18}, θ_{23}, and θ_{28}). This means that after the parameter ranking, the number of parameters to be used for model validation has already been reduced from 31 to 12, possibly to just 6.

5. The next stage is to study collinearity among parameters, and parameter identifiability. Recalling the kinetic rate for the UR

$$r_{\text{RIV}}^{\text{Me}} = -k_{\text{RIV}}^{\text{Me}} \exp\left(-\frac{E^{\text{Me}}}{RT}\right) \left(C_{\text{RIV}}^{\text{FeCl}_3}\right)^{\gamma_1^{\text{Me}}} \left(C_{\text{RIV}}^{\text{HCl}}\right)^{\gamma_2^{\text{Me}}} \left(w_{\text{RIV}}^{\text{Me}}\right)^{\gamma_3^{\text{Me}}}, \qquad (4.73)$$

it is relatively straightforward to see that E^{Me} and γ_3^{Me} are collinear regarding their effects on the selected outputs, i.e. the effect of a change in E^{Me} could be compensated by changing γ_3^{Me} appropriately. Figure 4.24 plots the sensitivities corresponding to E^{Me} and to γ_3^{Me}, which confirm again the collinearity among these parameters. Now, parameter identifiability of the subsets shown in table 4.14 is analyzed. We can conclude that the first two subsets are not identifiable due to collinearity between parameters. The subset $\{\theta_8,\ \theta_9,\ \theta_{10},\ \theta_{29}, \theta_{30},\ \theta_{31}\}$ has a collinearity index that is small enough for the nonlinear least squares estimation.

6. Once the subset of parameters has been chosen, parameter estimation is carried out by means of nonlinear least squares. The cost function to be

Table 4.13: Values of the parameter ranking index for the UR.

	$T_{\text{location 1}}$	$T_{\text{location 2}}$	$T_{\text{location 3}}$	$w^{\text{Fe}}_{\text{RIV},E}$	$w^{\text{Al}}_{\text{RIV},E}$	$w^{\text{Ca}}_{\text{RIV},E}$
θ_1	$2.6 \cdot 10^{-8}$	$7.6 \cdot 10^{-9}$	$1.0 \cdot 10^{-8}$	$7.2 \cdot 10^{-13}$	$1.8 \cdot 10^{-13}$	$8.4 \cdot 10^{-13}$
θ_2	$7.4 \cdot 10^{-10}$	$2.1 \cdot 10^{-10}$	$3.0 \cdot 10^{-10}$	$1.4 \cdot 10^{-14}$	$1.0 \cdot 10^{-14}$	$4.5 \cdot 10^{-14}$
θ_3	$9.1 \cdot 10^{-9}$	$2.6 \cdot 10^{-9}$	$3.7 \cdot 10^{-9}$	$2.5 \cdot 10^{-13}$	$9.2 \cdot 10^{-14}$	$3.2 \cdot 10^{-13}$
θ_4	$4.0 \cdot 10^{-10}$	$1.2 \cdot 10^{-10}$	$1.6 \cdot 10^{-10}$	$1.0 \cdot 10^{-14}$	$1.0 \cdot 10^{-14}$	$1.1 \cdot 10^{-14}$
θ_5	$1.3 \cdot 10^{-9}$	$3.8 \cdot 10^{-10}$	$5.4 \cdot 10^{-10}$	$7.6 \cdot 10^{-14}$	$2.7 \cdot 10^{-14}$	$2.2 \cdot 10^{-14}$
θ_6	$8.8 \cdot 10^{-11}$	$2.5 \cdot 10^{-11}$	$3.6 \cdot 10^{-11}$	$5.8 \cdot 10^{-15}$	$8.5 \cdot 10^{-15}$	$1.1 \cdot 10^{-14}$
θ_7	$1.8 \cdot 10^{-5}$	$5.4 \cdot 10^{-6}$	$7.5 \cdot 10^{-6}$	$5.1 \cdot 10^{-10}$	$1.0 \cdot 10^{-10}$	$5.6 \cdot 10^{-10}$
θ_8	$7.2 \cdot 10^{-8}$	$2.0 \cdot 10^{-8}$	$2.9 \cdot 10^{-8}$	**2.310**	$2.3 \cdot 10^{-13}$	$8.2 \cdot 10^{-13}$
θ_9	$4.6 \cdot 10^{-9}$	$8.2 \cdot 10^{-10}$	$1.2 \cdot 10^{-9}$	$2.1 \cdot 10^{-12}$	**2.002**	$3.3 \cdot 10^{-12}$
θ_{10}	$2.8 \cdot 10^{-9}$	$8.2 \cdot 10^{-10}$	$3.2 \cdot 10^{-15}$	$7.6 \cdot 10^{-14}$	$2.1 \cdot 10^{-14}$	**2.132**
θ_{11}	$3.2 \cdot 10^{-15}$	$2.2 \cdot 10^{-15}$	$1.8 \cdot 10^{-15}$	$2.0 \cdot 10^{-14}$	$3.1 \cdot 10^{-14}$	$1.2 \cdot 10^{-14}$
θ_{12}	$1.2 \cdot 10^{-17}$	$1.2 \cdot 10^{-15}$	$1.0 \cdot 10^{-15}$	$3.6 \cdot 10^{-14}$	$4.2 \cdot 10^{-14}$	$5.1 \cdot 10^{-14}$
θ_{13}	$3.0 \cdot 10^{-16}$	$2.7 \cdot 10^{-15}$	$3.7 \cdot 10^{-15}$	$8.2 \cdot 10^{-15}$	$6.0 \cdot 10^{-15}$	$3.2 \cdot 10^{-14}$
θ_{14}	$2.5 \cdot 10^{-8}$	$7.3 \cdot 10^{-9}$	$1.0 \cdot 10^{-8}$	$2.8 \cdot 10^{-6}$	$9.8 \cdot 10^{-14}$	$3.2 \cdot 10^{-13}$
θ_{15}	$3.6 \cdot 10^{-7}$	$1.1 \cdot 10^{-7}$	$1.5 \cdot 10^{-7}$	$\mathbf{4.1 \cdot 10^{-5}}$	$1.1 \cdot 10^{-12}$	$4.1 \cdot 10^{-12}$
θ_{16}	$6.5 \cdot 10^{-9}$	$1.9 \cdot 10^{-9}$	$2.6 \cdot 10^{-9}$	$8.5 \cdot 10^{-7}$	$3.8 \cdot 10^{-14}$	$6.8 \cdot 10^{-14}$
θ_{17}	$2.3 \cdot 10^{-8}$	$6.7 \cdot 10^{-9}$	$9.3 \cdot 10^{-9}$	$2.6 \cdot 10^{-6}$	$6.8 \cdot 10^{-14}$	$2.6 \cdot 10^{-13}$
θ_{18}	$3.6 \cdot 10^{-7}$	$1.1 \cdot 10^{-7}$	$1.5 \cdot 10^{-7}$	$\mathbf{3.4 \cdot 10^{-5}}$	$9.2 \cdot 10^{-13}$	$3.3 \cdot 10^{-13}$
θ_{19}	$8.7 \cdot 10^{-9}$	$2.5 \cdot 10^{-9}$	$3.5 \cdot 10^{-9}$	$4.3 \cdot 10^{-13}$	$1.5 \cdot 10^{-6}$	$6.6 \cdot 10^{-13}$
θ_{20}	$1.3 \cdot 10^{-7}$	$3.8 \cdot 10^{-8}$	$5.3 \cdot 10^{-8}$	$6.0 \cdot 10^{-12}$	$\mathbf{2.3 \cdot 10^{-5}}$	$9.3 \cdot 10^{-12}$
θ_{21}	$2.2 \cdot 10^{-9}$	$6.5 \cdot 10^{-10}$	$9.1 \cdot 10^{-10}$	$3.8 \cdot 10^{-14}$	$3.6 \cdot 10^{-7}$	$1.8 \cdot 10^{-13}$
θ_{22}	$7.9 \cdot 10^{-9}$	$2.3 \cdot 10^{-9}$	$3.2 \cdot 10^{-9}$	$7.8 \cdot 10^{-14}$	$1.3 \cdot 10^{-6}$	$5.6 \cdot 10^{-13}$
θ_{23}	$1.3 \cdot 10^{-7}$	$4.0 \cdot 10^{-8}$	$5.5 \cdot 10^{-8}$	$4.2 \cdot 10^{-13}$	$\mathbf{2.4 \cdot 10^{-5}}$	$9.7 \cdot 10^{-12}$
θ_{24}	$1.2 \cdot 10^{-9}$	$3.6 \cdot 10^{-10}$	$5.1 \cdot 10^{-10}$	$6.3 \cdot 10^{-12}$	$1.0 \cdot 10^{-14}$	$7.3 \cdot 10^{-6}$
θ_{25}	$1.6 \cdot 10^{-8}$	$4.7 \cdot 10^{-9}$	$6.5 \cdot 10^{-9}$	$3.9 \cdot 10^{-14}$	$9.8 \cdot 10^{-14}$	$\mathbf{9.6 \cdot 10^{-5}}$
θ_{26}	$3.2 \cdot 10^{-10}$	$9.4 \cdot 10^{-11}$	$1.3 \cdot 10^{-10}$	$3.3 \cdot 10^{-14}$	$1.5 \cdot 10^{-15}$	$1.9 \cdot 10^{-6}$
θ_{27}	$1.1 \cdot 10^{-9}$	$3.2 \cdot 10^{-10}$	$4.6 \cdot 10^{-10}$	$7.3 \cdot 10^{-14}$	$1.6 \cdot 10^{-14}$	$6.7 \cdot 10^{-6}$
θ_{28}	$1.6 \cdot 10^{-8}$	$4.6 \cdot 10^{-9}$	$6.5 \cdot 10^{-9}$	$4.1 \cdot 10^{-13}$	$9.9 \cdot 10^{-14}$	$\mathbf{9.5 \cdot 10^{-5}}$
θ_{29}	**2.833**	**0.715**	**1.128**	$1.1 \cdot 10^{-5}$	$1.2 \cdot 10^{-5}$	$2.0 \cdot 10^{-5}$
θ_{30}	**11.35**	**12.698**	**6.960**	$4.1 \cdot 10^{-17}$	$3.0 \cdot 10^{-17}$	$5.1 \cdot 10^{-17}$
θ_{31}	**0.048**	**0.055**	**0.036**	$1.1 \cdot 10^{-17}$	$1.5 \cdot 10^{-17}$	$1.3 \cdot 10^{-17}$

Table 4.14: Identifiability of UR parameter subsets.

Parameter Subsets	γ_K
$\{\theta_8,\ \theta_9,\ \theta_{10},\ \theta_{15},\ \theta_{18},\ \theta_{20},\ \theta_{23},\ \theta_{25},\ \theta_{28},\ \theta_{29},\ \theta_{30},\ \theta_{31}\}$	56823
$\{\theta_8,\ \theta_9,\ \theta_{10},\ \theta_{15},\ \theta_{20},\ \theta_{25},\ \theta_{29},\ \theta_{30},\ \theta_{31}\}$	7356
$\{\theta_8,\ \theta_9,\ \theta_{10},\ \theta_{29},\ \theta_{30},\ \theta_{31}\}$	76.86

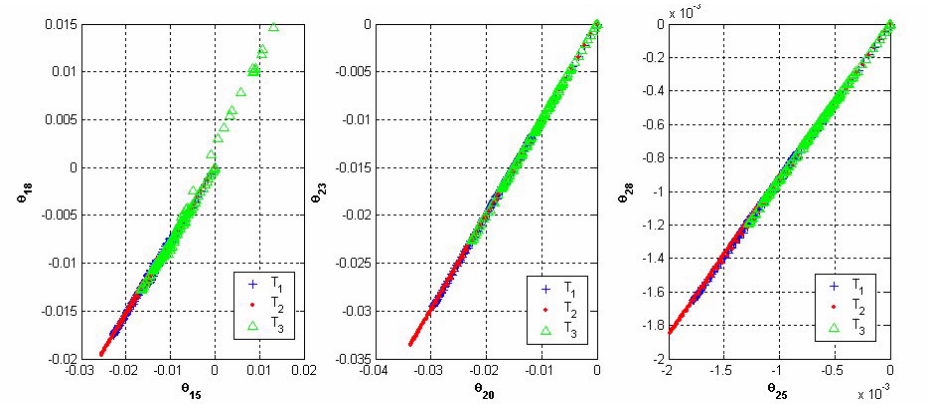

Figure 4.24: Collinearity betwen the activation energies $(\theta_{15}, \theta_{20}, \theta_{25})$ and the reaction orders $(\theta_{18}, \theta_{23}, \theta_{28})$ as regards their effect on the temperature at 3 locations in the UR.

minimized is thus

$$\min J \begin{pmatrix} \Delta\theta_8 \\ \Delta\theta_9 \\ \Delta\theta_{10} \\ \Delta\theta_{29} \\ \Delta\theta_{30} \\ \Delta\theta_{31} \end{pmatrix} = \sum_k \frac{1}{2} \left\{ e \begin{pmatrix} \Delta\theta_8 \\ \Delta\theta_9 \\ \Delta\theta_{10} \\ \Delta\theta_{29} \\ \Delta\theta_{30} \\ \Delta\theta_{31} \end{pmatrix} \right\}^T \mathrm{Sc} \left\{ e \begin{pmatrix} \Delta\theta_8 \\ \Delta\theta_9 \\ \Delta\theta_{10} \\ \Delta\theta_{29} \\ \Delta\theta_{30} \\ \Delta\theta_{31} \end{pmatrix} \right\}. \tag{4.74}$$

Nonlinear least squares provided the following estimates:

$$\begin{pmatrix} \Delta\hat{\theta}_8 \\ \Delta\hat{\theta}_9 \\ \Delta\hat{\theta}_{10} \\ \Delta\hat{\theta}_{29} \\ \Delta\hat{\theta}_{30} \\ \Delta\hat{\theta}_{31} \end{pmatrix} = \begin{pmatrix} -0.0127\ \theta_{8,\text{default}} \\ -0.0109\ \theta_{9,\text{default}} \\ 0.0308\ \theta_{10,\text{default}} \\ -0.0275\ \theta_{29,\text{default}} \\ 0.0105\ \theta_{30,\text{default}} \\ -\ 0.4243\,\theta_{31,\text{default}} \end{pmatrix}^T. \tag{4.75}$$

Figures 4.25 and 4.26 compare the experimental results with the simulation results with the default parameters. In turn, Figures 4.27 and 4.28 compare the experimental results with the simulated results with the estimated parameters. According to Figure 4.28, both the model and the experimental data show that the impurity fraction do not vary considerably during tapping. The model shows increasing trends with respect to tapping rate, which agrees with the model assumptions. In contrast, the experimental data does

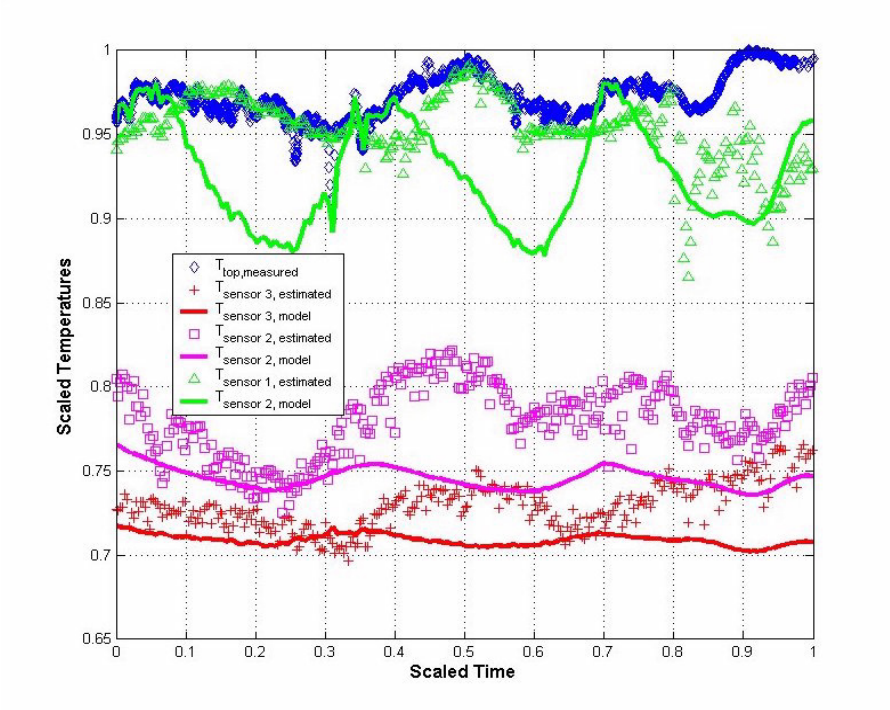

Figure 4.25: Experimental temperature values (markers) vs. simulated temperature values (lines) with default values for the parameters.

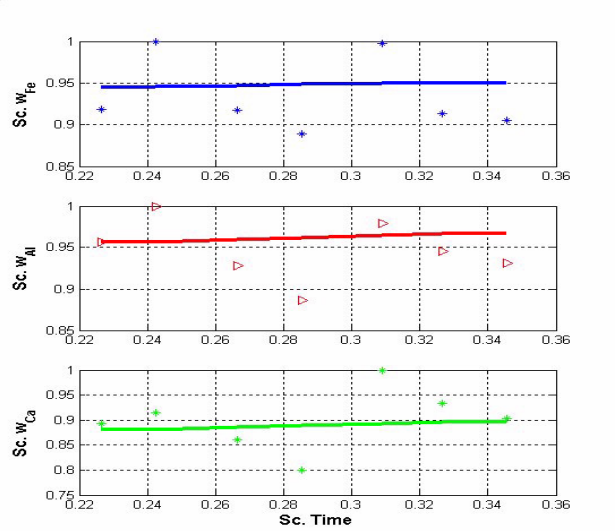

Figure 4.26: Experimental average metallic impurity fraction values (markers) vs. simulated results (lines) with default values for the parameters.

not show such a trend. Such a lack of trend may be due to sampling and/or measurement errors or due to funnel flow during tapping. But in any case, it is proven that the model gives results in the correct order-of-magnitude. As regards the temperature outputs, Figures 4.25 and 4.27 show that the approximation is better after parameter estimation than with the default parameter values. However, the fitting is not good. A systematic delay is observed between the simulations and the real data. When the temperatures inside the reactor were estimated from the measurements on the external surface, instantaneous heat transfer was assumed. Such an assumption is not realistic: the preprocessing of the data was not correct. A dynamic model of the heat transfer in the reactor wall should have been carried out to estimate the temperature profile in the reactor from the temperature profile on the external surface.

In order to achieve a more fair comparison between the simulated data and the measured data, a dynamic model of the heat transfer from the bulk slurry within the UR to the reactor external surface is developed. Such a heat transfer process could have been modeled by using an energy balance in the radial direction, but since such a process can easily be approximated by linear time invariant dynamics, an empirical model seems suitable for the purpose of data comparison. The *System Identification Toolbox* in MATLAB® is used to identify the linear models whose inputs are the temperatures calculated by the *Silgrain*® model, and whose

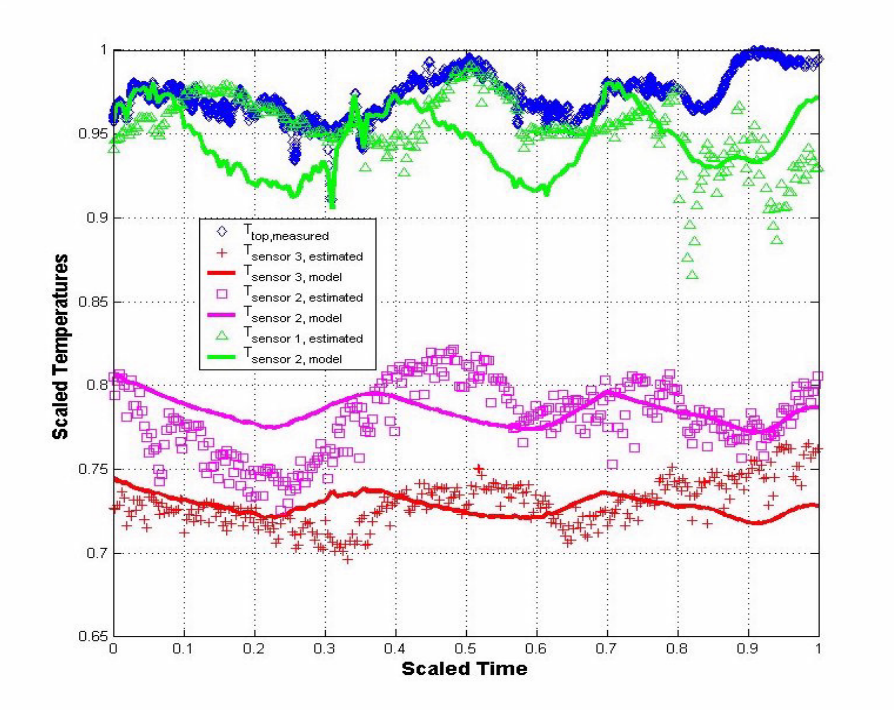

Figure 4.27: Experimental temperature values (markers) vs. simulated temperature values (lines) with estimated values for the parameters.

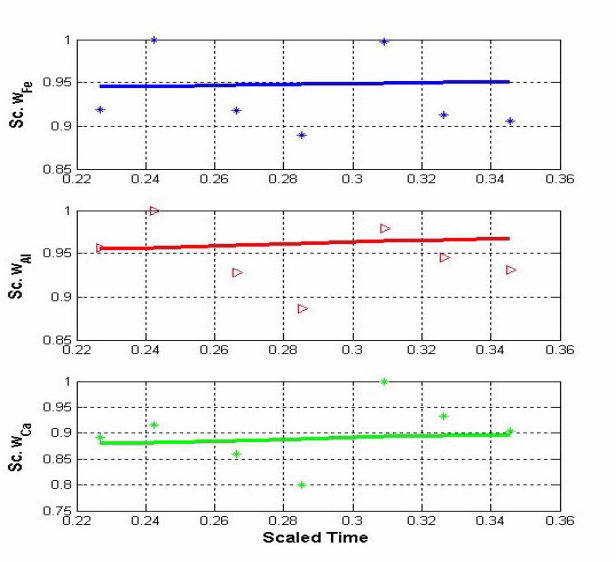

Figure 4.28: Experimental average metallic impurity fraction values (markers) vs. simulated results (lines) with the estimated values for the parameters.

outputs are the temperatures at the external surface of the UR. The input data are generated with the *Silgrain*® model, and using the parameter values after correcting with the estimated parameter changes shown in equation 4.75. Two types of model structures are tested:

1. ARX model structure, given by the following linear difference equation:

$$\begin{aligned} y_k + a_1 y_{k-1} + \ldots + a_{\mathrm{na}} y_{k-\mathrm{na}} &= b_0 u_{k-\mathrm{nk}} + b_1 u_{k-\mathrm{nk}-1} + \ldots + \\ & \quad b_{\mathrm{nb}} y_{k-\mathrm{nk}-\mathrm{nb}} + e_k, \end{aligned} \tag{4.76}$$

   where the modeler has to select the orders of the polynomials, i.e. na and nb, and the time delay nk.

2. ARMAX model structure, given by the following linear difference equation:

$$\begin{aligned} y_k + a_1 y_{k-1} + \ldots + a_{\mathrm{na}} y_{k-\mathrm{na}} &= b_0 u_{k-\mathrm{nk}} + b_1 u_{k-\mathrm{nk}-1} + \ldots + \\ & \quad b_{\mathrm{nb}} y_{k-\mathrm{nk}-\mathrm{nb}} + e_k + c_1 e_{k-1} + \ldots \\ & \quad c_{\mathrm{nc}} e_{k-\mathrm{nc}}, \end{aligned} \tag{4.77}$$

   where the modeler has to select the orders of the polynomials, i.e. na, nb, and nc, and the time delay nk.

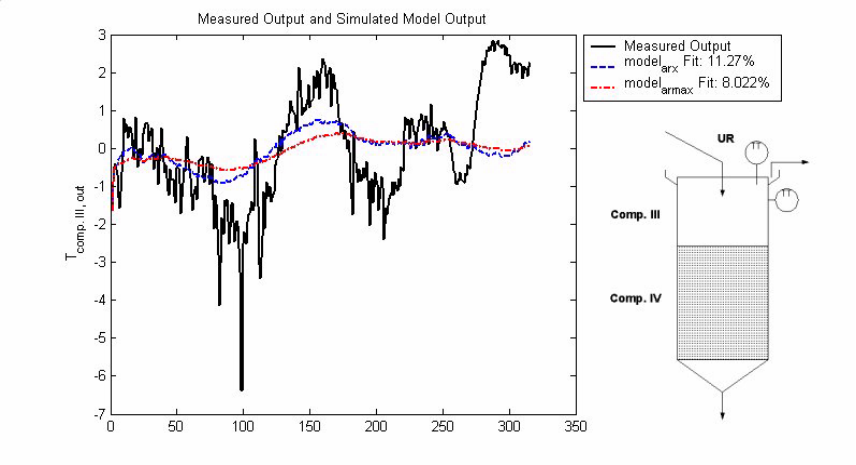

Figure 4.29: Comparison of the temperature on the outer surface predicted by the identified ARX and ARMAX models with the measured temperature.

For more information about model structures and model identification, see (Ljung 1999). Now, since there is a location in the reactor for which we do have a sensor inside the reactor, and a sensor on the external surface, we can use the resulting identified model as a reference to evaluate how good the fitting for the other 3 locations is. Figure 4.29 shows the resulting models for the case with measured input and output. As it can be observed, the fitting is not good, being particularly bad for the last 100 sample measurements. Some uncontrolled event may have happened with the process or with the sensors in that period. If we remove the last samples and run the identification again, then Figure 4.30 is obtained, which shows a much better approximation. Figures 4.31, 4.32, and 4.33 compare the model responses with the experimental data corresponding to the respective 3 sensor locations. The approximation is now satisfactory, and the model responses are much closer to the experimental data than in the comparison carried out in Figure 4.27. Note that, in most cases, the ARX models provide a better fitting than the ARMAX models. It is important to check whether the identified heat transfer models have similar or different dynamic behavior, i.e. time constants, delays, etc. Figure 4.34 shows the step responses of the identified ARX models for the different sensor locations. It can be observed that the model corresponding to the measurements inside and on the external surface shows a much smaller delay than the remaining three other models. Such a result may indicate that the heat transfer conditions in compartment III and compartment IV are quite different. In compartment III the solid/liquid ratio is much smaller than in compartment IV, while the turbulence is considerably stronger in the former than in the latter.

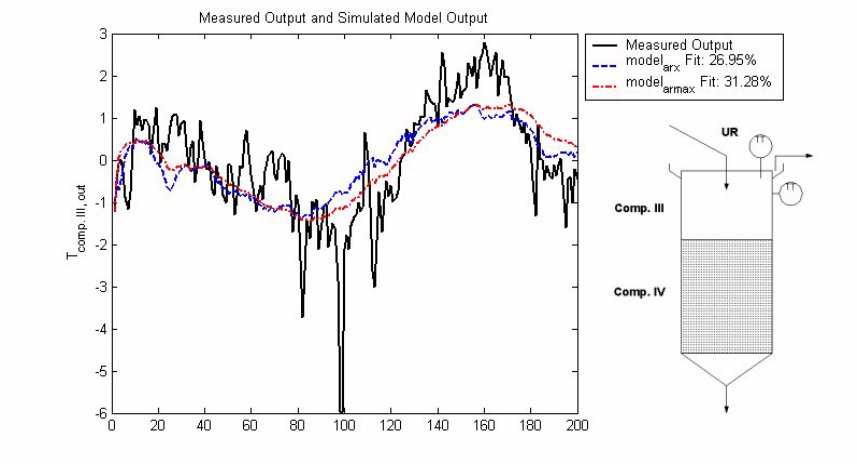

Figure 4.30: Comparison of the temperature on the outer surface predicted by the identified ARX and ARMAX models with the measured temperature (last samples ignored).

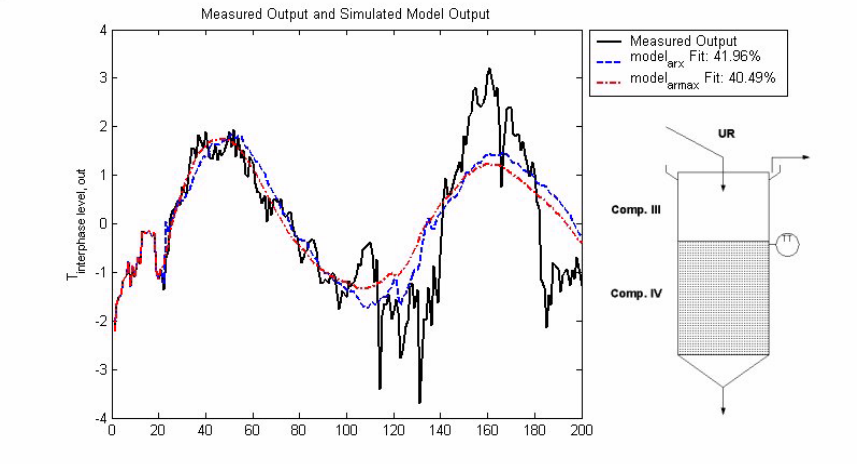

Figure 4.31: Identification of the heat transfer model for the sensor located at a height close to the interphase level between compartments III and IV.

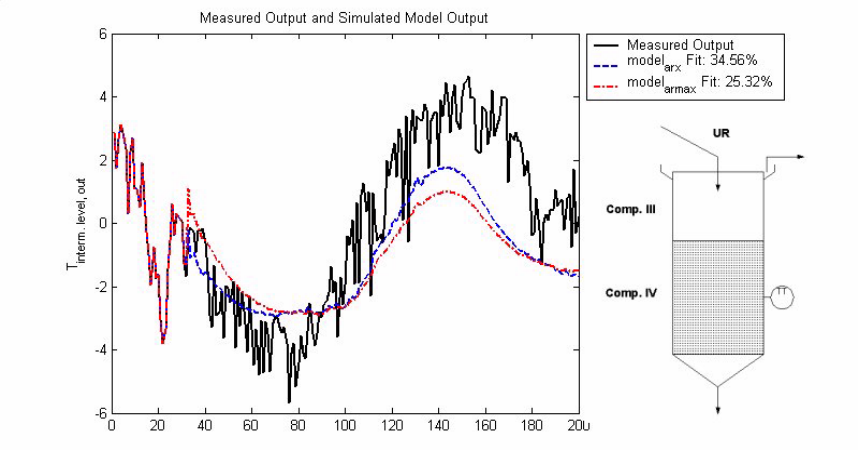

Figure 4.32: Identification of the heat transfer model for the sensor located at a height close to the intermediate level of compartment IV.

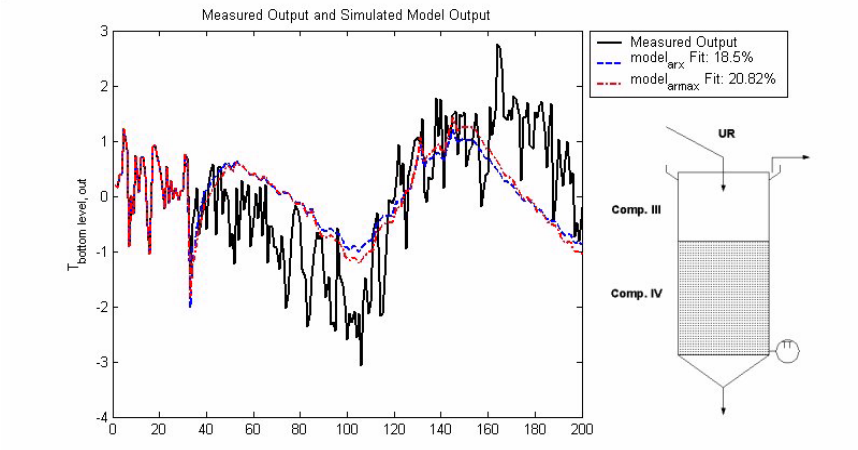

Figure 4.33: Identification of the heat transfer model for the sensor located at a height close to the bottom of compartment IV.

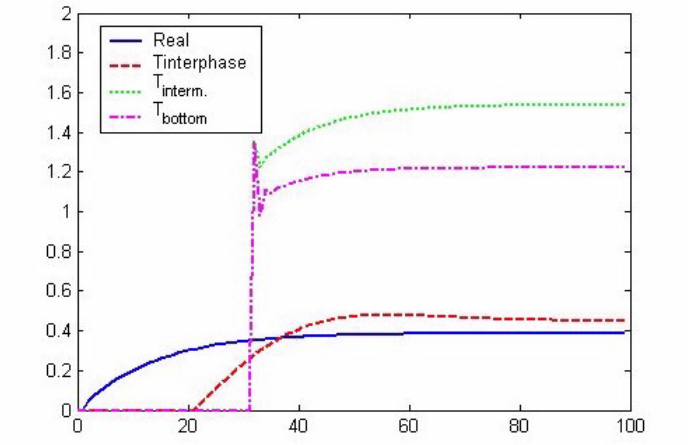

Figure 4.34: Comparison of the step response of the identified ARX models.

Therefore, a conclusion that may be derived from Figure 4.34 is that in compartment IV the limiting stage seems to be the heat transfer from the bulk (thick) slurry to the internal reactor wall. The parameter estimation for the UR model can be carried out again, now combining the *Silgrain*® model with a dynamic heat transfer model. We select ARX as the model structure, and keep the same polynomial orders and delays as the ones corresponding to Figures 4.31, 4.32, and 4.33. Note that the nonlinear least squares problem becomes more complex, since for each function evaluation 3 ARX models are identified. To reduce calculation time only parameters θ_{29}, θ_{30}, and θ_{31} are re-estimated, and the default values used are the corrected estimates after the previous parameter estimation run. Nonlinear least squares provides the following parameter estimates:

$$\begin{pmatrix} \Delta\hat{\theta}_{29} \\ \Delta\hat{\theta}_{30} \\ \Delta\hat{\theta}_{31} \end{pmatrix} = \begin{pmatrix} -0.0348\ \theta_{29,\text{new default}} \\ -0.0247\ \theta_{30,\text{new default}} \\ 0.1462\ \theta_{31,\text{new default}} \end{pmatrix}. \tag{4.78}$$

Figures 4.35, 4.36, and 4.37 compare the model responses after the last parameter estimation with the measured data. A certain improvement in the fitting can be noticed for the new parameters, as compared to Figures 4.31, 4.32, and 4.33.

Therefore, we can conclude that the fitting of the UR model to the available data is satisfactory. The choice of basis functions and of the collocation points in the UR model influence the model solution. However, the assumptions made for these elements in the solution method seem to be appropriate so far, since a good fitting to the experimental data is obtained. As regards the prediction ability of the model, no strong statement should be made yet, since the prediction

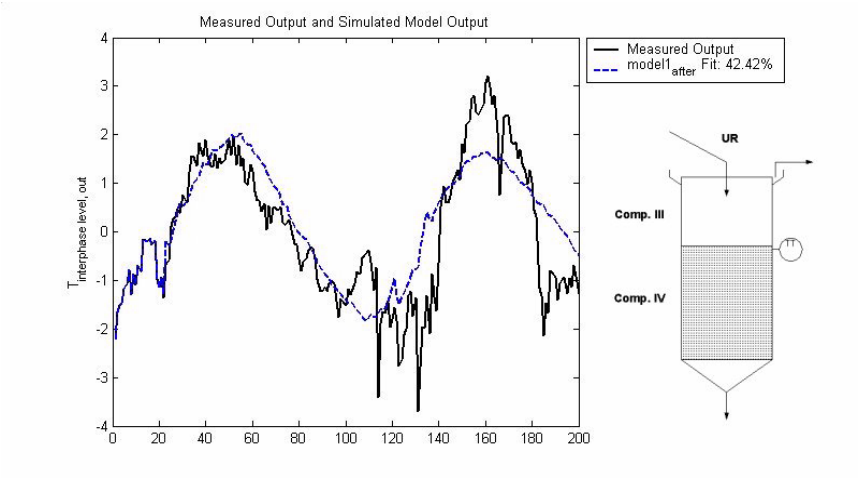

Figure 4.35: Comparison of the model outputs after parameter estimation with the real data, corresponding to the sensor located close to the interphase level between compartments III and IV.

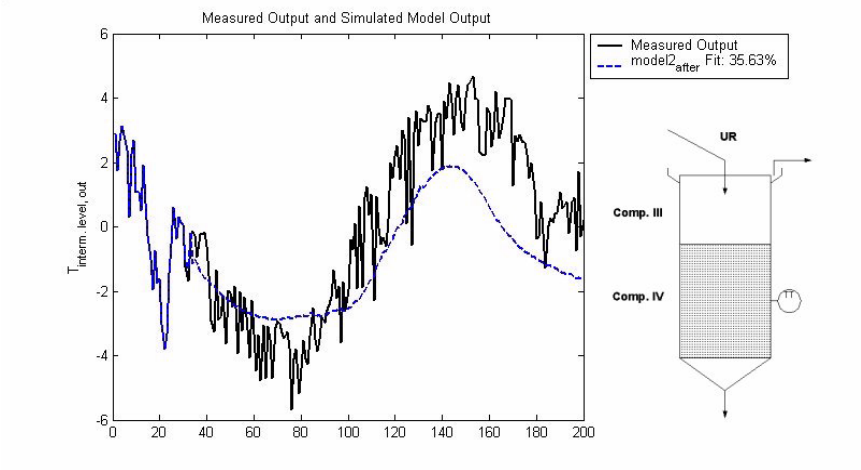

Figure 4.36: Comparison of the model outputs after parameter estimation with the real data, corresponding to the sensor located at a height close to the intermediate level of compartment IV.

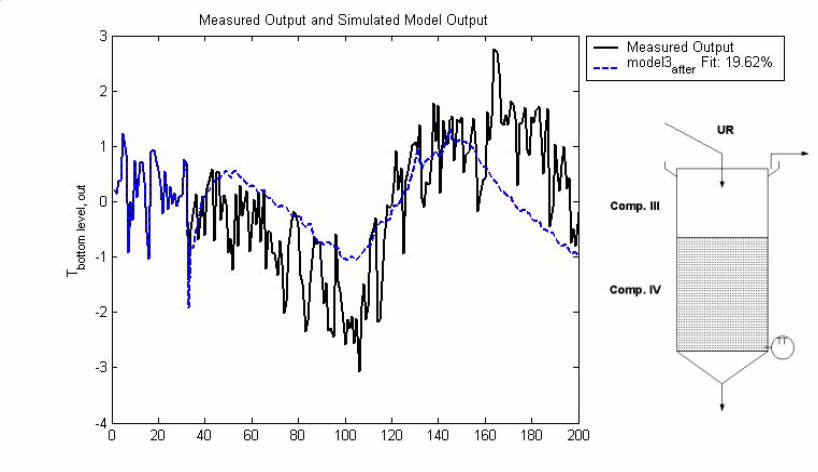

Figure 4.37: Comparison of the model outputs after parameter estimation with the real data, corresponding to the sensor located at a height close to the bottom of compartment IV.

abilities of the model have not been tested. Indeed, a more exhaustive parameter estimation and model validation campaign is recommended for the UR model. In such a campaign, it would be highly recommended to collect more measurements and to measure the initial profiles within the reactor, such that the model can be tested in a more proper way.

4.7.3 Some remarks about the parameter estimation of the model

The parameter estimation problems shown above are numerically demanding since we are dealing with large DAE systems. A common problem with these types of models is that parameters tend to be collinear, which results in poor identifiability. For this reason, using a method to analyze parameter sensitivity and parameter identifiability is particularly useful for these types of problems. Such an analysis provides a subset of parameters that is suited for parameter estimation, i.e. where the parameter subset has high sensitivity and low collinearity.

The parameter estimation corresponding to the UR model has provided two important lessons:

- A correct pre-treatment of the data is an essential stage in parameter estimation. Hence, it was proven how a static model of the heat transfer in the radial direction of the UR provided a fitting that was unsatisfactory,

while the introduction of a dynamic model of such a heat transfer provided a satisfactory fitting.

- Determining the initial state of the system is also key in parameter estimation. The initial state of the UR was not known. Hence, it is reasonable that the parameter identifiability analysis gave the initial conditions as the most important parameters to be identified.

4.8 Model uses

Dynamic models based on the balance laws can be used for different purposes. We distinguish here between applications in which the model is used off-line from those applications that use the model on-line.

4.8.1 Off-line applications

1. *System analysis* by simulation. The model can be used to simulate both the standard operation conditions, and non standard operation conditions. Moreover, simulations can be used to better understand the behavior of the system. In the real system it is not possible to measure all the states of the system, whereas in simulation these states can be calculated and analyzed. Analysis of the simulation results is a way to acquire knowledge about the system response to inputs or changes. Figures 4.38, 4.39, and 4.40 show a simulation with the standard operating conditions of the *Silgrain®* process. Figure 4.38 shows the feedrate and tapping conditions, and their effect on the interphase levels of the HR and UR, respectively. Figure 4.39 shows the evolution of PSDs at the inlet, within compartment I and at the overflow of compartment III. Figure 4.40 shows two examples of property profiles in compartment IV.

2. *Process optimization.* For safety and economic reasons, it is not possible to carry out neither considerable input changes or thorough experimental campaigns on the real system. However, when a model is available, the model can be used to test new patterns of operation, and to find optimal operation conditions. Once these conditions prove to be both optimal and safe on the model, then they can be tested on the real system. Figure 4.41 shows the response of the system to three types of feedstock rates: first the standard semibatch operation, then an equivalent semibatch operation with a lower cycle frequency, and finally the equivalent continuous operation. As observed, the influence of the type of operation on the system outputs is considerable. The higher the frequency of the cyclic input, the smaller the amplitude of

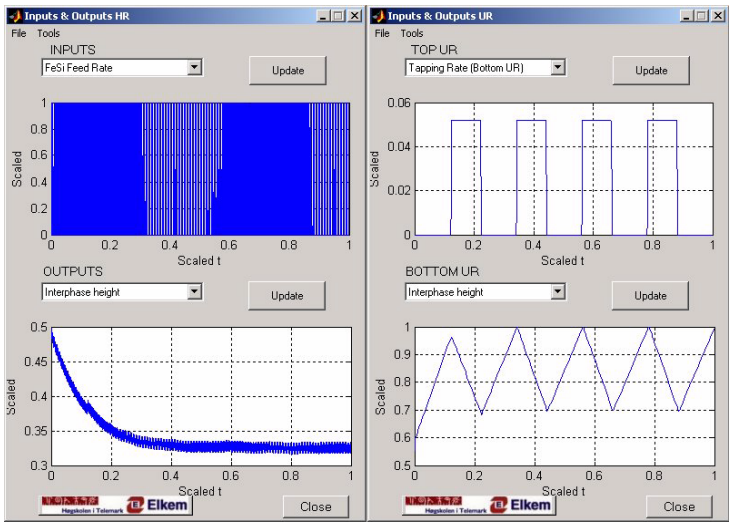

Figure 4.38: Standard operation of the *Silgrain*® process: feedrate and tapping, and their effect on the interphase level.

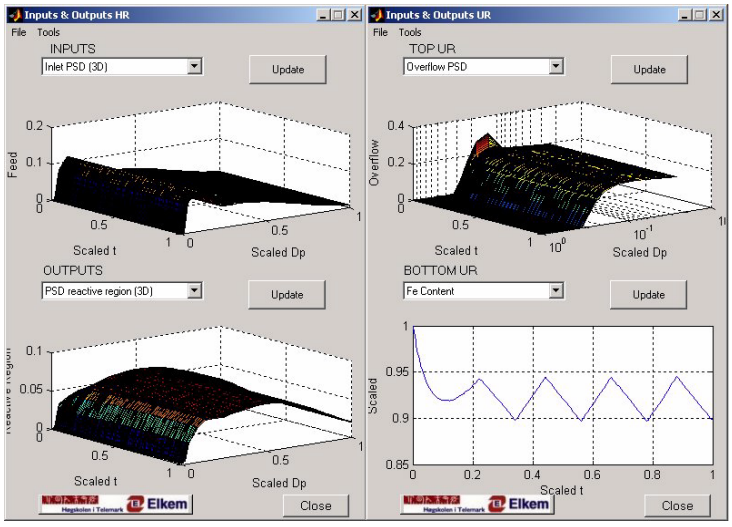

Figure 4.39: Standard operation of the *Silgrain*® process: PSDs.

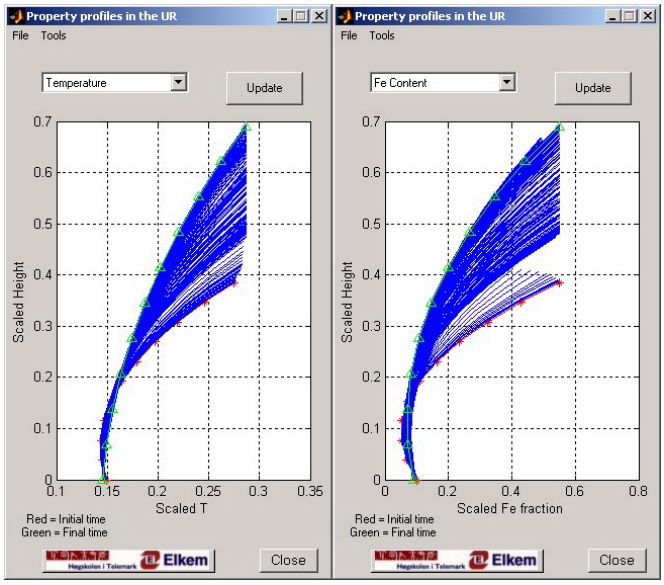

Figure 4.40: Standard operation of the *Silgrain*® process: profiles in compartment IV.

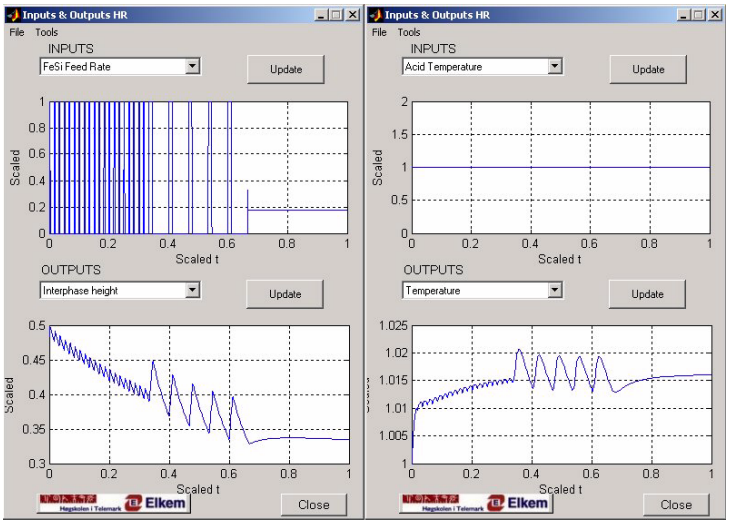

Figure 4.41: Response of the HR to three types of feedstock rates: standard semibatch rate, an equivalent semibatch rate of lower frequency, and continuous operation.

the resulting process outputs. This is an expected result: the process has a low filtering effect, and the simulator is able to give quantitative number of such an effect. Figure 4.42 shows a simulation of a possible start-up of the main reactor, after a shutdown. Material could be fed continuously, starting with a relatively cold acid, and then increasing the acid temperature to enhance disintegration, until the standard level and temperature conditions are achieved.

3. *Process design and roll-out.* When a new process is to be designed, and the basic assumptions and flow conditions in the system are decided, then a mechanistic model can be used to simulate the operation and to decide on design parameters, such as dimensions, or feed conditions. Roll-out consists in using the model of an existing plant, for another plant with a similar operation and just re-tune the values of the model parameters to use the same model for the new process. PBE models are thus suitable for process design and for roll-out.

4. *Controller design.* In order to design an automatic control system, it is necessary to decide on the variables that are used as controlled variables and manipulated variables. Moreover, knowledge about the dynamics of the system, i.e. the signs of the responses and the time constants, is required no matter the type of controller that is to be designed. Therefore, simulations on the model can be used to gather information about:

   - Input/output selection. The model can be used to analyze controllability of the outputs from the available inputs.
   - Required instrumentation. Measurements on the system are required for automatic control, and simulations can help to decide what and at which locations measurements should be taken.
   - Time constants of the system.

   The second part of this thesis is devoted to the use of the developed model to design a nonlinear controller.

5. *Training simulator.* The model, implemented in a graphical user interphase can be used to train new employees regarding the operation and behavior of the system. Appendix B shows the graphical user interphase that has been developed for the *Silgrain*® simulator as a part of this work.

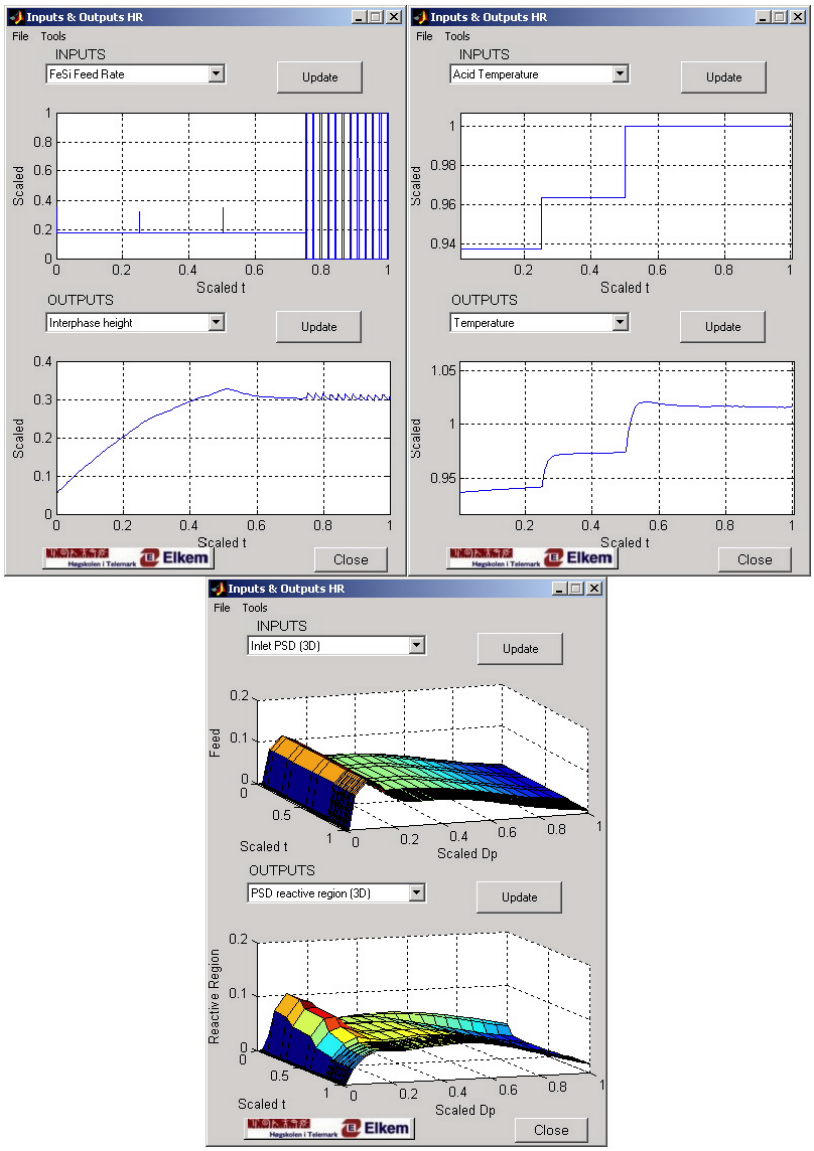

Figure 4.42: Simulation example of startup of the HR.

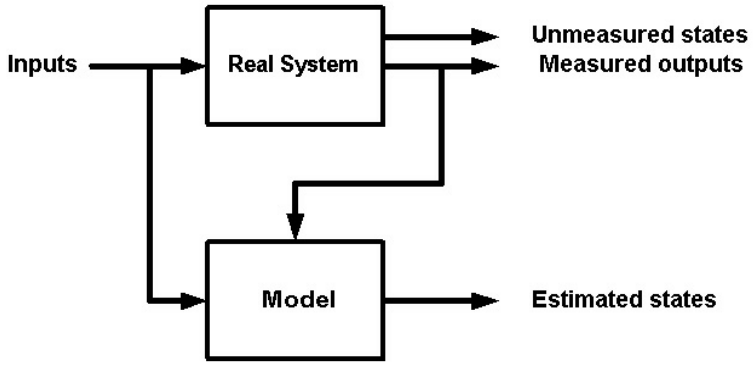

Figure 4.43: State estimator concept.

4.8.2 On-line applications

1. *State estimator, observer or soft sensor.* Some of the variables of the system are either impossible, difficult or too expensive to measure. However, once we have a validated model, and if there are enough measurements on the system such that the states we are interested in are observable from the measurements, then the model can be used to estimate them. Figure 4.43 illustrates the concept of a state estimator.

2. *Controller implementation.* There are many possible control techniques. Some of these techniques use predictions on the future behavior of the system to decide the control actions, such as model-based predictive control or optimal control. Other control techniques require estimates of states of the system that are not measured, such as nonlinear feedback linearization. Therefore, a model is required for the implementation of certain types of controllers.

3. *Statistical process control.* The model can also be used to control quality. Part III of this thesis explains how the model could be used for such a purpose.

We can thus conclude that mechanistic models offer the advantage that they can be used for a variety of purposes.

4.9 Conclusions

The main objective of this chapter has been to develop a model for the two reactors of the *Silgrain*® process that captures the essence of the process and that can be

used to obtain realistic predictions of the process behavior. A mechanistic model, based on the traditional balance laws of mass, energy and momentum and on the PBE, is chosen. Special emphasis has been put on the establishment of the model basis and assumptions. Hence, care is taken to avoid the common but unrealistic assumption of complete-mixing. In the *Silgrain®* process, four regions are distinguishable:

1. Compartment I (bottom HR) where mostly coarse material is localized, and where disintegration is the main event.

2. Compartment II (top HR) where grainy material is localized for a short residence time.

3. Compartment III (top UR) which operates as a separator of the particles from most of the acid.

4. Compartment IV (bottom UR) where the sedimented material is located, and where slow reaction and dissolution is the main phenomena.

A macroscopic balance is used *for* each of these distinguishable regions. Region volumes are allowed to vary, and a force balance on the particle is used to find the cut size, which relates the PSD in the effluent of the compartment to the PSD within the compartment. Compartments I, II, and III are modeled this way. A microscopic model is used for compartment IV, since property profiles are encountered in the axial direction.
Once the model structure is built, the model is "particularized" by defining the constitutive relations. A tailor-made experimental campaign at laboratory scale is carried out to find the birth and death terms of the PBE. The remaining constitutive relations are determined from the literature or from qualitative information of the process. Once the constitutive relations are established, a solution method is chosen. The system of equations corresponding to compartments I, II, and III are reduced to an index-0 DAE by discretization in the particle size coordinate. A nonequidistant fixed grid is used for discretization, and discretization is implemented such that mass is preserved. As regards the model of compartment IV, the resulting functional PDAE is first reduced to a standard PDAE by the method of moments, and subsequently reduced to a DAE by collocation.

The final stage is parameter estimation and model validation. An experimental campaign on the industrial plant has been carried out, and the systematic method for parameter identifiability analysis is tested with the *Silgrain®* model. Such a method has proved to be very useful. The parameter identifiability analysis reduces the number of parameters to be identified from 12 to 2 in the case of the HR, and from 31 to 6 in the case of the UR. After parameter estimation, the fitting of the

model to the experimental data from the industrial plant is satisfactory. However, the amount of experimental data is not large enough to divide the data into a set for parameter estimation and a test data set. It is thus recommended to carry out further experiments to test the prediction abilities of the model. Although the prediction abilities have not been validated, the fact that the model fits well to the experimental data after parameter estimation is a positive result, and confirms the potential of PBE models for predictive purposes.

Finally, some possible model uses have been described: system analysis, process optimization, process design, training simulator, controller design and implementation, soft sensoring, and quality control.

Although PBE models take time to develop, they can be developed quite systematically, they can represent fairly realistically the operation of industrial-scale units, and they can be used for a wide range of purposes.

Part II

Passivity-based control of particulate processes

Chapter 5

Introduction

5.1 Process control

Chemical process systems continuously exchange matter and energy with other units and/or the surroundings. The exchange of matter and energy keeps the system in a state that is not in equilibrium. If the system was isolated, according to classical thermodynamics, the state of the system would evolve towards the equilibrium state. One major aim of process control therefore is to manipulate the flows of matter and energy into and out of the system in such a way that the system is kept in desired nonequilibrium states. Such states may be periodic or aperiodic depending on the process specifications.

Automatic process control can:

- improve product quality;
- reduce emission of hazardous substances;
- reduce environmental impact;
- improve process safety;
- facilitate process optimization;

The implementation of process control has benefited from:

- improvement in measurement techniques, actuators, and computers;
- extensive research during the last 7 decades.

Many techniques for process control exist: Proportional-Integral-Derivative (PID) control, model-based predictive control, optimal control, nonlinear feedback linearization, adaptive control, etc. Note that these techniques have also been used in other areas, such as in shipsteering, rocket guidance, vibration control, water supply and many others. Obviously, some particular control techniques have had more acceptance in certain applications due to the main features of the system. Hence, PID control has been widely used for systems that have a more or less linear behavior, while optimal control has been much used for processes that operate in batch.

The development of a process controller requires the following stages:

1. System analysis. This includes gathering information about the dynamic features of the system, studying the availability of measurements and of manipulated variables, and the definition of the purpose of automatic control for the system under study.

2. Choice of control technique. This includes the definition of control objectives, like bandwidth, disturbance rejection, feedback and feedforward structures, design of filters and observers.

3. Controller design, including building the control algorithm and selecting the tuning parameters.

4. Controller implementation, which may include the development of new sensors where needed.

A good review of such a general approach can be found in the books by (Ogunnaike & Ray 1994) and (Seborg, Edgar & Mellichamp 2004).

5.2 Control of particulate processes

For several decades, extensive research has focused on the development of population balance models of particulate processes. In the last two decades, attention has shifted to the development of effective process control techniques for such processes, and on the exploitation of the available population balance models for process control. Several approaches have been tested but none of them have been widely accepted yet. Some of the challenges that are particular to the synthesis of controllers for particulate processes are:

- Particulate processes are often nonlinear. Open-loop instabilities, oscillatory behavior and long delays are common among particulate processes.

- Limited on-line measurement techniques are available for distributed properties.
- There are few feasible manipulated variables.
- Particulate processes often operate in batch or semibatch.

The first review paper on control of particulate processes (Rawlings, Miller & Witkowski 1993) reviewed model development, model solution, measurement techniques, parameter estimation and control of crystallization processes. In the paper, the authors wrote:

> We are only now seeing the advances in measurement and computing technologies necessary for successful industrial implementation of the ideas. It is reasonable to expect closed-loop crystal size distribution control to become part of accepted industrial practice in the near future (Rawlings et al. 1993).

This statement turned out to be too optimistic and there is still not a complete theory available for solving the distribution control problem. Nevertheless, there is no doubt that notable advances have been achieved in these areas at least from the theoretical point of view.

Another study on control of particulate processes is the controllability analysis suggested in (Semino & Ray 1995*a*) and its application to emulsion polymerization (Semino & Ray 1995*b*). In a series of papers authored by Christofides and coworkers, nonlinear output feedback controllers are developed for a crystallization process (Chiu & Christofides 1999), (Chiu & Christofides 2000) and an aerosol flow reactor (Kalani & Christofides 2000). To the best of my knowledge, Christofides is also the first author to come with a book on control of particulate processes (Christofides 2002). His methodological framework consists in first reducing the order of the population balance model by combining the method of weighted residuals and the concept of approximate inertial manifold. Once this is done, a nonlinear low-order output feedback controller that enforce exponential stability of the closed loop is synthesized using geometric and Lyapunov-based techniques. Some practical implementation issues such as the effect of input constraints (El-Farra, Chiu & Christofides 2001), and robustness (Chiu & Christofides 2000) are analyzed. However, the reported work is limited to theoretical development and simulation studies without experimental validation. Other nonlinear control techniques have been used, such as input-output decoupling control of a bioreactor (Kurtz, Zhu, Zamamiri, Henson & Hjortsø 1998). Model-based predictive control has also received a great deal of attention in the field of particulate processes, particularly for applications operating in batch or semibatch. Eaton & Rawlings

(1990) used nonlinear programming to solve the nonlinear model predictive control formulation of a batch crystallizer. Nonlinear model predictive control was also used by (Crowley, Meadows, Kostoulas & Doyle III 2000) and (Immanuel & Doyle III 2002) to optimize the performance of semibatch emulsion polymerization. Linear model predictive control has been proposed for the stabilization of oscillating microbial cultures in bioreactors (Kurtz et al. 1998) and (Zhu, Zamamiri, Henson & Hjortsø 2000), and for the emulsion polymerization of styrene (Zeaiter, Romagnoli, Barton & Gomes 2002). Linear control has been applied to crystallization (Vollmer & Raisch 2002) and (Patience & Rawlings 2001), and grinding (Galán, Barton & Romagnoli 2002). The vast majority of papers on control of particulate processes use closed-loop simulations to evaluate the performance of the controller. Practical implementation of process controllers are still rare and usually limited to laboratory scale plants, such as in (Patience & Rawlings 2001), (Immanuel & Doyle III 2002), and (Zeaiter, Romagnoli, Barton & Gomes 2002). Recent reviews on the status of process control of crystallization processes and granulation processes are given by (Braatz 2002) and (Wang & Cameron 2002).

In this work, a control approach called passivity-based control is chosen for control of particulate processes. The passivity theory is among the most powerful theories of control since it is based on input output behavior, and it applies to nonlinear and distributed systems quite easily. Passivity-based control has been widely use in the control of mechanical, electrical, and electromechanical systems. The technique has not been widely applied yet in the process engineering field despite of the nonlinear and distributed character of many of such systems. No references on the application of passivity-based control to particulate processes have been found. The reasons why passivity-based control looks appropriate for control of particulate processes are:

- passivity-based control is suited for systems that are nonlinear;
- the available population balance model can be exploited both for the design and implementation of the controller;
- stability is easy to ensure for passive systems;
- systems that are passive can be interconnected, leading to the resulting system also being passive.

Chapter 6 gives an introduction to passivity-based control theory and to the particular approach used in this work. A description of the methodological framework and the stability analysis are given. Examples of the application of the method to a simple reactor system and to the *Silgrain*® process are also given. Chapter 7 gives a further analysis of the control methodology, including the influence of

input constraints, the presence of disturbances, and the need of an observer. Some basic concepts of control theory are revised in appendix C. Any reader that is not familiar with nonlinear control theory should take a look at this appendix before reading the subsequent chapters.

Chapter 6

Inventory passivity-based control

6.1 Introduction

The notion of passivity has a long history in control and formed the basis for stability analysis of electrical circuits (Desoer & Vidyasagar 1975). Passivity can also be related to a more general notion called *dissipativity,* which was introduced by Willems (1972*a*) in the context of abstract operators.

> Dissipativity theory gives a framework for the design and analysis of control systems using an input-output description based on energy-related considerations. Dissipativity is a notion which can be used in many areas of science, and it allows the control engineer to relate a set of efficient mathematical tools to well known physical phenomena. (Lozano, Brogliato, Egeland & Maschke 2000)

The main idea behind the notions of passivity and dissipativity is that the dynamic behavior of physical systems can be explained in terms of the conservation, dissipation, and transport of a certain positive property of the system. The net increase in the positive property stored by a dissipative system in any given interval, is lower or, at most, equal to the amount of property supplied to the system in the given time interval. Such a behavior has implications for the stability of the system.

Ydstie and coworkers were the first to apply the passivity approach to process systems. A connection between macroscopic thermodynamics of process systems and the input-output passivity theory of nonlinear control was established in (Ydstie & Alonso 1997). This work continued with the development of passivity-based approaches for control of lumped process models (Farschman et al. 1998) and distributed process models (Alonso, Banga & Sanchez 2000), (Alonso & Ydstie 2001), (Ydstie 2002), respectively. The approach presented in (Farschman et al.

1998) exploits the structure of the first principle model directly in the formulation of the control law, which has the form of an output feedback linearization law. Stability of the closed loop is guaranteed by the fulfillment of the passivity inequality. There are other nonlinear control techniques that have also exploited the particular properties of process systems. Hence, a relationship between extensive thermodynamic variables and the dynamic modes of the system was first published in (Georgakis 1986), where such relationships were used for the synthesis of multivariable and nonlinear control structures. State feedback linearization and/or output feedback linearization from the balance laws is also used in control of positive systems, i.e. systems where the states and inputs are positive and upper bounded (Bastin & Provost 2002), (Imsland 2002). Stability of the closed loop is enforced by applying LaSalle's theorem subject to certain constraints on the system equations, but those constraints in some cases turn out to be too restrictive (Imsland 2002). In contrast to the passivity-based approach, no direct reference to the connection with thermodynamics is mentioned in control of positive systems.

The main ideas in dissipativity and passivity theory are presented in section 6.2. Section 6.3 describes the methodological framework of the inventory passivity-based approach. The nominal stability analysis of the inventory passivity-based approach is shown in section 6.4. A comparison with other nonlinear control approaches is given in section 6.5. Section 6.6 discusses in more detail the controllability and detectability requirements, and introduce techniques to check these requirements. Section 6.7 briefly discusses the connection of this approach to non-equilibrium thermodynamics. A simple chemical reactor is used as case study in section 6.8. The *Silgrain*® model is used in section 6.9 to illustrate the application of inventory passivity-based control to particulate processes, followed by a comparison with other methods used for control of particulate processes. Finally, this chapter ends with a summary of the main conclusions in section 6.10.

6.2 General passivity theory

Many dynamic systems, and in particular, many process engineering systems, can be described by a state-space representation that is affine in the manipulated variables

$$\begin{aligned} \frac{dx}{dt} &= f(x) + h(x)\,u \\ y &= g(x), \end{aligned} \tag{6.1}$$

where $x \in X = \mathbb{R}^n$ is the state, $u \in U = \mathbb{R}^m$ is the manipulated variable, $y \in Y = \mathbb{R}^p$ is the output.

Definition 6 (Dissipation Inequality (Willems 1972)) *A dynamic system Σ is said to be dissipative if there exists a nonnegative function $V : X \longrightarrow \mathbb{R}^+$, called the storage function, such that for all $(t_0, t_1) \in \mathbb{R}^2_+$, $u \in U$ and $x_0 \in X$, the following inequality holds*

$$V(x) - V(x_0) \leqslant \int_{t_0}^{t_1} w(\tau)\, d\tau. \tag{6.2}$$

where the supply rate *w is a real valued function defined on $U \times Y$, such that for any $(t_0, t_1) \in \mathbb{R}^2_+$, $u \in U$ and $y \in Y$, the function $w(t) = w(u(t), y(t))$ is locally integrable*

$$\int_{t_0}^{t_1} |w(t)|\, dt < \infty. \tag{6.3}$$

Remark 7 *Note that if the storage function $V(x)$ is differentiable, the dissipation inequality, i.e. equation 6.2, is equivalent to*

$$\frac{dV}{dt} \leq w(t) \qquad \forall t \geq 0 \tag{6.4}$$

that is, the rate of change of the property stored in the system is less than or at most equal to the supply rate (Willems 1972).

The key idea in dissipation theory is to find a suitable storage function V, and the corresponding supply function w, given a dynamic system Σ. As a general rule, the storage function $V(x)$ is not uniquely defined by the input/output behavior of the dynamic system Σ. This means that for the same dynamic system we may find several pairs (V, w) that fulfill the dissipation inequality. Indeed, one of the most difficult aspects of dissipativity-based control is to find an appropriate storage function.

Definition 8 *Passivity is a particular case of dissipativity, where the supply function w is given as the scalar product of outputs and inputs*

$$w = y^T u, \tag{6.5}$$

and where the storage function equals zero for the zero-state

$$V(0) = 0. \tag{6.6}$$

Note that in passivity, the number of outputs equals the number of manipulated variables, i.e. $m = p$, and that a particular structure for the supply function is given. However, the choice of storage function $V(x)$ remains as an open problem,

and it may be necessary to make particular choices of u and y in order to achieve a nonnegative storage function (Ortega, der Schaft, Mareels & Maschke 2001).

Note also that the broad range of applications of passivity theory has led to diverse ways of defining the notion of passivity in the literature. Such definitions are more specific, basically giving more information about the dissipation term. Definitions of state strictly passivity, input strictly passivity and output strictly passivity, among others, can be found in (Lozano et al. 2000), where relevant references are also given.

The main interest of disipassivity and passivity as applied to dynamic systems is that it is intimately related to stability. Only some technical conditions are required in order for passivity to imply stability of a steady-state at a local minimum of the storage function (Willems 1972). Therefore, a control strategy based on passivity theory would ensure stable operation and would guarantee the convergence of the system to the desired set point.

Note that the type of stability is determined by the type of passivity and by some properties of the dissipative system Σ, mainly its detectability. The internal states of a system are detectable from the outputs if when the outputs are fixed to zero, then the internal states evolve towards zero too. In mathematical terms, a dynamic system is said to be locally zero-detectable if there exists a neighborhood N of 0 such that for all $x \in N$ such that

$$y = g(x) = 0 \qquad \text{for all } t \geq 0 \Rightarrow \lim_{t \to \infty} x(t) = 0. \tag{6.7}$$

Theorem 9 (Byrnes, Isidori & Willems (1991)) *Assume that a system is passive with a positive definite storage function and it is locally zero-state detectable. Let $\Pi : Y \to U$ be any smooth function such that $\Pi(0) = 0$ and $y^T \Pi(y) > 0$ for each nonzero y. The control law*

$$u = -\Pi(y) \tag{6.8}$$

asymptotically stabilizes the zero-state $x = 0$.

Passivity-based control thus consists in finding the input-output description $[u, y]$, the storage function $V(x)$, and the control law $u = -\Pi(y)$ that renders the system passive.

The properties that make passivity-based control so valuable are:

- Stability. Stabilization of the closed-loop response is key in process control.
- Interconnectivity. When passive systems are interconnected, certain passivity properties are inherited (Lozano et al. 2000). Hence, a parallel interconnection of two passive systems Σ_1 and Σ_2 is always passive, whereas the

feedback interconnection of Σ_1 and Σ_2 is passive as long as some minor conditions are met (Lozano et al. 2000). Stability of interconnected systems is a relevant issue in process control, since processes consists of many units that interact with each other. The standard approach in process control is that controllers for the individual units are synthesized independently. But this can create instability of the overall plant. There is thus increasing interest in synthesizing controllers that ensure stabilization of the whole system. This is often referred to as *plantwide control* (Luyben, Tyreus & Luyben 1998). Therefore, the property of straightforward interconnectivity of passive systems can be very advantageous.

6.3 Inventory passivity-based control: Methodological framework

Inventory passivity-based control was first presented in (Farschman et al. 1998).

Definition 10 (Farschman et al. (1998)) *An inventory for a dynamic system Σ is an additive continuous (C^1) function $v : X \to \mathbb{R}_+$ so that if x_1 is the state of the system Σ_1 and x_2 is the state of another system Σ_2 then we have*

$$v(x) = v(x_1) + v(x_2). \tag{6.9}$$

Note that an inventory is an extensive measure, i.e. proportional to the size of the system. The thermodynamic states of a process system Σ, such as mass M, internal energy U or chemical mass of chemical species i M_i are inventories.

Farschman et al. (1998) suggested a storage function that only depends on inventories. They proved that a quadratic function measuring the distance between the measured or estimated inventories and their setpoints, is a suitable storage function. This ensures that the process is passive and that the process inventories converge to their setpoints.

A mechanistic model of the process system, based on the balance laws of mass, energy and momentum, and on the PBE if we are dealing with particulate processes, gives or can be reduced to a model of the following type:

$$\begin{aligned} \frac{dv}{dt} &= \phi(x)\, u + p(x) \\ v &= g(x), \end{aligned} \tag{6.10}$$

where the nomenclature introduced in (Farschman et al. 1998) is used: $v \in \mathbb{R}_+^{\dim v}$ are inventories (mass, energy, component mass,...), $u \in \mathbb{R}^{\dim u}$ are the manipulated variables (mass and energy flows), and $x \in \mathbb{R}_+^{\dim x}$ are intensive variables that are

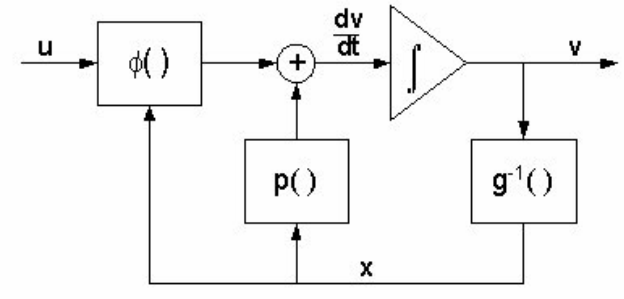

Figure 6.1: Block diagram of a process system. Note that the following functions: ϕ, p, and g, may be nonlinear.

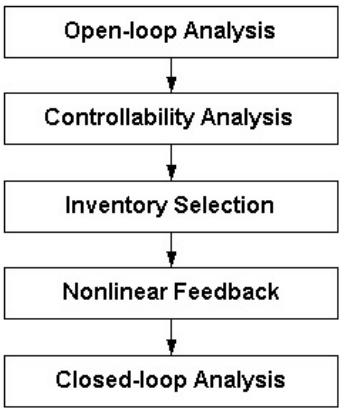

Figure 6.2: Methodology framework for the synthesis of an inventory passivity-based controller.

involved in the transport term ϕ and production term p of the balance laws (temperature, pressure, concentrations,...). We assume that the system of equations in 6.10 is complete, i.e. number of equations $= \dim v + \dim x$. Figure 6.1 shows a block diagram of the process model.

The methodology used for the synthesis of inventory passivity-based controllers of the form of equation is summarized in Figure 6.2, and consists of the following stages:

1. Open-loop analysis. This is the stage in which the control objectives are established, the available measurements and manipulated variables are identified, and the dynamic behavior of the open-loop system is quantified.

2. Controllability analysis and selection of inventories. Inventory-passivity based control assumes the same number of manipulated variables as controlled vari-

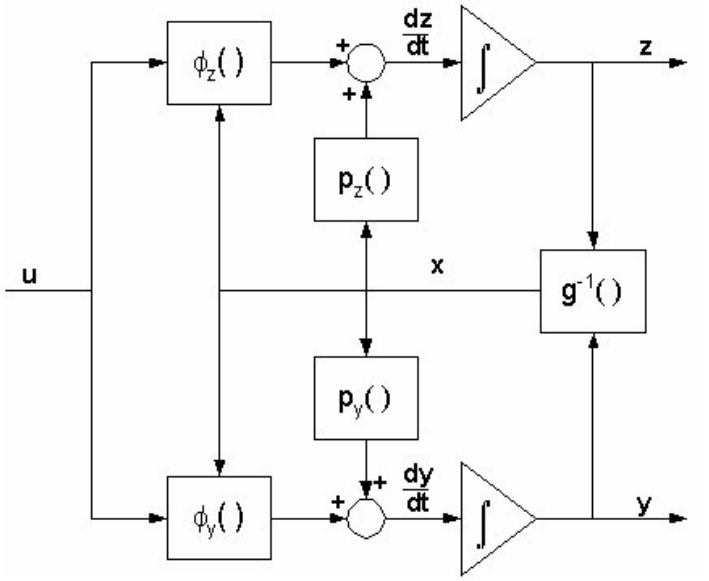

Figure 6.3: Block diagram of partitioned process model.

ables. The available manipulated variables were established in the previous stage, so we know the number of inventories that we have to select. The normal situation is that $\dim v > \dim u$. Thus, we have to carry out a partition of the inventory vector:

$$\begin{pmatrix} y \\ z \end{pmatrix} = Pv, \tag{6.11}$$

where $y \in \mathbb{R}_+^{\dim u}$ are the controlled inventories, $z \in \mathbb{R}_+^{\dim v - \dim u}$ are the uncontrolled inventories, and $P \in \mathbb{R}_+^{\dim v \,\times\, \dim v}$ is a permutation matrix. Similarly, the system in equation 6.10 can be rewritten as follows:

$$\begin{aligned} \frac{dy}{dt} &= \phi_y(x)\,u + p_y(x) \\ \frac{dz}{dt} &= \phi_z(x)\,u + p_z(x) \\ P^{-1}\begin{pmatrix} y & z \end{pmatrix}^T &= g(x)\,. \end{aligned} \tag{6.12}$$

Figure 6.3 shows the block diagram of the partitioned system. The selection of the partition matrix P is not arbitrary; certain controllability and detectability conditions must be fulfilled. Sometimes it is convenient that one or more of the controlled inventories is a linear combination of the inventories (for example, the sum of certain component masses). Therefore, P does not

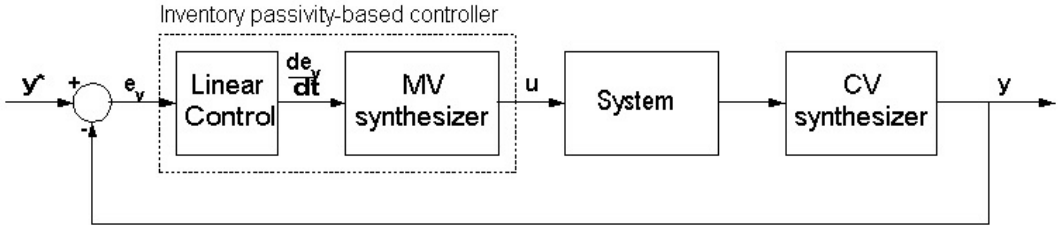

Figure 6.4: Closed-loop block diagram. MV - Manipulated variable; CV - Controlled variable.

necessarily have to be a permutation matrix. The only strict requirement is that P is invertible.

3. Nonlinear feedback law. Once the controlled inventories are chosen, the following feedback law is used:

$$\begin{aligned} \frac{de_y}{dt} &= -Ke_y \\ e_y &= y - y^*, \end{aligned} \tag{6.13}$$

where $K \in \mathbb{R}_+$ is a positive constant, called proportional constant, $y^* \in \mathbb{R}^{\dim y}$ is the desired setpoint and $e_y \in \mathbb{R}^{\dim y}$ is the output error. The nonlinear part of the feedback law consists in solving the following system of algebraic equations:

$$-Ke_y = \phi_y(x)\, u + p_y(x) - \frac{dy^*}{dt} \tag{6.14}$$

to obtain the value of the manipulated variable u. Figure 6.4 sketches a simplified block diagram the closed-loop. As shown by this figure, the control law consists of a linear calculation first (system of equations 6.13), followed by a nonlinear calculation of the manipulated variable (system of equations 6.14). To refer to this nonlinear calculation, we have adopted the nomenclature introduced by (Georgakis 1986): *manipulated variable synthesizer*. Note that Figure 6.4 also shows a *controlled variable synthesizer* block right after the system block, that represents the calculation of the controlled inventories from available measurements in the system, since inventories may not be measurable directly. We leave this issue for now, but it will be further discussed in chapter 7.

4. Analysis of the closed-loop operation. It is important to analyze the performance of the controller. The following questions may be noteworthy:

- Is offset-free tracking achieved?
- Are the closed-loop responses fast enough?
- Are the changes of the manipulated variables too aggressive?
- Are all the relevant states of the system stabilized?

If the performance of the closed-loop is not satisfactory, a retuning of the parameters of the controller may improve performance. If this is not the case, the synthesis procedure should be revised.

The methodology explained above is illustrated with the help of more detailed block diagrams. Two cases are studied.

1. Perfect model, the required measurements are available and all the inventories are used for control ($y = v$). Figure 6.5 shows the block diagram of the closed-loop. Since we assume that the model is perfect, there is a cancellation of terms. The closed-loop dynamics can thus be reduced, in this ideal case, to an equivalent linear system where the controller is a PID controller and the system is just an integrator. Therefore, inventory passivity-based control linearizes the dynamics, i.e. feedback linearization is achieved. The tuning of the PID controller should thus be relatively easy, and tuning methods from linear system theory can be used.

2. Perfect model, the required measurements are available, and a subset of inventories are used for control ($\dim y < \dim v$). Figure 6.6 shows the block diagram of the closed-loop. Again, there is a certain cancellation of terms. The closed-loop dynamics of the controlled inventories is again equivalent to a linear system where the controller is a PID controller and the system is just an integrator. Note, however, that the dynamics of the remaining inventories may still be nonlinear, and unless certain requirements are fulfilled, the response of the uncontrolled inventories may be unstable.

6.4 Inventory passivity-based control: Nominal stability analysis

The methodology presented in the previous section has not yet made use of the passivity concepts introduced in section 6.2. Passivity theory is needed to prove stability. A stability proof was presented in (Farschman et al. 1998), but that proof only established convergence of the controlled inventories, not examining the behavior of the remaining inventories or the internal model. The proof presented

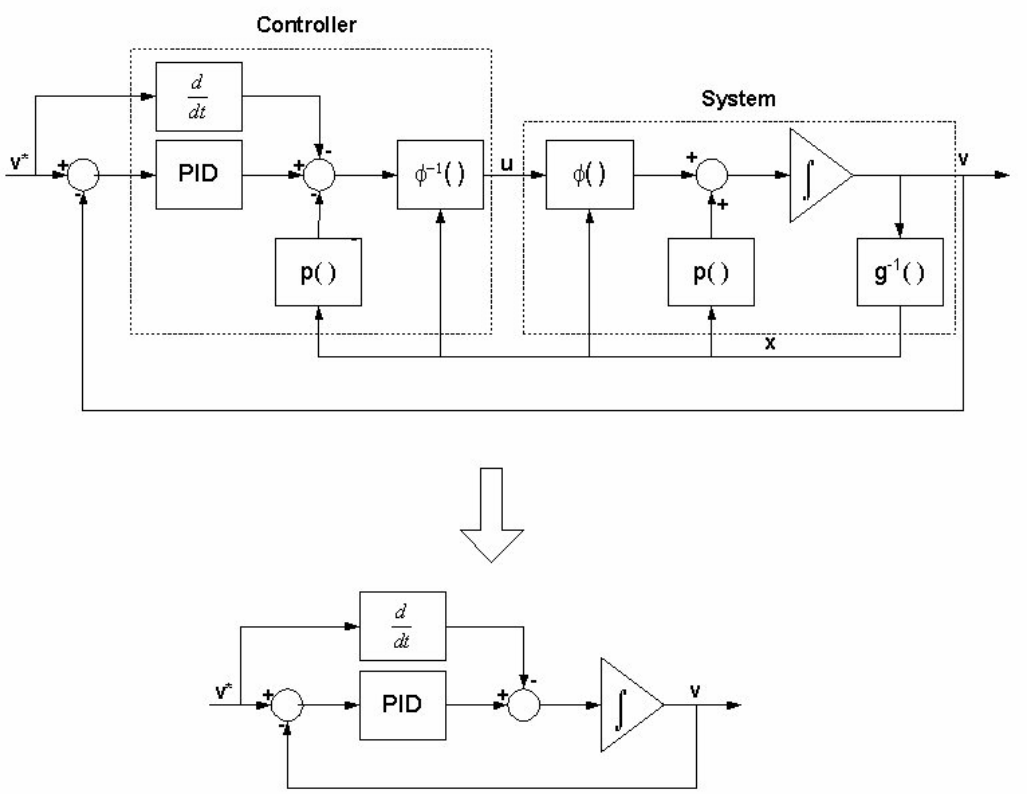

Figure 6.5: Block diagram of the closed-loop, under the assumptions of perfect model, available measurements, and $y = v$.

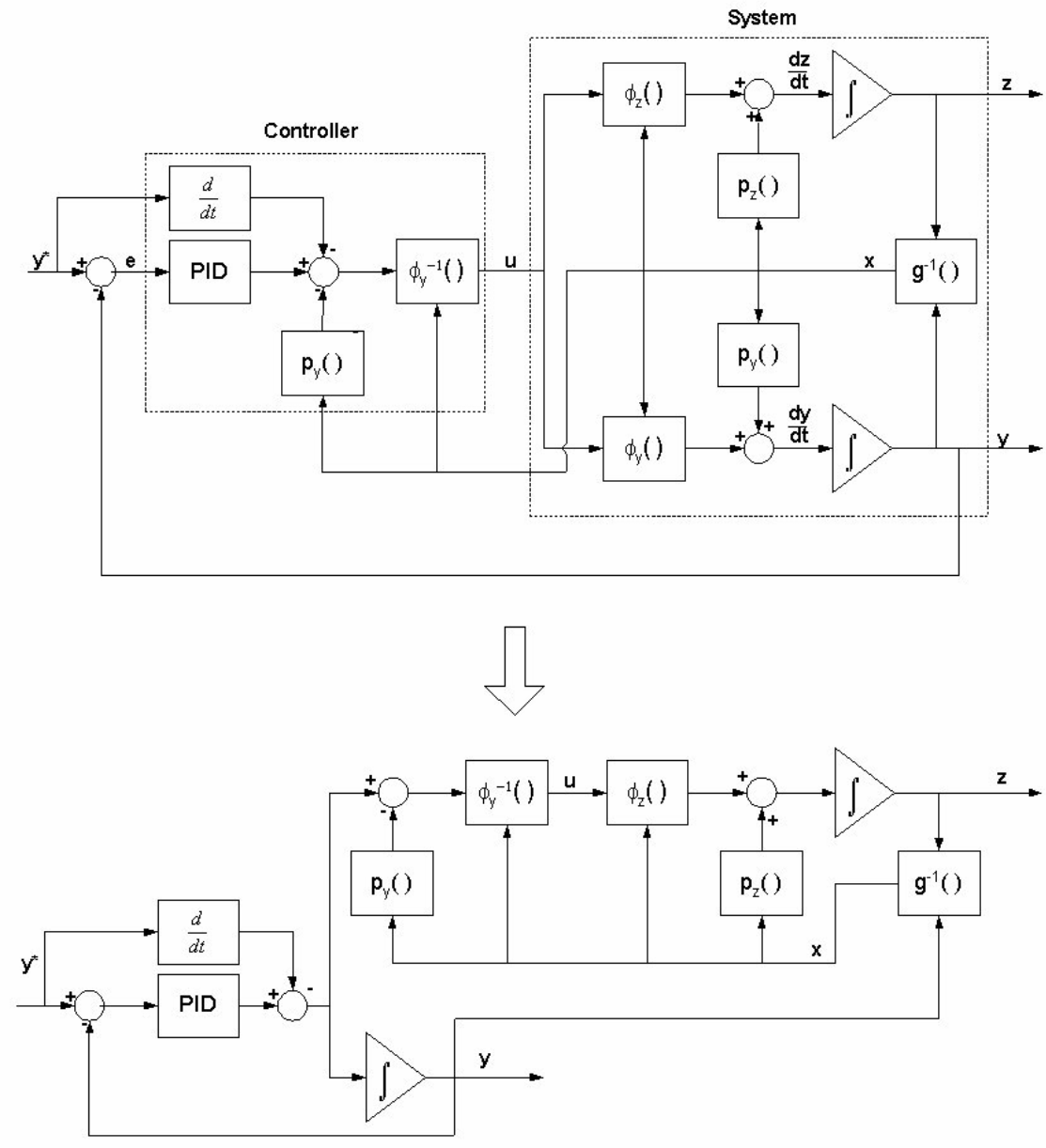

Figure 6.6: Block diagram of the closed-loop, under the assumptions of perfect model, available measurements, and $\dim y < \dim v$.

here can be applied to the cases where $\dim y < \dim v$. In order to make the proof as simple as possible, the linear controller used in the methodology is assumed to have only the proportional term, i.e. P-controller. But the same results would be obtained if a PID controller was used instead of a P-controller.

Let us define some terminology. The deviation of the controlled inventory y from the desired setpoint y^* is denoted by $\bar{y}$, the deviation of the uncontrolled inventories z from the final steady state z_{ss} is denoted by $\bar{z}$, and the instant time at which the controlled inventories y stabilize at the desired setpoint y^* is denoted by t^*. Let K be a diagonal positive matrix, and $\text{clip}(t)$ be a strictly increasing sigmoid function that starts at zero, flattens to 1 at $t = \hat{t} \geq t^*$, and its derivative has narrow local/exponential support

Theorem 11 *The thermodynamic system 6.10 is rendered passive with passive mapping*

$$\begin{aligned} \textit{passive input} &\rightarrow \phi_y(x)\, u + p_y(x) \\ \textit{passive output} &\rightarrow \bar{y} = y - y^* \end{aligned}$$

and storage function

$$V = \frac{1}{2}\bar{y}^T\bar{y} + \frac{1}{2}\bar{z}^T\bar{z}\,\text{clip}(t), \tag{6.15}$$

by the control law

$$-K\bar{y} = \phi_y(x)\, u + p_y(x) - \frac{dy^*}{dt}. \tag{6.16}$$

Passivity is ensured as long as the control law can be solved at any instant time t and as long as $\bar{z}$ is zero-state detectable from $\bar{y}$.

Proof. Let us assume that there exists a stationary state z_{ss} corresponding to $u = u^*$. The thermodynamic model can be rewritten in deviation form as follows

$$\frac{d\bar{y}}{dt} = \phi_y(x)\, u + p_y(x) \tag{6.17}$$

$$\frac{d\bar{z}}{dt} = \phi_z(x)\, u + p_z(x) \tag{6.18}$$

$$\bar{y} = y - y^*. \tag{6.19}$$

The condition of zero-state detectability implies that

$$\bar{y} = 0 \qquad \text{for all } t \geq 0 \Rightarrow \lim_{t\to\infty} \bar{z}(t) = 0. \tag{6.20}$$

Now the storage function to be used is

$$V = \frac{1}{2}\bar{y}^T\bar{y} + \frac{1}{2}\bar{z}^T\bar{z}\,\text{clip}(t). \tag{6.21}$$

Such a storage function is a positive definite function which only takes the zero value when the controlled inventories reach their setpoints and the uncontrolled inventories reach the steady-state. The passivity inequality is given by

$$V_f - V_0 \leq \int_{t_0}^{t_f} -\left(\bar{y}^T K \bar{y}\right) d\tau. \tag{6.22}$$

According to the control law, the dynamic behavior of $\bar{y}$ is given by

$$\frac{d\bar{y}}{dt} = -K\bar{y}, \tag{6.23}$$

which is a linear system of ODEs, with the following solution

$$\bar{y} = \exp\left(-K\left(t - t_0\right)\right)\bar{y}_0, \tag{6.24}$$

Now, if

$$t_0 = 0 \tag{6.25}$$
$$t_f \leq t^* \tag{6.26}$$

then

$$\begin{aligned} V_f &= \frac{1}{2}\bar{y}_f^T \bar{y}_f \\ V_0 &= \frac{1}{2}\bar{y}_0^T \bar{y}_0 \\ \int_{t_0}^{t_f} -\left(\bar{y}^T K \bar{y}\right)\, d\tau &= \int_{t_0}^{t_f} \left[\exp\left(-K\left(t - t_0\right)\right)\bar{y}_0\right]^T K \left[\exp\left(-K\left(t - t_0\right)\right)\bar{y}_0\right] dt \\ &= \frac{1}{2}\left|\left[\exp\left(-K\left(t - t_0\right)\right)\bar{y}_0\right]^T K \left[\exp\left(-K\left(t - t_0\right)\right)\bar{y}_0\right]\right|_{t_0}^{t_f} \\ &= \frac{1}{2}\left|\bar{y}^T \bar{y}\right|_{t_0}^{t_f} = \frac{1}{2}\bar{y}_f^T \bar{y}_f - \frac{1}{2}\bar{y}_0^T \bar{y}_0, \end{aligned} \tag{6.27}$$

and then the passivity inequality becomes an equality. If, on the contrary,

$$t_0 = 0 \tag{6.28}$$
$$t^* \leq t_f \leq \hat{t}. \tag{6.29}$$

then the integral term of the passivity inequality can be split into two terms so that

$$\begin{aligned} V_f - V_0 &\leq \int_{t_0}^{t^*} -\left(\bar{y}^T K \bar{y}\right)\, d\tau + \int_{t^*}^{t_f} -\left(\bar{y}^T K \bar{y}\right)\, d\tau \\ &\leq \int_{t_0}^{t^*} -\left(\bar{y}^T K \bar{y}\right)\, d\tau + 0, \end{aligned} \tag{6.30}$$

then

$$\begin{aligned} V_f &= 0 \\ V_0 &= \frac{1}{2}\bar{y}_0^T\bar{y}_0 \\ \int_{t_0}^{t^*} -\left(\bar{y}^T K\bar{y}\right)\ d\tau &= \frac{1}{2}\left|\bar{y}^T\bar{y}\right|_{t_0}^{t^*} = 0 - \frac{1}{2}\bar{y}_0^T\bar{y}_0, \end{aligned} \tag{6.31}$$

and again the passivity inequality becomes an equality. Finally for

$$t_0 = 0 \tag{6.32}$$

$$t_f \geq \hat{t} \tag{6.33}$$

the integral term of the passivity inequality can be split into two terms so that

$$\begin{aligned} V_f - V_0 &\leq \int_{t_0}^{t^*} -\left(\bar{y}^T K\bar{y}\right)\ d\tau + \int_{t^*}^{t_f} -\left(\bar{y}^T K\bar{y}\right)\ d\tau \\ &\leq \int_{t_0}^{t^*} -\left(\bar{y}^T K\bar{y}\right)\ d\tau + 0 \end{aligned} \tag{6.34}$$

$$V_f = \frac{1}{2}\bar{y}_f^T\bar{y}_f + \frac{1}{2}\bar{z}_f^T\bar{z}_f = 0 + \frac{1}{2}\bar{z}_f^T\bar{z}_f \tag{6.35}$$

$$V_0 = \frac{1}{2}\bar{y}_0^T\bar{y}_0 + \frac{1}{2}\bar{z}_0^T\bar{z}_0. \tag{6.36}$$

The passivity inequality is then

$$\frac{1}{2}\bar{z}_f^T\bar{z}_f - \frac{1}{2}\bar{y}_0^T\bar{y}_0 - \frac{1}{2}\bar{z}_0^T\bar{z}_0 \leq \frac{1}{2}\left|\bar{y}^T\bar{y}\right|_{t_0}^{t^*} \tag{6.37}$$

resulting in

$$\frac{1}{2}\bar{z}_f^T\bar{z}_f - \frac{1}{2}\bar{z}_0^T\bar{z}_0 \leq 0. \tag{6.38}$$

Since $\bar{z}$ is zero-detectable, and $\hat{t}$ is a variable that we can choose freely, then for a sufficient long $\hat{t}$, $z_f \leq z_0$, which means that the storage function fulfills the passivity inequality. ■

Remark 12 *The zero-detectability requirement is equivalent to requiring that the system is minimum phase. For a definition of minimum phase, see appendix C.*

Remark 13 *Note that the proof does not depend on the specific choice of* $\mathrm{clip}\,(t)$. *One possible function for* $\mathrm{clip}\,(t)$ *is the following:*

$$\mathrm{clip}\,(t) = t - (\hat{t} - t)\left(\frac{\arctan\left(\frac{\hat{t}-t}{0.01\hat{t}}\right)}{\pi} + 0.5\right) + (1.1\hat{t} - t)\left(\frac{\arctan\left(\frac{t-1.1\hat{t}}{0.01\hat{t}}\right)}{\pi} + 0.5\right), \tag{6.39}$$

where $\hat{t}$ *is the instant where all the states* z *evolve monotonically. It would equally work with another choice of* $\mathrm{clip}\,(t)$, *as long as it is a strictly increasing sigmoid function that starts at zero, flattens to* 1 *at* $t = \hat{t} \geq t^*$, *and its derivative has narrow local/exponential support.*

Theorem 11 states that if we formulate the model of a process system based on the balance equations, we may stabilize the whole system by using input-output feedback linearization, with a proper selection of a subset of the inventories as controlled outputs. In order to ensure passivity, and thus stability, two conditions must be fulfilled: the control law in equation 6.16 must have unique solution at all times, and the uncontrolled inventories must be zero-detectable. These two requirements limit the possible choice of inputs u and controlled inventories y, and they are typically hard to check for very complex nonlinear systems.

6.5 Comparison with other control methods

The trained eye will see that the proposed controller shares many similarities with other nonlinear control methods.

First of all, the suggested method is closely related to input-output feedback linearization. Input-output feedback linearization can be applied to nonlinear systems that have a well-defined *relative degree*, and that are *minimum phase*. Local stability of the resulting closed-loop follows from the asymptotic stability of the zero-dynamics, but input-output feedback linearization theory is lacking from systematic global stability results (Slotine & Li 1991). The inventory-passivity based approach can be considered a specific application of input-output feedback linearization in which the particular structure of the nonlinear system is exploited to find the linearizing control law in a straightforward manner and to ensure global stability of the closed-loop. Hence, if the controlled inventories are selected according to the requirements in theorem 11:

1. the system has automatically partial relative degree $(1, 1, \ldots, 1)$ and total relative degree $r = m$, where m is the number of manipulated variables u. No differentiation of the nonlinear system is needed to calculate the relative degree, since the controlled output is just a subset of the state vector.

2. the system is minimum phase.

3. there exists a Lyapunov-type function (the storage function in equation 6.21) that ensures not only local stability of the closed-loop, but also global stability of the closed-loop if the system is globally minimum phase.

Global stability of nonlinear systems that are rendered passive by feedback linearization was studied in (Byrnes, Isidori & Willems 1991). It was shown that not only minimum phase but also weakly minimum phase nonlinear systems having relative degree $(1, 1, \ldots, 1)$ can be globally asymptotically stabilized by input-output feedback linearization, provided that suitable controllability-like rank conditions are satisfied. This means that the requirement of zero-state detectability in our approach might be weakened even further.

There are parallels between inventory passivity-based control and the state feedback controller for a class of positive systems presented in (Imsland 2002) and (Imsland & Foss 2003). Positive systems are dynamic systems in which the state is nonnegative, and the input is nonnegative and upper bounded. Hence, inventory models of the form 6.10 can be considered positive systems if the inputs u have upper bounds. The state feedback controller used by Imsland (2002) is constructed by dividing the model into $m = \dim u$ subsets, each subset associated to one of the elements in the input vector. The sum of the states in each subset is the controlled output associated to the corresponding input. Strong assumptions are made on the terms of the nonlinear system to ensure controllability. Local and global convergence of the state of the system to an invariant set is proved by means of LaSalle's invariance theorem. Stabilization (in the sense of Lyapunov) of the system relies thus on the existence of an invariant set for the closed-loop dynamics for the given control law, which is thus related to requiring stable internal dynamics. As indicated by Imsland (2002), some of the assumptions used in the approach to ensure controllability may be too strong for certain systems.

The search for general theorems that establish the conditions which make a nonlinear system stabilizable is a topic that has attracted a good deal of attraction. Probably the most general result so far is the notion of input-output stability introduced by Liberzon, Morse & Sontag (2002). This theory does not rely on zero dynamics or normal forms and is not restricted to affine systems. A system is defined as input-output stable if its state and input eventually become small when the output and derivatives of the output are small. This notion thus is related to the concept of a minimum-phase nonlinear system. Systems fulfilling the requirements of the inventory passivity-based approach fall under the definition of input-output stability.

6.6 A closer look at the controllability and detectability requirements

Theorem 9 states that the closed-loop is passive, and thus stable, if two requirements are fulfilled. The first requirement is that the selected controlled inventories y are controllable with respect to the manipulated variables u. The control law

$$-K\bar{y} = \phi_y(x)\,u + p_y(x) - \frac{dy^*}{dt} \tag{6.40}$$

must therefore have solution for u given by

$$u = \phi_y(x)^{-1}\left(-K\bar{y} - p_y(x) + \frac{dy^*}{dt}\right). \tag{6.41}$$

Hence, we have to solve a system of algebraic equations. Depending on the complexity of the terms $p_y(x)$ and $\phi_y(x)$, the system of equations 6.41 will be solved analytically or numerically. Note also that the states involved in the control law have to be available. If they can not be measured, then they must be estimated by means of an observer. We assume in this chapter that the states that appear in the control law are measured. This controllability requirement implies *static* controllability of the selected inventories with respect to the manipulated variables u, i.e. for a constant value u_{ss}, then y reaches a certain steady-state value after a certain finite time interval:

$$u = u_{ss} \Rightarrow y \rightarrow y_{ss}. \tag{6.42}$$

The second requirement of Theorem 9 is that the uncontrolled inventories are detectable from the controlled inventories, or equivalently, the internal dynamics are stable. However, to prove that the internal dynamics are stable is not trivial for general nonlinear systems. Fortunately, process systems have certain structural features that can be exploited for analyzing the stability of the internal dynamics. In particular, we focus here on chemical reaction systems, since many particulate systems can be understood as a large network of chemical reactions. The process systems that exhibit the widest range of nonlinear behavior (multiple steady-states, oscillatory limit cycles, etc.), are precisely the systems where chemical reaction is present. Indeed, the nonlinear dynamic behavior of chemical systems has attracted a good deal of attention since the discovery of an homogeneous oscillating reaction by Belousov in the 1950s. Such a discovery attracted the interest of the thermodynamics community, but also of the nonlinear dynamics community. This resulted in the development of powerful theories on the existence and uniqueness of equilibria for reaction networks. In particular, the theory developed in a series of papers by Feinberg, Horn and Jackson (Horn & Jackson 1972),

(Feinberg & Horn 1974), (Feinberg 1980), (Feinberg 1991), (Feinberg 1995*a*), and (Feinberg 1995*b*) is of remarkable importance, and worth reading. Some of the main results in this theory are summarized here, and coupled with the inventory passivity-based approach. These results are new since chemical reaction systems were not studied in (Farschman et al. 1998).

Feinberg and coworkers thought of a chemical reaction mechanism as a network that connects the various reactants, intermediates and products. The motivation of their work was the following:

> Although the governing differential equations vary markedly from one chemical system to another, the equations themselves are determined in a rather precise way by the underlying network of chemical reactions. Thus, one can hope to draw firm connections between aspects of reaction network structure and the variety of dynamics that can be admitted by the corresponding system of differential equations. (Feinberg 1987)

This was quite a challenging goal: being able to state whether the governing differential equations of a chemical system have the capacity to admit certain kinds of qualitative behavior by just inspecting the network of chemical reactions. A chemical reaction network consists of three sets:

- the set of chemical species in the network, denoted by n_s.
- the set of complexes of the network, which are the set of objects that appear before and after the reaction arrows (Horn & Jackson 1972). The number of complexes is denoted as n_c.
- the set of reactions in the network.

Figure 6.7 shows two examples of Feinberg's diagrams. Once the diagram is built, one has to count the number of *linkage classes* l. A *linkage class* is a group of complexes that are connected by reaction arrows. Hence, it is simply the number of separate "pieces" of which the diagram is built. For example, mechanism a) in Figure 6.7 has 2 linkage classes, while mechanism b) has 1 linkage class. Now, consider a reaction network with n_s species. A reaction vector in $\mathbb{R}^{n_s}$ is associated to each reaction in the network, obtained by subtracting the "reactant" complex vector from the "product" complex vector. Then, the *rank* of the reaction network s is the number of linearly independent vectors in the mechanism. Essentially, s represents the smallest number of reactions required such that all reaction stoichiometries in the mechanism can be constructed as linear

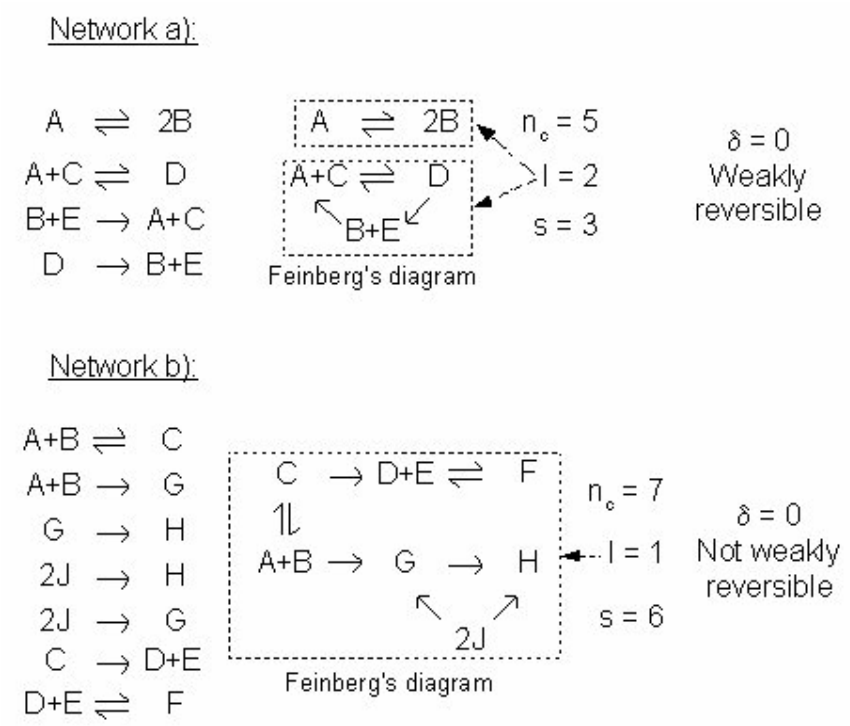

Figure 6.7: Examples of the construction of Feinberg's diagrams (Feinberg 1995*a*).

combinations of this set. The *deficiency* δ of a reaction network is a nonnegative integer index defined by the formula

$$\delta = n_c - l - s. \tag{6.43}$$

This index contains much information about the type of behavior that the network may admit. It is also possible to calculate a deficiency index for each individual linkage class. Both reaction networks in Figure 6.7 have deficiency zero.

Before we can present the theorems, we need some additional definitions. Two complexes in the same class are *strongly linked* if they "ultimately react" to each other, either by a reversible reaction, or through a sequence of (reversible or not reversible) reactions. The linkage class can thus be partitioned into equivalence classes called the *strong-linkage classes*. A *terminal strong-linkage class* is a strong-linkage class containing no complex that reacts to a complex in a different strong-linkage class. For example, network b) in Figure 6.7 has two terminal strong-linkage classes $\{D + E, F\}$ and $\{G, H, 2J\}$. A chemical reaction network is *reversible* if its "react to" reaction is symmetric, i.e. for every reaction in the network, its reverse reaction does also exist. A chemical reaction network is *weakly reversible* if its "ultimately react to" reaction is symmetric, i.e. for any pair of complexes connected with a directed arrow path in one direction, there exists an arrow path in another direction that also connect those complexes. In a weakly reversible network each linkage class is a terminal strong-linkage class. Network a) in Figure 6.7 is weakly reversible, while network b) is not weakly reversible. Finally, a reaction is said to have *mass action* kinetics when the rate function for each reaction is determined by the stoichiometry of the reaction, being the kinetic order of each reactant equal to the corresponding stoichiometric coefficient.

Theorem 14 (The Deficiency Zero Theorem (Feinberg 1987)) *For any reaction network of deficiency zero the following statements hold true:*
(i) If the network is not weakly reversible then, for arbitrary kinetics (not necessarily mass action), the differential equations for the corresponding reaction system can not admit a positive steady state (i.e. a steady-state where none of the reactants is depleted).
(ii) If the network is not weakly reversible then, for arbitrary kinetics (not necessarily mass action), then the differential equations for the corresponding reaction system can not admit a cyclic composition trajectory along which all species concentrations are positive.
(iii) if the network is weakly reversible then, for mass action kinetics (but regardless of the positive values the rate constants take), the differential equations for the corresponding reaction system have the following properties: There exist within each positive stoichiometric compatibility class precisely one steady-state;

that steady-state is asymptotically stable; and there is no nontrivial cyclic composition trajectory along which all species concentrations are positive.

Theorem 15 (The Deficiency One Theorem (Feinberg 1987)) *Consider a mass action system for which the underlying reaction network has l linkage classes, each containing just one terminal strong linkage class. Suppose that the deficiency of the network and the deficiencies of the individual linkage classes satisfy the following conditions:*
(i) $\delta_i \leq 1,\ i = 1,\ 2, \ldots, l$
(ii) $\delta = \sum_{i=1}^{l} \delta_i$.
Then, no matter what (positive) values the rate constants take, the corresponding differential equations can admit no more than one steady state within a positive stoichiometric compatibility class. If the network is weakly reversible, the differential equations admit precisely one steady state in each positive stoichiometric compatibility class.

Corollary 16 *A mass action system for which the underlying reaction network has just one linkage class can admit multiple steady states within a positive stoichiometric compatibility class only if the deficiency of the network or the number of its terminal strong linkage classes exceeds one.*

Some remarks may be useful:

- The method is not limited to small networks. It can be applied to very intrincate networks. This is quite practical, because the deficiency of the network can be calculated and the linkage classes can be studied even before one has written the system of differential equations.

- The method is not limited to closed reactors, as it may seem at first glance. Indeed, open reactors, heterogeneous reactions, and reactors where certain species concentrations are kept constant, can all be accommodated within the framework, by incorporating into the network certain pseudoreactions. Hence, if we have a continuous stirred tank reactor (CSTR), a pseudoreaction $B \xrightarrow{q} 0$ would account for the presence of B in the effluent stream q, whereas $0 \xrightarrow{q} A$ would account for the presence of A in the feed stream. Theorems 15 and 15 would then be applied to the *augmented* reaction network. Some examples can be found in (Feinberg 1979) and (Feinberg 1987).

- The strongest (and most useful) statements in the theorems apply only to networks with mass-action kinetics. This may sound as a strong limitation, but one should remember that mass-action kinetics are very widely used,

even in the field of particulate processes. Although the theorems can not give so strong results when dealing with non mass-action kinetics, they still provide some information about the existence or non-existence of certain dynamic behaviors.

- It may seem that most chemical reaction networks probably violate theorems 14 and 15, but this is false. Indeed, deficiency zero networks and deficiency one networks arise frequently.

- Although isothermal conditions are required, some of the conclusions are valid regardless of the values the kinetic constants may take.

In the context of inventory passivity-based control, we can make use of Feinberg's theory to study the stability of internal dynamics of systems with chemical reaction. Typically, the controlled inventories will be the energy, one or several component mole number, and/or total mass. Then, once the controlled inventories are tracked to their respective setpoints, the system whose dynamics we have to analyze is an open reactor with certain species regarded as constant. Then, the theorems are applied to the resulting *augmented* network. The goal of the controller is that our selection of controlled inventories are such that the remaining system of equations is a *deficiency zero* and *weakly reversible* network with mass action kinetics. Then, a steady-state compatible with any initial conditions does exist, is unique, and globally asymptotically stable. In other words, the internal dynamics are globally asymptotically stable and stabilization of the whole set of states will be achieved.

In the cases where the deficiency zero and deficiency one theorem can not confirm or deny the existence, uniqueness and stability of steady-states, other techniques of nonlinear kinetic dynamics may be used. Hence, a graphical method specific for CSTR, called the *species-complex-linkage graph*, was developed in (Schlosser & Feinberg 1994). Such a graph allows to conclude whether a kinetic network with mass-action kinetics can or can not give rise to multiple steady states for any combination of the residence time, rate constants and feed concentrations. This technique has certain similarities with Feinberg's approach but is not deficiency oriented. Another ambitious approach is the *stoichiometric network analysis (SNA)* by (Clarke 1980), that identifies critical subnetworks within a complex reaction mechanism that can result in instability. Although SNA is very powerful, it is not as easy to apply as Feinberg's technique:

> There is much in this chapter that would be of practical value to experimental chemists if they could only understand it. (Clarke 1980)

If none of these methods can provide conclusions on stability, then a local bifurcation analysis has to be carried out. In such an approach, the steady-state

values are plotted with respect to different values of the manipulated variables. Bifurcation plots may require extensive simulations and the results are not globally valid.

6.7 Connection to thermodynamics

Chapter 5 began with a description of control from a thermodynamic point of view. Control theory very seldom mentions thermodynamics, but there is a strong connection between the two fields (Ydstie & Alonso 1997) and (Luyben et al. 1998). Inventory passivity-based control is probably the approach that uses such a connection in the most direct way.

Thermodynamics is the science that studies various properties of a macroscopic system, the relationship between these various properties, and the transformations of states of matter (Kondepudi & Prigogine 1998). *Classical* thermodynamics was born as a result of the invention of heat engines, in an attempt to explain and define the limits of operation of such engines. It is founded on essentially two fundamental laws, one concerning *energy* and one concerning *entropy*. *Classical* thermodynamics only applies to *isolated*[1] systems and to *closed*[2] systems that are very near the state of *thermodynamic equilibrium*. The state of *thermodynamic equilibrium* is a fundamental concept in *classical* thermodynamics. A characteristic feature of *thermodynamic equilibrium* is the existence of *extremum principles*, i.e. there exist functions of the state called thermodynamic potentials which are extrema (minima or maxima) at the equilibrium. A fluctuation leading to a deviation from equilibrium is followed by a response which brings the system back to the extremum of the thermodynamic potential. The *thermodynamic equilibrium* is thus a stable state. For isolated systems, entropy is the corresponding thermodynamic potential and is maximized at equilibrium. For closed systems at constant entropy and volume, energy is the corresponding thermodynamic potential and is minimized at equilibrium.

Nonequilibrum thermodynamics, on the other hand, applies to *open*[3] systems, and to *closed* systems that are far from the equilibrium state. Note that the concept of *thermodynamic equilibrium* does not apply to open systems. Instead, the term *steady-state* is used to denote a time-invariant state of an open system. *Nonequilibrium* thermodynamics has its roots in the phenomenological laws of viscous flow, and accounts both for irreversible processes and states far from equilibrium. In contrast to *classical* thermodynamics, there is no guarantee that an extremum principle that predicts the state to which a nonequilibrium system will

[1] systems that do not exchange energy or matter with the exterior
[2] systems that exchange energy with the exterior but not matter
[3] systems that exchange both energy and matter with the exterior

evolve, exists. As a result, any fluctuations from a steady-state may no longer be damped, and a variety of phenomena that never appear in equilibrium systems, such as oscillating concentrations in a chemical system, may be observed. See (Kondepudi & Prigogine 1998) for an introduction to dissipative structures and order through fluctuations. Some nonequilibrium systems do have an extremum principle. Hence, an extremum principle, the principle of *minimum entropy production*, exists for nonequilibrium systems that are in the so-called linear regime, and that fulfill the Onsager's reciprocal relations:

> In the linear regime, the total entropy production in a system subject to flow of energy and matter, reaches a minimum value at the nonequilibrium steady-state. (Kondepudi & Prigogine 1998).

Now, note that systems fulfilling the criteria of inventory passivity-based control, are open systems that have stable nonequilibrium steady-states. Hence, the storage function V suggested in the inventory passivity-based approach is a thermodynamic potential that is minimized at the nonequilibrium steady-states. An extremum principle exists for passive process systems. Indeed, the storage function suggested in (Ydstie & Alonso 1997) was proven to be closely related to Keenan's thermodynamic availability. In (Coffey & Ydstie 1999), a new stored function named generalized availability was introduced. According to (Luyben et al. 1998), the storage function suggested in (Ydstie & Alonso 1997) is also related to the exergy function. Finally, a criterion of stability of general nonequilibrium steady-states are found in (Kondepudi & Prigogine 1998), that is based on Lyapunov theory, and where the excess entropy production is considered a Lyapunov functional. We can thus conclude that the storage function suggested in theorem 11 is a thermodynamic potential, related to the curvature of the entropy function.

6.8 Case study: *van der Vusse* reactor

A benchmark problem for nonlinear control design was proposed in (Chen, Kremling & Allgöwer 1995). The reactor under consideration is a continuous stirred tank reactor (CSTR) with a cooling jacket. The main reaction is given by the transformation of cyclopentadiene (species A) to the product cyclopentenol (species B). Cyclopentadiene reacts in an unwanted parallel reaction to the by-product dicyclopentadiene (substance D). Furthermore, cyclopentanediol (species C) is formed in an unwanted consecutive reaction from the product cyclopentenol. Such a reaction mechanism is called *van der Vusse* reaction, and is given by:

$$A \rightarrow B \rightarrow C \tag{6.44}$$

$$2A \rightarrow D. \tag{6.45}$$

The balance equations for such an homogenous reactor are given by

$$\begin{pmatrix} \frac{dN_A}{dt} \\ \frac{dN_B}{dt} \\ \frac{dN_C}{dt} \\ \frac{dN_D}{dt} \end{pmatrix} = \begin{pmatrix} C_{A,f} - C_A \\ C_{B,f} - C_B \\ C_{C,f} - C_C \\ C_{D,f} - C_D \end{pmatrix} q + \begin{pmatrix} -1 & 0 & -2 \\ 1 & -1 & 0 \\ 0 & 1 & 0 \\ 0 & 0 & 1 \end{pmatrix} \begin{pmatrix} r_1 V \\ r_2 V \\ r_3 V \end{pmatrix} \tag{6.46}$$

$$\frac{dU}{dt} = q\rho C_p \left(T_f - T\right) + (-\Delta H) r V + Q_{\text{he}} \tag{6.47}$$

$$\begin{pmatrix} N_A \\ N_B \\ N_C \\ N_D \\ U \end{pmatrix} = \begin{pmatrix} C_A V \\ C_B V \\ C_C V \\ C_D V \\ V\rho C_p \left(T - T_{\text{ref}}\right) \end{pmatrix} \tag{6.48}$$

$$\begin{pmatrix} r_1 \\ r_2 \\ r_3 \end{pmatrix} = \begin{pmatrix} k_{1,0} \exp\left(-\frac{E_1}{RT}\right) C_A \\ k_{2,0} \exp\left(-\frac{E_2}{RT}\right) C_B \\ k_{3,0} \exp\left(-\frac{E_2}{RT}\right) C_A^2 \end{pmatrix} \tag{6.49}$$

$$(-\Delta H) r V = \begin{pmatrix} -\Delta H_1 & -\Delta H_2 & -\Delta H_3 \end{pmatrix} \begin{pmatrix} r_1 V \\ r_2 V \\ r_3 V \end{pmatrix}, \tag{6.50}$$

where N_A, N_B, N_C, and N_C represent the number of moles in the reactor of species A, B, C, and D, respectively; C_A, C_B, C_C, and C_C represent molar concentration in the reactor; $C_{A,f}$, $C_{B,f}$, $C_{C,f}$, and $C_{D,f}$ represent molar concentration in the feed stream; V is the reactor volume; U indicates the internal energy within the reactor; T and T_f are the reactor and feed temperature, respectively; C_p is the fluid heat capacity; ρ is the fluid density; ΔH_1, ΔH_2 and ΔH_3 are the heat of reactions corresponding to reaction 1, 2, and 3, respectively; and Q_{he} is the exchanged heat flow between the reactor and cooling jacket. The reactions are assumed to have mass-rate kinetics, and the dependence of the kinetic constant with temperature follows Arrhenius' law. Table 6.1 summarizes the values of parameters for the model (the kinetic parameters are taken from (Chen et al. 1995)).

The manipulated variables are the flowrate q and the exchanged heat flow Q_{he}. The species of interest is species B. Therefore, the standard control goal would be to maximize the yield of B, and operate the reactor at isothermal conditions. If we chose the number of moles of species B and the internal energy as controlled

Table 6.1: Kinetic, thermodynamic and design parameters of the van der Vusse reactor.

$k_{1,0}$	$1.287 \cdot 10^{12}\,\mathrm{h}^{-1}$
$k_{2,0}$	$1.287 \cdot 10^{12}\,\mathrm{h}^{-1}$
$k_{3,0}$	$4.5215 \cdot 10^{9}\,(\mathrm{h\,mol/l})^{-1}$:
$\frac{E_1}{R}$	9758.3 K
$\frac{E_2}{R}$	9758.3 K
$\frac{E_3}{R}$	8560 K
ΔH_1	$4.2\,\mathrm{kJ/mol}A$
ΔH_2	$-11\,\mathrm{kJ/mol}B$
ΔH_2	$-41.85\,\mathrm{kJ/mol}A$
V	100 l
$C_{A,\mathrm{in}}$	5.10 mol/l
$C_{B,\mathrm{in}}$	0 mol/l
$C_{C,\mathrm{in}}$	0 mol/l
$C_{D,\mathrm{in}}$	0 mol/l
ρ	0.9342 kg/l
C_p	3.01 kJ/kg h

inventories, we would have the following control law:

$$\begin{pmatrix} -K_B\,(N_B - N_B^*) \\ -K_U\,(U - U^*) \end{pmatrix} = \begin{pmatrix} C_{B,f} - C_B & 0 \\ \rho C_p\,(T_f - T) & 1 \end{pmatrix} \begin{pmatrix} q \\ Q_{\mathrm{he}} \end{pmatrix} + \begin{pmatrix} 1 & -1 & 0 \\ -\Delta H_1 & -\Delta H_2 & -\Delta H_3 \end{pmatrix} \begin{pmatrix} r_1 V \\ r_2 V \\ r_3 V \end{pmatrix}. \quad (6.51)$$

We have to check if a unique solution for q and Q_{he} exists for any value the states may take, and if static controllability is achieved. We can begin by studying if there exists a value q^* and Q_{he}^* that can stabilize the controlled inventories to the setpoints, i.e.

$$\begin{pmatrix} 0 \\ 0 \end{pmatrix} = \begin{pmatrix} C_{B,f} - C_B^* & 0 \\ \rho C_p\,(T_f - T^*) & 1 \end{pmatrix} \begin{pmatrix} q^* \\ Q_{\mathrm{he}}^* \end{pmatrix} + \begin{pmatrix} 1 & -1 & 0 \\ -\Delta H_1 & -\Delta H_2 & -\Delta H_3 \end{pmatrix} \begin{pmatrix} k_1^* C_A V \\ k_2^* C_B^* V \\ k_3^* C_A^2 V \end{pmatrix}. \quad (6.52)$$

Some formulae manipulation gives

$$q^* = \frac{k_2^* C_B^* V - k_1^* C_A V}{C_{B,f} - C_B^*}. \quad (6.53)$$

In order for q^* to be constant, then C_A has to have reached a steady-state C_A^{SS}, i.e.

$$0 = \left(C_{A,f} - C_A^{SS}\right) q^* - k_1^* C_A^{SS} V - k_3^* \left(C_A^{SS}\right)^2 V. \tag{6.54}$$

Now, if equation 6.53 is substituted into equation 6.54, and $C_{B,f} = 0$, then we obtain

$$\left(k_3^* C_B^* + k_1^*\right)\left(C_A^{SS}\right)^2 - \left(k_2 C_B^* + k_1\left(C_{A,f} - C_B^*\right)\right)\left(C_A^{SS}\right) + k_2 C_B^* C_{A,f} = 0, \tag{6.55}$$

which means that there exists values of the kinetic constants that provide two positive solutions for equation 6.55, and consequently, for equation 6.53. Therefore, we can not select N_B as controlled inventory.

Let us thus choose the number of moles of species A and the internal energy as controlled inventories, yielding the following control law

$$\begin{pmatrix} -K_A\left(N_A - N_A^*\right) \\ -K_U\left(U - U^*\right) \end{pmatrix} = \begin{pmatrix} C_{A,f} - C_A & 0 \\ \rho C_p\left(T_f - T\right) & 1 \end{pmatrix} \begin{pmatrix} q \\ Q_{\text{he}} \end{pmatrix} + \begin{pmatrix} 1 & 0 & -2 \\ -\Delta H_1 & -\Delta H_2 & -\Delta H_3 \end{pmatrix} \begin{pmatrix} r_1 V \\ r_2 V \\ r_3 V \end{pmatrix}. \tag{6.56}$$

Let us check whether the available manipulated variables can lead the new controlled inventories to the given setpoint, i.e. whether the following system of equations has unique solution:

$$\begin{pmatrix} 0 \\ 0 \end{pmatrix} = \begin{pmatrix} C_{A,f} - C_A^* & 0 \\ \rho C_p\left(T_f - T^*\right) & 1 \end{pmatrix} \begin{pmatrix} q^* \\ Q_{\text{he}}^* \end{pmatrix} + \begin{pmatrix} 1 & 0 & -1 \\ -\Delta H_1 & -\Delta H_2 & -\Delta H_3 \end{pmatrix} \begin{pmatrix} k_1^* C_A^* V \\ k_2^* C_B V \\ k_3^*\left(C_A^*\right)^2 V \end{pmatrix}. \tag{6.57}$$

After some formulae manipulation we obtain

$$q^* = \frac{\left(k_1^* C_A^* + k_3^*\left(C_A^*\right)^2\right) V}{C_{A,f} - C_A^*} \tag{6.58}$$

$$Q_{\text{he}}^* = -q^* \rho C_p\left(T_f - T^*\right) + \Delta H r^* V. \tag{6.59}$$

Hence, there exists a unique value of the manipulated variables (for each selected pair of setpoints and initial conditions, and within the logic range of operation $0 \leq C_A^* < C_{A,f}$) that can keep the system in the selected setpoint once reached. Note however, that in order for Q_{he}^* to get to a constant value, C_B has to reach

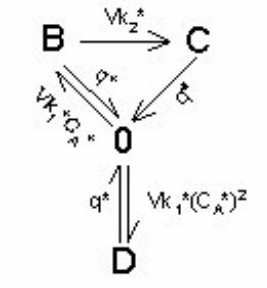

Figure 6.8: Feinberg's diagram corresponding to the Van der Vusse kinetics, when N_A and U are kept constant.

the steady-state too (C_B appears in $\Delta H r^* V$). Similarly, the control law can be solved with respect to the manipulated variables at each instant:

$$q(t) = -K_A \frac{C_A - C_A^*}{C_{A,f} - C_A} V + \frac{(k_1 + k_3 C_A)}{C_{A,f} - C_A} C_A V \tag{6.60}$$

$$Q_{\text{he}}(t) = -q^* \rho C_p (T_f - T^*) + \Delta H r V - K_U (U - U^*). \tag{6.61}$$

Now we can use Feinberg's theory to study the stability of the internal dynamics. Let us assume that N_A and U have reached their respective setpoints, and the manipulated variables are kept in the corresponding steady-state value. What happens then with the dynamics of N_B, N_C and N_D? Does a steady-state exist for them? Is the steady-state unique? Is the steady-state asymptotically stable? These kinds of questions can be answered by Feinberg's theorem. The system of equations under study is thus:

$$\begin{pmatrix} \frac{dN_B}{dt} \\ \frac{dN_C}{dt} \\ \frac{dN_D}{dt} \end{pmatrix} = \begin{pmatrix} C_{B,f} - C_B \\ C_{C,f} - C_C \\ C_{D,f} - C_D \end{pmatrix} q^* + \begin{pmatrix} 1 & -1 & 0 \\ 0 & 1 & 0 \\ 0 & 0 & 1 \end{pmatrix} \begin{pmatrix} k_1^* C_A^* V \\ k_2^* C_B V \\ k_3^* (C_A^*)^2 V \end{pmatrix} \tag{6.62}$$

$$\begin{pmatrix} \frac{dN_A}{dt} \\ \frac{dU}{dt} \end{pmatrix} = \begin{pmatrix} 0 \\ 0 \end{pmatrix}. \tag{6.63}$$

Figure 6.8 shows the corresponding Feinberg's network. Note that the *zero*-complex is used to account for the fact that we are dealing with an open reactor.

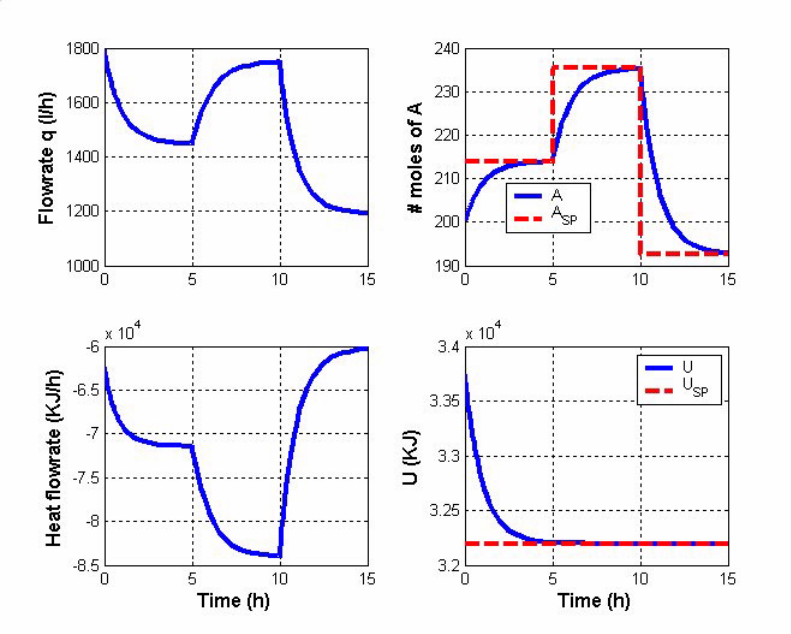

Figure 6.9: Closed-loop simulation of the Van der Vusse reactor. Manipulated variables and controlled inventories.

It is also straightforward to see that:

$$\begin{aligned} n_c &= 4 \\ l &= 1 \\ s &= \operatorname{rank} \begin{pmatrix} -1 & 1 & 0 & 0 \\ 0 & -1 & 1 & 0 \\ -1 & 0 & 1 & 0 \\ 0 & 0 & 1 & -1 \end{pmatrix} = 3 \\ \delta &= 0. \end{aligned}$$

Therefore, we have a deficiency-zero network. Moreover, the network is *weakly reversible*. Then, by application of theorem 14, we can conclude that there exists a steady-state for the uncontrolled inventories, the steady-state is unique (but distinct for each positive pair of N_A^* and U^*), and is asymptotically stable. Therefore, the conditions of theorem 11 are fulfilled, and when N_A and U are chosen as controlled inventories, the closed-loop is passive. Figures 6.9 and 6.10 show the results of closed-loop simulation of the suggested control structure. The initial conditions for the simulations are shown in Table 6.2, and the controller parameters and the setpoints are shown in Table 6.3. As expected, not only the controlled inventories reach their respective setpoints, but also the uncontrolled inventories

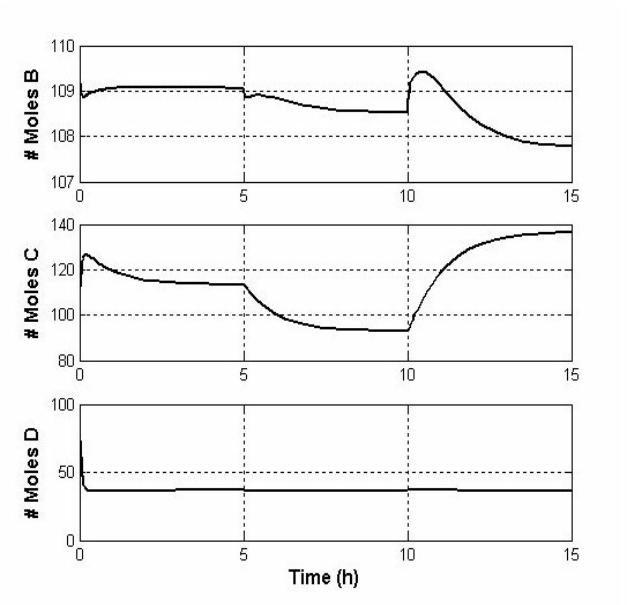

Figure 6.10: Closed-loop simulation of the Van der Vusse reactor. Uncontrolled inventories.

Table 6.2: Initial conditions for Van der Vusse reactor.

$N_A(0)$	$200\,\mathrm{mol}$
$N_B(0)$	$110\,\mathrm{mol}$
$N_C(0)$	$100\,\mathrm{mol}$
$N_D(0)$	$100\,\mathrm{mol}$
$U(0)$	$33743\,\mathrm{kJ}$

Table 6.3: Controller parameters and setpoints for the van der Vusse reactor.

K_A	$1\,\mathrm{h}^{-1}$
N_A^*	$\begin{cases} 214\,\mathrm{mol} & 0 \le t < 5\,\mathrm{h} \\ 235.4\,\mathrm{mol} & 5 \le t < 10\,\mathrm{h} \\ 192.6\,\mathrm{mol} & 10 \le t < 15\,\mathrm{h} \end{cases}$
K_U	$1\,\mathrm{h}^{-1}$
U^*	$100\,\mathrm{kJ}$

reach a steady-state. The suggested control is multivariable. Observe that when the setpoint for N_A is changed, both manipulated variables are moved in order to reach the new setpoint. Note also that the first setpoint for N_A corresponds to the steady-state that maximizes the yield of B for the selected temperature. This is confirmed by Figure 6.10. Therefore, even though we could not select B as controlled inventory, we can still achieve optimal conditions of B by a proper selection of the setpoints of the controller. In other words, the inventory passivity-based controller could be part of a multi-level hierarchy of control functions. The suggested controller would ensure stabilization of the system, and on top of it an optimizer could determine the optimal settings for the inventory passivity-based controller. In fact, the same process model could be used in both control levels.

Remark 17 *A P-controller was used. Alternatively, a PI- or a PID-controller might have been used. The choice of the controller parameters influences the velocity at which the controlled inventories reach their setpoints, the overshoot experienced by the uncontrolled inventories, and the extent of the change applied to the manipulated variables.*

Remark 18 *The change of setpoints was assumed to occur as a step change. We could have used a "smoother" version, for example, a first order model of the setpoint change and account for this in the control law 6.61.*

One of the manipulated variables used in the inventory passivity-based controller is the heat flow exchanged by the reactor and the cooling jacket. Obviously, this is not the actual manipulated variable. Heat flow in the cooling jacket is typically regulated by manipulating the flowrate of cooling fluid in the cooling jacket. Hence, a basic control loop is required to achieve the desired heat exchange. We could use inventory-passivity based control to design such an inner loop. Taking into account that the exchanged heat flow is given by

$$Q = -h_{\text{he}} S \left(T - T_{\text{he}}\right), \tag{6.64}$$

where h_{he} is the overall heat transfer coefficient, S is the surface available for heat transfer between the reactor and the cooling jacket, and T_{he} is the temperature in the cooling jacket. Complete-mix conditions are assumed in the cooling jacket, giving the following heat balance

$$\frac{dU_c}{dt} = q_{\text{he}} \rho_{\text{he}} C_{p,\text{he}} \left(T_{f,\text{he}} - T_{\text{he}}\right) - Q, \tag{6.65}$$

where ρ_{he} is the density of the cooling fluid, $C_{p,\text{he}}$ is its heat capacity, $T_{f,\text{he}}$ is the temperature of the cooling jacket at the inlet, V_{he} is the volume of the cooling

jacket and U_c is the internal energy stored in the cooling jacket. The control loop for the inner loop can thus be designed as follows

$$-K_{U_c}(U_c - U_c^*) = q_{\text{he}}\rho_{\text{he}}C_{p,\text{he}}\left(T_{f,\text{he}} - T_{\text{he}}\right) - Q, \tag{6.66}$$

where q_{he} is the manipulated variable, and U_c^* is the setpoint for this loop, given by

$$U_c^* = \rho_{\text{he}}C_{p,\text{he}}V_{\text{he}}\left(T + \frac{Q}{h_{\text{he}}S} - T_{\text{ref}}\right). \tag{6.67}$$

Hence, we have a cascade controller, in which the inner loop 6.66 should be designed with faster dynamics than the outer loop 6.61. The controllability and detectability conditions are still fulfilled, such that the closed-loop remain passive. Figures 6.11 and 6.12 show the simulation with the cascade controller. As expected, the controlled inventories reach their respective setpoints, and the uncontrolled inventories stabilize to a certain setpoint.

6.9 Case study: *Silgrain*® HR

This section illustrates how inventory passivity-based control can easily be applied to particulate processes. Only the main reactor (HR) of the *Silgrain*® process is considered for control purposes, for a number of reasons. First of all, the HR is the bottleneck of the process. Hence, only the material that has undergone disintegration in the HR, and is fine enough to be transported with the upcoming acid flow, is further processed in the remaining stages of the process. Since disintegration is thus the key stage, it is reasonable to focus the control efforts on disintegration. Moreover, the feasible manipulated variables are inputs to the HR. In contrast, as the *Silgrain*® process is today, the possibilities to manipulate the UR are restricted to manipulating the tapping rate, i.e. the residence time of the material in the reactor. Longer residence times in the UR may improve the chemical quality of the product, but at the cost of decreasing the production rate. If we want to improve both the product quality and the production rate, then disintegration has to be enhanced.

In practice, the FeSi feedstock is fed in a semibatch way. However, to test inventory passivity-based control, continuous feed of the FeSi feedstock is assumed. Semibatch feed is used in the real plant due to the structural set up of the process. Continuous feed in the simulations is not a limitation, since it is possible to design an equivalent semibatch operation from the continuous control moves given by the controller. Moreover, when constrained control is introduced in the next chapter, it will be shown that the semibatch operation can be achieved by simply using the proper setpoint signal.

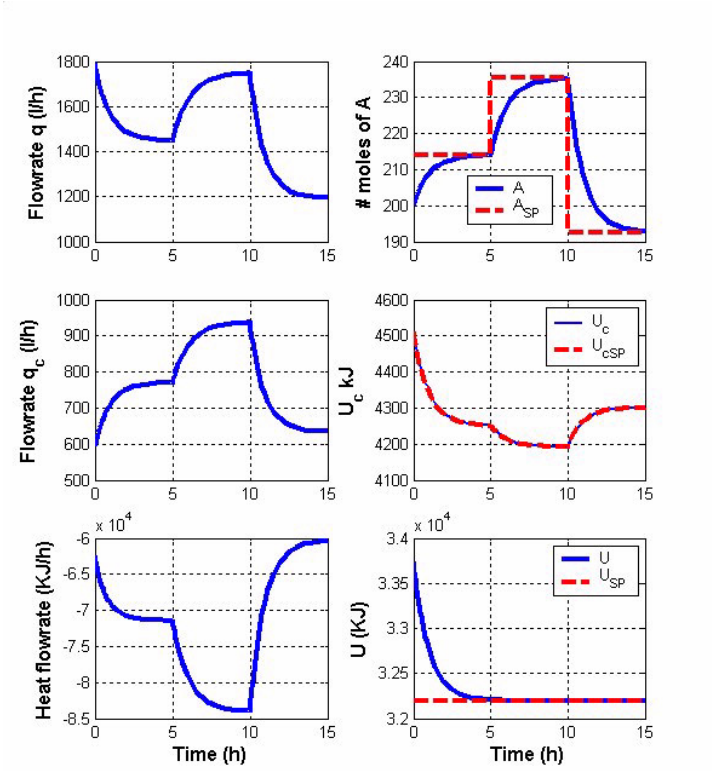

Figure 6.11: Closed-loop simulation of the Van der Vusse reactor for the cascade configuration. Manipulated variables and controlled inventories.

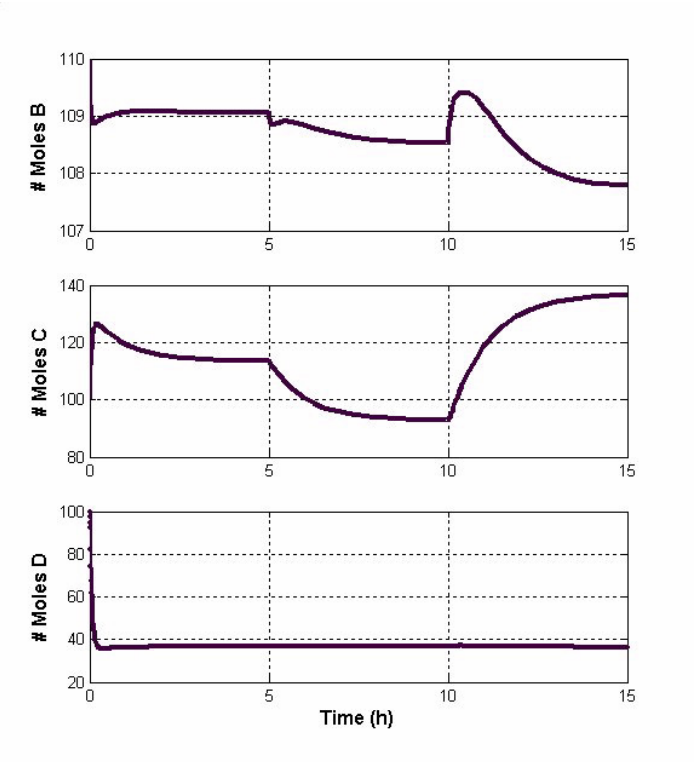

Figure 6.12: Closed-loop simulation of the Van der Vusse reactor for the cascade configuration. Uncontrolled inventories.

There are two available manipulated variables: the FeSi feedrate, $\dot{M}_{\text{feed}}$, and the temperature of the acid feed to the HR, $T_{\text{feed}}^{\text{acid}}$. Disintegration depends to a great extent on temperature, it is therefore clear that the internal energy should be one of the controlled inventories. As second controlled variable, the mass of particles within compartment I, $M_{\text{RI}}^{\text{active}}$, is chosen, i.e. the mass of particles that are still too large to be transported by the acid. The balances for the chosen inventories, considering the discretized PBE model, are:

$$\begin{aligned} \frac{dM_{\text{RI}}^{\text{active}}}{dt} &= \sum_{i=1}^{N} \frac{d\ \Phi_{i\,\text{RI}}^{\text{active}}}{dt} = \left(1 - w_{\text{feed}}^{\text{inert}}\right) \dot{M}_{\text{feed}} - \sum_{i=1}^{N} \dot{\Phi}_{i\,\text{RI,out}}^{\text{active}} \\ \left(V_1\ \rho c_{p\,1} + V_2\ \rho c_{p\,2}\right) \frac{dT}{dt} &= \dot{H}_{\text{in}} - \dot{H}_{\text{out}} + \sum_{\text{Me}} \left(-\Delta H_{\text{Me}}\right) r_{\text{RI}}^{\text{Me}} V_{\text{RI}} - \dot{Q}_{\text{surroundings}} \end{aligned} \tag{6.68}$$

where

$$\begin{aligned} \dot{H}_{\text{in}} &= \dot{M}_{\text{feed}} c_{p\text{solid}} \left(T_{\text{feed}}^{\text{solid}} - T_{\text{ref}}\right) + q_{\text{feed}}^{\text{acid}} \rho_{\text{acid}} c_{p\text{acid}} \left(T_{\text{feed}}^{\text{acid}} - T_{\text{ref}}\right) \\ \dot{H}_{\text{out}} &= q_{\text{RII,out}} \left|\rho c_p\right|_{\text{RII}} \left(T_{\text{HR}} - T_{\text{ref}}\right) \\ \rho c_{p\,i} &= \rho_{\text{acid}} c_{p\text{acid}} \varepsilon_i + \rho_{\text{solid}} c_{p\text{solid}} \left(1 - \varepsilon_i\right) \quad i = \text{RI, RII} \\ \Delta H_{\text{Me}} &= \Delta H_{\text{Me}}^{0} + \Delta H_{\text{Me}}^{T} T \\ \dot{Q}_{\text{surroundings}} &= u_{\text{overall}}\ S\ \left(T - T_{\text{surroundings}}\right). \end{aligned}$$

Note that the energy balance is expressed in terms of the derivative of T, instead of the derivative of an extensive variable. This is due to the assumptions made in the model, and due to the need of expressing the energy balance as a function of available information, i.e. reaction enthalpies, etc. However, this is not any inconvenience. We can still use inventory passivity-based control without any change, where one of the controlled variables is now an intensive variable: T. Inventory passivity-based control is based on using the inventory balances in the control law. It does not matter if one or some of the inventory balances are expressed in an intensive variable instead of an extensive variable. The control law is

$$-Ke_y = \phi_y u + p_y \tag{6.69}$$

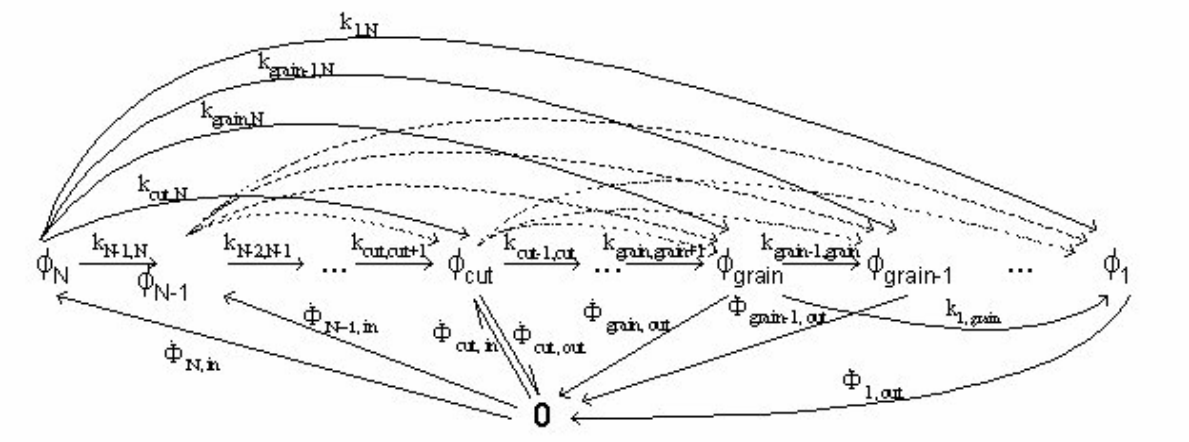

Figure 6.13: Feinberg diagram of the discretized HR dynamics.

where

$$
\begin{aligned}
-Ke_y &= \begin{pmatrix} -K_M & 0 \\ 0 & -K_T\left(V_1\,\rho c_{p\,1} + V_2\,\rho c_{p\,2}\right) \end{pmatrix} \begin{pmatrix} M_{\mathrm{RI}}^{\mathrm{active}} - M^* \\ T - T^* \end{pmatrix} \\
\phi_y u &= \begin{pmatrix} \left(1 - w_{\mathrm{feed}}^{\mathrm{inert}}\right) & 0 \\ c_{p\mathrm{solid}}\left(T_{\mathrm{feed}}^{\mathrm{solid}} - T_{\mathrm{ref}}\right) & q_{\mathrm{feed}}^{\mathrm{acid}}\rho_{\mathrm{acid}}c_{p\mathrm{acid}} \end{pmatrix} \begin{pmatrix} \dot{M}_{\mathrm{feed}} \\ T_{\mathrm{feed}}^{\mathrm{acid}} \end{pmatrix} \\
p_y &= \begin{pmatrix} -\sum_{i=1}^{N} \dot{\Phi}_{i\,\mathrm{RI,out}}^{\mathrm{active}} \\ -\dot{H}_{\mathrm{out}} + \sum_{\mathrm{Me}} \left(-\Delta H_{\mathrm{Me}}\right) r_{\mathrm{RI}}^{\mathrm{Me}} V_{\mathrm{RI}} - \dot{Q}_{\mathrm{surroundings}} \end{pmatrix}.
\end{aligned}
$$

Such a control law has a unique solution at any instant, since the matrix ϕ_y is invertible for all physically realizable states ($w_{\mathrm{feed}}^{\mathrm{inert}} < 1$, $q_{\mathrm{feed}}^{\mathrm{acid}} > 0$), and the production term p_y is bounded at any instant. Moreover, the selected inventories are statically controllable from the selected inputs as long as the internal dynamics are stable, since the control law depends on some of the internal states.

The dynamics of compartment II are stable. Similarly, the simple kinetic model used in compartment I and presented in section 4.5.2 also has stable dynamics. Therefore, the only states that may show unstable dynamic behavior are the particle size distributions of the active and inert material in compartment I, which are the states being closely related to disintegration. The dynamics of the PSD of active feedstock can be studied in the framework of Feinberg's theory. Indeed, we can interpret disintegration as the reaction network shown in Figure 6.13. The disintegration process is thus equivalent to a network of series and parallel reactions among N isomers, ϕ_1, ϕ_2, $\ldots$, ϕ_N, where isomer i reacts to any isomer k as long as $k < i$, and $i >$ grain. Isomers ϕ_N, ϕ_{N-1}, $\ldots$, ϕ_{cut} are fed to the reactor but

do not leave the reactor, while the remaining isomers are not present in the feed but leave the reactor. Such an inlet and outlet flow of compounds are represented in Feinberg's diagram with reactions with the zeroth complex. It is also straightforward to note that ϕ_N is the amount of particles of largest size, ϕ_1 is the amount of particles of smallest size, ϕ_{cut} is the amount of particles of the cut size and ϕ_{grain} is the amount of particles of the smallest grains that can still disintegrate. The kinetic constants k_{ij} are a function of the birth and death functions, as follows:

$$k_{ij} = \bar{b}\left(x_i, x_j\right) a_j.$$

Although the resulting Feinberg's network seems quite complex, it is straightforward to calculate the deficiency. The number of complexes, the number of linkage classes, the rank, and the deficiency are, respectively,

$$\begin{aligned} n_c &= N+1 \\ l &= 1 \\ s &= N \\ \delta &= 0. \end{aligned}$$

Now, the reaction network shown in Figure 6.13 is weakly reversible, and the disintegration kinetics in the HR-model are assumed to be mass-action. Hence, all requirements of theorem 14 are met, and we can conclude that even though the reaction network apparently is very complex, the system can not experience complicated nonlinear behavior. There exists a steady-state that corresponds to each pair of constant values of $\dot{M}_{\text{feed}}$ and $T_{\text{feed}}^{\text{acid}}$. Such steady-states not only exist; they are also unique and asymptotically stable. Therefore, static controllability is achieved. Since all the requirements of theorem 11 are fulfilled, the closed-loop is passive and stable when using the control law in equation 6.69.

Before showing the simulation analysis, it is noteworthy to take a closer look at the Feinberg diagram in Figure 6.13. The network is weakly reversible due to the presence of the zeroth complex, i.e. because of being an open system. If there were neither feedstock flowing in, nor material flowing out of the compartment, then we would have the network in Figure 6.14. Such a network has also deficiency zero:

$$\begin{aligned} n_c &= N \\ l &= 1 \\ s &= N-1 \\ \delta &= 0 \end{aligned}$$

but is not weakly reversible. Then, according to theorem 14, it is not possible to have a positive steady-state, i.e. a steady-state where none of the reactants is

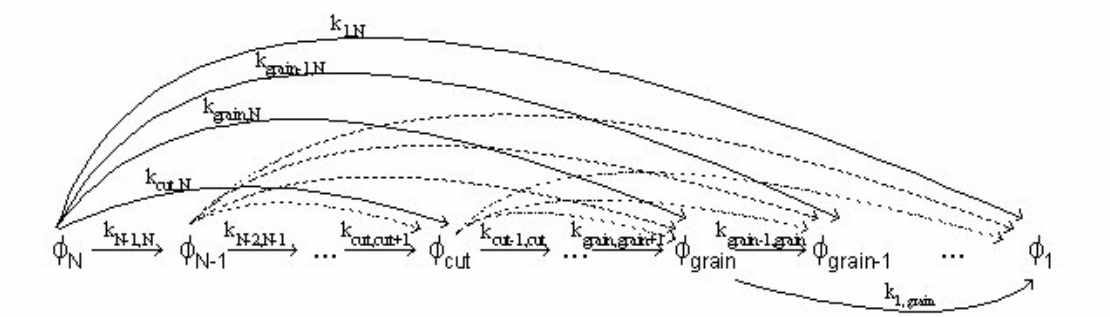

Figure 6.14: Feinberg diagram of batch disintegration.

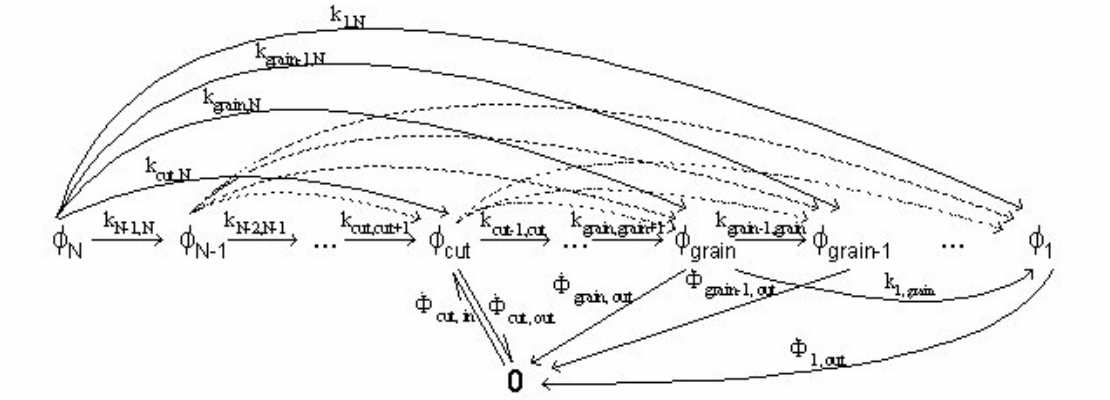

Figure 6.15: Feinberg diagram of disintegration when there is not FeSi feedstock, but there is outflow.

depleted. Such a result is not really new, we know that if we carry out the disintegration in a batch reactor, after a certain period of time all the FeSi feedstock would have disintegrated into particles of smaller size than D_{grain}. Figure 6.15 shows Feinberg's network corresponding to the part of a semibatch operation at which there is not FeSi feedstock, but there is outflow. Again, the kinetic network has deficiency zero, and is not weakly reversible. Therefore, no positive steady-state is possible: the larger particles will all be depleted after a sufficiently long period of time. Such a conclusion was again expected. Finally, note that for the continuous operation (and the semibatch operation), particles with $D_i < D_{\text{cut}}$ have an outflow $\dot{\Phi}_{i,\text{out}}$ that equals the sum of produced particles of this size from breakage of larger particles. Therefore, ϕ_i is actually equal to zero within compartment I, as assumed in the model. This means that we could have simplified the network

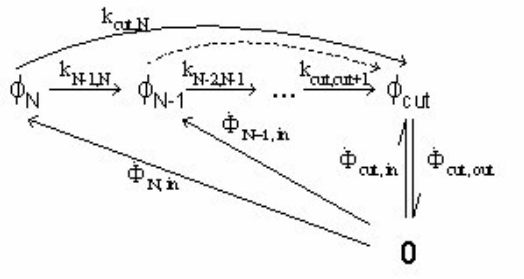

Figure 6.16: Simplified (Deficiency-zero) Feinberg network of disintegration in compartment I of the HR.

in Figure 6.13 to the simpler network in Figure 6.16 if we were only interested in the steady-state within compartment I. However, since we are interested in the whole HR, the best is to use the network in Figure 6.13.

As regards the inert fraction of the FeSi feedstock, it is quite straightforward to see that the manipulated variables in the suggested control law in equation 6.69 can not stabilize the states related to the inert fraction $(\Phi_i{}_{\mathrm{RI}}^{\mathrm{inert}}, V_{\mathrm{RI}})$. In other words, such states are not detectable from the controlled inventories. This is not a surprising result; it is well-known that the inert fraction of the FeSi feedstock accumulates in compartment I unless inert tapping is carried out. Since the inert fraction is small, inert tapping is carried out only a few times per year. We could consider the inert tapping flowrate as a third manipulated variable: $q_{\mathrm{RI,tapping}}^{\mathrm{inert}}$, and select the total mass of inert material in compartment I, $M_{\mathrm{RI}}^{\mathrm{inert}} = \sum_{i=1}^{N} \Phi_i{}_{\mathrm{RI}}^{\mathrm{active}}$, as third control inventory. We would need the following additional control loop:

$$-K_{M_{\mathrm{inert}}} \left(M_{\mathrm{RI}}^{\mathrm{inert}} - M_{\mathrm{inert}}^{*}\right) = w_{\mathrm{feed}}^{\mathrm{inert}} M_{\mathrm{in}} - q_{\mathrm{RI,tapping}}^{\mathrm{inert}} (1 - \varepsilon_{\mathrm{RI}}) w_{\mathrm{RI}}^{\mathrm{inert}}. \tag{6.70}$$

If we did so, then all the states of the system would be detectable from the controlled inventories, and then the whole system would be stabilized by the suggested (3 MV, 3 CV) inventory passivity-based control strategy. However, in practice, it is more suitable to carry out inert tapping a few times a year, than attempting continuous inert tapping. Therefore, in the simulation analysis, the (2 MV, 2 CV) control law shown in equation 6.69 is used, and we account for that the states related to the inert material will not stabilize when $w_{\mathrm{feed}}^{\mathrm{inert}} > 0$.

Figure 6.17 shows the time evolution of the manipulated variables and controlled variables. As expected, the controlled variables converge smoothly to their respective setpoints, without overshoot or oscillations. Note also that the control is multivariable, since a change in any of the setpoints involves changes in both manipulated variables. Figure 6.18 shows the time evolution of some selected variables of the system, assuming that no inert is present in the FeSi feedstock. As

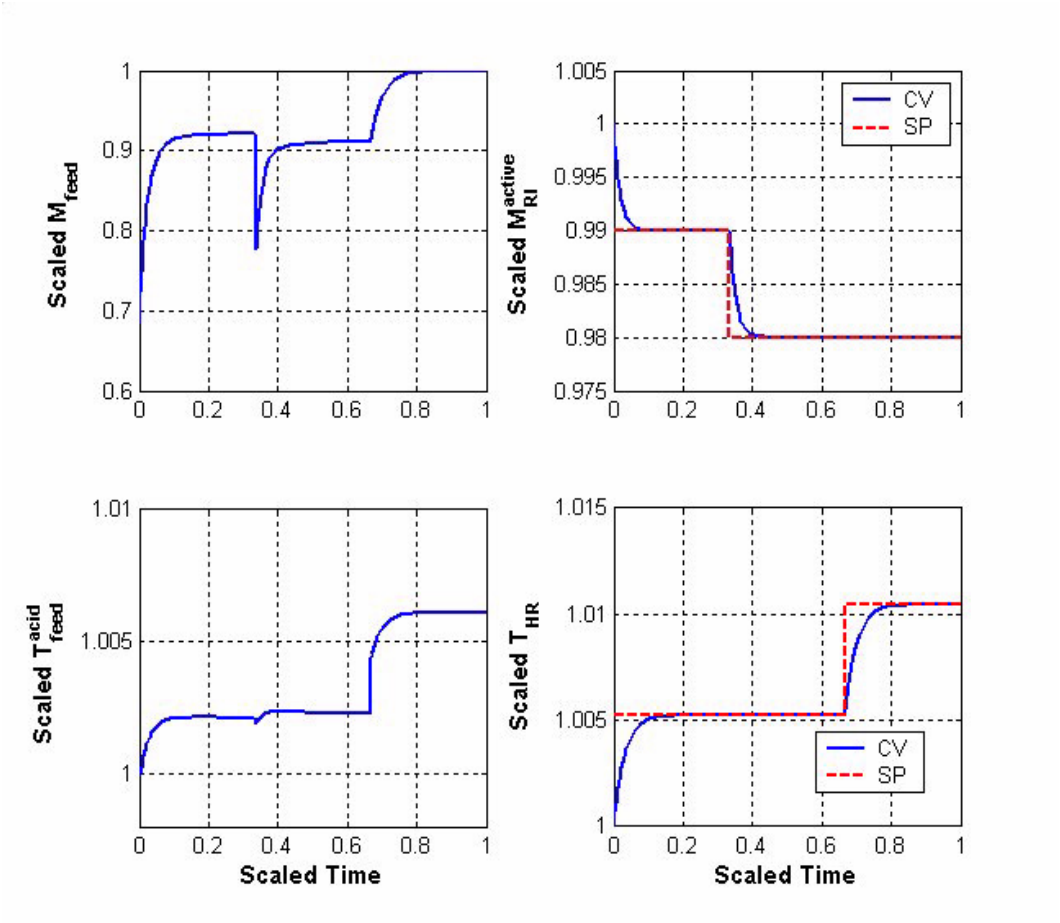

Figure 6.17: Closed-loop simulation of the HR. Manipulated variables and controlled inventories.

expected, all the states stabilize and reach a steady-state. Figure 6.19 shows the time evolution of the same states as shown in Figure 6.18, but when some inert material is present in the FeSi feedstock. The fraction of inert material is unrealistically high, to facilitate comparison with Figure 6.18. As discussed before, the states related to the inert material do not stabilize now. The remaining states do still stabilize. The states related to the inert material could be stabilized by adding the additional control loop in equation 6.70.

Note that although the states of the system stabilize, the rates at which the states reach the steady-state vary considerably among different states. Some of them have rapid dynamics, while others evolve in a sluggish manner. Note also that the manipulated variable $T_{\text{feed}}^{\text{acid}}$ requires, in turn, a basic control loop to be manipulated. A small heat exchanger would be needed upstream of the HR, where $T_{\text{feed}}^{\text{acid}}$ is the controlled output, and the fluid flow in the heating/cooling jacket is the manipulated variable. Such a situation is similar to the cascade controller suggested for the van der Vusse reactor in the previous section.

Remark 19 *Since the controlled inventories have a predictable first-order response under closed-loop operation, the tuning of the controller parameters may seem relatively straightforward. However, in addition to the response velocity of the controlled inventories, some other factors to consider when tuning the inventory passivity-based controller are:*
- the larger the values of the proportional constants K_M and K_U, the shorter the time it takes for the controlled inventories to reach the setpoints, but the more aggressive the moves of the manipulated variables.
- the values of the proportional constants influence the dynamics of the remaining inventories and states.
- the selection of the setpoints influences the values at which the uncontrolled inventories and states stabilize. Hence, we can indirectly control one or more of the states of the system by a proper selection of the controller setpoints. For example, in the Silgrain® *process we may be interested in controlling/optimizing the mass rate of disintegrated material leaving the* HR *and entering the* UR*. Then, we should integrate the inventory-passivity based controller in a multi-level hierarchy of control functions.*

6.9.1 Comparison with other methods for control of particulate processes

Despite having a large-scale, nonlinear particulate system, it has been proved that a proper choice of a few inputs and outputs of the system, combined with a nonlinear feedback law, may stabilize the whole system, assuming perfect model and available state measurements. Such assumptions may seem both strict and

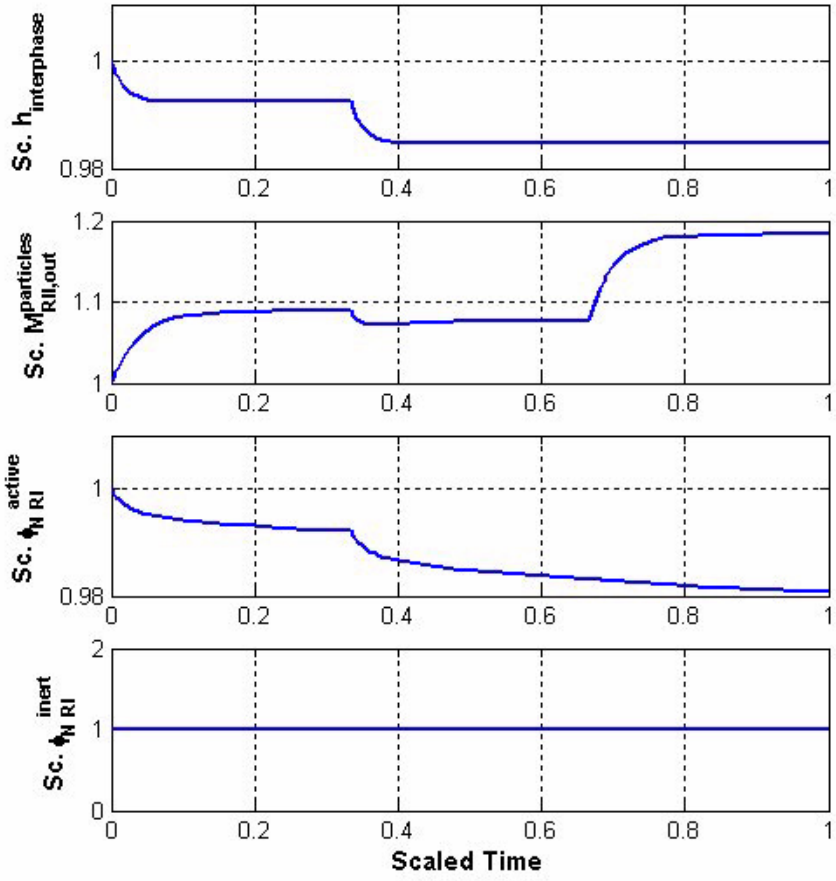

Figure 6.18: Closed-loop simulation of the HR when $w_{\text{feed}}^{\text{inert}} = 0$. Selected variables: interphase level between compartments I and II, mass flowrate of particles leaving compartment II, mass of particles of active feedstock with size x_N within compartment I, and mass of particles of inert feedstock with size x_N, within compartment I.

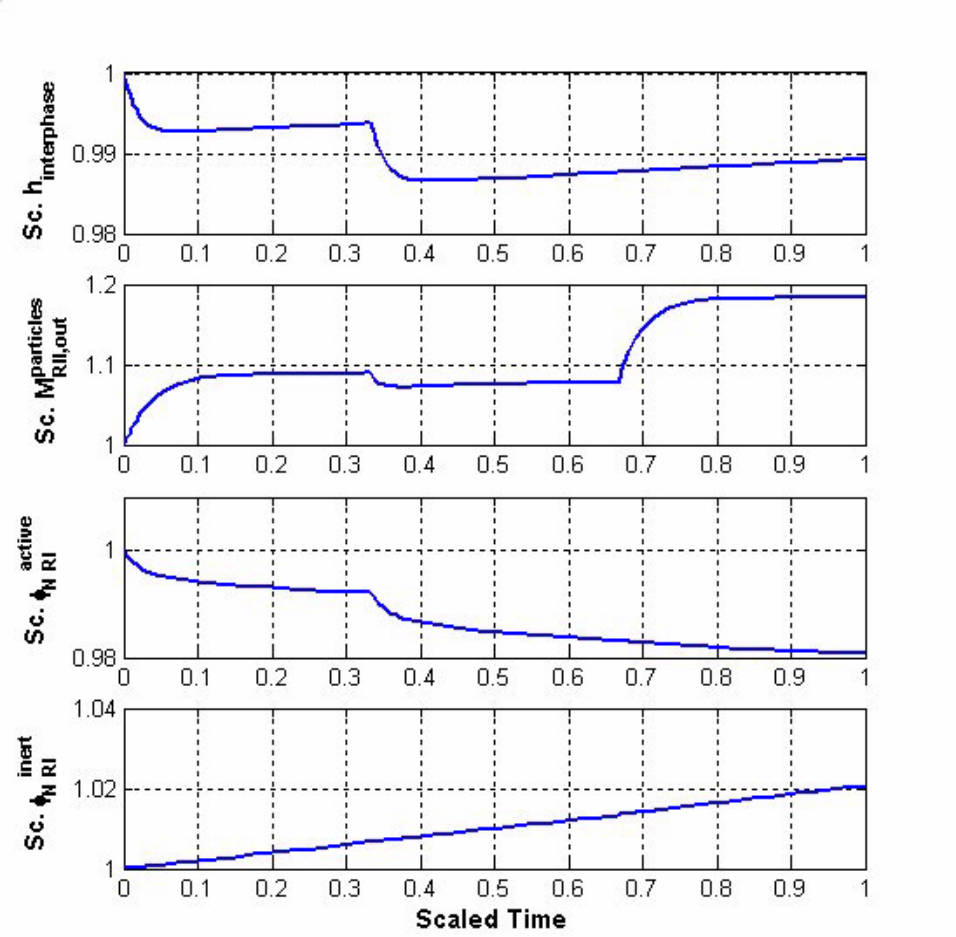

Figure 6.19: Closed-loop simulation of the HR when $w_{\text{feed}}^{\text{inert}} > 0$. Selected variables: interphase level between compartments I and II, mass flowrate of particles leaving compartment II, mass of particles of active feedstock with size x_N within compartment I, and mass of particles of inert feedstock with size x_N, within compartment I.

unrealistic, since models are never perfect, and often some of the states that may be involved in the control law are not measurable in particulate systems. However, note that all published material on model-based control of particulate processes do make the same assumptions of perfect model and available state measurements, and still none of them can prove global stability. Most methods evaluate the performance of the closed-loop controller by a mere simulation analysis. Others just prove local stability.

Particulate process models are large-scale models due to the distributed nature of particulate processes. In order to design a controller that may be implementable in practice, only a few outputs can be controlled. In most of the references in the literature, a heuristic selection of the controlled outputs is carried out (Zhu et al. 2000), (Zeaiter, Romagnoli, Barton & Gomes 2002), and (Mantzaris, Srienc & Dautidis 2002). Interestingly, in some cases this heuristic selection is a subset of the original state vector (Zhu et al. 2000). A different approach, suggested by Christofides et al., consists in first obtaining a low-order ODE approximation of the particulate process model, and then use such a model for the synthesis of an output feedback controller (Chiu & Christofides 1999), (Christofides 2002). The model reduction procedure is based on a combination of the method of weighted residuals and the concept of approximate inertial manifold. They recognize that many particulate processes exhibit low-dimensional dynamic behavior:

> We note that even though many particulate processes exhibit low-dimensional dynamic behavior, the delicate mathematical question of rigorously establishing the existence of inertial manifolds for particulate process model, at this stage is unresolved. (Chiu & Christofides 1999)

Christofides et al. use some approximate mathematical methods to find a low-dimensional model that captures the dominant dynamics of the process. The inventory passivity-based approach suggested in this chapter also takes advantage of the low-dimensional dynamic behavior of particulate processes. This is the reason why choosing a low-order subset of the inventories is sufficient to stabilize many particulate processes. Inventory passivity-based control uses well-established techniques of kinetic network theory to make sure that the selected inventories capture the dominant dynamics of the process and that the internal dynamics are stable. Such techniques are relatively straightforward to use and do not require as high level of advanced mathematics as the approximate inertial manifold concept (except for SNA by (Clarke 1980), which requires knowledge of topology). Finally, and most important, these techniques may provide global results, as opposed to the approximate inertial manifold.

As mentioned above, the main advantage of inventory passivity-based control is that it provides global stability results. The method by Christofides et al.

only proves local exponential stability. The approaches based on model predictive control study the performance of the closed-loop response mainly by computer simulations (Zhu et al. 2000), (Mantzaris et al. 2002), and in some instances by comparison with experimental results from a laboratory-scale plant (Zeaiter, Romagnoli, Barton & Gomes 2002).

6.10 Conclusions

The original theory for inventory passivity-based control by Farschman, Viswanath & Ydstie (1998) shows that the balance equations of process systems can be used to define a controller using feedback linearization that brings the controlled inventories to their setpoints by adjusting flows. The methodological framework is extended in this chapter to include reactive process systems and particulate process systems. Such processes show considerably more complicated nonlinear behavior than the process systems without reaction. The stability proof considered previously by Farschman, Viswanath & Ydstie (1998) considered only the convergence of the controlled inventories to their setpoints. The extended proof given in this thesis proves also stability of the remaining states of the system provided that certain controllability and detectability requirements are met. The relevance of the stability property is emphasized by comparing the approach with other well-known approaches of nonlinear control. A more detailed description of the controllability and detectability requirements is given. Proving detectability is particularly difficult for nonlinear systems. However, there exist powerful theories in the field of nonlinear chemical dynamics that may be used to check detectability in chemical reaction systems. The chemical network approach by Feinberg; Horn and Jackson is introduced and connected with the inventory passivity-based control concept. A brief discussion about the link to nonequilibrium thermodynamics is given in section 6.7. It is concluded that process systems fulfilling the requirements of the inventory passivity-based approach are nonequilibrium systems for which an extremum principle exist. The storage function is the corresponding thermodynamic potential. The control design methodology is illustrated with two examples: the van der Vusse reactor, and the *Silgrain*® process. It is shown that inventory-passivity based control can be easily applied to particulate processes. A discussion of the advantages of the suggested approach compared to other approaches for control of particulate processes is also discussed.

Despite all the advantages of the inventory passivity-based method, there are still some important questions that should be investigated:

- How does the presence of input constraints affect stability and controller performance?

- How does the presence of model errors affect stability and controller performance?
- How does the presence of an observer affect stability and controller performance?
- What is the role of inventory passivity-based control in the framework of plantwide control?
- Can inventory passivity-based control be combined with statistical process monitoring?

These questions will be the focus of the next chapter.

Chapter 7

Advanced issues in inventory passivity-based control

7.1 Introduction

The previous chapter discussed the performance of the controller under ideal conditions. Models are not perfect, there are disturbances, there are constraints on the manipulated variables, and there are states that can not be measured or that are too expensive to measure. It is thus relevant to evaluate the performance of the suggested control methodology under more realistic conditions.

Section 7.2 discusses the effect of input constraints, and the ability of inventory passivity-based control to handle them. Section 7.3 shows how an approach reported in literature, that combines inventory passivity-based control and sliding control, handles model errors and disturbances in a robust way, and how the approach is directly applicable to systems with chemical reaction and to particulate systems. The importance and potential of using observers is discussed in section 7.4, and although no observer is developed for the *Silgrain*® process, the most recent developments in nonlinear observers are reviewed. Section 7.5 shows that inventory passivity-based control can be used to automate processes that operate in semibatch. Finally, section 7.6 discusses the role of inventory passivity-based control in the framework of plantwide control, as well as the advantages of combining inventory passivity-based control with statistical process control.

7.2 Constrained control

Constraints on the manipulated variables are always present due to the inherent limitations of the actuators. Hence, a valve has a limited range of operation: it can not be open less then 0% or more than 100%. Such constraints that are related

to physical limitations are often referred to as *hard* constraints. There are other types of constraints that may be considered in the design of the controller, such as bounds in process outputs, quality constraints, safety margins, etc. Such types of constraints that can be relaxed are often referred to as *soft* constraints. The attention here is focused on hard constraints, since they can not be avoided.

A typical way to introduce input constraints on the controller is by a saturation function or selector:

$$u = \begin{cases} u_{\max} & \text{if} \quad u_{\text{calculated}} > u_{\max} \\ u_{\text{calculated}} & \text{if} \quad u_{\min} \leq u_{\text{calculated}} \leq u_{\max} \\ u_{\min} & \text{if} \quad u_{\text{calculated}} < u_{\min}. \end{cases} . \tag{7.1}$$

Note that such a control law is nonlinear as a result of the saturation. Moreover, constrained control poses important limitations on the ability to steer processes:

- Some setpoints may not be possible to reach under constrained control, irrespective of the choice of the control strategy. The set of unfeasible setpoints depends on the range of the constraints. Hence, the tighter the range $[u_{\min},\ u_{\max}]$, the larger the set of unfeasible setpoints.

- A performance deterioration of the closed loop response may occur when the manipulated variable is saturated, in the form of sluggishness of response or even loss of stability.

- The controller becomes more difficult to tune. In addition, wind-up problems may appear when the controller has integral compensation and the constraints are active.

In the field of control of particulate processes, the effect of constraints has seldom been accounted for, mainly because most of the reported works are exclusively based on simulation studies. A notable exception is the work reported in (El-Farra et al. 2001) and (Christofides 2002). The methodology reported in these references starts with an explicit characterization of the set of admissible setpoints that can be achieved in the presence of constraints. This information, together with a reduced order ODE model of the process, is used as the basis for the synthesis of a nonlinear bounded output feedback controller that enforces locally exponential stability in the closed-loop system. Such a controller is synthesized via Lyapunov-based control methods.

In general control applications, the detrimental effects of input constraints have been widely recognized and studied. Model predictive control is possibly the framework in which the most notable contributions have been achieved to deal with constraints. Linear model predictive control accounting for input constraints has

been applied to particulate processes, see for example (Zhu et al. 2000), but linear models can not always represent the dynamics of particulate processes well.

Constraint handling in the framework of inventory passivity-based control can be carried out in a relatively straightforward way, as long as the conditions of theorem 11 (proving stabilization of chemical reaction networks) are met for the nominal control. The synthesis of a bounded controller involves some additional stages as compared to the procedure presented in section 6.3:

1. Determination of constraints. The limitations of the actuators have to be studied, and a decision on the range of operation of each actuator

$$[u_{i,\min},\ u_{i,\max}] \qquad \forall u_i \tag{7.2}$$

has to be done.

2. Investigation of the feasibility of the desired setpoints. The approach by (Christofides 2002) consists in characterizing the steady-state feasibility, i.e. the set of admissible setpoints for the given constraints. This is done by solving the system of algebraic equations resulting from forcing the accumulation term of the dynamic model to be equal to zero and by considering a given value of $u_i \in [u_{i,\min},\ u_{i,\max}]$, i.e. for an inventory model solving the following system of equations

$$0 = \phi_y u_i + p_y. \tag{7.3}$$

Then, by repeating such a calculation for different values of u_i, a dependence of the steady-states with the input value can be identified. Note that this analysis is independent of the specific control strategy. An alternative approach could just be to analyze whether the specific setpoints for the inventories that we are interested in can be achieved for a steady-state value of the manipulated variables that lies within the constraints or not.

3. Investigation of the controllability of the desired setpoint. Although a setpoint is steady-state feasible, there is not guarantee that such a setpoint can be achieved under a given controller and starting from any given initial condition (Christofides 2002). Since the manipulated variables are now constrained, the controllability requirement is more difficult to fulfill than in the nominal case. In (Farschman 1998) a controllability requirement adapted to constrained control, named ϵ-controllability, was introduced.

Definition 20 (Farschman (1998)) *Let $\epsilon > 0$ be a real number. An inventory $y(x)$ is said to be ϵ-controllable if there exists a $u \in [u_{i,\min},\ u_{i,\max}]$ such that for*

all x, the following is true,

$$-\epsilon \leq \frac{dy}{dt} \leq \epsilon. \tag{7.4}$$

Now, theorem 11 can be reformulated to account for constrained control as follows:

Corollary 21 *The thermodynamic system 6.10 is rendered passive with passive mapping*

$$\begin{array}{rcl} \textit{passive input} & \rightarrow & \phi_y(x)\,u + p_y(x) \\ \textit{passive output} & \rightarrow & \bar{y} = y - y^* \end{array}$$

and storage function

$$V = \frac{1}{2}\bar{y}^T\bar{y} + \frac{1}{2}\bar{z}^T\bar{z}\,\mathrm{clip}(t), \tag{7.5}$$

by the control law

$$\begin{array}{rcl} -K\bar{y} & = & \phi_y(x)\,u_{\text{calculated}} + p_y(x) - \dfrac{dy^*}{dt} \\ u & = & \begin{cases} u_{\max} & \textit{if} \quad u_{\text{calculated}} > u_{\max} \\ u_{\text{calculated}} & \textit{if} \quad u_{\min} \leq u_{\text{calculated}} \leq u_{\max} \\ u_{\min} & \textit{if} \quad u_{\text{calculated}} < u_{\min} \end{cases}. \end{array} \tag{7.6}$$

Passivity is ensured as long as the setpoint is feasible, the inventories are ϵ-controllable at any instant time t and as long as $\bar{z}$ is zero-state detectable from $\bar{y}$. Under these conditions, the inventories converge to their respective setpoints, and the remaining states stabilize to a certain steady-state value.

Proof. The proof is very similar to the proof corresponding to theorem 11. The main difference is when one or several constraints are active. Let us assume that during the interval $[t_{c,1}, t_{c,2}]$ one or some constraints are active. Then, for one or several of the controlled inventories, the evolution of the output error is given by:

$$\frac{d\bar{y}_i}{dt} \leq -\epsilon. \tag{7.7}$$

Those inventories that are not affected by the constrained manipulated variables have the following dynamics:

$$\frac{d\bar{y}_j}{dt} = -K_j\bar{y}_j. \tag{7.8}$$

Then, the passivity inequality can be written as

$$V_{c,1} - V_{c,2} \leq \int_{t_{c,1}}^{t_{c,2}} \left(\sum_i -\epsilon + \sum_j -K_j\bar{y}_j^2 \right) d\tau, \tag{7.9}$$

and the inequality becomes an equality. Therefore, the requirement of ϵ-controllability ensures that the inventories reach their respective steady-states, since the inventory derivatives can be forced to have positive or negative value at any instant. Once the setpoints are reached, the stabilization of the remaining uncontrolled states takes place in an equivalent way to that in unconstrained control. ■

In the case that the requirements of corollary are violated, stabilization can still be ensured for certain types of systems. In this work special attention is being paid to particulate systems, that in many cases can be interpreted as a chemical reaction network.

Corollary 22 *Chemical reaction networks (including particulate processes) for which the selection of controlled inventories yields to internal dynamics that have zero deficiency, show stable closed-loop dynamics regardless of the chosen setpoint. Hence, if the setpoint is feasible, then the inventories will converge to the setpoint values, whereas if the setpoint is not feasible, then the inventories will converge to a steady-state that is distinct from the setpoint, i.e. there will be an offset, but the system is still stable.*

Proof. If the setpoint is feasible, corollary 21 is valid. If the setpoint is not feasible, the constrained control law in equation 7.6 will provide a value of the manipulated variable which is saturated at a constraint value, i.e. the control law ends up reduced to

$$u = u_{\text{constraint}}. \tag{7.10}$$

Then, the dynamics of the closed loop become:

$$\begin{aligned} \frac{dy}{dt} &= \phi_y(x)\, u_{\text{constraint}} + p_y(x) \\ \frac{dv}{dt} &= \phi_v(x)\, u_{\text{constraint}} + p_v(x)\,. \end{aligned} \tag{7.11}$$

The uncontrolled inventories v fulfill the requirements of the deficiency zero theorem (see theorem 14). Hence, for the states v there exists one unique steady-state corresponding to each stoichiometric class. In other words, v stabilizes for any constant value of the manipulated variable. And since the selection of controlled inventories was done such that they fulfill a steady-state controllability requirement (see theorem 11), then the controlled inventories y do also reach a steady-state for any given value of the manipulated variable. Hence the whole state stabilizes. ■

Figures 7.1 and 7.2 show a simulation run with equivalent setpoint conditions to the ones used in Figures 6.17 and 6.18, but constrained control is now used. The constraints to the manipulated variables have been chosen such that the last setpoint is not feasible. As can be observed in Figures 7.1 and 7.2, the feasible setpoints are reached in an identical way as in Figures 7.1 and 7.2, whereas in the

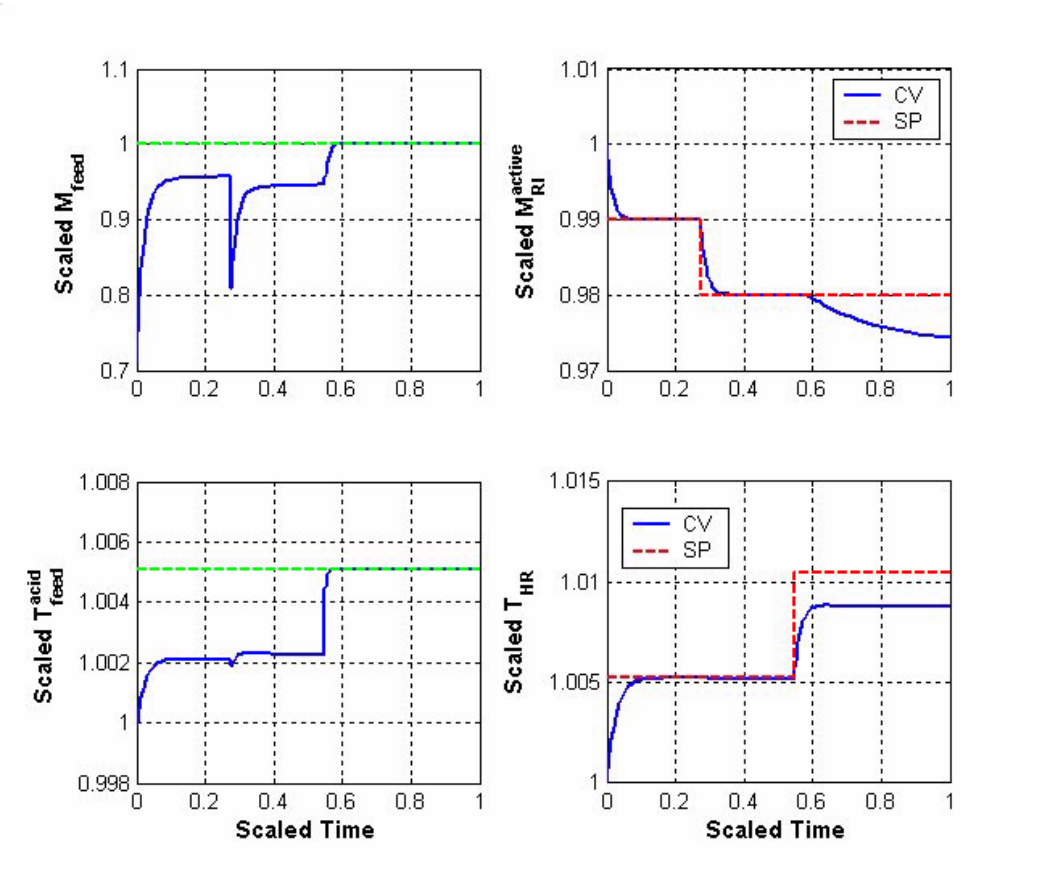

Figure 7.1: Closed-loop simulation of the HR with constrained control. Manipulated variables (first column) and controlled inventories (second column).

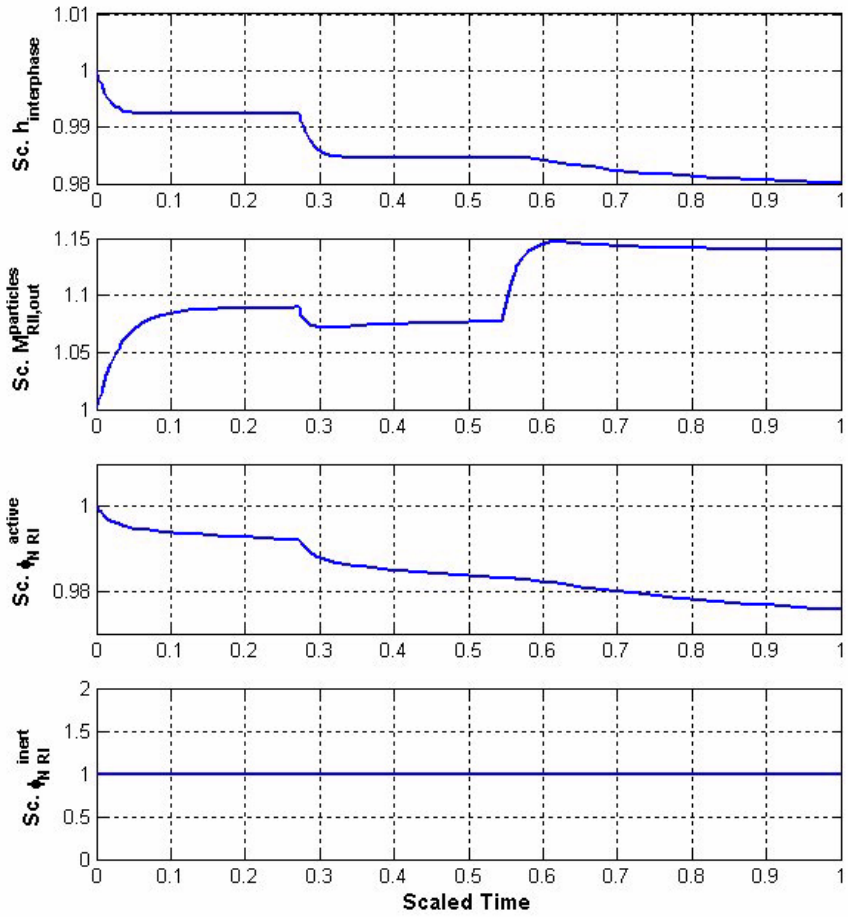

Figure 7.2: Closed-loop simulation of the HR when $w_{\text{feed}}^{\text{inert}} = 0$, and using constrained control. Selected variables: interphase level between compartments I and II, mass flowrate of particles leaving compartment II, mass of particles of active feedstock with size x_N within compartment I, and mass of particles of inert feedstock with size x_N, within compartment I.

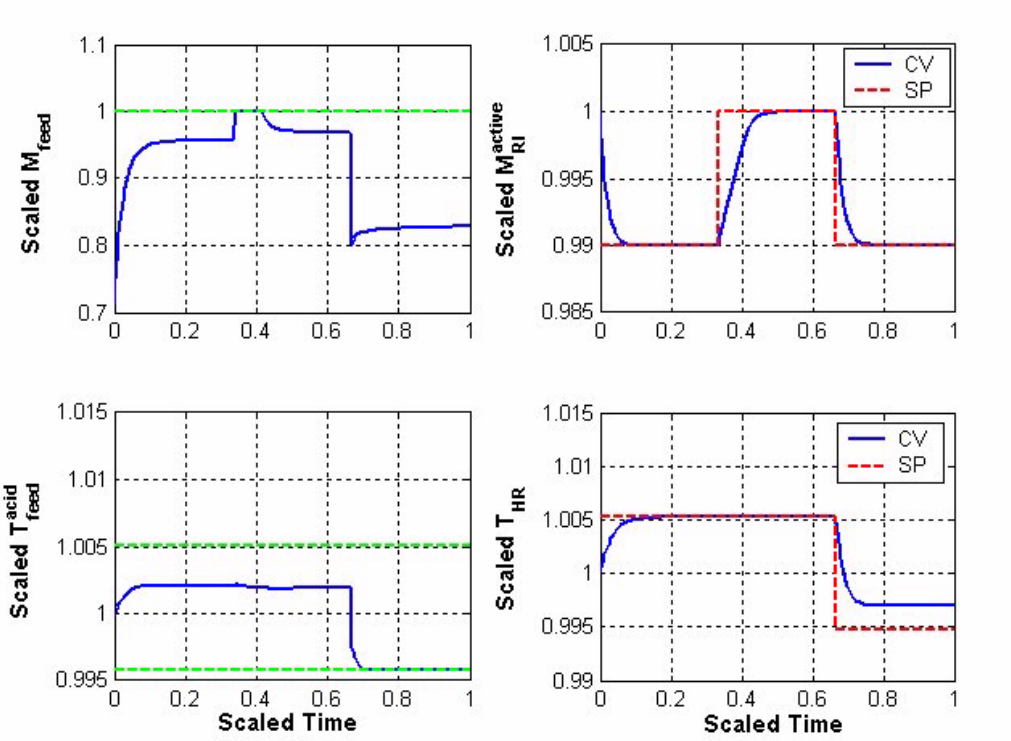

Figure 7.3: Closed-loop simulation of the HR with constrained control. Manipulated variables (first column) and controlled inventories (second column).

case of the unfeasible setpoint, an offset is obtained for both controlled inventories, but stabilization of all inventories and states is achieved. Figure 7.3 shows other setpoint conditions. Note that the second setpoint is feasible, and the inventory converges to the setpoint, but one of the constraints is active for a certain time, and this makes the response more sluggish than when no saturation takes place. Note also that the last temperature setpoint is unfeasible, and again the closed-loop stabilizes at a steady-state, but an offset is obtained.

7.3 Robust inventory-passivity based control

Mathematical models are never perfect. Models are built on assumptions that facilitate the establishment of the mathematical system of equations. However, these assumptions make the behavior of the model different from that of the real system. In control literature, such systems whose behavior are only partially known are referred to as *uncertain* systems. Some sources of *uncertainty* in process models

are (Christofides 2002):

- uncertain variables, such as unknown process parameters and unknown disturbances,
- unmodeled dynamics, such as fast actuator and sensor dynamics that are not taken into account and time-varying parameters.

In terms of analysis and control design, there are several approaches to classify and handle uncertainties, see for example (Qu 1998) for a thorough discussion.

> The problem of controlling uncertain systems, also referred to as the robust control problem, is to design a fixed (i.e. uncertainty independent) controller which guarantees the design requirements in the presence of significant uncertainties that are bounded in size by either some constant or some well-defined functions of the state and time. If it exists, such a stabilizing control is called robust control, and the resulting stability or performance is called robust stability or performance, respectively. The adjective "robust" is used to refer to the fact that the specific property holds for all possible uncertainties within their bounds (or bounding functions). (Qu 1998)

The number of references dealing with robust control of particulate processes is quite limited. A method for the synthesis of robust nonlinear controllers for spatially homogeneous particulate processes including time-varying uncertain variables and unmodeled dynamics, was reported in (Chiu & Christofides 2000) and (Christofides 2002). The controllers are synthesized via Lyapunov's direct method, and enforce the desired stability in the closed-loop system and attenuation of the effect of uncertain variables. However, the reported method relies on three strong assumptions that may not be fulfilled for some processes, and the procedure requires knowledge of advanced nonlinear control. Robust linear control has also been reported in the literature (Vollmer & Raisch 2002), (Galán et al. 2002), but such an approach is only useful when the dynamics of the particulate process can be approximated by a linear model, and the linear model is accurate enough to preserve the main features of the original system.

As regards inventory passivity-based control, a robust controller has recently been reported (Wang & Ydstie 2004*b*). The reported approach consists in combining inventory passivity-based control with high gain (sliding mode) adaptive control to handle the system uncertainties caused by modelling errors and unmeasured disturbances.

Theorem 23 (Wang & Ydstie 2004) *Consider the following uncertain inventory system*

$$\frac{dv}{dt} = p(x) + \Phi(x)\, u + \Delta, \tag{7.12}$$

where Δ is a lumped uncertainty which is possibly nonlinear and time-varying. The sliding mode controller

$$p(x) + \Phi(x)\, u = -K\left(v - v^*\right) + \frac{dv^*}{dt} - \hat{\delta}\,\mathrm{sign}\left(S(t)\right), \tag{7.13}$$

where

$$S(t) = \left(\frac{d}{dt} + K\right) \int \left(v - v^*\right) d\tau \tag{7.14}$$

$$\|\Delta\| \leq \hat{\delta}, \tag{7.15}$$

and with the following adaptation algorithm

$$\frac{d\hat{\delta}}{dt} = \alpha \|\Delta\|,$$

where α is a positive constant, makes the controlled system asymptotically convergent to the switching surface $S(t) = 0$, and further guarantees that the system is stable. The above sliding mode design is equivalent to the passivity-based control. The mapping

$$p(x) + \Phi(x) \rightarrow \left(v - v^*\right) \tag{7.16}$$

is passive with the storage function

$$V\left(S(t), \tilde{\delta}\right) = \frac{1}{2}S^2 + \frac{1}{2}\tilde{\delta}^2, \tag{7.17}$$

and the supply function

$$w = \|S(t)\|\left(\|\Delta\| - \delta\right), \tag{7.18}$$

where

$$\tilde{\delta} = \hat{\delta} - \delta,$$

being δ the real bound on the uncertainty.

The method reported in (Wang & Ydstie 2004*b*) was only tested with square systems, i.e. systems where the number of inventories equals the number of manipulated variables ($\dim v = \dim u$). However, the method can be applied to rectangular systems ($\dim u < \dim v$) as long as the conditions of the stability theorem of rectangular system (theorem 11) and of the robust inventory passivity-based

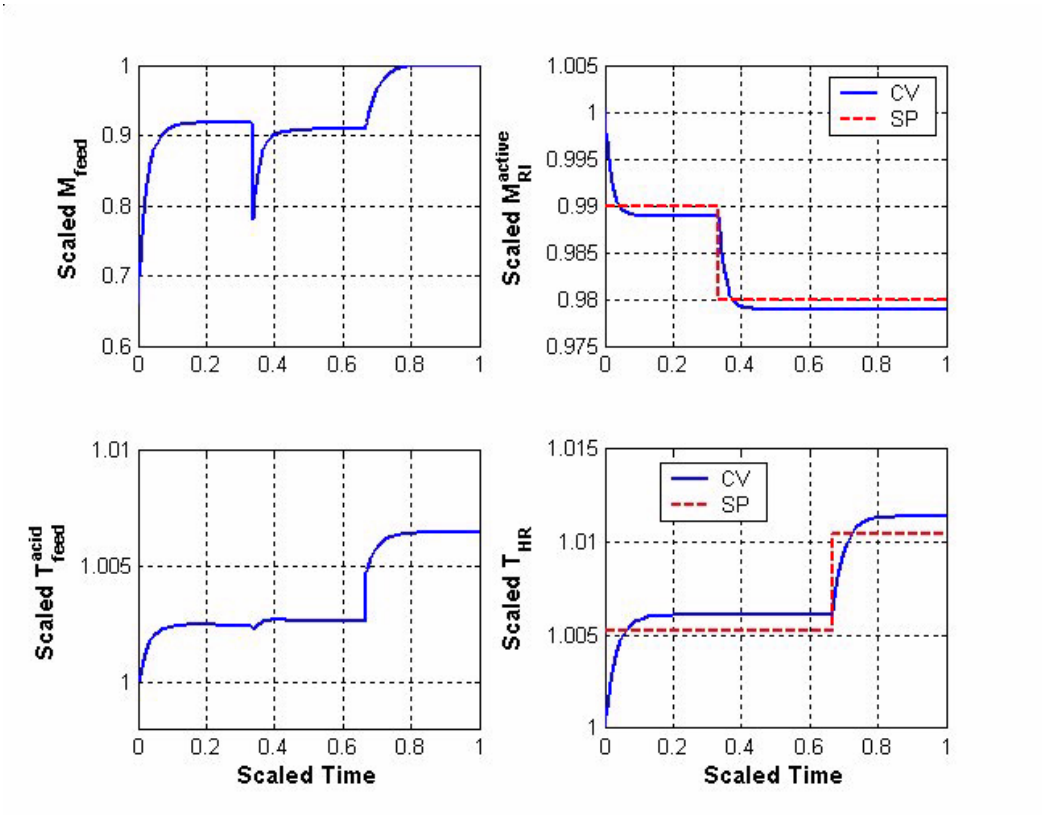

Figure 7.4: Closed-loop simulation of the HR with an erroneous value of parameter k_a in the controller. Manipulated variables (first column) and controlled inventories (second column).

control theorem (theorem 23) are all met. This means that the sliding mode controller can be applied to the *Silgrain*® process. Let us start considering a constant uncertainty in the parameters. In section 4.7, it was proved that the parameter affecting disintegration the most, was k_a in the *breakage frequency* function, see equation 4.8. Let us assume that the real parameter is constant but unknown, such that the value used in the model is not correct. Figures 7.4 and 7.5 show the same closed-loop simulation as that corresponding to Figures 6.17 and 6.18, except that an erroneous value of k_a in the nominal controller is now used. Figure 7.4 shows that the controlled variables stabilize, but an offset exists. By comparing Figures 7.5 (perfect model) and 6.18, it can be noticed that the steady-state reached by the uncontrolled variables is also slightly displaced. Figures 7.6 and 7.7 show the same closed-loop simulation as previously, again with an erroneous value of k_a in the controller law, but now the controller law is robust and is synthe-

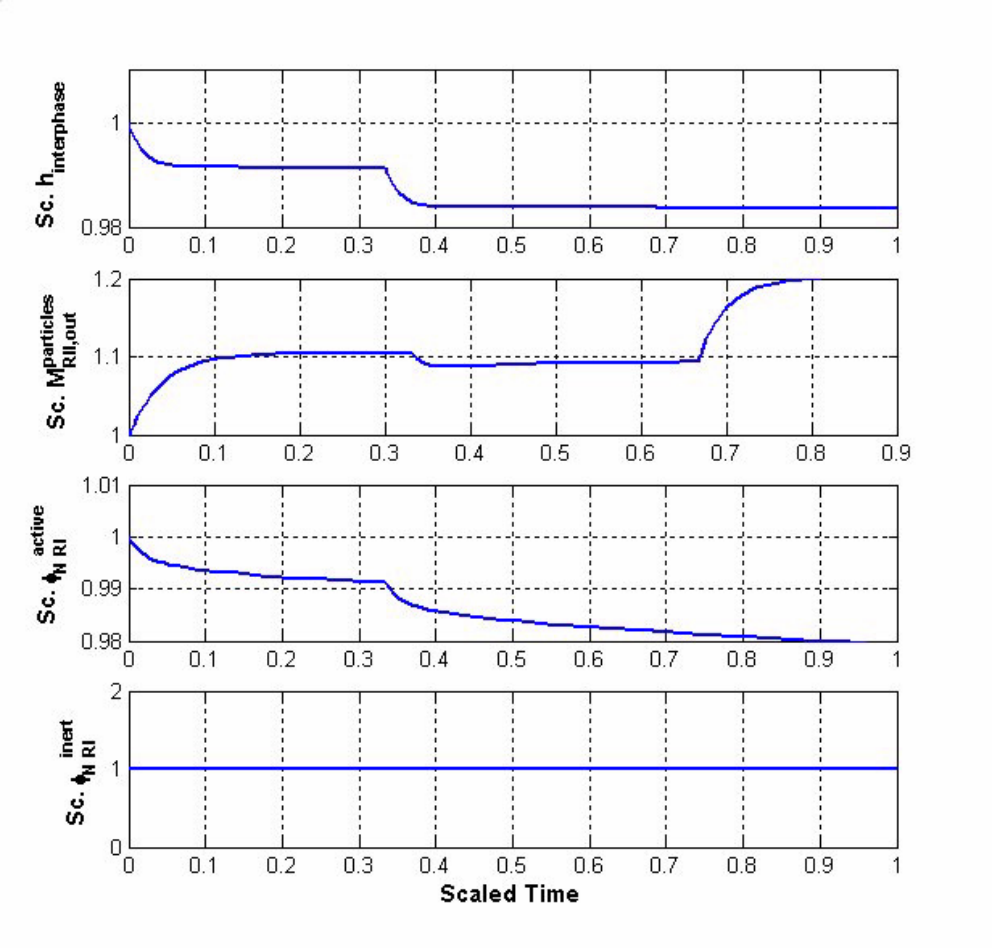

Figure 7.5: Closed-loop simulation of the HR with an erroneous value of parameter k_a in the controller. Selected variables: interphase level between compartments I and II, mass flowrate of particles leaving compartment II, mass of particles of active feedstock with size x_N within compartment I, and mass of particles of inert feedstock with size x_N, within compartment I.

sized according to equation 7.13. As it can be observed, the inventories converge to their setpoints, and the selected variables converge to the same setpoints as in Figure 6.18. This means that the sliding-mode controller has an integral action. Moreover, the integral action is adaptive. For this reason, the sliding mode controller should work in more complex situations than a constant error on one parameter. Let us assume now that for each of the setpoint conditions the value of k_a is constant but different, i.e. k_a acquires 3 different values along the simulation, and these 3 values are changed in a random way. Figures 7.8 and 7.9 show the closed-loop response of the nominal controller, while Figures 7.10 and 7.11 show the closed-loop response of the robust controller. The nominal controller stabilizes the inventories, but offsets from the setpoints are observed. In contrast, the robust controller makes the inventories to converge to their setpoints.

In (Wang & Ydstie 2004*b*), an example is given where the uncertainty of the parameter is assumed to be a random variable. Such an stochastic model was simulated, and the sliding mode controller gave a satisfactory performance. Reproducing the conditions of white noise in a parameter of the *Silgrain*® model is not straightforward due to numerical difficulties. The *Silgrain*® model is large in size and is stiff, thus a variable-order solver for stiff problems is required (`ode15s` command in MATLAB® is used in this work). Solvers using variable time step size can not solve stochastic equations without further modification. This problem is discussed in (Lie 2004).

For the ODE

$$\frac{dx}{dt} = f(x, u), \tag{7.19}$$

it is possible to write this as

$$dx = f(x, u)\, dt. \tag{7.20}$$

By integrating dx from x_t to $x_{t+\Delta t}$ and $f(x, u)\, dt$ from t to $t + \Delta t$, this gives:

$$x_{t+\Delta t} - x_t = \int_t^{t+\Delta t} f(x, u)\, dt.$$

If $f(x, u)$ varies slowly over the time interval, this intuitively leads to the Explicit Euler approximation:

$$x_{t+\Delta t} - x_t \approx \Delta t \cdot f(x_t, u_t).$$

However, if $f(x, u)$ varies rapidly over the time interval Δt, this approximation is not valid. One example of such systems is if u is

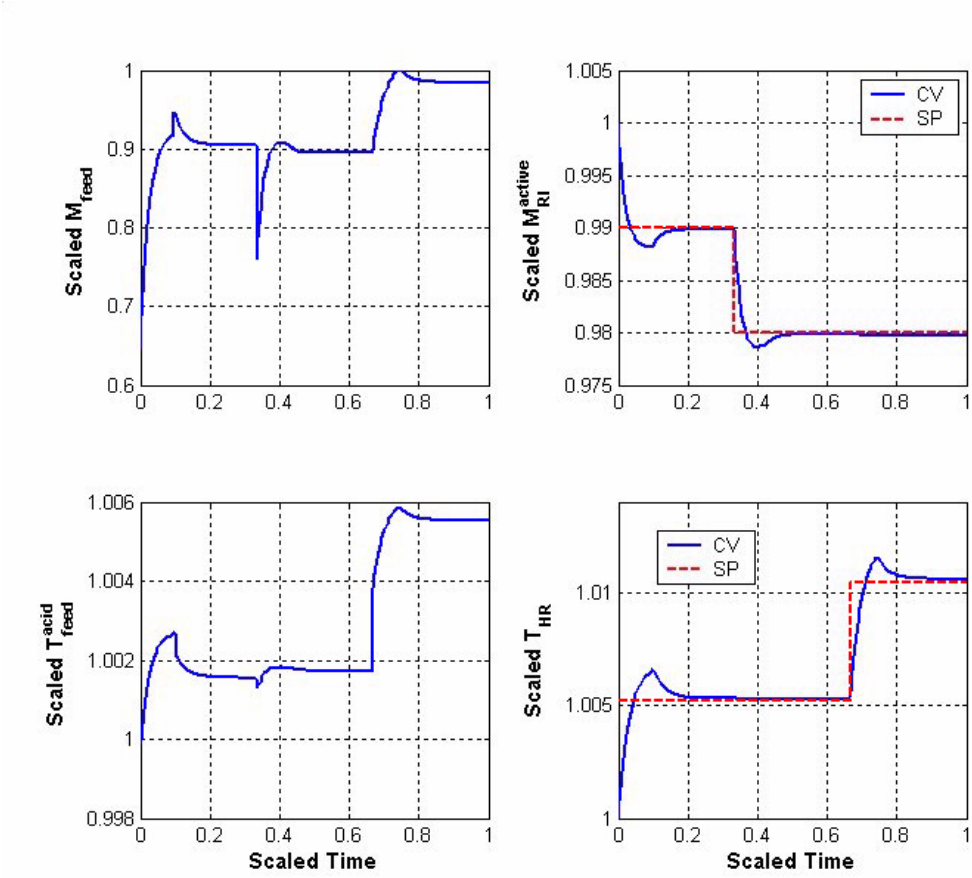

Figure 7.6: Closed-loop simulation of the HR with an erroneous value of parameter k_a in the controller, and a robust inventory passivity-based controller. Manipulated variables (first column) and controlled inventories (second column).

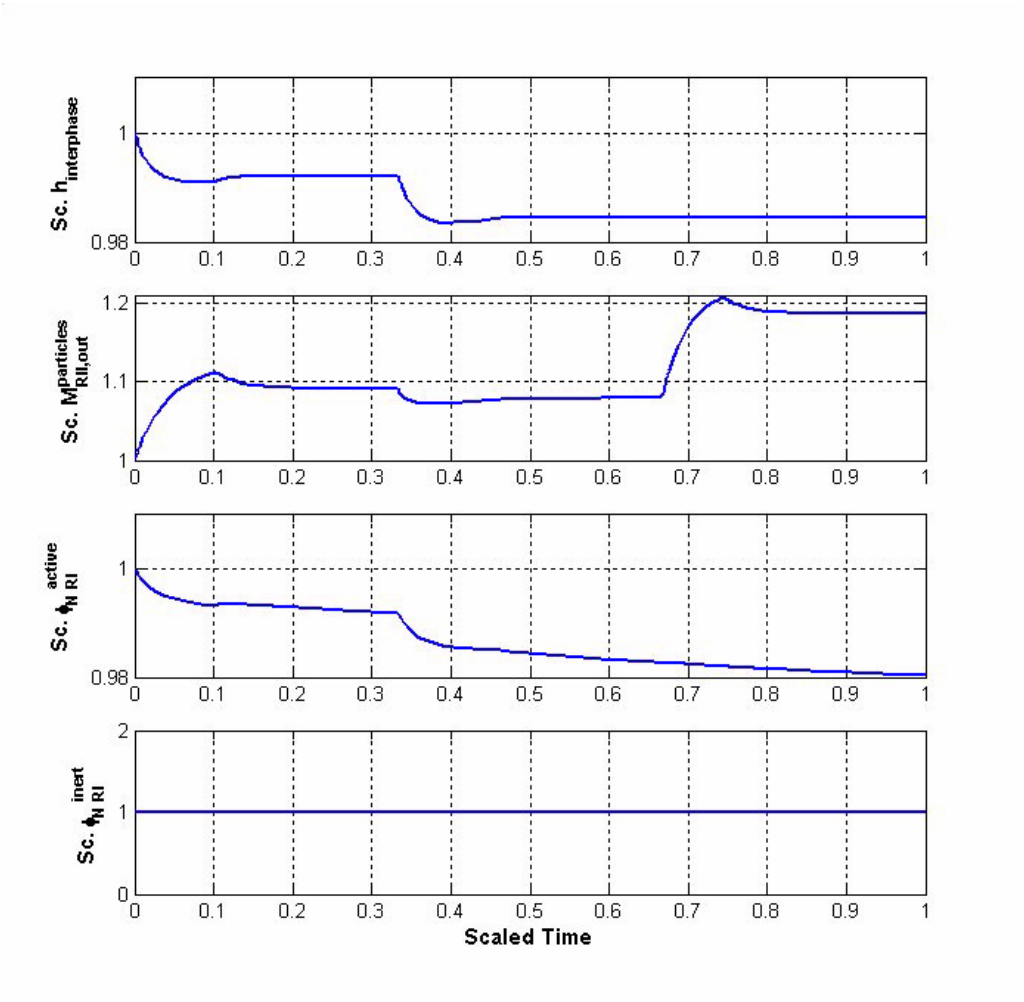

Figure 7.7: Closed-loop simulation of the HR with an erroneous value of parameter k_a in the controller, and a robust inventory-passivity based controller. Selected variables: interphase level between compartments I and II, mass flowrate of particles leaving compartment II, mass of particles of active feedstock with size x_N within compartment I, and mass of particles of inert feedstock with size x_N, within compartment I.

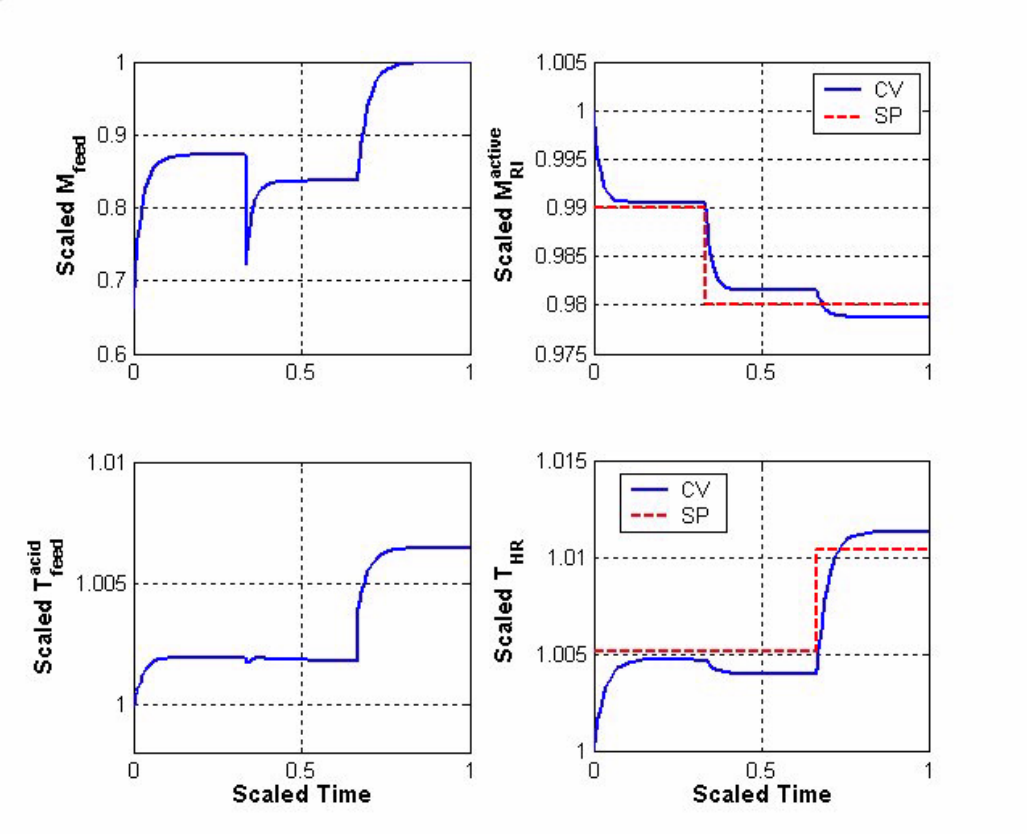

Figure 7.8: Closed-loop simulation of the HR with a time-varying k_a, and using the nominal controller. Manipulated variables (first column) and controlled inventories (second column).

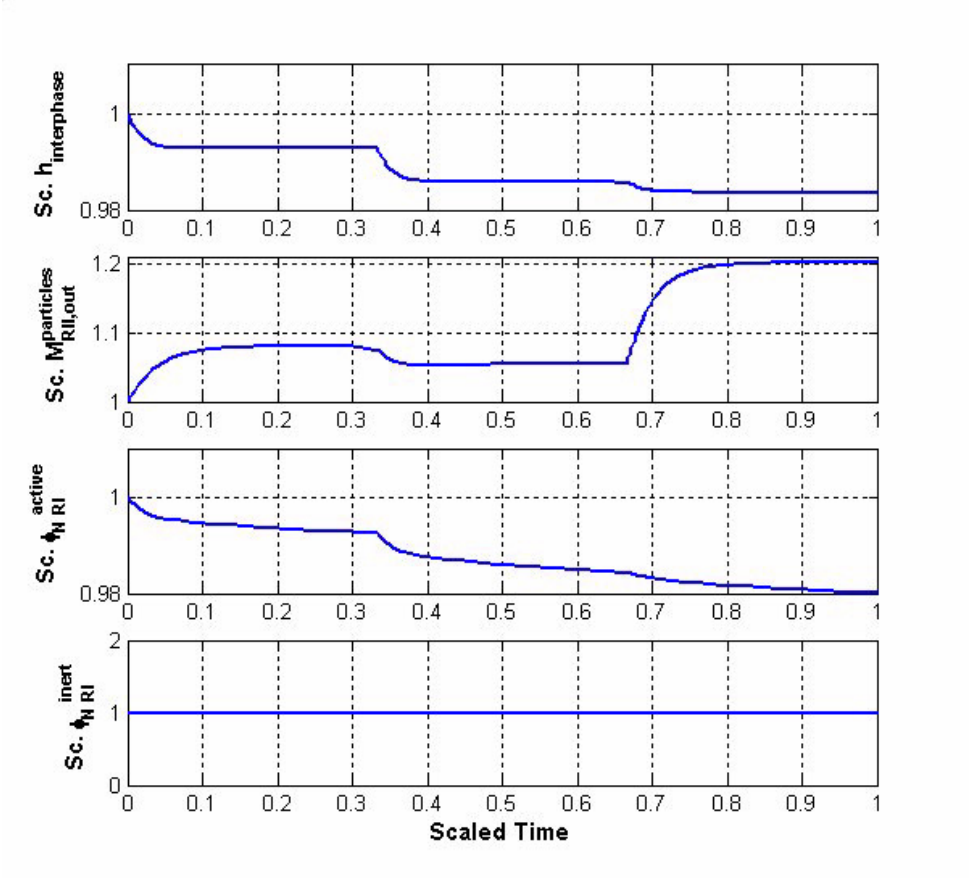

Figure 7.9: Closed-loop simulation of the HR with with a time-varying k_a, and using the nominal controller. Selected variables: interphase level between compartments I and II, mass flowrate of particles leaving compartment II, mass of particles of active feedstock with size x_N within compartment I, and mass of particles of inert feedstock with size x_N, within compartment I.

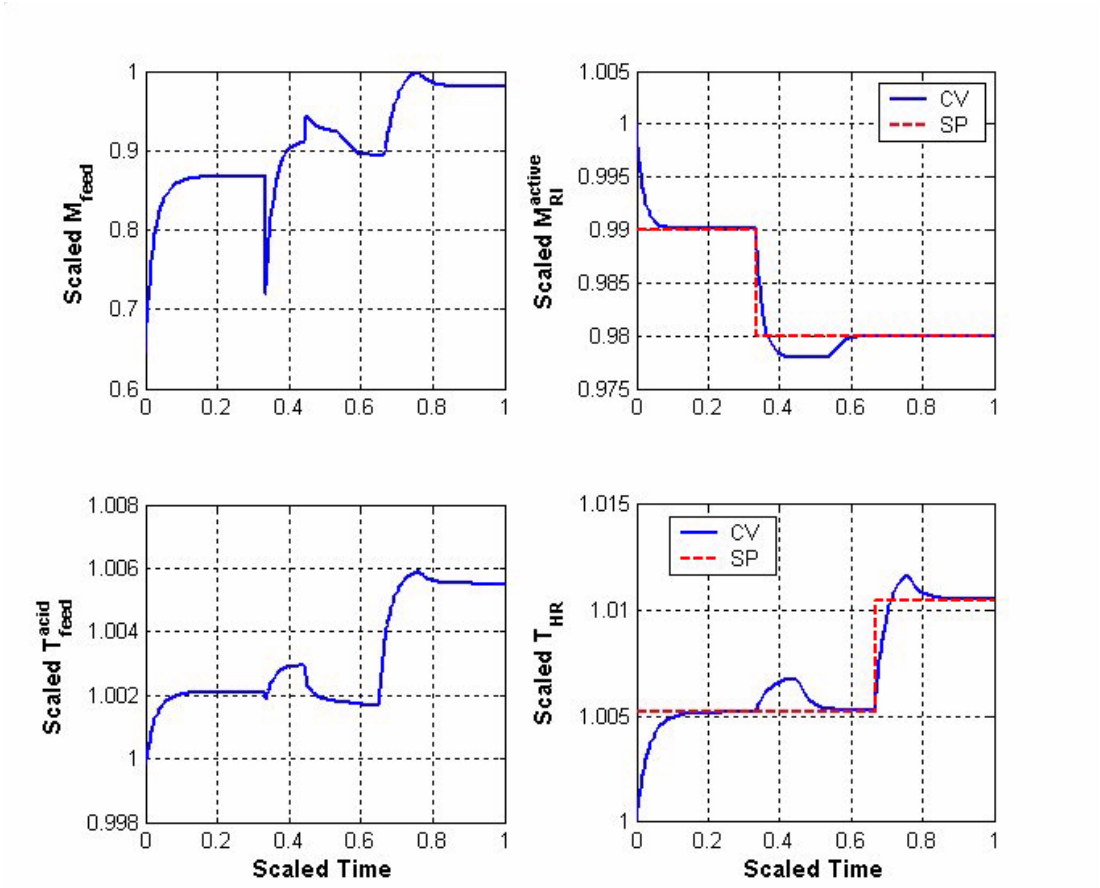

Figure 7.10: Closed-loop simulation of the HR with a time-varying k_a, and using the robust controller. Manipulated variables (first column) and controlled inventories (second column).

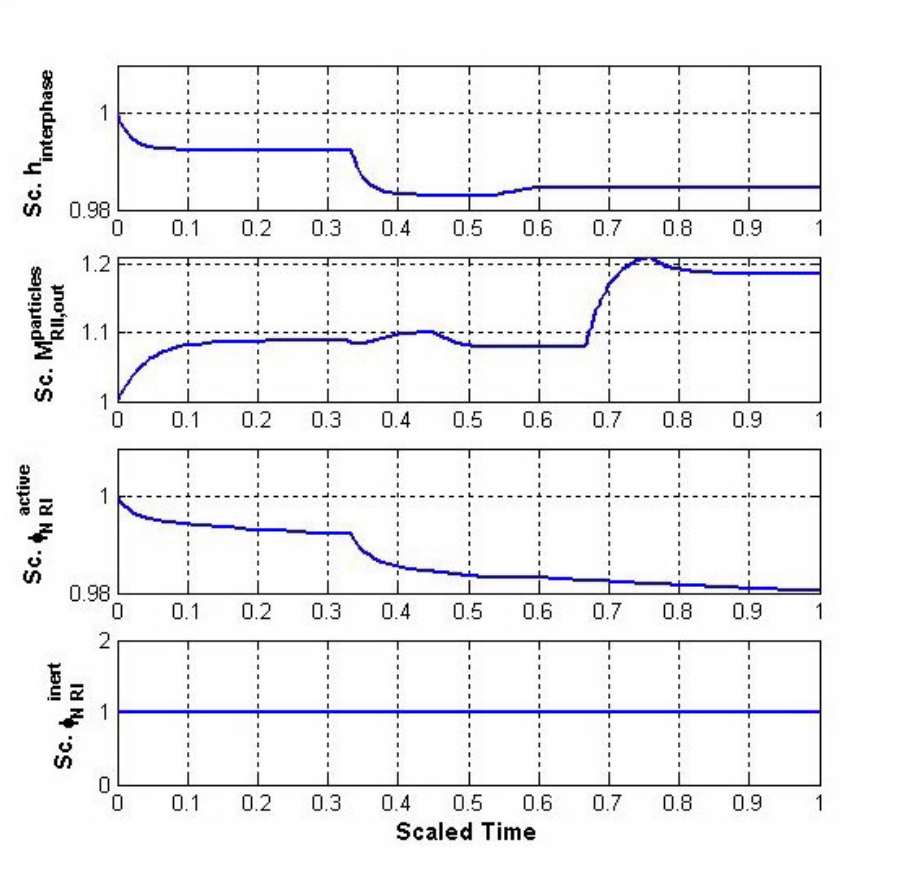

Figure 7.11: Closed-loop simulation of the HR with with a time-varying k_a, and using the robust controller. Selected variables: interphase level between compartments I and II, mass flowrate of particles leaving compartment II, mass of particles of active feedstock with size x_N within compartment I, and mass of particles of inert feedstock with size x_N, within compartment I.

so-called white noise. When u is white noise, it is even problematic to write the system as

$$\frac{dx}{dt} = f(x, u),$$

because $f(x, u)$ will hardly be continuous, and hence x is not really differentiable. Because of this, mathematicians tend to write such stochastic differential equations as in equation 7.20. For the general case of such systems, it is even difficult to find an Euler-type approximation. For the case of additive/multiplicative white noise u, i.e.

$$f(x, u) = g(x) + S(x)\, u, \tag{7.21}$$

where $S(x)$ is a matrix, it can be shown that the Euler approximation takes the form

$$x_{t+\Delta t} - x_t \approx \Delta t \cdot g(x_t) + \ell_u(\Delta t) \cdot S(x_t) \cdot u_t.$$

For the special case when the white noise is drawn from either the *Gaussian* distribution or the *uniform* distribution, function $\ell_u(\Delta t)$ takes the form

$$\ell_u(\Delta t) = \sqrt{\Delta t},$$

see e.g. (Artemiev & Averina 1997). For higher order methods such as Runge-Kutta methods, the scheme becomes even more complicated when u is white noise. The same is valid for variable step-length methods. If we treat the problem as an ODE with fixed variance in the random number generator, instead of adapting the variance to the step-length, serious problems may show up, and they are especially serious if a variable step-length method is used. (Lie 2004)

In the simulations attempted with the *Silgrain*® model, treating the problem with fixed variance in the random number generator, the following difficulties were observed: the simulation time was very large, when a small step-length is used the controller apparently worked better than it will do in reality, as the step length increased the problem became unrealistically difficult to control and the controlled system got sluggish, and in some occasions the problem eventually became unstable. This behavior can be explained by the erroneous expression

$$\ell_u(\Delta t) = \Delta t.$$

Hence, the simulation result was not representative of the closed loop behavior that would be found when using the designed controller on the real system.

A question that may be raised is: Is it realistic to assume that the uncertainty is white noise? In (Bryson & Ho 1975), the following point of view appears on an uncertainty:

> ..., in "worst case designs", we assume that nature is perverse enough to determine the worst disturbance; but we do not assume that nature is perverse enough to actually change the disturbance as the game evolves. (Bryson & Ho 1975)

In any case, it can be concluded that the robust controller suggested in (Wang & Ydstie 2004*b*) may provide a better performance than the nominal inventory passivity-based control in the presence of uncertainty. Note that the robust controller can be applied to the type of systems reported in this work, i.e. rectangular systems with $\dim v < \dim u$. The robust controller ensures stabilization of the whole set of variables and inventory convergence to the setpoints as long as all the requirements of the stability theorem of rectangular system (theorem 11) and of the robust inventory passivity-based control theorem (theorem 23) are met.

Finally, note that the robust controller has integral action. Therefore, some anti-windup strategy should be used if there exists constraints on the manipulated variables.

7.4 Observer-based control

The inventory passivity-based control law, both in the nominal mode (equation 6.16) and in the sliding mode (equation 7.13), is typically a function not only of the controlled inventories and model parameters, but also a function of other internal states or transformation of the states (for example, intensive variables). However, for many particulate processes, the availability of instrumentation and measurements is limited. This means that in practice not all the states required in the control law are available. Fortunately, for many particulate processes, relatively realistic mechanistic models are available or can be developed. Therefore, the available process measurements together with the process knowledge (in the form of a model) can be used to estimate the state of the system. This is what an *observer* or *state estimator* does. The concept of an observer for a dynamic process was introduced in 1966 by Luenberger (Luenberger 1966), but actually observers had already been in use since the invention of the Kalman filter in the late 1950*s*. One possible way to define an observer is the following:

> An observer for a dynamic system $S(x, y, u)$ with state x, output y and input u is another dynamic system $\hat{S}(\hat{x}, y, u)$ having the property that the state $\hat{x}$ of the process of the observer $\hat{S}$ converges to the state x of the system S, independent of the input u or the state x. (Friedland 1996)

Figure 7.12 shows a block diagram of an observer.There are various ways

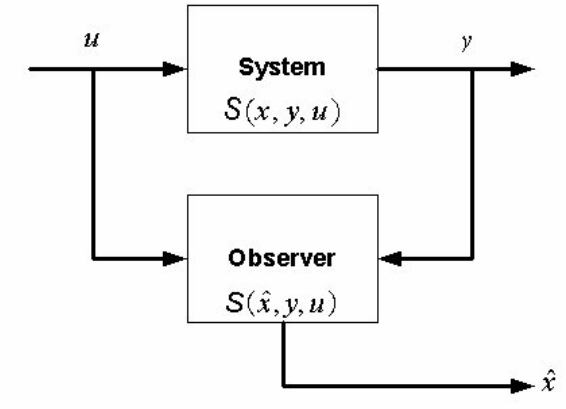

Figure 7.12: Observer block diagram.

to classify observers. Hence, if the observer has the same order as the system ($\dim \hat{x} = \dim x$) irrespective of the number of independent observations, then a *full-order* observer is obtained. In contrast, a *reduced-order* observer is obtained if the dimension of the estimated vector is smaller than the dimension of the system's state vector ($\dim \hat{x} = \dim x - \dim y$). If the measurements are assumed to be noise-free, the observer is *deterministic*. If measurement noise is accounted for, the observer is *stochastic*. Depending on the type of system, the observers can be *linear* or *nonlinear*. The Kalman filter is one of the most widely used observers, and is a linear stochastic full-order observer that is optimized for the noise present in the measurements and inputs of the process. In the framework of inventory passivity-based control of particulate processes, it is more convenient to use *nonlinear deterministic full-order observers*, for the following reasons:

- The available models, i.e. population balance models, are typically nonlinear.
- Population balance models have a large number of states. Hence, using reduced-order observers would not present any considerable advantage.
- Stochastic observers require knowledge of the probabilistic nature of measurement noise.

Among the various applications of observers, perhaps the most important is for the implementation of closed-loop control algorithms designed by state-space methods (Friedland 1996). Figure 7.13 sketches the function of the observer in the framework of inventory passivity-based control. Notice that the controlled inventories in many cases can not be measured directly. Therefore, the symbol y_m is used to indicate measurements, while y is used to indicate the controlled

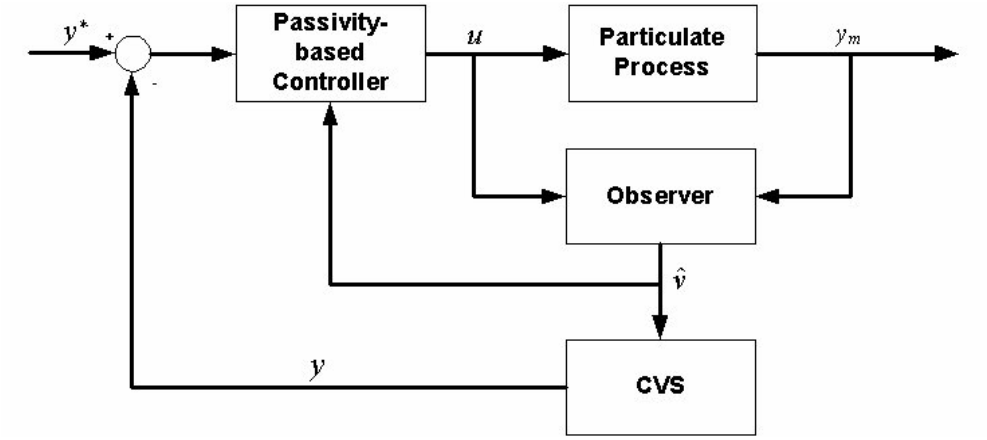

Figure 7.13: The function of an observer in the framework of inventory passivity-based control (CVS = Controlled Variable Synthesizer).

inventories. In mathematical terms, the observer corresponding to the system in equation 6.10 is:

$$\begin{aligned} \frac{d\hat{v}}{dt} &= \phi(\hat{x})\,u + p(\hat{x}) - L(y_m - \hat{y}_m) \\ \hat{v} &= g(\hat{x}) \\ \hat{y}_m &= h(\hat{v}), \end{aligned} \tag{7.22}$$

where L is the observer gain, and h is the transformation function that relates the measurements to the state variables, i.e. to the inventories.

The main performance requirement of an observer is that the estimation error:

$$\hat{e} = \hat{v} - v \tag{7.23}$$

converges to zero in a finite time interval, and irrespective of u and v. In order for this to be achieved, the information about the state v must be recoverable from knowledge of the available measurements y_m and from the observer equations. Such a requirement is referred to as *observability*. Therefore, the observer design problem is to find the observer gain L that makes the state v observable from the available measurements y_m, and that guarantees that the estimation error $\hat{e}$ converges to zero in a reasonable time interval. For linear systems, there exists methods that ensure existence and convergence of observers, see (Friedland 1996) for a review. In contrast, for nonlinear systems, establishing generally applicable conditions for existence and convergence of observers is an open and active area of research (Chaves & Sontag 2002).

Despite the potential advantage of observers in the field of particulate processes, the amount of reported material on the design of observers for such systems is scarce. The extended Kalman filter, which is an extension of the Kalman filter to nonlinear systems, could be used since it has proven to give satisfactory results in many other applications. However, no convergence proof is available for the extended Kalman filter. A Luenberger-type observer is used in (Christofides 2002) to estimate the states required for the implementation of a nonlinear state feedback controller. The design is carried out under the hypothesis that the system is locally observable.

An observer-based control strategy which combines inventory passivity-based control with a state observer has recently been reported (Wang & Ydstie 2004*a*), where it was shown that the observer error converges to zero if the local linearized system is observable and if a Lipschitz condition for the high order terms is satisfied. The reported work proves that such an observer combined with the sliding mode controller in equation 7.13 makes the state estimate converge, and the controlled system will be stable. The development of such an observer for the *Silgrain*® model is possible, but not straightforward, so it falls outside the scope of this work.

The *Silgrain*® model can be considered a deficiency zero chemical reaction network. The explicit construction of globally convergent observers for these type of reaction networks has been reported in (Chaves & Sontag 2002). In the reported method, the measurements are a subset of the state variables, or more generally, monomials in state variables. A detectability requirement must be fulfilled, but the observer design method provides a straightforward way to check this requirement, that is based on linear algebra. Detectability can be checked by analyzing the rank of the sum of two subspaces: one of them is the stoichiometric subspace of the reaction network, and the other subspace is the column space of the transpose of the observer gain. Unfortunately, the method reported in (Chaves & Sontag 2002) can not be directly used for reaction networks with a zero complex, and the *Silgrain*® model does contain a zero complex.

The development of nonlinear observers for particulate processes should attract attention from the research community in the future, since realistic models are available, measurements are difficult, and the potential advantages of using model based control, i.e. observer based control, are notable.

7.5 Semibatch control

The *Silgrain*® process operates in a semibatch way as regards the feeding of the FeSi feedstock. Inventory passivity-based control can still be applied. The only changes that have to be considered for control design are that:

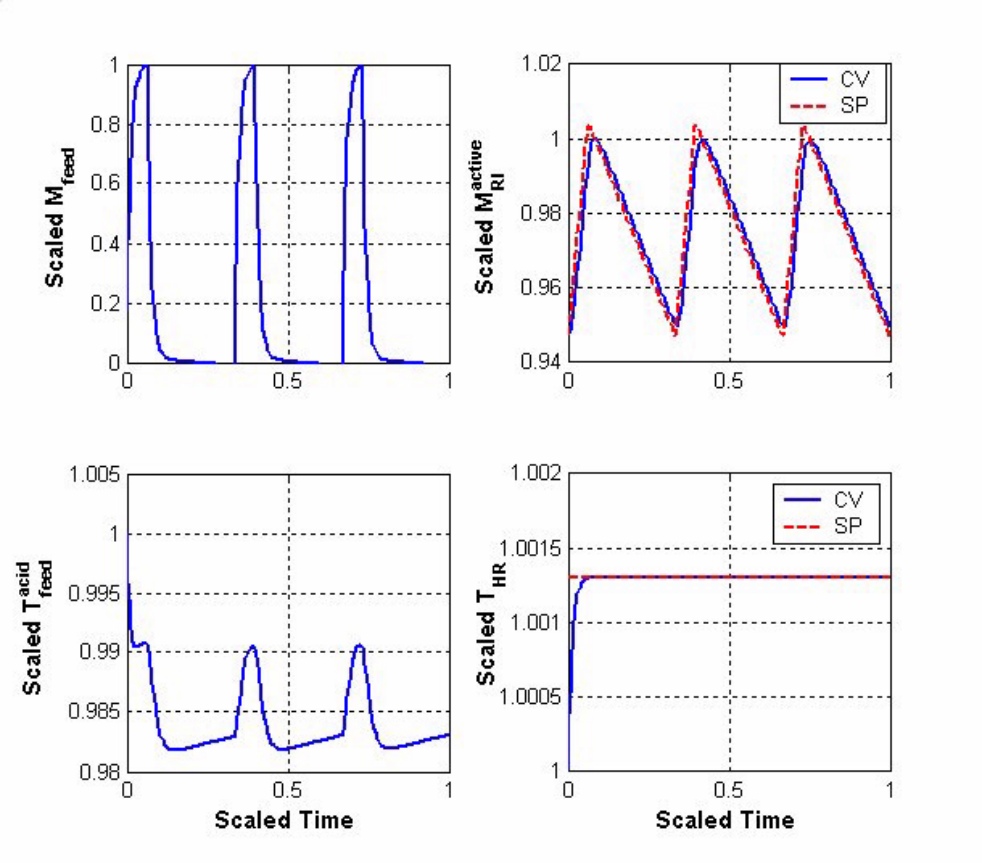

Figure 7.14: Semibatch control of the HR of the *Silgrain*® process using inventory passivity-based control. Manipulated variables (first column) and controlled inventories (second column).

- The reference v^* is no longer an specific setpoint, but a trajectory, more precisely, a cyclic trajectory.
- Some constraints may be active in certain parts of the cycle, so it is natural to use constrained inventory passivity-based control. Then, special care should be taken such that the whole reference trajectory is feasible.

Figure 7.14 shows the closed-loop response that would be obtained if inventory passivity-based control was used to automate the semibatch feeding of the HR in the process. Note that in Figure 7.14, inventory passivity-based is used to keep the temperature constant at a desired setpoint even though FeSi feeding is semibatch. In contrast, in the current manual operation of the process, the temperature varies. Keeping the temperature constant is important to reduce

the variability of the quality of the product. Therefore, using inventory-passivity based control in the *Silgrain*® process is advantageous, regardless of the semibatch feeding of raw material (in an automatic way).

7.6 Plantwide control and SPM

So far, inventory passivity-based control has been used for the design of a control strategy for a unique process unit, without considering the rest of the plant. However, the interaction among units in a plant has an effect on the overall performance of the plant. It is known that apparently appropriate control schemes for a process unit may actually lead to an inoperable plant when the unit is connected to other unit operations in a process with recycle streams and energy integration (Luyben et al. 1998). *Plantwide process control* involves the systems and strategies required to control an entire chemical plant consisting of many interconnected unit operations (Luyben et al. 1998). Because of the problem's complexity, approaches to plantwide control often rely on heuristics and experience. But also optimization and simulation are useful for plantwide control.

> The primary mathematical tools employed in this book is a rigorous, nonlinear mathematical model of the entire plant. This model must faithfully capture the nonlinearity and constraints encountered in the plant under consideration. Any plantwide control scheme must be tested on this type of model, because linear, unconstrained models are not adequate to predict many of the important plantwide phenomena. So mathematical modelling and simulation are vital tools in the solution of the plantwide control problem. (Luyben et al. 1998)

Using inventory passivity-based control to design the individual unit control-loops may present some advantages as regards plantwide control, since:

- it is based on rigorous nonlinear models. If nonlinear models of the units are available, it should be relatively straightforward to build a nonlinear model of the whole plant,
- systems that are rendered passive by passivity-based control retain the stability properties when they are interconnected (Lozano et al. 2000).

It is also important to remember that inventory passivity-based control is part of a multi-level hierarchy of control functions. This is illustrated in Figure 7.15, where inventory passivity-based control would lie in the area of advanced control. At the bottom of the structure is the basic control, that manipulates the actuators

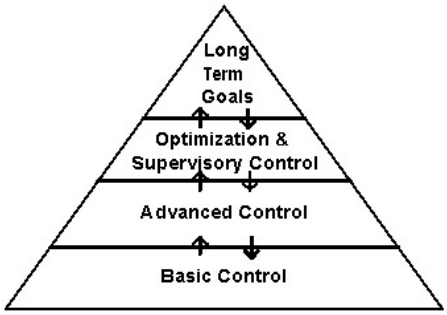

Figure 7.15: Hierarchy of the control functions in a typical process plant. Similar figures can be found in references (Prett & García 1988) and (Qin & Badgwell 1997).

directly. The advanced control improves the performance of the basic controllers. The following level (optimization and supervisory control) takes into consideration operational constraints and economical factors to optimize the overall operation of the plant. Finally at the top of the structure another optimizer takes into account the long-term and global economic goals of the plant. Similar hierarchical structures have been described in the field of model predictive control, see for example, (Prett & García 1988) and (Qin & Badgwell 1997).

Automatic control in general, and inventory passivity-based control in particular, aim at reducing the variability of a process. There is another field that shares such a goal: *statistical process monitoring (SPM)*, also sometimes referred to as *statistical quality control*. *Quality* is difficult to define, since it has many dimensions. For instance, according to (Garvin 1988) the main dimensions of quality are: performance, reliability, durability, serviceability, aesthetics, features, perceived quality, and conformance to standards. The traditional definition of quality is based on the viewpoint that products and services must meet the requirements of those who use them, i.e. "quality is fitness for use". However, a more appropriate definition is "quality is inversely proportional to variability" (Montgomery 1996), since if variability in the main characteristics of a product decreases, the quality of the product increases. *Quality improvement* is thus the reduction of variability in processes and products. Process control reduces the variability of a process, thus being a way to improve quality. SPM uses statistical methods to describe variability, to determine whether the variability is due to random variation or to assignable causes, and then take action depending on the cause of variation. Therefore, the main elements of an SPM system are:

- The quality characteristics to be followed up, i.e. equivalent to the controlled outputs of a process controller.

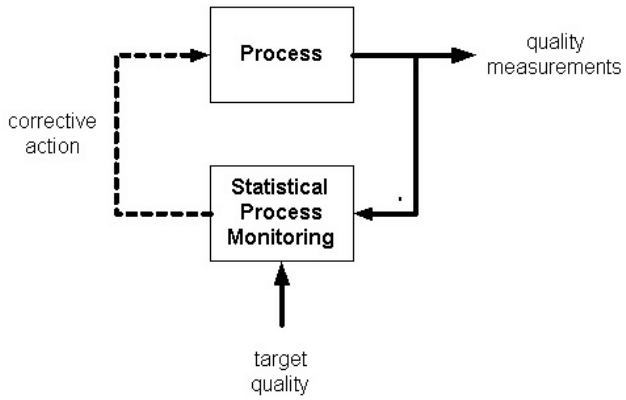

Figure 7.16: Statistical process monitoring.

- The nominal or target value for the quality characteristic, i.e. equivalent to the setpoint values of a process controller.
- A statistical method to determine whether the quality characteristic is *in statistical control*, i.e. the characteristic has a value within the target values where there are no unusual sources of variability present, or if on the contrary, the quality characteristic is *out of statistical control* due to the presence of assignable causes.
- A decision-taking method to solve the situations in which the quality characteristic is out of statistical control.

Figure 7.16 illustrates the concept of SPM.

There are many problem-solving tools that are used in the context of SPM, such as: histograms, check lists, pareto chart, cause and effect diagram, defect concentration diagram, scatter diagram and control chart. Control charts plot the quality characteristic against the nominal value. Hence, control charts are very similar to the plots used in process control. Originally, the control charts were used for univariate statistics, such as the mean value chart, dispersion chart, the cumulative sum chart, the exponentially moving average chart, etc. Control charts for multivariate statistics have also been developed such as the Hotelling T^2 control chart (Johnson & Wichern 1998).

SPM regards the quality variables as random variables. Traditional SPM methods assume that these random components of the in-control variation are independent and identically distributed (iid). However, the measurements made on chemical processes usually violate the iid assumption. Process measurements tend to be autocorrelated, and specially this is so when feedback control loops are present.

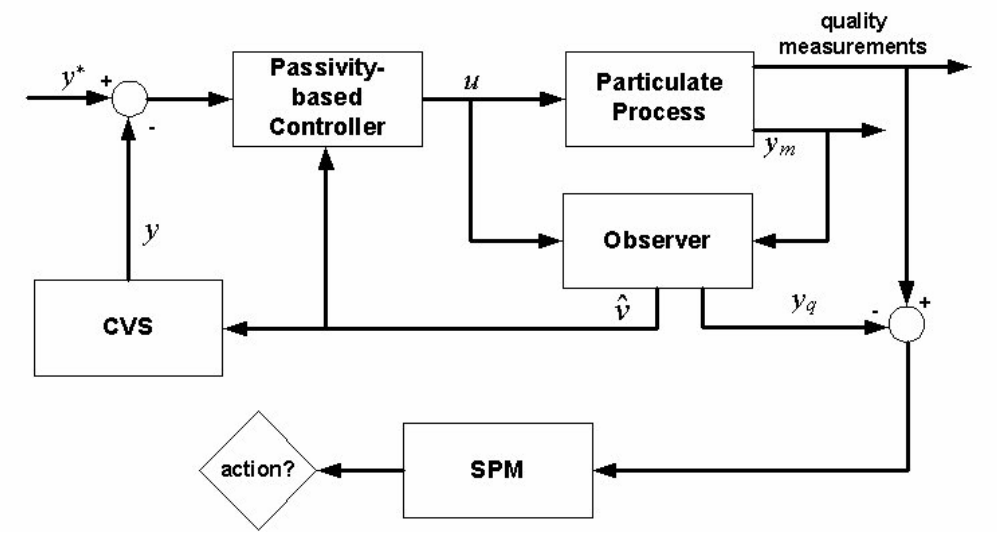

Figure 7.17: Integration of inventory passivity-based control and statistical process monitoring. CVS = Controlled variable synthesizer.

An approach that has proven useful in dealing with autocorrelated data is to model the correlative structure with an appropriate time series model, use that model to remove the autocorrelation from the data, and apply control charts to the residuals (Montgomery 1996). The residuals are not autocorrelated (white noise), and therefore the residual at each instant time contains new information not carried out in the previous values of the residual. For this reason, the residuals are often referred to as *innovations* in estimation literature. An alternative approach was reported in (Negiz 1995) and (Negiz & Cinar 1997), consisting in describing the in-control variability by means of a canonical-variate (CV) state-space model, and a T^2 statistic based on the CV state variables is used for developing a SPM procedure.

Although SPM and process control share the same ultimate goal, they use different techniques and different information to achieve such a goal. There is considerable interest in combining them (Negiz 1995), (Montgomery 1996), since they are complementary. Properly designed control systems reduce variability. However, when certain types of disturbances and assignable causes occur, then the process control system may not handle them properly, and variability may increase. These assignable causes could then be detected by the SPM procedure, and proper actions could be taken. Figure 7.17 illustrates how inventory passivity-based control could be combined with an SPM approach. Since a fairly representative model is available, the same model can be used as a basis for the SPM procedure. The quality measurements are compared with the quality variables predicted by the

model, and then control charts for the innovations or for the T^2 statistic based on the innovations are constructed. Control charts can be constructed because the autocorrelation is eliminated, and the residuals are approximately white noise. When the process is out of statistical control, appropriate corrective measurements could be adopted such as: modifying the feedstock to the normal values, re-tune the controller or the model, etc.

7.7 Conclusions

In the practical implementation of inventory passivity-based control, the manipulated variables are often constrained. The presence of such constraints may make certain sets of setpoints unfeasible, and the controller performance may deteriorate. These issues come up on all control designs since the constraints are imposed by the process equipment and the process physics. Therefore, a prior analysis of setpoint feasibility is necessary, regardless of the method used for control. Section 7.2 shows that inventory passivity-based control ensures convergence of the controlled inventories to their setpoints, and stabilization of the remaining states, provided that the selected setpoint are feasible and ϵ-controllable. For chemical reaction networks of zero deficiency, the closed-loop is stable even in the case of unfeasible setpoints. In such case, the system stabilizes but an offset is obtained.

The effect of disturbances and model errors is analyzed in section 7.3. Wang & Ydstie (2004*b*) recently suggested a method which combined inventory passivity-based control and sliding mode control. The method has been tested on the *Silgrain*® process with satisfactory results. The inventories converge to the desired setpoints and the remaining states stabilize, even in the presence of disturbances and model errors, as long as certain conditions are met. Moreover, the design of the controller is nearly as simple as in the nominal design.

One of the main limitations of inventory passivity-based control is the need of knowing the state of the system in order to calculate the control law. Unfortunately, full state measurements may not be available. However, relatively realistic models are available or can be developed for most particulate processes. Therefore, observers can be constructed to calculate the unmeasured states. Proving convergence of nonlinear observers is an area of active research; some promising results have been reported, and are reviewed in section 7.4.

Many particulate processes operate in semibatch, such as the case under study. Section 7.5 shows that inventory passivity-based control can be used in a straightforward way to automate such a semibatch operation.

A brief discussion of the role of inventory passivity-based control within the overall operation of a plant is given. Inventory passivity-based control is just an element in the hierarchy of control functions in a chemical plant. It is mentioned

how the stability of interconnections that characterizes passivity-based control can be advantageous in the framework of plantwide control. Finally, a brief discussion is given about the potential benefits of combining inventory passivity-based control with statistical process monitoring.

Part III

Thesis conclusions

Chapter 8

Conclusions and future directions

8.1 Discussion and conclusions

The main goal of this thesis has been to establish a systematic strategy for the development of PBE models of particulate processes to be used for the purposes of design and implementation of automatic control. Particulate processes are encountered in a great number of industrial processes. Although particulate processes have been studied for several decades now, there are still many challenges associated to the development of realistic models and control strategies for such processes.

Special emphasis has been put on the development of models that represent realistically the dynamic behavior of industrial-scale units, while keeping a reasonable degree of mathematical complexity. A real industrial particulate process: the *Silgrain*® process, has been used as case study. The approach to PBE modeling suggested in this thesis does not differ to a great extent from the general approach to modeling of chemical reaction units, but attention has been stressed in certain stages to account for the special features of particulate processes. Special consideration has been given to the establishment of model foundations. The widely-used assumption of complete-mixing turns out to be unrealistic for the PBE in many instances, and should thus be avoided. A compartmentalization of the unit based on distinguishable regions in the unit is suggested in this thesis to achieve more realistic models. A PBE is thus written for each compartment, and the connections among compartments are defined based on the physics and hydrodynamics of the process. For the *Silgrain*® process, a division into 4 compartments proves adequate. Once the balance equations are written, the next stage consists in establishing the constitutive equations, which is relatively straightforward for the continuous phase, but more striving for the disperse phase. Hence, for the *Silgrain*® model a tailor-made experimental campaign at laboratory scale

was required in order to determine the constitutive equations describing particle disintegration. Once the constitutive equations are defined, the next stage is the selection of a solution method for the mathematical equations. PBE models are in general more challenging to solve than other process models, but the modeler can benefit from the extensive research results that are available in the literature. For the *Silgrain*® model, a numerical discretization method on the particle size coordinate, that ensures mass preservation, is used to solve the system equations corresponding to compartments I, II and III. Compartment IV is solved by a combination of the method of moments and the collocation method. Once the model can be solved and simulated, an important stage is that of parameter estimation and model validation. Despite of the importance that this stage plays for the applications in which PBE models are used as realistic representations of the particulate processes, there is still limited reported material on this topic. For this reason, special attention is dedicated to these tasks in this thesis. An experimental campaign on the industrial plant has been carried out to gather data for parameter estimation and model validation, and a systematic method for parameter identifiability analysis is discussed and tested with the *Silgrain*® model. Such a method proves to be very useful, since it provides a subset of parameters that can be identified from the available data. After parameter estimation, the fitting of the model to the experimental data from the industrial plant is satisfactory. Although the prediction abilities of the model have not been tested due to the limited amount of available data, the fact that the model fits well to the experimental data after parameter estimation is a positive result, and confirms the potential of PBE models for predictive purposes.

As regards automatic control, the attention is focused on a particular strategy: inventory passivity-based control. Although this control approach had never been applied to particulate processes before, and has seldom been applied to chemical processes, inventory passivity-based control has been chosen here because it possesses some properties that can be advantageous, and which are not found in other approaches. First of all, the control law is directly based on the model, is multivariable, and accounts for the nonlinearities of the process. Secondly, convergence of the controlled outputs to their setpoints and stabilization of the remaining states of the system, can be ensured under certain conditions. The interconnection of systems that are rendered passive by the control law, is also passive and thus stable. In this thesis, the main ideas behind dissipativity, passivity, and inventory passivity-based control theory are summarized. The methodological framework of inventory passivity-based control is extended to include reactive process systems and particulate process systems. The approach relies on certain controllability and detectability requirements. Although a general method to study detectability may not be possible, a method is suggested in this thesis that may be applied to a

large number of systems. It is based on a powerful theory in the field of nonlinear chemical dynamics: The chemical network approach by Feinberg. This method is applied to the *Silgrain®* model, thus demonstrating that inventory passivity-based control can relatively easily be used for control of particulate processes. Some issues that are relevant for the practical implementation of inventory passivity-based control have also been discussed, namely: the presence of constraint inputs, the effect of uncertainties and model errors, the need of an observer, the possibility for semibatch control, and the importance of the controller in plantwide control. It is discussed how the presence of constrained inputs may deteriorate the performance of controllers in general, and how it may even lead to infeasibility of the setpoints. However, if certain precautions are taken, inventory passivity-based control may perform in a satisfactory way in the presence of input constraints. Regarding model uncertainties, a reported method in the literature for robust control has been tested with the *Silgrain®* model, with quite good results. Some promising results in the search for convergent nonlinear observers are reviewed. Finally, a discussion is given on how inventory passivity-based control can be advantageous for the purpose of plantwide control, and how the control approach can be combined with statistical process monitoring to achieve a further reduction in the variability of the process and the products, and thus improving the quality of the processes and products.

Based on the results presented in this thesis, it can be concluded that relatively realistic PBE models of industrial process units can be developed in a systematic way, and that inventory passivity-based control can be applied for the design and implementation of control strategies for particulate processes. Inventory passivity-based control exploits the knowledge of the process contained in the PBE model, can ensure stabilization of the process, can be used for continuous or semibatch operation, and has other certain advantageous features. A model of an industrial leaching process, the Silgrain® process, has been developed, and a control strategy based on inventory passivity-based control has been suggested, with promising results (in simulation).

8.2 Future directions

Speculation about the directions that the *academic* and *industrial* communities will adopt in the future is not an easy task. In most cases, the statements made on future directions tend to be too optimistic. This is so because the response time constant of the academic community to technological advances/discoveries is several orders of magnitude smaller than the corresponding time constant of the industrial community. There are a number of reasons that explains this: limited budgets for research, high employee mobility, economic cycles, etc. I hope this will

change in the future, such that the technological results studied by the academic community, will also be quickly adopted by the industrial community. Considerable time and resources are used by many academic institutions nowadays to develop PBE models, but are these models exploited by industry? Unfortunately, not to the extent they could. So, here I throw my *hopes* about future directions:

- Sensor technology will improve, and the new sensors will be used in industry. The areas that will benefit from a better instrumentation are: process understanding, model development and validation, process control, process monitoring, and process optimization.
- PBE model development will be more systematic, and even automatic: specific software for model development may be developed, in which many of the modeling tasks will be carried out automatically.
- Results on the phenomenological laws of particulate processes will make it easier to establish the constitutive equations, with less need for tailor-made experiments.
- A large number of tools and advances from systems engineering will be regularly used in PBE model development and the use of PBE models.
- The use of PBE models for off-line and on-line uses in industrial plants will be routine. PBE models will be used as the basis for design and implementation of unit control, plantwide control and statistical process monitoring. A better integration between these fields will be achieved.
- Controller design and controller implementation will be more straightforward, more systematic, and the resulting controller algorithm will have well-known and favorable features. Inventory passivity-based control will be encountered in many particulate processes.
- A better integration of process control and statistical process monitoring will be achieved.

As regards, the case study: the *Silgrain*® process, my hopes are that:

- The instrumentation in the plant will be improved.
- The model will be further validated, and improved if new knowledge of the process is available.
- The model will be used for the following tasks: training simulator, process optimization, process control, and statistical process monitoring.

- The control strategy, based on inventory passivity-based control, will be implemented.

Part IV

Appendices

Appendix A

DAE vs. ODE

Ordinary differential equations (ODE) and differential and algebraic equations (DAE) arise when using mathematical modeling techniques for describing dynamic phenomena. An ODE system is given by equations of the type

$$\frac{dx}{dt} = f\left(t, x, u\right), \tag{A.1}$$

where x are the variables whose dynamic behavior we are interested in, u are specified input variables, and t represents time. In turn, a DAE system is given by equations of the type

$$F\left(t, y, \frac{dy}{dt}\right) = 0, \tag{A.2}$$

i.e. in addition to differential equations the system contains algebraic equations.

Historically, sets of DAEs were frequently restated and solved as ODEs, by differentiation and/or extensive algebraic manipulation, often destroying the natural structure of the system. Today, it is becoming more common to deal with such problems in their original, natural DAE form, mainly because the variables in the original DAE typically have some physical significance, whereas those that result after manipulation into an ODE may not (Lefkopoulos & Stadherr 1993). However,

> *DAEs are not ODEs* (Petzold 1985).

A number of difficulties can arise when numerical methods are used to solve DAE systems of the form shown in equation A.2. Many of the DAE systems can be solved using numerical methods which are commonly used for solving stiff systems of ODEs, such as Backward Differentiation Formulas (BDF). Others can be solved using such methods but only after substantial modification to the strategies usually used in codes implementing those methods (Petzold 1985).

DAE systems can be characterized using the concept of *index*. The index can be thought of as a measure of the variation of the DAE structure from a standard ODE system (Lefkopoulos & Stadherr 1993). The index can be defined as the minimum number of times we must differentiate all or part of the system A.2 with respect to time t in order to determine $y' = dy/dt$ as a continuous function of y and t. More formally, it can be stated that the index of a DAE is the smallest nonnegative integer ν such that the nonlinear system:

$$\begin{aligned} F\left(t, y, y'\right) &= 0 \\ \frac{d}{dt}F\left(t, y, y', y''\right) &= \frac{dF}{dy}y' + \frac{dF}{dy'}y'' + \frac{\partial F}{\partial t} = 0 \\ &\vdots \\ \frac{d^{\nu}}{dt^{\nu}}F(t, y, y', y'', ..., y^{\nu}, y^{\nu+1}) &= 0 \end{aligned}$$

when viewed as relating $t,\ y,\ y', y'', ..., y^{\nu}, y^{\nu+1}$ as independent variables, is solved for y' uniquely in terms of y and t, i.e. there is an underlying ODE $y' = y'\left(z, t\right)$. The definition implies that any pure ODE is an index-zero DAE, and a system of algebraic equations has an index-one provided the system of equations is nonsingular.

Another difference between ODEs and DAEs is that in the latter we must specify *consistent initial conditions*, and this can become a challenging problem for certain DAEs. For a set of initial conditions to be consistent, it must satisfy the system at an initial time t_0

$$F(t_0, y_0, y_0') = 0. \tag{A.3}$$

Note that the term initial conditions is used to refer to the vector (y_0, y_0') rather than simply to y_0. This is a necessary condition, but not always sufficient for consistency. Usually, some or all of the equations resulting from differentiating F ν times with respect to time have to be satisfied, too.

Appendix B

The *Silgrain*® Simulator

In order to make the *Silgrain*® model user-friendly and available to users that may not be very familiar with programming in MATLAB®, a graphical user interface (GUI) has been developed with the help of *the GUI Design Environment* in MATLAB®.

The simulator is started by typing `Silgrain` in the command line of MATLAB®. The window shown in Figure B.1 appears. By clicking on the `First Run` button, a new simulation is initiated. The windows shown in Figures B.2 and B.3 appear, where the user types the values of the inputs and the initial conditions corresponding to the HR and to the UR, respectively. Default values are given in the windows, but they have been removed here to protect confidential information. Note that some of the inputs are considered to have constant values during the simulation, while others can change in a cyclical pattern. This means that we can simulate diverse modes of operation: continuous, semibatch or batch operation of certain inputs, such as the FeSi feed or the tapping of the UR . Figure B.4 indicates the kind of cyclic inputs that may be simulated. Once the values of the initial conditions and inputs in Figures B.2 and B.3 are typed, and the `OK` buttons are clicked, the window shown in Figure B.5 pops up, where the user introduces the desired simulation time. When the `OK` button is clicked, the simulation starts. Once the calculations are finished, the standard (Windows) `Save` window appears, where the user can select the folder, the filename and save the simulation results as a data file (format `.mat` in MATLAB®). Once the data are saved, a window with a question of whether plotting unscaled or scaled variables appears. Once the choice is made, plotting is carried out. The windows shown in Figure B.6 then appear, where the user can select variables from the pop-up menus and plot them by clicking on the corresponding `Update` buttons. Some options are available for modifying the plots, for example zoom, and for saving the figures in some of the most common formats (`.gif`, `.jpg`, etc).

Simulations that were calculated and saved can be continued. The values of the

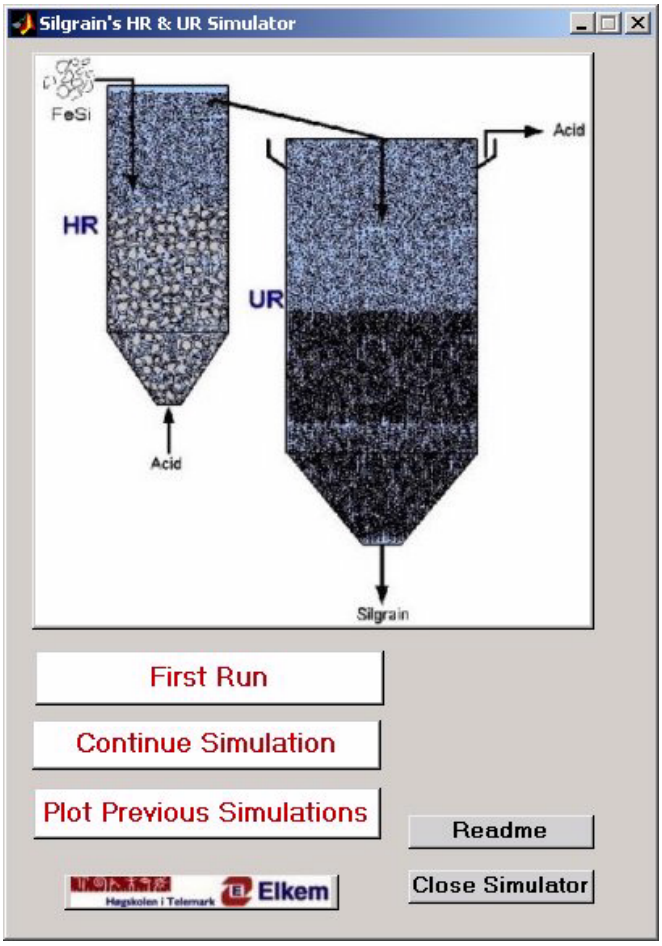

Figure B.1: Main window of the *Silgrain*® simulator.

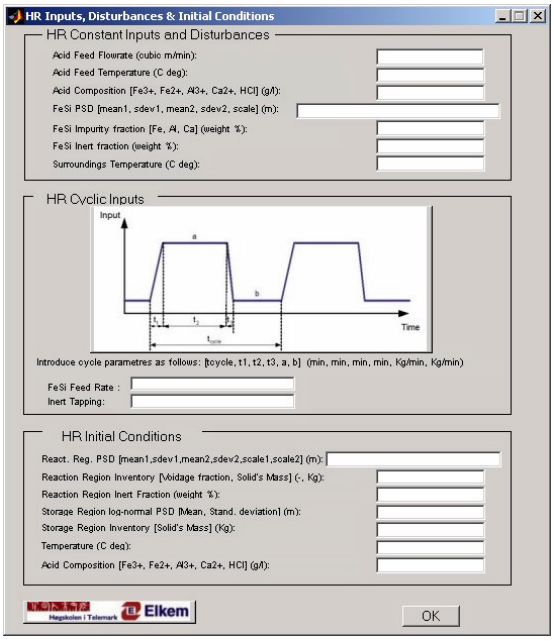

Figure B.2: HR inputs and initial conditions.

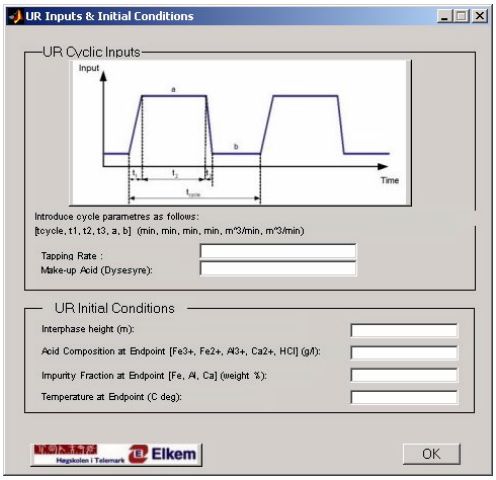

Figure B.3: UR inputs and initial conditions.

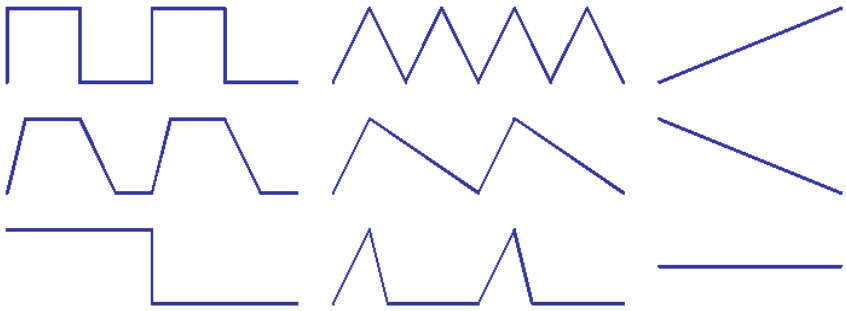

Figure B.4: Types of cyclic inputs that can be used in the *Silgrain*® simulator.

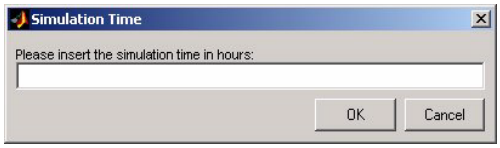

Figure B.5: Simulation time window.

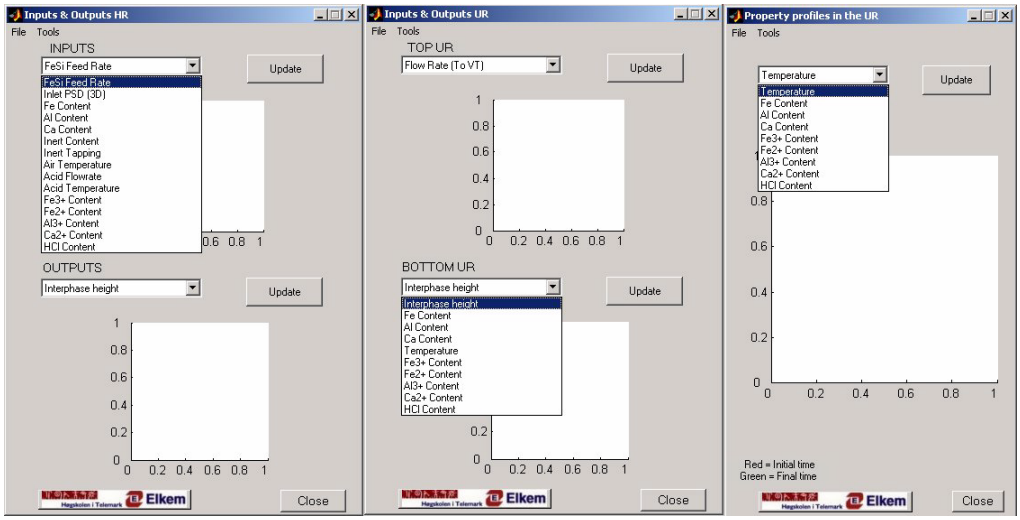

Figure B.6: Plot windows.

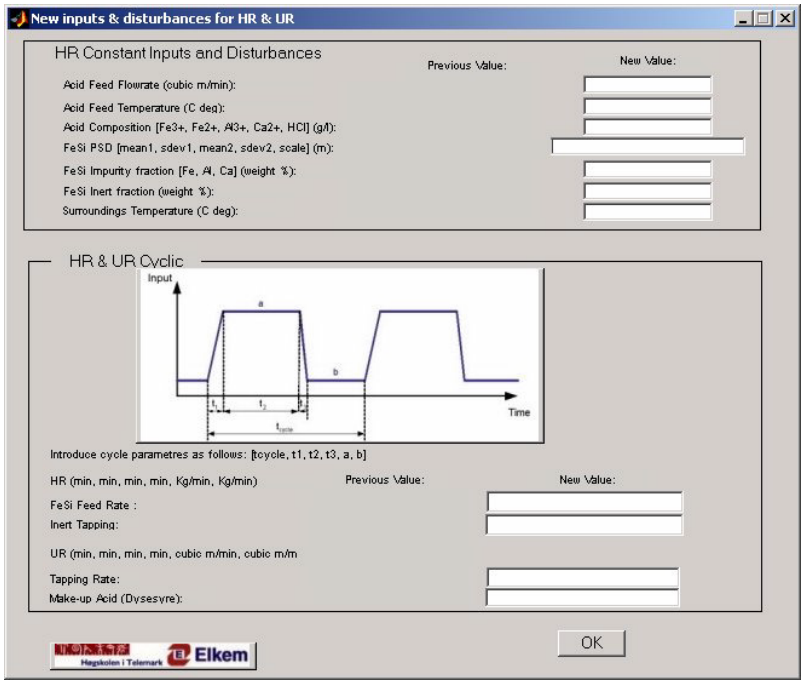

Figure B.7: New inputs and disturbances window.

variables at the last simulated time instant thus become the initial conditions for the new simulation. This allows the user for example to make changes in the inputs, or carry out simulations that otherwise would be too long. In order to continue a previous simulation, the user has to click on the `Continue Simulation` button in the main window (shown in Figure B.1). The standard `Open file` window appears. The user thus selects the folder and filename of the simulation data to be loaded. Once the file is loaded, the window shown in Figure B.7 appears, where the user can type the values of the new inputs to the system. The values used in the previous simulation are shown, but they have been removed here to protect confidential information. When, the `OK` button is clicked, the window in Figure B.5 appears, where the user introduces the simulation time. Once the calculations are finished, the standard `Save` window appears, and once the data are saved, the plot windows shown in Figure B.6 appear.

Finally, saved data can be loaded anytime for plotting, by using the `Plot Previous Simulation` button in the main window (shown in Figure B.1).

Appendix C

Some concepts in nonlinear control theory

The theory presented in this appendix is a summary of material presented in introductory books to nonlinear control (Slotine & Li 1991), (Khalil 1996).

C.1 Autonomous and nonautonomous nonlinear systems

A nonlinear dynamic system can usually be represented by a set of nonlinear differential equations in the form

$$\frac{dx}{dt} = f(x,t) \tag{C.1}$$

where f is a nonlinear function, and x is the state of the system. Note that although equation C.1 does not explicitly contain the control input as variable, it can represent the closed-loop dynamics of a feedback system, with the control input being substituted by a function of the state x or time.

The nonlinear system C.1 is said to be autonomous if f does not depend explicitly on time, i.e. the system's state equation can be written

$$\frac{dx}{dt} = f(x) \tag{C.2}$$

Otherwise, the system is called non-autonomous.

Autonomous and non-autonomous systems are equivalent to linear time-invariant and linear time-variant systems, respectively, in linear system theory. The properties of closed-loop systems, in particular stability, are easier to analyze for autonomous systems than for non-autonomous systems. Moreover, the state trajec-

tory of an autonomous system is independent of the initial time, while that of an non-autonomous system is dependent on the initial time.

Definition 24 *A state x^{ss} is said to be an steady-state of the system if once $x(t)$ is equal to x^{ss}, it remains equal to x^{ss} for all future time.*

If we are interested in studying the properties of an steady-state that is not the origin, it is common to make the following change of variables

$$x_{\text{new}} = x - x^{ss}, \tag{C.3}$$

formulating the system of equations in term of the new set of variables x_{new}, and studying the behavior of the new system in the neighborhood of the origin.

In some practical problems we are not interested in stability around an steady-state, but rather with the stability of a *motion*, i.e. whether a system will remain close to its original motion trajectory if slightly perturbed away from it. This kind of problem can also be transformed into an equivalent stability problem around an equilibrium point, but the equivalent system is non-autonomous.

C.2 Stability

Stability theory has a central role in systems theory and engineering. Qualitatively, a system is described as stable if starting the system somewhere near the desired operating point, the system will stay close to the operating point ever after. Stability is the first and most important performance feature of a controller, at least for systems operating in a continuous way. Note that since nonlinear systems may have complex behavior, refinements of the stability notion are needed to describe the essential features of the system.

C.2.1 Stability of a steady-state for autonomous systems

Definition 25 *The steady-state $x = 0$ of equation C.2 is:*
- stable if, for each $\varepsilon > 0$, there is $\delta = \delta(\varepsilon) > 0$ such that:

$$\|x(0)\| < \delta \quad \Rightarrow \quad \|x(t)\| < \varepsilon, \quad \forall t \geq 0$$

- unstable if it is not stable.
- asymptotically stable if it is stable and δ can be chosen such that:

$$\|x(0)\| < \delta \quad \Rightarrow \quad \lim_{t \to \infty} x(t) = 0$$

- marginally stable if it is stable but not asymptotically stable.
- exponentially stable if there exist two strictly positive numbers a and λ such that

$$\|x(0)\| < \delta \quad \Rightarrow \quad \|x(t)\| < a\|x(0)\| e^{-\lambda t}, \quad \forall t \geq 0$$

- globally asymptotically stable if asymptotic stability holds for any initial states.
- locally asymptotically stable if asymptotic stability only holds for certain initial states.

Therefore, asymptotic stability is a harder requirement than marginal stability. Asymptotic stability requires the state to converge to the origin as time goes to infinity, while marginal stability only requires the state to remain close to the origin at all times. When the origin is asymptotically stable, we are often interested in determining how far from the origin the trajectory can be and still converge to the origin as t approaches ∞. This gives rise to the definition of the *region (or domain) of attraction*. If this region is equal to the whole state space, then we have global asymptotic stability. Otherwise, we have local asymptotic stability.

C.2.2 Stability of a steady-state for non-autonomous systems

The concepts of stability for non-autonomous systems are quite similar to those of autonomous systems. However, due to the dependence of non-autonomous system behavior on initial time t_0, the definitions of these stability concepts include t_0 explicitly. Furthermore, the concept of *uniformity* is necessary to characterize non-autonomous systems.

Definition 26 *The steady-state $x = 0$ of equation C.1 is:*
- stable if, for each $\varepsilon > 0$, there is $\delta = \delta(\varepsilon, t_0) > 0$ such that:

$$\|x(t_0)\| < \delta \quad \Rightarrow \quad \|x(t)\| < \varepsilon, \quad \forall t \geq t_0 \geq 0 \tag{C.4}$$

- unstable if it is not stable.
- uniformly stable if, for each $\varepsilon > 0$, there is $\delta = \delta(\varepsilon) > 0$, independent of t_0, such that condition C.4 is satisfied.
- asymptotically stable if it is stable and $\delta = \delta(\varepsilon, t_0)$ can be chosen such that:

$$\|x(t_0)\| < \delta \quad \Rightarrow \quad \lim_{t \to \infty} x(t) = 0$$

- globally asymptotically stable if asymptotically stability holds for any initial states.

- uniformly asymptotically stable if it is uniformly stable and there is a positive constant δ, independent of t_0, such that

$$\|x(t_0)\| < \delta \quad \Rightarrow \quad \lim_{t\to\infty} x(t) = 0$$

uniformly in t_0; that is, for each $\eta > 0$, there is $T = T(\eta) > 0$ such that

$$\|x(t)\| < \eta, \quad \forall t \geq t_0 + T(\eta), \quad \forall \|x(t_0)\| < c.$$

- globally uniformly asymptotically stable if it is uniformly stable, $\delta(\varepsilon)$ can be chosen to satisfy

$$\lim_{\varepsilon\to\infty} \delta(\varepsilon) = \infty,$$

and, for each pair of positive numbers η and c, there is $T = T(\eta, c) > 0$ such that

$$\|x(t)\| < \eta, \quad \forall t \geq t_0 + T(\eta, c), \quad \forall \|x(t_0)\| < c.$$

Here, asymptotic stability requires that there exists a region of attraction for every initial time t_0. Uniformly asymptotic stability implies that there exists a region of attraction, independent of t_0, such that any system trajectory with initial states in such a region converges to the origin uniformly in time. Globally uniformly asymptotic stability requires that the region of attraction is independent of t_0 and equal to the whole state space.

C.2.3 Determination of stability: Lyapunov theory

Having defined stability, the next question is to find ways to determine stability. Lyapunov stability theorems are widely used, and indeed, they are the basis for many nonlinear control approaches. The method shown here is called Lyapunov's direct method.

Theorem 27 (Lyapunov's direct method) *Let $x = 0$ be an steady-state point for the autonomous system C.2 and $D \subset \mathbb{R}^n$ be a domain containing $x = 0$. Let $V : D \to \mathbb{R}$ be a scalar, continuously differentiable function of the state such that*

$$V(0) = 0 \quad \text{and} \quad V(x) > 0 \quad \text{in} \quad D - \{0\} \tag{C.5}$$

$$\frac{dV}{dt} \leq 0 \quad \text{in} \quad D, \tag{C.6}$$

i.e. V is a positive definite function and its time derivative is negative semi-definite, then $x = 0$ is stable.
If, in addition,

$$\frac{dV}{dt} < 0 \quad \text{in} \quad D - \{0\}, \tag{C.7}$$

i.e. the time derivative of V is negative definite, then $x = 0$ is asymptotically stable.
If, in addition,

$$\lim_{\|x\|\to\infty} V(x) = \infty$$

then the steady-state is globally asymptotically stable.

A continuously differentiable function $V(x)$ satisfying conditions C.5 and C.6 is called a *Lyapunov function*. Lyapunov's direct method can be applied without solving the system of differential equations. Unfortunately, there is no systematic method for finding candidate Lyapunov functions. Many Lyapunov functions may exist for the same system. On the other hand,

> If engineering insight and physical properties are properly exploited, an elegant and powerful Lyapunov analysis may be possible for very complex systems. (Slotine & Li 1991)

Note also that the theorem's conditions are only sufficient. Failure of a candidate function to satisfy the conditions for stability or asymptotic stability does not mean that the steady-state is not stable or asymptotic stable.

However, asymptotic stability is such a desirable property of a system, that other theorems have been established to be able to draw conclusions on stability when Lyapunov's conditions are not met. Thus, if we have a Lyapunov function that is only positive semidefinite (instead of positive definite), then LaSalle's invariant set theorem can be used to draw conclusions on stability. A set Ω is said to be *invariant* if every system trajectory which starts at a point in Ω remains in Ω for all future time, i.e.

$$x(0) \in \Omega \quad \Rightarrow \quad x(t) \in \Omega, \quad \forall t \in \mathbb{R}.$$

A set is said to be positively invariant if

$$x(0) \in \Omega \quad \Rightarrow \quad x(t) \in \Omega, \quad \forall t \geq 0.$$

Theorem 28 (LaSalle's invariance principle) *Let $\Omega \subset D$ be a compact set that is positively invariant with respect to the autonomous system C.2. Let $V : D \to \mathbb{R}$ be a scalar, continuously differentiable, function of the state such that*

$$\frac{dV}{dt} \leq 0 \quad in \quad \Omega.$$

Let E be the set of all points in Ω where

$$\frac{dV}{dt} = 0.$$

Let M be the largest invariant set in E. Then every solution starting in Ω approaches M as $t \to \infty$.
Now, suppose that no solution can stay identically in M, other than the trivial solution $x(t) \equiv 0$. Then, the origin is asymptotically stable.
Finally, if the conditions for asymptotic stability are met, and V is radially unbounded, i.e.

$$\frac{dV}{dt} \leq 0 \quad in \quad \mathbb{R}^n$$

then the origin is globally asymptotic stable.

Lyapunov theory for autonomous systems can be extended to non-autonomous systems. The conditions required in the treatment of non-autonomous systems are more complicated and more restrictive. These conditions are not shown here, but can be found in introductory texts to nonlinear control, such as (Slotine & Li 1991). LaSalle's invariance principle does not have a counterpart for non-autonomous systems, though.

Although there are not systematic methods to find candidate Lyapunov functions for a general nonlinear system, there exist theorems that are concerned with the existence of Lyapunov functions for a given system, and these are called *converse Lyapunov theorems*. There are also instability theorems based on Lyapunov's direct method.

C.3 Feedback linearization

The main idea of feedback linearization is to algebraically transform a nonlinear system dynamics into a fully or partly linear one, such that linear control techniques can be applied. *Input-state* feedback linearization is used when the dynamics are fully linearized, transforming a nonlinear system of the form

$$\frac{dx}{dt} = f(x, u) \tag{C.8}$$

where $x \in \mathbb{R}^n$ is the state vector, and $u \in \mathbb{R}^m$ is the input vector, into an equivalent linear time-invariant system

$$\frac{dz}{dt} = Az + Bv \tag{C.9}$$

by a certain state transformation

$$z = z(x) \tag{C.10}$$

and a certain input transformation

$$v = v(x, u).$$

Then, standard linear techniques are used to design v.

Very often we deal with tracking problems in which it is desired that certain outputs $y \in \mathbb{R}^p$ of the system

$$y = g(x) \tag{C.11}$$

track a reference signal r, and then it may be more beneficial to linearize the input-output map even at the expense of leaving part of the state equation nonlinear. In such cases, *Input-output* feedback linearization is used, where the nonlinear system composed of equations C.8 and C.11 is transformed into a linear system of the type

$$\begin{aligned} \frac{ds}{dt} &= v \\ y &= s \end{aligned} \tag{C.12}$$

by a certain input transformation

$$v = v(x, y, u). \tag{C.13}$$

Then, the original state x is transformed into

$$\begin{pmatrix} y \\ z \end{pmatrix} = \varphi(x) \tag{C.14}$$

where y is the external state and z is the internal state described by

$$\frac{dz}{dt} = k(z, y). \tag{C.15}$$

Linear feedback is then used to design v. However, some catches about input-output feedback linearization are:

1. Not all nonlinear systems are feedback linearizable. There must be a certain structural property of the nonlinear system that allows us to perform nonlinear cancellations. This required property is that the system has a well-defined *relative degree*.

2. Since the linearized input-output map does not account for all the dynamics of the system, we have to make sure that the "unobservable" part of the dynamics is well-behaved. This is done through the concept of *internal dynamics*.

Definition 29 *A system has relative degree r if we need to differentiate the output of a system r times to generate an explicit relationship between the output y and the input u. A single-input single-output nonlinear system of the form*

$$\begin{aligned} \frac{dx}{dt} &= f(x) + g(x)u \\ y &= h(x) \end{aligned} \tag{C.16}$$

where $x \in \mathbb{R}^n$, $u \in \mathbb{R}$, and $y \in \mathbb{R}$, has a relative degree r $(1 \leq r \leq n)$ in a region Ω, if $\forall x \in \Omega$

$$\begin{aligned} L_g L_f^i h(x) &= 0 \qquad 0 \leq i < r-1 \\ L_g L_f^{r-1} h(x) &\neq 0 \end{aligned} \tag{C.17}$$

where the Lie derivatives L_f and L_g are given by

$$\begin{aligned} L_f h(x) &= \frac{\partial h(x)}{\partial x} f(x) \\ L_f^i h(x) &= L_f L_f^{i-1} h(x) = \frac{\partial \left(L_f^{i-1} h(x) \right)}{\partial x} f(x) \\ L_g L_f^i h(x) &= \frac{\partial \left(L_f^i h(x) \right)}{\partial x} g(x). \end{aligned}$$

Then, the new controlled outputs control law that is used to achieve linearization is

$$u = \frac{1}{L_g L_f^{r-1} h(x)} \left(-L_f^r h(x) + v \right). \tag{C.18}$$

If we have a multiple-input multiple-output system in the affine form C.16, where $x \in \mathbb{R}^n$, $u \in \mathbb{R}^m$, and $y \in \mathbb{R}^m$, the system is said to have a relative degree $(r_1, r_2, \ldots, r_m)$ and a total relative degree $r = r_1 + r_2 + \ldots + r_m$, where r_i is the number of times we have to differentiate the output y_i such that at least one of the inputs appears explicitly, i.e.

$$L_{g_j} L_f^{r_i - 1} h_i(x) \neq 0 \quad \textit{for at least one } j.$$

Input-output linearization decomposes the dynamics of a nonlinear system into an external (input-output) part and an internal part. The *internal dynamics*, as shown by equation C.15, depend on the output vector. Well-behaveness of the internal dynamics is thus essential to ensure good control. In order to make some conclusions about the internal dynamics, it is common to study the zero-dynamics of the system, i.e. the system's internal dynamics when the input is chosen such that the output is maintained at zero

$$\begin{aligned} \frac{dy}{dt} &= 0 \\ \frac{dz}{dt} &= k(z, 0). \end{aligned} \tag{C.19}$$

Definition 30 *A nonlinear system is said to be:*
- minimum phase if its zero-dynamics is asymptotically stable.

- weakly minimum phase if its zero-dynamics are stable in the sense of Lyapunov, but not necessary asymptotically stable.
- globally minimum phase if its zero-dynamics are asymptotically stable for any $z(0)$.
- globally weakly minimum phase if its zero-dynamics is stable in the sense of Lyapunov for any $z(0)$.

As in any controller design we are interested in analyzing the stability of the closed-loop. The input-ouput feedback linearization law stabilizes the system locally provided that the zero-dynamics is asymptotically stable. However, global asymptotic stability of the zero-dynamics does not guarantee global stability of the closed-loop.

References

Aas, H. (1971), The Silgrain process: Silicon metal from 90% ferrosilicon, *in* 'Light Metals 1971: Proceedings of Symposia 100th AIME Annual Meeting', number A71-47, pp. 650–667.

Alonso, A. A., Banga, J. R. & Sanchez, I. (2000), 'Passive control design for distributed process systems: Theory and application', *AIChE J.* **46**(8), 1593–1606.

Alonso, A. A. & Ydstie, B. E. (2001), 'Stabilization of distributed systems using irreversible thermodynamics', *Automatica* **37**(11), 1739–1755.

Alopaeus, V., Koskinen, J., Keskinen, K. I. & Majander, J. (2002), 'Simulation of the population balances for liquid-liquid systems in a nonideal stirred tank. part 2 — parameter fitting and the use of the multiblock model for dense dispersions', *Chem. Eng. Sci.* **57**, 1815–1825.

Andreassen, J.-P. (1995), Løselighetsforhold for jern og aluminium ved syrebehandling av ferrosilisium, Master's thesis, Department of Inorganic Chemistry. University of Trondheim.

Aris, R. (1999*a*), *Elementary Chemical Reactor Analysis*, Dover Publications, Inc., New York.

Aris, R. (1999*b*), *Mathematical Modeling. A Chemical Engineer's Perspective*, Academic Press, San Diego, CA.

Artemiev, S. S. & Averina, T. A. (1997), *Numerical Analysis of Systems of Ordinary and Stochastic Differential Equations*, VSP, Utrecht, the Netherlands.

Bastin, G. & Provost, A. (2002), Feedback stabilisation with positive control of dissipative compartmental systems, *in* 'Electronic Proceedings of 15th International Symposium on the Mathematical Theory of Networks and Systems', University of Notre Dame, South Bend, Indiana (USA).

Bathia, S. K. & Chakraborty, D. (1992), 'Modified MWR approach: Application to agglomerative precipitation', *AIChE J.* **38**(6), 868–878.

Bird, R. B., Stewart, W. & Lightfoot, E. (2002), *Transport Phenomena*, 2nd edn, John Wiley & Sons, Inc., New York.

Braatz, R. D. (2002), 'Advanced control of crystallization processes', *Annu. Rev. Contr.* **26**, 87–99.

Brun, R., Reichert, P. & Künsch, H. R. (2001), 'Practical identifiability analysis of large environmental simulation models', *Water Resour. Res.* **37**(4), 1015–1030.

Bryson, A. E. & Ho, Y. (1975), *Applied Optimal Control. Optimization, Estimation and Control*, Hemisphere Publishing Corporation, Washington D. C.

Byrnes, C. I., Isidori, A. & Willems, J. C. (1991), 'Passivity, feedback equivalence, and the global stabilization of minimum phase nonlinear systems', *IEEE T. Automat. Contr.* **36**(11), 1228–1240.

Chaves, M. & Sontag, E. D. (2002), 'State-estimators for chemical reaction networks of Feinberg-Horn-Jackson zero deficiency type', *Eur. J. Control* **8**(4), 343–359.

Chen, H., Kremling, A. & Allgöwer, F. (1995), Nonlinear predictive control of a benchmark CSTR, *in* 'Proceedings of 3rd European Control Conference', pp. 3247–3252.

Chen, Z., Prüss, J. & Warbecke, H. (1998), 'A population balance model for disperse systems: Drop size distribution in emulsion', *Chem. Eng. Sci.* **53**(5), 1059–1066.

Chiu, T. & Christofides, P. (1999), 'Nonlinear control of particulate processes', *AIChE J.* **45**(6), 1279–1297.

Chiu, T. & Christofides, P. (2000), 'Robust control of particulate processes using uncertain population balances', *AIChE J.* **46**(2), 266–280.

Christofides, P. D. (2002), *Model-Based Control of Particulate Processes*, Kluwer Academic Press, Dordrecht, The Netherlands.

Clarke, B. L. (1980), 'Stability of complex reaction networks', *Adv. Chem. Phys.* **43**, 1–215.

Coffey, D. P. & Ydstie, B. E. (1999), Process networks: Passivity, stability and feedback control, *in* 'Annual Meeting of the AIChE, Dallas, TX'.

Coulson, J. M. & Richardson, J. F. (1978), *Chemical Engineering. Fluid Flow, Heat Transfer and Mass Transfer*, Vol. 1, Pergamon Press, Inc., Oxford.

Crowley, T. J., Meadows, E. S., Kostoulas, E. & Doyle III, F. J. (2000), 'Control of particle size distribution described by a population balance model of semibatch emulsion polymerization', *J. Process Contr.* **10**, 419–432.

Crundwell, F. & Bryson, A. (1992), 'The modelling of particulate leaching reactors — the population balance approach', *Hydrometallurgy* **29**, 275–295.

Desoer, C. A. & Vidyasagar, M. (1975), *Feedback Systems: Input-Output Properties*, Academic Press, New York.

Diemer, R. B. & Olson, J. H. (2002), 'A moment methodology for coagulation and breakage problems: Part 2 — moment models and distribution reconstruction', *Chem. Eng. Sci.* **57**, 2211–2228.

Dixon, D. G. (1995), 'Improved methods for the design of multistage leaching systems', *Hydrometallurgy* **39**, 337–351.

Dixon, D. G. (1996), 'The multiple convolution integral: A new method for modelling multistage continuous leaching reactors', *Chem. Eng. Sci.* **51**, 4759–4767.

Dueñas Díez, M. (2001), Report on the laboratory study related to the mechanistic modeling of the main reactor in the Silgrain process (confidential), Technical report, Elkem A.S. and Telemark University College.

Dueñas Díez, M. (2003), Suggestion of a measurement campaign for validation of the HR and UR model, Technical report, Telemark University College and Elkem ASA.

Dueñas Díez, M., Andersen, E., Fjeld, M. & Lie, B. (2004), Validation of a compartmental population balance model of an industrial leaching process: The Silgrain process, *in* '2nd International Conference on Population Balance Modelling', Valencia (Spain). Submitted to Chem. Eng. Sci.

Dueñas Díez, M., Ausland, G., Fjeld, M. & Lie, B. (2001), Simulation of a hydrometallurgical leaching reactor modeled as a DAE system, *in* 'Proceedings of the 42nd SIMS Simulation Conference — SIMS 2002', Telemark University College, Porsgrunn (Norway).

Dueñas Díez, M., Ausland, G., Fjeld, M. & Lie, B. (2002), 'Simulation of a hydrometallurgical leaching reactor modeled as a DAE system', *Mod. Ident. & Cont.* **23**(2), 93–115.

Dueñas Díez, M., Ausland, G. & Lie, B. (2003*a*), Silisium produksjon: Utfordringer, modelltilpasning, og anvendelser av dynamisk modell av Silgrain-prosessen, *in* 'Servomøtet', Trondheim, Norway.

Dueñas Díez, M., Ausland, G. & Lie, B. (2003*b*), Towards realistic population balance models, *in* 'Proceedings of the Annual AIChE Meeting, San Francisco (USA)'. Submitted to Powder Technol.

Dueñas Díez, M. & Lie, B. (2000), Modelling and simulation of a hydrometallurgical leaching reactor, *in* B. Elmegaard, N. Houbak, A. Jakobsen & F. J. Wagner, eds, 'Proceedings of the 41st SIMS Simulation Conference — SIMS 2001', Scandinavian Simulation Society and Technical University of Denmark, Lyngby (Denmark), pp. 199–225.

Dueñas Díez, M. & Lie, B. (2003*a*), Mechanistic modeling and nonlinear control of particulate processes, *in* 'Nordic Process Control Workshop', Trondheim, Norway.

Dueñas Díez, M. & Lie, B. (2003*b*), Nonequilibrium thermodynamics and process control, *in* 'Proceedings of the 4th European Congress of Chemical Engineering', European Federation of Chemical Engineering, Granada, Spain.

Dueñas Díez, M. & Lie, B. (2003*c*), Towards realistic macroscaled models of particulate processes, *in* '5th UK Particle Technology Forum', Sheffield, UK.

Dueñas Díez, M., Lie, B. & Ydstie, B. E. (2001), Passivity-based control of particulate processes, *in* 'Annual AIChE Meeting', Reno, USA.

Dueñas Díez, M., Ydstie, B. E. & Lie, B. (2002*a*), En passivitetstilpasset strategi for prosessregulering, *in* 'Servomøtet', Kongsberg (Norway).

Dueñas Díez, M., Ydstie, B. E. & Lie, B. (2002*b*), Passivity-based control of particulate processes modeled by population balance equations, *in* 'Proceedings of the 4th World Congress on Particle Technolgy — WCPT4', Sydney (Australia).

Eaton, J. W. & Rawlings, J. B. (1990), 'Feedback control of chemical processes using on-line optimization techniques', *Comput. & Chem. Eng.* **14**(4), 469–479.

Edgar, T. F., Himmelblau, D. M. & Ladson, L. S. (2001), *Optimization of Chemical Processes*, 2nd edn, McGraw-Hill, New York.

Efron, B. & Tibshirani, R. J. (1993), *An Introduction to the Bootstrap*, Chapman and Hall, Boca Raton, Florida.

El-Farra, N. H., Chiu, T. Y. & Christofides, P. D. (2001), 'Analysis and control of particulate processes with input constraints', *AIChE J.* **47**(8), 1849–1865.

Farschman, C. A. (1998), On the Stabilization of Process Systems Described by the Laws of Thermodynamics, PhD thesis, Carnegie Mellon University.

Farschman, C. A., Viswanath, K. P. & Ydstie, B. E. (1998), 'Process systems and inventory control', *AIChE J.* **44**(8), 1841–1857.

Feinberg, M. (1979), *Lectures on Chemical Reaction Networks. University of Wisconsin-Madison*, 4.5 of 9 lectures delivered at the Mathematics Research Centre, University of Wisconsin-Madison.

Feinberg, M. (1980), Chemical oscillations, multiple equilibria and reaction network structure, *in* W. E. Stewart, W. H. Ray & C. C. Conley, eds, 'Dynamics and Modelling of Reactive Systems', Academic Press, pp. 59–159.

Feinberg, M. (1987), 'Chemical reaction network structure and the stability of complex isothermal reactors — I. The deficiency zero and deficiency one theorems', *Chem. Eng. Sci.* **42**, 2229–2268.

Feinberg, M. (1991), *Some Recent Results in Chemical Reaction Network Theory*, Vol. 37 of *The IMA Volumes in Mathematics and its Applications*, Springer Verlag, pp. 43–70.

Feinberg, M. (1995*a*), 'The existence and uniqueness of steady states for a class of chemical reaction networks', *Arch. Rational Mech. Anal.* **132**, 311–370.

Feinberg, M. (1995*b*), 'Multiple steady states for chemical reaction networks of deficiency one', *Arch. Rational Mech. Anal.* **132**, 371–406.

Feinberg, M. & Horn, F. J. M. (1974), 'Dynamics of open chemical systems and the algebraic structure of the underlying reaction network', *Chem. Eng. Sci.* **29**, 775–787.

Fogler, H. (1992), *Elements of Chemical Reaction Engineering*, Prentice-Hall, Inc., Englewood Cliffs, New Jersey.

Friedland, B. (1996), *The Control Handbook*, CRC Press, chapter 37, pp. 607–618.

Froment, G. & Bischoff, K. (1990), *Chemical Reactor Analysis and Design*, 2nd edn, John Wiley & Sons, Inc., New York.

Galán, O., Barton, G. W. & Romagnoli, J. (2002), 'Robust control of a SAG mill', *Powder Technol.* **124**, 264–271.

Garvin, D. A. (1988), *Managing Quality*, Vol. Sept.-Oct., The Free Press, New York.

Gelbardt, F. & Seinfeld, J. H. (1978), 'Numerical solution of the dynamic equation for particulate systems', *J. Comput. Phys.* **28**, 357–375.

Georgakis, C. (1986), 'On the use of extensive variables in process dynamics and control', *Chem. Eng. Sci.* **41**(6), 1471–1484.

Gerstlauer, A., Motz, S., Mitrovic, A. & Gilles, E. D. (2002), 'Development, analysis and validation of population balance models for continuous and batch crystallizers', *Chem. Eng. Sci.* **57**, 4311–4327.

Glemmestad, B., Ertler, G. & Hillestad, M. (2002), Advanced process control in a Borstar PP plant, *in* 'ECOREPII, 2nd European Conference on the Reaction Engineering of Polyolefins. Lyon, France, 1-4 July 2002'.

Greenwood, N. N. & Earnshaw, A. (1997), *Chemistry of the Elements*, 2nd edn, Butterworth-Heinemann.

Hauge, T. A. (2003), Roll-Out of Model Based Control with Application to Paper Machines, PhD thesis, Norwegian University of Science and Technology and Telemark University College.

Herbst, J. (1979), Rate processes in multiparticle metallurgical systems, *in* H. Sohn & M. Wadsworth, eds, 'Rate Processes in Extractive Metallurgy', Plenum Press, pp. 53–112.

Herbst, J. & Asihene, S. (1993), Modelling and simulation of hydrometallurgical processes using the population balance approach, *in* V. Papangelakis & G. Demopoulos, eds, 'Modelling, Simulation and Control of Hydrometallurgical Processes. Proceedings of the 32nd Annual Conference of Metallurgists of CIM', Canadian Institute of Mining, metallurgy and petroleum, Quebec, pp. 3–44.

Horn, F. J. M. & Jackson, R. (1972), 'General mass action kinetics', *Arch. Rational Mech. Anal.* pp. 81–116.

Hulburt, H. M. & Katz, S. (1964), 'Some problems in particle technology — A statistical mechanical formulation', *Chem. Eng. Sci.* **19**, 555–574.

Immanuel, C. D., Cordeiro, C. F., Sundaram, S. S., Meadows, E. S., Crowley, T. J. & Doyle III, F. J. (2002), 'Modeling of particle size distribution in emulsion co-polymerization: Comparison with experimental data and parametric sensitivity studies', *Chem. Eng. Sci.* **26**, 1133–1152.

Immanuel, C. D. & Doyle III, F. J. (2002), 'Open-loop control of particle size distribution in semi-batch emulsion copolymerization using a generic algorithm', *Chem. Eng. Sci.* **57**, 4415–4427.

Imsland, L. & Foss, B. A. (2003), State feedback set stabilization for a class of positive systems, *in* 'Proceedings of IFAC POSTA', Rome.

Imsland, L. S. (2002), Output Feedback Stabilization and Control of Positive Systems, PhD thesis, Norwegian University of Science and Technology.

Johnson, R. A. & Wichern, D. W. (1998), *Applied Multivariate Statistical Analysis*, Prentice Hall, Upper Saddle River, New Jersey.

Kalani, A. & Christofides, P. D. (2000), 'Modeling and control of a Titania aerosol reactor', *Aerosol Sci. & Tech.* **32**, 369–391.

Kapur, P. (1995), Particle population balance in granulation of iron ores by an auto-layering mode, *in* S. Mehrotra & R. Shekhar, eds, 'Mineral Processing. Recent Advances and Future Trends.', Allied Publishers ltd, pp. 703–717.

Khalil, H. A. (1996), *Nonlinear Systems*, Prentice Hall, Inc., Upper Saddle River, New Jersey.

Kolflaath, J. A. (1960), United States Patent 2,923,167: Method of refining ferrosilicon material, Technical report, Oslo, Norway.

Kondepudi, D. & Prigogine, I. (1998), *Modern Thermodynamics*, John Wiley & Sons, Inc., Chichester, England.

Kumar, S. & Ramkrishna, D. (1996*a*), 'On the solution of population balance equations by discretization — I. A fixed pivot technique', *Chem. Eng. Sci.* **51**(8), 1311–1332.

Kumar, S. & Ramkrishna, D. (1996*b*), 'On the solution of population balance equations by discretization — II. A moving pivot technique', *Chem. Eng. Sci.* **51**(8), 1333–1342.

Kumar, S. & Ramkrishna, D. (1997), 'On the solution of population balance equations by discretization — III. Nucleation, growth and aggregation of particles', *Chem. Eng. Sci.* **52**(24), 4659–4679.

Kunii, D. & Levenspiel, O. (1991), *Fluidization Engineering*, 2nd edn, Butterworth-Heinemann, Boston.

Kurtz, M. J., Zhu, G.-Y., Zamamiri, A., Henson, M. A. & Hjortsø, M. A. (1998), 'Control of oscillating microbial cultures described by population balance models', *Ind. Eng. Chem. Res.* **37**, 4059–4070.

Lefkopoulos, A. & Stadherr, M. A. (1993), 'Index analysis of unsteady-state chemical process systems — I. An algorithm for problem formulation', *Comput. & Chem. Eng.* **17**(4), 399–413.

Lehmann, E. L. (1998), *Elements of Large-Sample Theory*, Springer Verlag, New York.

Lestage, R., Pomerleau, A. & Hodouin, D. (2002), 'Constrained real-time optimization of a grinding circuit using steady-state linear programming supervisory control', *Powder Technol.* **124**, 254–263.

Levenspiel, O. (1972), *Chemical Reaction Engineering*, 2nd edn, John Wiley & Sons, Inc.

Levenspiel, O. (1999), *Chemical Reaction Engineering*, 3rd edn, John Wiley & Sons, New York.

Liberzon, D., Morse, A. S. & Sontag, E. D. (2002), 'Output-input stability and minimum-phase nonlinear systems', *IEEE T. Automat. Contr.* **47**, 422–436.

Lie, B. (2002), Model reduction by collocation. Lecture Notes.

Lie, B. (2004), Simulation of systems with uncertainty. Written communication.

Litster, J. D. (2003), 'Scale-up of wet granulation processes: Science not art', *Powder Technol.* **130**, 35–40.

Litster, J. D., Smit, D. J. & Hounslow, M. J. (1995), 'Adjustable discretised population balance for growth and aggregation', *AIChE J.* **41**(3), 591–603.

Ljung, L. (1999), *System Identification: Theory for the User*, 2nd edn, Prentice-Hall, Inc., Upper Saddle River, New Jersey.

Lozano, R., Brogliato, B., Egeland, O. & Maschke, B. (2000), *Dissipative Systems Analysis and Control. Theory and Applications.*, Springer Verlag, London.

Luenberger, D. (1966), 'Observers for multivariable systems', *IEEE T. Automat. Contr.* **11**, 190–197.

Luyben, W. L., Tyreus, B. D. & Luyben, M. (1998), *Plantwide Process Control*, McGraw-Hill, New York.

Ma, D. L., Braatz, R. D. & Taffi, D. K. (2002), 'Compartmental modeling of multidimensional crystallization', *Int. J. Mod. Phys.* **16**(1-2), 383 – 390.

Mahoney, A. W., Doyle III, F. J. & Ramkrishna, D. (2002), 'Inverse problems in population balances. Particle growth and nucleation from dynamic data', *AIChE J.* **48**(5), 981–990.

Mantzaris, N. V., Srienc, F. & Dautidis, P. (2002), 'Nonlinear productivity control using a multi-staged cell population balance model', *Chem. Eng. Sci.* **57**, 1–14.

Margarido, F., Figueiredo, M. O., Queiróz, A. M. & Martins, J. P. (1997), 'Acid leaching of alloys within the quaternary system Fe-Si-Ca-Al', *Ind. Eng. Chem. Res.* **36**, 5291–5295.

Margarido, F., Martins, J. P., Figueiredo, M. O. & Bastos, M. H. (1993*a*), 'Kinetics of acid leaching refining of an industrial Fe-Si alloy', *Hydrometallurgy* **34**, 1–11.

Margarido, F., Martins, J. P., Figueiredo, M. O. & Bastos, M. H. (1993*b*), 'Refining of Fe-Si alloys by acid leaching', *Hydrometallurgy* **32**, 1–8.

Martins, J. P. & Margarido, F. (1996), 'The cracking shrinking model for solid-fluid reactions', *Mater. Chem. and Phys.* **44**, 156–169.

Matthews, H. B., Miller, S. M. & Rawlings, J. B. (1996), 'Model identification for crystallization: Theory and experimental verification', *Powder Technol.* **88**, 227–235.

Mersmann, A., Braun, B. & Löffelmann, M. (2002), 'Prediction of crystallization coefficients of the population balance', *Chem. Eng. Sci.* **57**, 4267–4275.

Mohan, R. & Myerson, A. S. (2002), 'Growth kinetics: A thermodynamic approach', *Chem. Eng. Sci.* **57**, 4277–4285.

Montgomery, D. C. (1996), *Introduction to Statistical Quality Control*, John Wiley & Sons, Inc., New York.

Negiz, A. (1995), Statistical Dynamic Modeling and Monitoring Methods for Multivariable Continuous Processes, PhD thesis, Ilinois Institute of Technology.

Negiz, A. & Cinar, A. (1997), 'Statistical monitoring of multivariable dynamic processes with state-space models', *AIChE J.* **43**, 2002–2020.

Nelles, O. (2001), *Nonlinear System Identification*, Springer Verlag, Berlin.

Nocedal, J. & Wright, S. J. (1999), *Numerical Optimization*, Springer Verlag, New York.

Ogunnaike, B. A. & Ray, W. H. (1994), *Process Dynamics, Modeling, and Control*, Oxford University Press, New York.

Ortega, R., der Schaft, A. V., Mareels, I. & Maschke, B. (2001), 'Putting energy back in control', *IEEE Contr. Syst. Mag.* (April), 18–33.

Park, J. & Levenspiel, O. (1975), 'The crackling core model for the reaction of solid particles', *Chem. Eng. Sci.* **30**, 1207–1214.

Pathath, P. K. & Kienle, A. (2002), 'A numerical bifurcation analysis of nonlinear oscillations in crystallization processes', *Chem. Eng. Sci.* **57**, 4391–4399.

Patience, D. B. & Rawlings, J. B. (2001), 'Particle-shape monitoring and control in crystallization processes', *AIChE J.* **47**, 2125–2130.

Perry, R. H. & Green, D. W. (1984), *Perry's Chemical Engineer's Handbook*, 5th edn, McGraw-Hill Inc., New York.

Petzold, L. R. (1985), 'Differential-algebraic equations are not ODEs', *SIAM J. Sci. Stat. Compt.* **3**(3), 49–95.

Pietsch, W. (2001), *Agglomeration Processes — Phenomena, Technologies, Equipment*, Wiley-VCH.

Prett, D. M. & García, C. E. (1988), *Fundamental Process Control*, Butterworth-Heinemann, Boston.

Qin, S. J. & Badgwell, T. A. (1997), An overview of industrial model predictive control technology, *in* J. Kantor, C. E. Garcia & B. Carnahan, eds, 'Proceedings of the International Conference on Chemical Process Control', Tahoe, California, pp. 232–256.

Qu, Z. (1998), *Robust Control of Nonlinear Uncertain Systems*, John Wiley & Sons, Inc., New York.

Ramkrishna, D. (1971), 'Solution of population balance equations', *Chem. Eng. Sci.* **26**, 1136–1139.

Ramkrishna, D. (1973), 'On problem-specific polynomials', *Chem. Eng. Sci.* **28**, 1362–1365.

Ramkrishna, D. (1985), 'The status of population balances', *Rev. Chem. Eng.* **3**, 49–95.

Ramkrishna, D. (2000), *Population Balances. Theory and Applications to Particulate Systems in Engineering*, Academic Press, London.

Randolph, A. D. (1964), 'A population balance for countable entities', *Can. J. Chem. Eng.* **42**, 280–281.

Randolph, A. D. & Larson, M. A. (1988), *Theory of Particulate Processes. Analysis and Techniques of Continuous Crystallization*, 2nd edn, Academic Press, Inc., San Diego.

Rawlings, J. B. & Ekerdt, J. G. (2002), *Chemical Reactor Analysis and Design Fundamentals*, Nob Hill Publishing, Madison.

Rawlings, J. B., Miller, S. M. & Witkowski, W. R. (1993), 'Model identification and control of solution crystallization processes: A review', *Ind. Eng. Chem. Res.* **32**, 1275–1296.

Rice, J. A. (1995), *Mathematical Statistics and Data Analysis*, Duxbury Press, Belmont, CA.

Richardson, J. F. & Harker, J. H. (2002), *Coulson and Richardson's Chemical Engineering. Particle Technology and Separation Processes*, 5th edn, Butterworth-Heinemann, Oxford.

Rubisov, D. H. & Papangelakis, V. G. (1995), 'Model-based analysis of pressure oxidation autoclave behaviour during process upsets', *Hydrometallurgy* **39**, 377–389.

Rubisov, D. H. & Papangelakis, V. G. (1996*a*), 'Mathematical modelling of the transient behaviour of CSTRs with reactive particulates: Part 1— The population balance framework', *Can. J. Chem. Eng.* **74**, 353–362.

Rubisov, D. H. & Papangelakis, V. G. (1996*b*), 'Mathematical modelling of the transient behaviour of CSTRs with reactive particulates: Part 2 — Application to pyrite pressure oxidation', *Can. J. Chem. Eng.* **74**, 363–371.

Sarti, D. & Einhaus, R. (2002), 'Silicon feedstock for the multi-crystalline photovoltaic industry', *Sol. Energ. Mat. and Sol. C.* **72**, 27–40.

Schlosser, P. M. & Feinberg, M. (1994), 'A theory of multiple steady states in isothermal homogeneous CFSTRs with many reactions', *Chem. Eng. Sci.* **49**(11), 1749–1767.

Seborg, D. E., Edgar, T. F. & Mellichamp, D. A. (2004), *Process Dynamics and Control*, Wiley, Hoboken, New Jersey.

Semino, D. & Ray, W. H. (1995*a*), 'Control of systems described by population balance equations — I. Controllability analysis', *Chem. Eng. Sci.* **50**(11), 1805–1824.

Semino, D. & Ray, W. H. (1995*b*), 'Control of systems described by population balance equations — II. emulsion polymerization with constrained control action', *Chem. Eng. Sci.* **50**(11), 1825–1839.

Shampine, L. F., Reichelt, M. W. & Kierzenka, J. A. (1999), 'Solving index-1 DAEs in Matlab and Simulink', *SIAM Rev.* **41**(3), 538–552.

Slotine, J.-J. E. & Li, W. (1991), *Applied Nonlinear Control*, Prentice-Hall Inc., Englewood Cliffs, New Jersey.

Tavare, N. S. (1995), *Industrial Crystallization. Process Simulation, Analysis and Design*, Plenum Press, New York.

Verkoeijen, D., Pouw, G. A., Meesters, G. M. H. & Scarlett, B. (2002), 'Population balances for particulate processes — a volume approach', *Chem. Eng. Sci.* **57**, 2287–2303.

Vollmer, U. & Raisch, J. (2002), 'Population balance modelling and H∞ - controller design for a crystallization process', *Chem. Eng. Sci.* **57**, 4401–4414.

Walter, E. & Pronzato, L. (1997), *Identification of Parametric Models from Experimental Data*, Springer Verlag, Berlin.

Wang, F. Y. & Cameron, I. T. (2002), 'Review and future directions in the modelling and control of continuous drum granulation', *Powder Technol.* **124**, 238–253.

Wang, J. & Ydstie, B. E. (2004*a*), 'Observer-based inventory control', *Submitted to Automatica* .

Wang, J. & Ydstie, B. E. (2004*b*), Robust inventory control systems, *in* 'Proceedings of the American Control Conference, ACC2004', Submitted to Automatica.

Wauters, P. A. L. (2001), Modelling and Mechanisms of Granulation, PhD thesis, Delft Technical University.

Willems, J. C. (1972), 'Dissipative dynamical systems. Part I: General theory', *Arch. Rational Mech. Anal.* **45**, 321–351.

Ydstie, B. E. (2002), 'Passivity based control via the second law', *Comput. & Chem. Eng.* **26**, 1037–1048.

Ydstie, B. E. & Alonso, A. A. (1997), 'Process systems and passivity via the Clausius-Planck inequality', *Syst. and Control Lett.* **30**, 253–264.

Zeaiter, J., Romagnoli, J. A., Barton, G. & Gomes, V. (2002), Modelling, optimisation and control of particulate systems: On-line application to emulsion polymerisation processes, *in* 'Proceedings of the 4th World Congress on Particle Technolgy — WCPT4', Sydney (Australia).

Zeaiter, J., Romagnoli, J. A., Barton, G. W., Gomes, V. G., Hawkett, B. S. & Gilbert, R. G. (2002), 'Operation of semi-batch emulsion polymerisation reactors: Modelling, validation and effect of operating conditions', *Chem. Eng. Sci.* **57**, 2955–2969.

Zhu, G.-Y., Zamamiri, A., Henson, M. A. & Hjortsø, M. A. (2000), 'Model predictive control of continuous yeast bioreactors using cell population balance models', *Chem. Eng. Sci.* **55**, 6155–6167.